Characterization of Monomers and Heteromers of the Dopamine and Histamine Receptor Families Using Bioluminescence- and Radioactivity-Based Techniques

Dissertation

zur Erlangung des Doktorgrades der Naturwissenschaften (Dr. rer. nat.)

an der Fakultät für Chemie und Pharmazie

der Universität Regensburg

vorgelegt von

Denise Mönnich

aus Plauen

im Jahr 2024

Characterization of Monomers and Heteromers of the Dopamine and Histamine Receptor Families Using Bioluminescence- and Radioactivity-Based Techniques

Dissertation

zur Erlangung des Doktorgrades der Naturwissenschaften (Dr. rer. nat.)

an der Fakultät für Chemie und Pharmazie

der Universität Regensburg

vorgelegt von

Denise Mönnich

aus Plauen

im Jahr 2024

Die vorliegende Arbeit entstand im Zeitraum von Mai 2020 bis April 2024 unter der Anleitung von PD Dr. Steffen Pockes an der Fakultät für Chemie und Pharmazie der Universität Regensburg.

Der Promotionsgesuch wurde eingereicht im April 2024.

Tag der mündlichen Prüfung: 11. Juni 2024

Vorsitzender des Prüfungsausschusses:	Prof. Dr. Jörg Heilmann
Erstgutachter:	PD Dr. Steffen Pockes
Zweitgutachter:	Prof. Dr. Joachim Wegener
Drittprüfer:	Prof. Dr. Max Keller

Acknowledgments

An dieser Stelle möchte ich mich bei allen Personen bedanken, die zum Entstehen dieser Arbeit beigetragen und mich über die Jahre begleitet haben. Insbesondere möchte ich mich bedanken bei:

Herrn PD Dr. Steffen Pockes für die Vergabe dieses interessanten Themas, die Betreuung und den Freiraum in der Projektgestaltung, die Unterstützung bei allen Publikationen, die Durchsicht dieser Arbeit, sowie die Erstellung des Erstgutachtens. Außerdem danke ich dir für die schönen gemeinsamen Lehrstuhlausflüge und die grandioseste Pizza Regensburgs.

Herrn Prof. Dr. Sigurd Elz für die Aufnahme in den Arbeitskreis und die finanzielle Unterstützung meines Projektes;

Herrn Prof. Dr. Joachim Wegener für die Bereitschaft das Zweitgutachten zu erstellen;

Herrn Prof. Dr. Max Keller für die Teilnahme an der Promotionsprüfung als Drittgutachter;

Herrn Prof. Dr. Jörg Heilmann für die Nutzung der Sterilbank und für die Übernahme des Vorsitzes meiner Promotionsprüfung;

Herrn Prof. Dr. Pierre Koch für die Zurverfügungstellung aller Geräte für die Klonierungs- und Radioaktivlaborarbeiten, sowie für die Nutzung des EnSpires und der Tecan-Geräte.

allen Co-Autoren für die angenehme Zusammenarbeit und fachlichen Austausch, ohne die die Publikationen nicht möglich gewesen wären. Insbesondere möchte ich mich bedanken bei: Dr. Laura J. Humphrys, Dr. Carina Höring und Dr. Lisa Forster für die fachliche und zeitliche Investitionen für die Erstellung der Dopaminies Publikation und Dr. Martin Nagl, dass du mit mir meine erste First-Autor Publikation gemacht und einem shared-first zugestimmt hast und Dr. Niklas Rosier für die Unterstützung in der Entstehung dieser Publikation;

Frau Gabriele Brunner für die Unterstützung in der Zellkultur und organisieren der Materialien am Lehrstuhl von Prof. Heilmann;

Frau Vivien Czipper und Frau Maria Beer-Krön für die hervorragende Unterstützung bei den experimentellen Arbeiten im Labor und für die ständige Bereitschaft zu helfen, sowohl bei meinen oder externen Projekten, bei der Revision für die Dopaminies Publikation oder bei anderen Problemchen;

bei meinen Studierenden im Rahmen des Wahlpflicht- oder Forschungspraktikums für ihr Interesse an meinen Projekten und die experimentelle Unterstützung, die teilweise in Kapitel 4 und 5 eingeflossen sind: Herrn Andreas Beutel und Herrn Dominik Fuchs, Frau Julia Mauch, Frau Anna Scholz, Frau Iman Slim, Herrn Ahmad Jabal, Frau Tina Meier und Frau Anna-Maria Schuhböck;

Frau Dr. Laura J. Humphrys für das Korrekturlesen und dass du Teil des Team Dopaminies warst, für die gute fachliche Zusammenarbeit und deinen Input zu meinem Projekt;

meinem Mädels-Chem.-Cup Team für all den Spaß, den wir hatten und dass ihr so motiviert wart, auch wenn es die ein oder andere Verletzung gab und wir die Notaufnahme kurzzeitig überflutet haben;

dem LS Med. Chem. II mit seinen derzeitigen und ehemaligen Mitgliedern, für die schönen gemeinsamen Ausflüge zu Dult, zum Bowling oder das gemeinsame Feierabendbier;

dem AK Pockes mit seinen derzeitigen und ehemaligen Mitgliedern, die mich in der Zeit der Promotion begleitet und diese verschönert haben;

bei den ehemaligen und derzeitigen Heilfrauen, dass ihr mich so liebevoll adoptiert habt und wir viele lustige Abende verbracht haben. Besonderer Dank gilt Frau Leonie Kayser, Frau Carola Aumer, Frau Liza Dreisbusch und Iris Huber fürs Zuhören und all die außergewöhnlichen Abende in eurer Küche, beim Fasching, Erstsemester-Feiern, Palmator oder Berg;

Herrn Dr. Niklas Rosier und Herrn Dr. Martin Nagl für die Bereitstellung zahlreicher Liganden, ohne die, diese Arbeit nicht möglich gewesen wäre, sowie den fachlichen Austausch bei Problemen, die angenehme Zusammenarbeit für Publikationen und im Laboralltag und alle lustigen Momente bei außer-universitären Aktivitäten - vor allem bei der Konferenz in Leipzig;

Herrn Dr. Merlin Bresinsky, Herrn Alexander Hubmann und Herrn Jonas Daschner für das angenehme Arbeitsklima, das ein oder andere Bier und die Gespräche, um mich auf andere Gedanken zu bringen und für ihr außergewöhnliches Bowlingtalent, dass uns fast den Sieg gebracht hat;

Herrn Dr. Lukas Grätz für deine unendliche Geduld und Zeit mit mir Probleme zu besprechen und dass du immer nach einer Lösung gesucht hast, um mir zu helfen;

Frau Dr. Lisa Forster, dass du meine Einsamkeit im Labor beendet hast und so eine angenehme und lustige Laborkollegin warst, sowie für das Korrekturlesen von Kapitel 4;

Herrn Dr. Stanislav Andreev für deinen Humor, der mich immer aufmuntern konnte, egal wie doof der Tag auch war;

Frau Dr. Carina Höring für die guten Gespräche, sowohl fachlich als auch privat bei einer Tasse Kaffee oder einem Bier;

Frau Dr. Lisa Schindler für die schönen Spätzle-Abende und dafür, dass du nicht müde wurdest mir zu sagen, dass ich für mich Einstehen muss und deine Unterstützung – *Motzen statt Kotzen!*;

Frau Sabrina Zölch, zum einen für das Korrekturlesen dieser Arbeit, jedoch viel mehr dafür, dass du in den letzten Jahren immer ein offenes Ohr für alle Probleme hattest, mich immer auf andere Gedanken gebracht hast (auch wenn das meist mit Kopfschmerzen verbunden war), einfach immer da warst und eine wundervolle Freundin bist (: ;

all meinen nicht-universitären Freunden, die mich während der Promotion aufgebaut und mir Mut zugesprochen haben. Danke, dass ihr nicht müde wurdet, euch immer das gleiche anzuhören. Insbesondere danke ich Frau Katharina Ackermann, dass du dir bei unzähligen Abendessen das Rumgeheule angehört hast und für all deine aufbauenden Nachrichten. Frau Pia Rudlof, Frau Fenja Offermanns und Frau Salyna Alizad für die vielen Zoom-Calls und Urlaube / Unternehmungen, damit ich etwas abschalten konnte. Frau Tina Brandscher für deinen Humor und unverblümte Ehrlichkeit, Frau Juliane Diessl für diverse Kochabende und Sneak -Besuche und Herrn Robert Sommer dafür, dass ich immer eine Zuflucht aus der Uni hatte, sodass zumindest eine gewisse Zeit der Stress vergessen war.

Ein besonders großer Dank gilt meinen wundervollen Eltern und Großeltern, die mich seit vielen Jahren unterstützen - auch über die Promotion hinaus und ihr menschenmöglichstes gegeben haben, dass ich es bis hierhergeschafft habe.

Zu guter Letzt, danke ich der Person, die mich in den letzten Jahren immer zum Lachen bringen konnte, egal wie schlimm der Tag war, die immer für mich da war und mit mir 100 Berge hochgewandert ist, um dem Laboralltag zu entfliehen. Du warst fast seit Tag eins an meiner Seite und hast mir unendlich viel Kraft gegeben, um das durchzustehen. Danke für Alles Lukas.

Publications and Presentations

Publications (peer-reviewed articles)

(published prior to the submission of this thesis)

Mönnich, D.*; Humphrys, L. J.*; Höring, C.; Hoare, B. L.; Forster, L.; Pockes, S. Activation of Multiple G Protein Pathways to Characterize the Five Dopamine Receptor Subtypes Using Bioluminescence Technology. *ACS Pharmacol Transl Sci* **2024**. DOI: 10.1021/acsptsci.3c00339.
*contributed equally

Rosier, N.; **Mönnich, D.**; Nagl, M.; Schihada, H.; Sirbu, A.; Konar, N.; Reyes-Resina, I.; Navarro, G.; Franco, R.; Kolb, P.; Annibale, P.; Pockes, S. Shedding Light on the D1 -Like Receptors: A Fluorescence-Based Toolbox for Visualization of the D1 and D5 Receptors. *Chembiochem* **2023**, e202300658. DOI: 10.1002/cbic.202300658.

Nagl, M.; **Mönnich, D.**; Rosier, N.; Schihada, H.; Sirbu, A.; Konar, N.; Reyes-Resina, I.; Navarro, G.; Franco, R.; Kolb, P.; Annibale, P.; Pockes, S. Fluorescent Tools for the Imaging of Dopamine D2 -Like Receptors. *Chembiochem* **2023**, e202300659. DOI: 10.1002/cbic.202300659.

Mönnich, D.*; Nagl, M.*; Forster, L.; Rosier, N.; Igel, P.; Pockes, S. Discovery of a Tritiated Radioligand with High Affinity and Selectivity for the Histamine H3 Receptor. *ACS Med Chem Lett* **2023**, 14 (11), 1589–1595. DOI: 10.1021/acsmedchemlett.3c00413.
*contributed equally

Jacob, H.; Braekow, P.; Hofmann, B.; Kirchhefer, U.; Forster, L.; **Mönnich, D.**; Humphrys, L. J.; Pockes, S.; Neumann, J.; Gergs, U. Ergometrine stimulates histamine H2 receptors in the isolated human atrium. *Naunyn-Schmiedeberg's Arch Pharmacol* **2023**, 396 (12), 3809–3822. DOI: 10.1007/s00210-023-02573-8.

Szczepańska, K.; Podlewska, S.; Dichiara, M.; Gentile, D.; Patamia, V.; Rosier,N.; **Mönnich,D.**; Ruiz Cantero, C. M.; Karcz, T.; Łażewska, D.; Siwek, A.; Pockes, S.; Cobos, E. J.; Marrazzo, A.; Stark, H.; Rescifina, A.; Bojarski, A. J.; Amata, E.; and Kieć-Kononowicz, K. Structural and Molecular Insight into Piperazine and Piperidine Derivatives as Histamine H3 and Sigma-1 Receptor Antagonists with Promising Antinociceptive Properties. *ACS Chem Neurosci* **2022**, 13 (1), 1–15. DOI: 10.1021/acschemneuro.1c00435.

Szczepańska, K.; Pockes, S.; Podlewska, S.; Höring, C.; Mika, K.; Latacz, G.; Bednarski, M.; Siwek, A.; Karcz, T.; Nagl, M.; Bresinsky, M.; **Mönnich, D.**; Seibel, U.; Kuder, K. J.; Kotańska, M.; Stark, H.; Elz, S.; Kieć-Kononowicz, K. Structural modifications in the distal, regulatory region of histamine H3 receptor antagonists leading to the identification of a potent anti-obesity agent. *Eur J Med Chem* **2021**, 213, 113041. DOI: 10.1016/j.ejmech.2020.113041.

Tropmann, K.; Bresinsky, M.; Forster, L.; **Mönnich, D.**; Buschauer, A.; Wittmann, H.-J.; Hübner, H.; Gmeiner, P.; Pockes, S.; Strasser, A. Abolishing Dopamine D2long/D3 Receptor Affinity of Subtype-Selective Carbamoylguanidine-Type Histamine H2 Receptor Agonists. *J Med Chem* **2021**, 64 (12), 8684–8709. DOI: 10.1021/acs.jmedchem.1c00692.

Forster, L.; Grätz, L.; **Mönnich, D.**; Bernhardt, G.; Pockes, S. A Split Luciferase Complementation Assay for the Quantification of β-Arrestin2 Recruitment to Dopamine D2-Like Receptors. *Int J Mol Sci* **2020**, 21 (17), 6103. DOI: 10.3390/ijms21176103.

Höring, C.; Seibel, U.; Tropmann, K.; Grätz, L.; **Mönnich, D.**; Pitzl, S.; Bernhardt, G.; Pockes, S.; Strasser, A. A dynamic, split-luciferase-based mini-G protein sensor to functionally characterize ligands at all four histamine receptor subtypes. *Int J Mol Sci* **2020**, 21 (22), 8440. DOI: 10.3390/ijms21228440.

Poster Presentations

(only contributions as presenting author are listed)

Mönnich, **D.**; Rosier, N.; Nagl, M.; Forster, L.; Pockes, S.; Characterization of the D1R-H3R heteromer in a co-expressing system using bivalent ligands. *Conference of the German Pharmaceutical Society (DPhG)* (2023, Tübingen, Germany)

Mönnich, **D.**; Rosier, N.; Nagl, M.; Pockes, S.; Characterization of the D1R-H3R and D2R-H3R heteromers in co-expressing systems using bivalent ligands. *4GPCRnet international symposium* (2022, Leipzig, Germany).

Mönnich, D.; Höring, C.; Pockes, S.; A Split-Luciferase-Based Mini-G Protein Sensor to Functionally Characterize Dopamine D1-like Receptor Ligands. *Frontiers in Medicinal Chemistry 2022* (GDCh) (2022, virtual meeting)

Mönnich, D.; Höring, C.; Pockes, S.; Development of a Split-Luciferase-Based Mini-G Protein Assay for the Functional Characterization of Dopamine D1-like Receptors Ligands. *Conference of the German Pharmaceutical Society (DPhG)* (2021, virtual meeting)

Table of Content

1. General Introduction

1.1. G Protein-Coupled Receptors

G protein-coupled receptors (GPRCs) are cell surface receptors consisting of seven transmembrane (TM) domains, connected through three extracellular loops (ECL) and three intracellular loops (ILC), with more than 800 members encoded in the human genome.[1–3] Currently, the superfamily of GPCRs is classified into six classes, whereas family A (rhodopsin-like receptors), family B (secretin receptors), family C ($GABA_B$-receptors, metabotropic glutamate receptors and calcium-sensing receptors) and family F (frizzled receptors) are the well-known representatives.[4,5] All transduce the signal of triggers like photons, nucleotides, ions, hormones, peptides, chemokines, and others with their heterotrimeric G protein, followed by a downstream cellular response.[6] Thus, the superfamily of GPCRs is one of the most studied drug targets with currently about 35% of all approved drugs addressing these receptors.[7,8]

1.2. G Protein Induced Signaling Pathways

GPCRs are generally addressed by ligands divided into full or partial agonists, inverse agonists, or antagonists, which stabilize the respective receptor in different states.[9] While antagonists bind to GPCRs in any conformation, inverse agonists prefer the stabilization of the inactive conformation and in contrast, agonists or partial agonists preferable stabilize the activated conformation.[10,11] In general, GPCRs consist of a heterotrimeric G protein, comprising an α, β and γ subunit, whereas the Gα subunit, can be divided into the $\alpha_{s/olf}$-, $\alpha_{i/o}$-, $\alpha_{q/11}$- and $\alpha_{12/13}$-family.[12–14] After the activation by a ligand, a conformational change of the respective receptor is induced and the Gα subunit exchanges intracellular guanosine diphosphate (GDP) with guanosine triphosphate GTP. Thus, the Gβ- and Gγ subunit dissociate as a dimer from the receptor-G-protein-complex and both initiate further downstream effector proteins or lead to internalization and desensitization of the receptor.[15–17] According to the Gα subunit, the $G\alpha_s$ family activates adenylyl cyclase (AC), which causes a cytosolic increase of the second messenger cyclic adenosine monophosphate (cAMP). In contrast, an activation of the $G\alpha_{i/o}$ family leads to inhibition of AC.[18,19] Furthermore, addressing the $G\alpha_{q/11}$ subunit stimulates phospholipase C, followed by an increase of inositol triphosphate (IP_3) and diacylglycerol (DAG).[20] Despite that, the βγ-dimer enables the activation of potassium channels and the positive regulation of AC or phospholipase C-β (PLC-β) (Figure 1.1).[21,22] Moreover, the dissociation of the βγ-dimer from the Gα subunit is responsible for an increase in affinity of the α-subunit to GDP with a following exchange of GTP by GDP.[23,24] Thus, the GPCRs are considered for further activation and signal transmitting.[25]

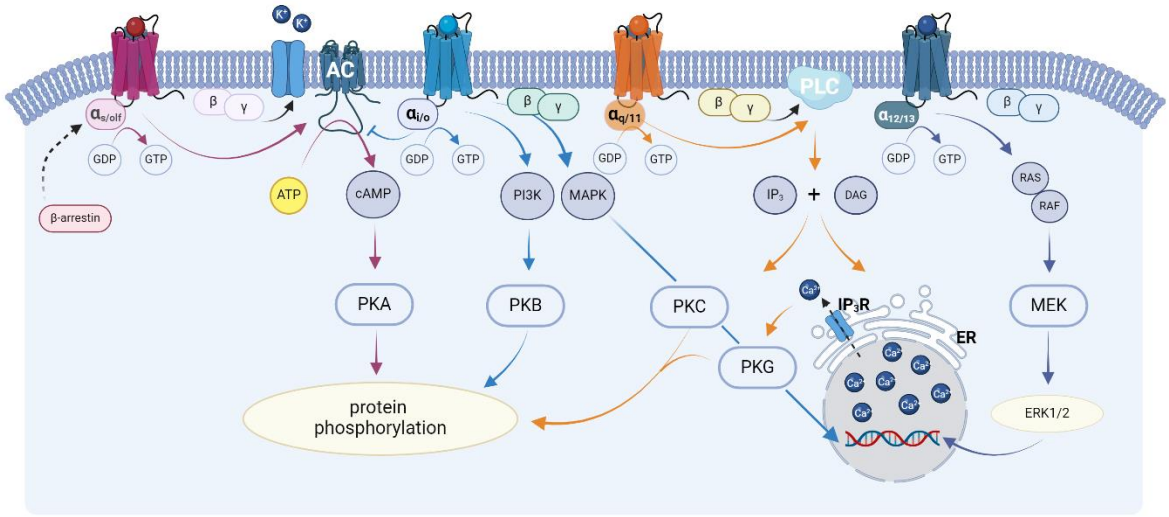

Figure 1.1: Simplified schematic signaling pathway of GPCRs coupled through different G proteins. (Adapted from Panula et al. 2015).[20] Abbreviations used: AC – adenylyl cyclase, ATP – adenosine triphosphate, cAMP- cyclic adenosine monophosphate, DAD – diacylglycerol, ERK 1/ 2 - extracellular signal-regulated kinase 1/ 2, IP3 – inositol-1,4,5-trisphosphate, MAPK or MEK - mitogen-activated protein kinase, PI3K – phosphoinositide-3-kinase, PKA - protein kinase A, PKB - protein kinase B, PKC protein kinase C, PLC – phospholipase C, RAS – rat sarcoma virus (protein), and RAF - rapidly accelerated fibrosarcoma (protein). Created with BioRender.com.

Due to an overlap in downstream signaling pathways by potential G protein and βγ-dimer activation and possible β-Arestin recruitment, unwanted on-target side effects are induced by potential drugs.[26] To overcome this drawback, bias signaling has been in focus of modern drug discovery to distinguish conceivable ligands inducing functional selectivity towards specific G proteins or indeed other signal transducers such as β-arrestins.[27] Already known ligands,[28] allosteric modulators,[29] or bitopic ligands, composed of an orthosteric binding pocket pharmacophore and an allosteric pharmacophore,[30] are investigated as bias ligands. Likewise, addressing heteromers or oligomers by bivalent ligands results in possible improved or altered physiological responses.[31]

1.2.1. Dopamine Receptors and Its Signaling

The famous neurotransmitter dopamine elicits its multifaceted modulatory functions by activating five dopamine receptors, which belong to the class A family of GPCRs.[32,33] In general, the dopamine receptors are divided into two subtype families, whereas the D_1-like family comprises the D_1 receptor (D_1R) and D_5 receptor (D_5R), which share a high structural homology and activate the second messenger pathway through AC.[34,35] Despite that, the D_2 receptor (D_2R), D_3 receptor (D_3R) and D_4 receptor (D_4R) form the D_2-like family, which inhibits, in contrast, the cAMP-initiated second messenger cascade.[36] However, the dopamine receptors are key constituents of the central nervous system (CNS) and are highly expressed in ventral tegmental areas and substantia nigra pars compacta[37], where dopaminergic pathways are involved for various vital central nervous functions,[38] like learning processes,[39] motivation,[40] and motorial

output.[41] Otherwise, dysregulation of the catecholamine dopamine is associated with different diseases, such as schizophrenia,[42] Parkinson's disease,[43] drug addiction,[44] and bipolar disorders.[45] Therefore, the re-regulation of these functions by specific drugs plays diverse roles in drug therapy. Thus, this is currently realized by addressing the D_2-like receptors by approved drugs like pramipexole, selegilin, and levodopa for the treatment of Parkinson's disease[46–48] or antipsychotic drugs as haloperidol, risperidone or olanzapine for bipolar disorders and schizophrenia.[49,50] Especially the latter ones are not selective for the D_2-like receptors and show a broad side effect profile. These are referred as 'dirty drugs'[51] and selective alternatives are being researched in current drug development and promising candidates are in clinical trials like brilaroxazine (Phase III)[52] and sodium benzoate (Phase II / III).[53] For the D_1-like receptors upon this time point only one approved drug is available as emergency treatment for hypertensive crisis (Fenoldopam).[54]

1.2.2. Histamine Receptors and Its Signaling

The family of histamine receptors comprises four receptors, which are coupled to three different G-proteins. The H_1 receptor (H_1R) predominantly activates the pathway of $G\alpha_{q/11,}$ the H_2 receptor (H_2R) the $G\alpha_s$ subunit and in contrast, the signal of H_3 receptor (H_3R) and H_4 receptor (H_4R) is mediated via the $G\alpha_{i/o}$ subunits.[20,55] Histamine, as the endogenous ligand, is associated as a neurotransmitter[56] and is involved in inflammatory regulations.[57] Thus, in pathogenesis the histamine receptors are addressed by drugs as anti-histamines (H_1R antagonists), for the management of allergies[58] like cetirizine, diphenhydramine, or loratadine.[59,60] At the same time the H_2R antagonists famotidine and ranitidine are used for the treatment of gastrointestinal disorders[61,62] and the H_3R ligand pitolisant, characterized as an inverse agonist, to treat narcolepsy, a CNS disorder.[63,64] The H_4R plays a crucial rule in immune-related diseases[65] and therefore, the H_4R antagonist JNJ-39758979 was a promising candidate for the treatment of atopic dermatitis but was discontinued in phase II clinical trial.[66,67] Upon this timepoint, there is no approved drug available and research is still ongoing.[68–70] Due to the involvement of histamine receptors in diseases described above, the development of novel drugs and the investigation of binding properties through the development of new test systems is necessary.[71,72]

1.3. Chimeric Gα-Subunit Proteins – miniG Proteins as a Novel Tool for the Investigation of G Protein Interactions

The Gα subunit, a subunit of the heterotrimeric G protein can be functionally classified into the Gα-GTPase domain and α-helical domain (Gα-AH), both involved in conformational changes of the activated GPCR.[73] As Gα-surrogates, minimal G (miniG) proteins were originally designed to stabilize GPCRs in their active conformation for crystallization, in order to evolve the understanding of GPCR structure and drug design.[74] The crystallization of GPCRs was quite challenging, due to the transient nature of the interaction,[73] as well as the GPCR stabilization by heterotrimeric G proteins due to their large size, conformational dynamics and instability in detergents.[75] Consequently, the engineered miniG proteins consist of the GTPase domain of Gα proteins, comprising 97% of the G protein binding surface to an activated GPCR, including mutations for increased thermostability and reduced nucleotide affinity.[74,76] Based on this concept, several miniG proteins with similar coupling properties to GPCRs such as the Gα families α_s, α_{si}, α_{sq} and α_o have been successfully developed[74,76] and were involved in cryo-EM structures for several GPCRS.[77–79] Furthermore, miniG proteins in combination with the Split-Nano luciferase (NanoLuc) complementation technology were applied to investigate coupling characteristics of GPCRs.[72,76,80]

1.4. Bioluminescence in GPCR Research

In order to observe not only interactions between different proteins, receptors or ligand-receptor interactions, but moreover the functional triggered signal, bioluminescent-based techniques are a useful tool. This includes nano luciferase bioluminescence resonance energy transfer (NanoBRET)-studies,[81,82] miniG-recruitment,[72] G-CASE sensors, which is a BRET-based method created from the TRUPATH system,[83] or the CAMYEN BRET-based biosensor as variations of a well-established technique.[80] To ensure a bioluminescence is measurable a moiety emits light in the presence of a substrate, which undergoes an oxidation and decarboxylation process. In contrast, in Förster Resonance Energy Transfer (FRET)-based studies, an extern laser excites a fluorophore, resulting in a fluorescent emission[84] and causing a high background signal due to the external light source.[85] Moreover, in further common techniques radioisotopes are necessary, resulting in increasing costs by waste disposal and safety issues.[85,86]

1.4.1. Split Luciferase Complementation (SLC)

A commonly used method is the split luciferase complementation (SLC) technique, where two inactive split fragments of an original protein can be restored in close proximity under total catalytic function.[87,88] There are already several fusion proteins implementing the SLC on designed fragments of firefly luciferase,[89] optimized nano luciferase, D-luciferin-based click beetle green or click beetle red luciferases.[90] These strategies are offering the monitoring of protein–protein interactions of biological processes in real-time. However, this is applied by the generation of fusion proteins with the respective interacting counterparts and the split luciferase fragments. Through the merge of the two host proteins the complementation takes place by restoring the reporter fragments with its catalytic function.[91]

One well-known representative is the split Nano luciferase (NanoLuc), consisting of a small bit (NlucC; 1.3 kDa, also known as smBiT[92]) fused to one interacting protein and the large bit (NlucN; 18 kDa, also known as LgBiT[92]), which is introduced to the respective other protein. The NanoLuc is a genetically engineered luciferase, derived from a natural luciferase in the deep-sea shrimp *Oplophorus gracilirostris* with more favorable brightness and size compared to the firefly luciferase.[93] Additionally, by modification of the small bit fragment, auto-affinity was distinguished in order to reduce background signal.[94] If both proteins are in close proximity, bioluminescence at a wavelength of λ = 460 nm is measurable upon reconstitution of the two split fragments in the presence of a substrate, like Coelenterazine-h or Furimazine (Figure 1.2).[95]

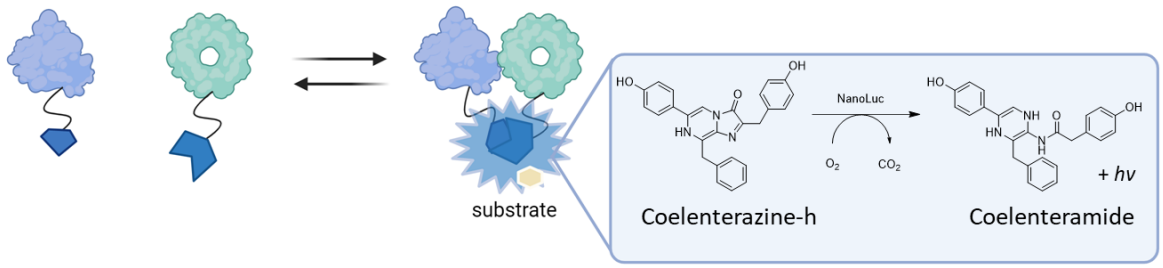

Figure 1.2: Schematic illustration of SLC principle for protein-protein interactions in the presence of the substrate Coelenterazine-h. Created with BioRender.com.

1.4.2. BRET-Based Techniques in Current Research

The first BRET was a naturally occurring phenomenon in marine organisms such as *Aequoria victora* and *Renilla reniformis*[96] and was applied in research to study protein-protein interactions, like CCAAT/enhancer binding protein alpha (C/EBPalpha) in the mammalian nucleus,[97] protein dimerization,[98–100] or β-Arrestin recruitment.[91,101] Over the last years, BRET-based techniques have been improved towards brighter and smaller luminescent proteins[93,102], greater spectral separation and red-shifted fluorescent proteins.[103–105] The first application to GPCRs was to investigate the dimerization of β_2 adrenergic receptors.[106] Thus, a donor and acceptor, with an overlap of donor emission- and acceptor excitation spectra were fused to the respective proteins

or receptors of interest. Thus, a non-radiative energy transfer between the donor and acceptor takes place when both are in close proximity (≤ 10 nM) within a favorable orientation to each other (Figure 1.3, A).[107] In general, techniques taking advantage of *Renilla* luciferase with variants of YFP employing Coelenterazine-h as substrate are commonly referred to as BRET[1] while a combination of *Renilla* luciferaseII, DeepBlueC™ (Coelenterazine-400a) and variants of GFP is assigned as BRET[2].[108–110]

Stoddart et al. 2015 recently applied the NanoBRET technique to investigate ligand binding to several GPCRs (assigned to BRET[2]).[107] Cells expressing one fusion protein are subsequently incubated with the corresponding substrate, allowing the BRET donor to produce luminescence. Using the brighter NanoLuc as a fusion protein to increase sensitivity, in the presence of Furimazine bioluminescence at a wavelength of λ = 460 nm is produced and transfers the non-radiative energy to the donor, like a TAMRA coupled fluorescent ligand, resulting in fluorescence ($\lambda \geq 610$ nm) (Figure 1.3, B). This setup enables monitoring the binding of a ligand in real-time, with low non-specific binding, high sensitivity and the possibility for high-throughput screening.[107,111,112]

To elucidate the (canonical) coupling of G proteins of orphan receptors or well-studied GPCR, the G-case sensor created from the TRUPATH system is an excellent tool.[113] In this system the different G proteins are C-terminally fused to the NanoLuc transferring the energy to a cp-Venus fluorescent protein as BRET acceptor, which is coupled to the βγ dimer resulting in BRET signal. Binding of a ligand to the receptor then causes a conformational change while the βγ subunit dissociates from the respective G protein leading to a lower BRET signal (Figure 1.3, C).[83]

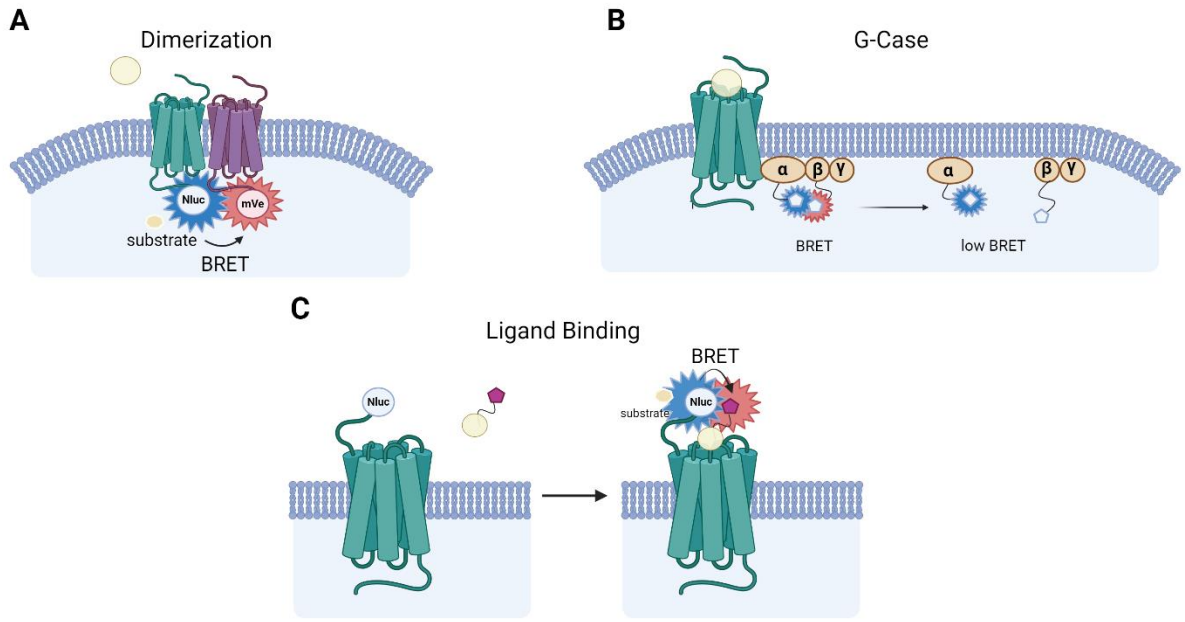

Figure 1.3: Various bioluminescence techniques applied to several GPCRs. **A:** NanoBRET-based investigation of receptor dimerization, where the donor (NanoLuc) and the acceptor (mVenus) are C-terminally fused to each protomer. In the presence of a substrate a BRET-signal is measurable. **B:** Scheme of the G-CASE assay, where the NanoLuc is introduced into the Gα subunit of a G protein trimer, and the cpVenus protein is cloned to the N-terminus of the corresponding Gγ subunit. After receptor activation by a ligand, the Gα-NanoLuc donor and cpVenus-Gγ acceptor proteins are spatially displaced, decreasing the BRET ratio and enabling measurement of the specific activation of a chosen Gα subunit. **C:** Principle of BRET-based GPCR ligand binding assay. The NanoLuc as donor is N-terminally fused to the respective receptor, while the corresponding acceptor as fluorophore is coupled to the ligand of interest. The BRET signal results in low proximity (≤ 10 nM) of the donor and the acceptor after catalytic oxidation of the substrate through the NanoLuc. Created with BioRender.com.

1.5. Heterodimerization of Receptors of the Class A Family: Current State of the Art

Until a few years ago, it was assumed that class A receptors, unlike class C receptors, only occur as monomers, but results from radioligand binding studies or immunoprecipitation experiments gave first hints for the formation of homo- or heterodimers and higher-order oligomers of class A receptors.[114–116] With the development of techniques like BRET and FRET,[117–119] protein complementation,[106,120] and imaging,[121,122] the existence of dimers and oligomers was supported. However, up to this point, no crystal structure of any (human) class A GPCR heteromer or oligomer was reported. A homodimer is referred as a cross-interaction between two identical transmembrane receptors, whereas a heterodimer (also known as a heteromer) consists of two distinct receptors.[123] The formation of homomers is considered, to rely predominantly on TM interactions. In contrast, for heteromers or oligomers, the binding energy between the receptors is crucial, but these cross-interactions are still under-researched, as well as the sufficient stoichiometric receptor ratio to form functional complexes *in vivo*.[124,125]

With the application of bioluminescence techniques, like NanoBRET or spilt complementation, the existence of several dimers as the D_2R-D_2R or H_3R-H_3R homodimer,[100,126] or the D_2R-NTS_1R and D_3R-NTS_1R heterodimer was confirmed.[127,128] Unlike the class C family, the homo-, hetero- or oligomerization of class A family receptors is not necessary for functioning signaling but can lead to distinct pharmacological properties compared to the respective monomers.[129,130]

1.5.1. Dimerization Alters Pharmacological Properties

From the traditional perspective of ligand-receptor-theory a drug interacts with a receptor, whereby the magnitude of the receptor-mediated effect is proportional to the concentration of the drug-receptor-complex. Therefore, the activation initiates a conformational change and induces a downstream signal cascade, while the presence of homo-, hetero-, or oligomerization leads to a higher complexity of GPCR signaling. However, dimerization can modulate existing capacities and induce new pharmacological effects with a switch in signaling transduction, signal amplification or reduction compared to the monomeric structure (Figure 1.4.).[15,131,132]

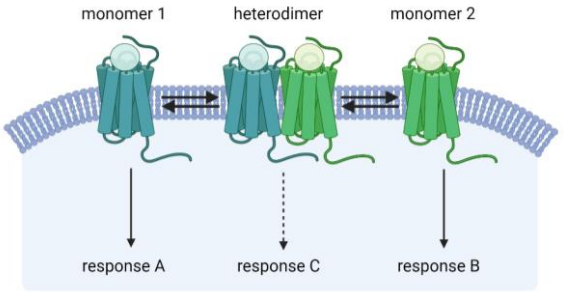

Figure 1.4: Altered signal transduction of receptors due to dimerization. Created with BioRender.com.

During this cross-interaction, the TMs of each protomer undergo conformational changes, initiating possible novel pharmacological properties due to crosstalk. Thus, binding of a ligand possibly leads to an induced conformational change that is transmitted to the second protomer and results in an increased or decreased binding affinity, described as positive or negative cooperativity.[127,133] Evidence for a positive cooperativity was recently observed for the δ-opioid receptor – μ-opioid receptor heterodimer,[134] and likewise, for the muscarinic M_3 receptor homodimer to recruit ß-Arrestin-1.[135] A negative cooperativity of the D_2R homodimer was elucidated for specific antagonists.[136] Another possible event is the positive or negative modulation as for the D_2R-H_3R heterodimer where an H_3R receptor-mediated negative modulation of the $D_{2l}R$ function was demonstrated. This evolve novel opportunities as a new therapeutic target for the Parkinson's disease.[137] Despite that, the binding of a ligand can alter the affinity of one protomer to the respective other, indicating a dissociation as for the D_2R homodimer in the presence of the D_2R antagonist spiperone.[138,139]

1.5.2. Addressing Heteromers by Bivalent Ligands

In order to induce a possibly positive or negative cooperativity or modulation or in general targeting homo- or heteromers, the design of bivalent ligands was implemented by combining two pharmacophores linked by a spacer of appropriate length and suitable biochemical properties.[140,141] While bitopic ligands are considered to address one orthosteric and the adjacent allosteric binding pocket of a monomeric receptor, bivalent ligands simultaneously recognize two orthosteric binding sites of a receptor homo- or heteromer.[142] Thus, the bivalent ligand can bind monovalent to one protomer and might increase the local concentration of the second protomer by binding the tethered pharmacophore[128] or induce a protomeric signal cascade (Figure 1.5, A), as well as binding with both pharmacophores to the dimer, leading to possibly crosstalk effects and second messenger pathways (Figure 1.5, B and C).[143] The gain in entropy results due to an increased concentration of the second pharmacophore in close distance to the homo- or heteromer, after the binding to one protomer (Figure 1.5, C).[144]

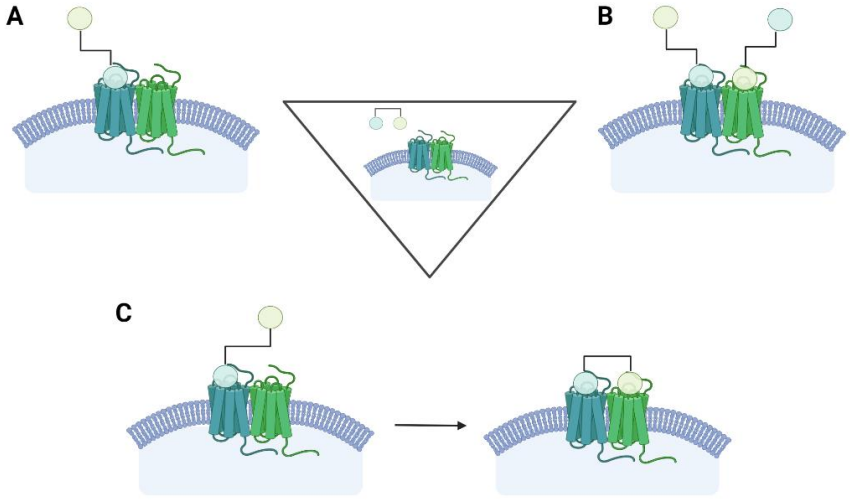

Figure 1.5: Schematic illustration of possible binding modes of a bivalent ligand to a receptor heteromer inducing different pharmacological effects. **A:** Monovalent binding of one pharmacophore of the bivalent ligand to the respective protomer. **B:** Monovalent binding of two bivalent ligands to the respective protomer. **C:** Binding of the bivalent ligand with one pharmacophore, followed by pushing the second one in the vicinity of the second binding site. Created with BioRender.com.

For characterization and analysis of bivalent ligands these possible binding modes are supposed to be considered. It is assumed, that a bivalent ligand binds preferentially to the heteromer, to gain in entropic energy and stabilize the heteromer relative to that of the monomeric counterpart,[145] resulting in a higher affinity.[128,146] Nevertheless, other factors, like an potential loss in conformational entropy for flexible linkers or the influence of the respective linker length need to be considered for favorable binding.[145,147]

However, the design of specific bivalent ligands addressing homo- or heteromers with high affinity has been a successful approach and has been applied to show various GPCR cross-interactions.[146,148,149] Despite that, their large size and high molecular weight, lead to different

adsorption, distribution or metabolism, which has disadvantages for *in vivo* studies. Therefore, further investigations and modifications are necessary for a clinical application.[29,128,150]

1.5.3. Dopamine and Histamine Interconnectivity

In the striatum, dopamine and histamine receptors are highly comprised and the histaminergic system has an impact towards the modulation of dopaminergic neurotransmission.[151] Thus, the cross-interaction as D_1R-H_3R or D_2R-H_3R heteromers is not surprising.[137,152] The formation of functional entities regulates different biochemical processes, which can differ from the monomeric units, that need to be further understood.[152,153]

Both, the D_1R and H_3R belong to the class A family of GPCRs, whereas the D_1R canonical couples to the $G\alpha_s$ subunit leading to the activation of AC and in contrast, the H_3R inhibits the AC signal cascade mediated by the $G\alpha_{i/o}$ protein.[20,34] Due to the formation of the D_1R-H_3R heteromer, the induced signal cascade by the H_3R agonist (*R*)-α-methyl-histamine was altered, allowing the activation of the mitogen-activated protein kinase (MAPK) pathway.[154] Furthermore, the H_3R antagonist thioperamide was able to reduce the D_1R-induced cell death and neuronal degeneration, which plays a crucial role in Huntington's disease.[155] Moreno et al. 2020 showed the possible formation of the D_1R-H_3R heteromer with an additional subunit of *N*-methyl-D-aspartate (NMDA)- receptor, which belongs to the family of ionotropic glutamate receptors,[156] conducting a negative cooperativity by inhibition of this complex.[157] The initiated signal pathway elicits its effect to a reduced dopamine-, NMDA- or $\beta_{1\text{-}42}$-amyloid-induced cell death. This $\beta_{1\text{-}42}$-amyloid-induced cell death was observed as a possible initiator for Alzheimer's disease.[158] Therefore, addressing this oligomer is a potential target for neurodegenerative diseases using selective bivalent ligands.[159,160]

A second representative for dopamine and histamine interconnectivity is the D_2R-H_3R heteromer, which occurs in the striatal tissue of the human brain.[137] In contrast to the D_1R-H_3R heteromer, both involved protomers canonically couple to the $G\alpha_{i/o}$ subunit.[20,36] The existence of the cross-interaction was proven by Ferrada et al. 2009, as well as the negative cooperativity to the signal cascade of the D_2R protomer by activating the H_3R protomer,[137] which can be a useful tool for the regulation of dopaminergic side effects in Parkinson's disease by addressing the D_2R-H_3R heteromer with novel bivalent ligands.[161] Furthermore, Xu et al. 2023 confirmed recently the predicted cross-interaction and assumed an effect of H_3R and D_2R agonists on the regulation of GSK3β by targeting the D_2R-H_3R heteromer.[137,162]

1.6. Scope and Aim of this Thesis

In GPCR research there is still an interest in the investigation of well-studied drug targets like dopamine receptors aiming new approaches to ligand design, addressing favorable signaling pathways and increasing (functional) selectivity, as well as the characterization of potential new drug targets like receptor heteromers. The aim of this thesis was to elucidate the binding properties and signaling pathways of both, monomeric receptors (dopamine receptor family) and receptor heteromers (D_1R-H_3R and $D_{2l}R$-H_3R). For the investigation of cross-interactions between the D_1R or $D_{2l}R$ with the H_3R novel bivalent ligands, synthesized by Dr. Niklas Rosier and Dr. Martin Nagl in-house (Thesis Rosier et al. 2022 and Nagl et al. 2022), were used for the characterization. Unfortunately, during the development process the used radioligand [^{3}H]UR-PI294 was inappropriate, due to high non-specific binding in radioligand binding experiments. Thus, a novel H_3R selective radioligand was synthesized by Dr. Martin Nagl and had to be characterized (Figure 1.6).

With a focus on functional efficacy and selectivity, as well as on the investigation of possible G protein coupling, the split luciferase-based miniG protein recruitment technique, CAMYEN BRET-based biosensors and G-case sensors derived from the TRUPATH system[80] had to be applied to all five (human) dopamine receptors. Consequently, in the case of the miniG recruitment assay the small bit of the split NanoLuc had to be fused to the C-terminus of the respective dopamine receptor, while the large bit had to be introduced N-terminally to the (canonical) miniG protein. For the CAMYEN BRET assay the whole NanoLuc had to be fused to the C-terminus of an Epac cAMP binding domain, and mCitrine to the N-terminus, while in the case of the G-case sensor the whole Nanoluc had to be cloned into the Gα subunit of a G protein trimer, and the cpVenus protein had to be fused to the N-terminus of the corresponding Gγ subunit. With these three assays functional selectivity of G protein subunits had to be analyzed and may help with dopamine receptor targeting and their downstream effects.

In recent studies the cross-interaction between the D_1R or D_2R with the H_3R was shown.[152,154] The characterization and the identification of the triggered pharmacological pathways on the respective heterodimer by bivalent ligands represents both a major challenge and an opportunity in drug design for novel therapeutics for the treatments of diseases like Huntington's disease, Alzheimer's disease or Parkinson's disease.[137,152,155] To study both, the D_1R-H_3R and $D_{2l}R$-H_3R heteromer had to be co-expressed in HEK293T cells. However, from previous BRET-based studies a receptor ratio of 1:2 for the D_1R-H_3R heteromer is predicted to result in functional complexes *in vitro* and had to be considered as target ratio in this thesis.[163] Nevertheless, other ratios for the formation of D_1R-H_3R heteromers had to be supposed for further investigation. As there is no predicted receptor ratio for the D_2R-H_3R heteromer, but the 1:2 ratio in general for class A GPCRs heteromers,[164] different ratios, including the 1:2 ratio, had to be generated likewise. Moreover,

the binding affinities of the specifically synthesized bivalent ligands had to be investigated, as well as a possible bivalent binding mode to the respective receptor heteromers.[141] Thus, the development of a radioligand-based test system for the D_1R-H_3R and $D_{2l}R$-H_3R heteromers, respectively, co-expressing both protomers, was intended. In addition, the goal was to develop a functional assay for the investigation of possible positive or negative cooperativity or modulations between the $D_{2l}R$ and H_3R protomers induced by D_2R or H_3R standard ligands, as well as by bivalent ligands within the $D_{2l}R$-H_3R heteromer.

Another project was to investigate the potential binding affinities of novel ligands at all five (human) dopamine receptors using the NanoBRET technique, established for GPCRs by Stoddart et al. 2015.[107] This set-up represents a suitable alternative for radioligand binding experiments allowing to overcome drawbacks like safety issues and increased costs for waste disposal.[85,86] To implement this technique the NanoLuc had to be fused to the N-terminus of the respective dopamine receptor, acting as BRET-donor, to produce luminescence in the presence of a substrate (λ = 460 nM). After binding of a fluorescent ligand (BRET-acceptor) a non-radiative energy transfer takes place, when both counterparts are in close proximity and fluorescence is emitted (λ >600 nM).[86] This method enables real-time monitoring of ligand binding, as well as real-time kinetic measurements at all five dopamine receptors, with low non-specific binding, high sensitivity and the possibility for high-throughput screening.[107,111,112]

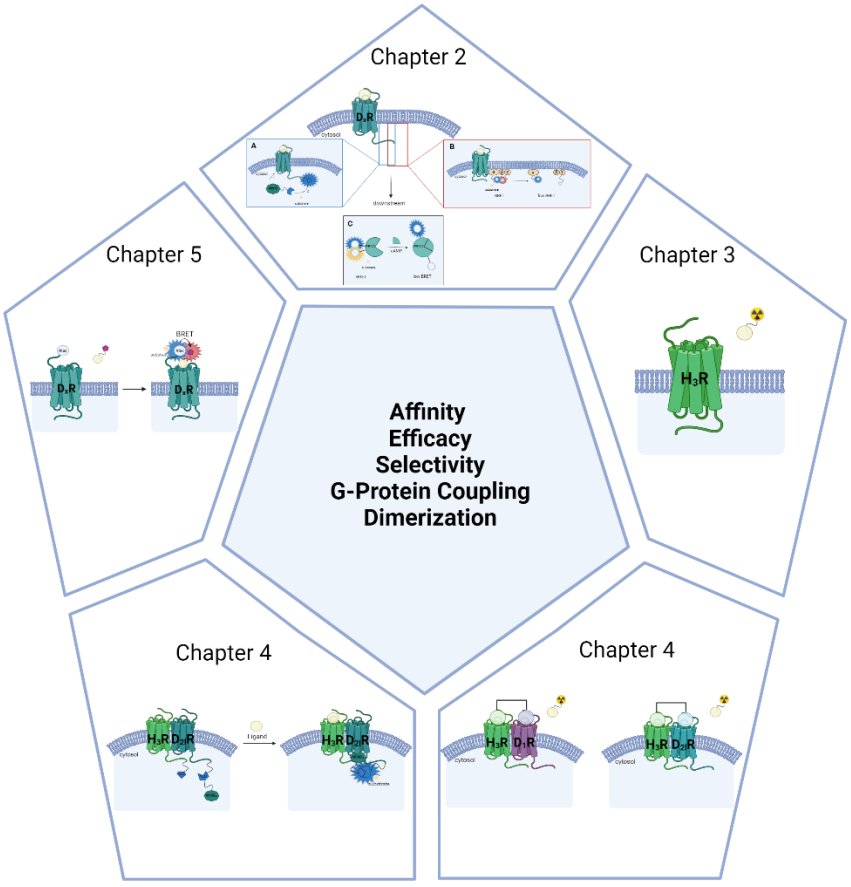

Figure 1.6: Schematic illustration of the aim of this thesis.

1.7. References

(1) Scholz, N.; Langenhan, T.; Schöneberg, T. Revisiting the classification of adhesion GPCRs. *Annals of the New York Academy of Sciences* **2019**, *1456* (1), 80–95. DOI: 10.1111/nyas.14192.

(2) Rosenbaum, D. M.; Rasmussen, S. G. F.; Kobilka, B. K. The structure and function of G-protein-coupled receptors. *Nature* **2009**, *459* (7245), 356–363. DOI: 10.1038/nature08144.

(3) Guo, S.; Zhao, T.; Yun, Y.; Xie, X. Recent progress in assays for GPCR drug discovery. *American journal of physiology. Cell physiology* **2022**, *323* (2), C583-C594. DOI: 10.1152/ajpcell.00464.2021. Published Online: Jul. 11, 2022.(4) Kolakowski, L. F. GCRDb: a G-protein-coupled receptor database. *Receptors & channels* **1994**, *2* (1), 1–7.

(5) Attwood, T. K.; Findlay, J. B. Fingerprinting G-protein-coupled receptors. *Protein engineering* **1994**, *7* (2), 195–203. DOI: 10.1093/protein/7.2.195.

(6) Bondar, A.; Lazar, J. Optical sensors of heterotrimeric G protein signaling. *The FEBS journal* **2021**, *288* (8), 2570–2584. DOI: 10.1111/febs.15655.

(7) Hauser, A. S.; Attwood, M. M.; Rask-Andersen, M.; Schiöth, H. B.; Gloriam, D. E. Trends in GPCR drug discovery: new agents, targets and indications. *Nature reviews. Drug discovery* **2017**, *16* (12), 829–842. DOI: 10.1038/nrd.2017.178.

(8) Sriram, K.; Insel, P. A. G Protein-Coupled Receptors as Targets for Approved Drugs: How Many Targets and How Many Drugs? *Molecular pharmacology* **2018**, *93* (4), 251–258. DOI: 10.1124/mol.117.111062.

(9) Creese, I.; Burt, D. R.; Snyder, S. H. Dopamine receptor binding: differentiation of agonist and antagonist states with 3H-dopamine and 3H-haloperidol. *Life sciences* **1975**, *17* (6), 933–1001. DOI: 10.1016/0024-3205(75)90454-3.

(10) Laeremans, T.; Sands, Z. A.; Claes, P.; Blieck, A. de; Cesco, S. de; Triest, S.; Busch, A.; Felix, D.; Kumar, A.; Jaakola, V.-P.; Menet, C. Accelerating GPCR Drug Discovery With Conformation-Stabilizing VHHs. *Frontiers in molecular biosciences* **2022**, *9*, 863099. DOI: 10.3389/fmolb.2022.863099.

(11) Seifert, R.; Wenzel-Seifert, K.; Gether, U.; Kobilka, B. K. Functional differences between full and partial agonists: evidence for ligand-specific receptor conformations. *The Journal of pharmacology and experimental therapeutics* **2001**, *297* (3), 1218–1226.

(12) Hilger, D.; Masureel, M.; Kobilka, B. K. Structure and dynamics of GPCR signaling complexes. *Nature structural & molecular biology* **2018**, *25* (1), 4–12. DOI: 10.1038/s41594-017-0011-7.

(13) Simon, M. I.; Strathmann, M. P.; Gautam, N. Diversity of G proteins in signal transduction. *Science (New York, N.Y.)* **1991**, *252* (5007), 802–808. DOI: 10.1126/science.1902986.

(14) Oldham, W. M.; Hamm, H. E. Structural basis of function in heterotrimeric G proteins. *Quarterly reviews of biophysics* **2006**, *39* (2), 117–166. DOI: 10.1017/S0033583506004306.

(15) Tuteja, N. Signaling through G protein coupled receptors. *Plant signaling & behavior* **2009**, *4* (10), 942–947. DOI: 10.4161/psb.4.10.9530.

(16) Trewavas, A. J.; Malho, R. Signal Perception and Transduction: The Origin of the Phenotype. *The Plant cell* **1997**, *9* (7), 1181–1195. DOI: 10.1105/tpc.9.7.1181.

(17) Gether, U. Uncovering molecular mechanisms involved in activation of G protein-coupled receptors. *Endocrine reviews* **2000**, *21* (1), 90–113. DOI: 10.1210/edrv.21.1.0390.

(18) Kristiansen, K. Molecular mechanisms of ligand binding, signaling, and regulation within the superfamily of G-protein-coupled receptors: molecular modeling and mutagenesis approaches to receptor structure and function. *Pharmacology & therapeutics* **2004**, *103* (1), 21–80. DOI: 10.1016/j.pharmthera.2004.05.002.

(19) Alspaugh, J. A.; Pukkila-Worley, R.; Harashima, T.; Cavallo, L. M.; Funnell, D.; Cox, G. M.; Perfect, J. R.; Kronstad, J. W.; Heitman, J. Adenylyl cyclase functions downstream of the Galpha protein Gpa1 and controls mating and pathogenicity of Cryptococcus neoformans. *Eukaryotic cell* **2002**, *1* (1), 75–84. DOI: 10.1128/EC.1.1.75-84.2002.

(20) Panula, P.; Chazot, P. L.; Cowart, M.; Gutzmer, R.; Leurs, R.; Liu, W. L. S.; Stark, H.; Thurmond, R. L.; Haas, H. L. International Union of Basic and Clinical Pharmacology. XCVIII. Histamine Receptors. *Pharmacological reviews* **2015**, *67* (3), 601–655. DOI: 10.1124/pr.114.010249.

(21) Rondard, P.; Iiri, T.; Srinivasan, S.; Meng, E.; Fujita, T.; Bourne, H. R. Mutant G protein alpha subunit activated by Gbeta gamma: a model for receptor activation? *Proceedings of the National Academy of Sciences of the United States of America* **2001**, *98* (11), 6150–6155. DOI: 10.1073/pnas.101136198.

(22) Smrcka, A. V. G protein βγ subunits: central mediators of G protein-coupled receptor signaling. *Cellular and molecular life sciences: CMLS* **2008**, *65* (14), 2191–2214. DOI: 10.1007/s00018-008-8006-5.

(23) Syrovatkina, V.; Alegre, K. O.; Dey, R.; Huang, X.-Y. Regulation, Signaling, and Physiological Functions of G-Proteins. *Journal of molecular biology* **2016**, *428* (19), 3850–3868. DOI: 10.1016/j.jmb.2016.08.002.

(24) Mafi, A.; Kim, S.-K.; Goddard, W. A. The mechanism for ligand activation of the GPCR-G protein complex. *Proceedings of the National Academy of Sciences of the United States of America* **2022**, *119* (18), e2110085119. DOI: 10.1073/pnas.2110085119.

(25) Ross, E. M.; Wilkie, T. M. GTPase-activating proteins for heterotrimeric G proteins: regulators of G protein signaling (RGS) and RGS-like proteins. *Annual review of biochemistry* **2000**, *69*, 795–827. DOI: 10.1146/annurev.biochem.69.1.795.

(26) Gurevich, V. V.; Gurevich, E. V. Biased GPCR signaling: Possible mechanisms and inherent limitations. *Pharmacology & therapeutics* **2020**, *211*, 107540. DOI: 10.1016/j.pharmthera.2020.107540.

(27) Wisler, J. W.; Rockman, H. A.; Lefkowitz, R. J. Biased G Protein-Coupled Receptor Signaling: Changing the Paradigm of Drug Discovery. *Circulation* **2018**, *137* (22), 2315–2317. DOI: 10.1161/CIRCULATIONAHA.117.028194.

(28) Inoue, A.; Raimondi, F.; Kadji, F. M. N.; Singh, G.; Kishi, T.; Uwamizu, A.; Ono, Y.; Shinjo, Y.; Ishida, S.; Arang, N.; Kawakami, K.; Gutkind, J. S.; Aoki, J.; Russell, R. B. Illuminating G-Protein-Coupling Selectivity of GPCRs. *Cell* **2019**, *177* (7), 1933-1947.e25. DOI: 10.1016/j.cell.2019.04.044.

(29) Hao, J.; Beck, J. P.; Schaus, J. M.; Krushinski, J. H.; Chen, Q.; Beadle, C. D.; Vidal, P.; Reinhard, M. R.; Dressman, B. A.; Massey, S. M.; Boulet, S. L.; Cohen, M. P.; Watson, B. M.; Tupper, D.; Gardinier, K. M.; Myers, J.; Johansson, A. M.; Richardson, J.; Richards, D. S.; Hembre, E. J.; Remick, D. M.; Coates, D. A.; Bhardwaj, R. M.; Diseroad, B. A.; Bender, D.; Stephenson, G.; Wolfangel, C. D.; Diaz, N.; Getman, B. G.; Wang, X.-S.; Heinz, B. A.; Cramer, J. W.; Zhou, X.; Maren, D. L.; Falcone, J. F.; Wright, R. A.; Mitchell, S. N.; Carter, G.; Yang, C. R.; Bruns, R. F.; Svensson, K. A. Synthesis and Pharmacological Characterization of 2-(2,6-Dichlorophenyl)-1-((1S,3R)-5-(3-hydroxy-3-methylbutyl)-3-(hydroxymethyl)-1-methyl-3,4-dihydroisoquinolin-2(1H)-yl)ethan-1-one (LY3154207), a Potent, Subtype Selective, and Orally Available Positive Allosteric Modulator of the Human Dopamine D1 Receptor. *Journal of medicinal chemistry* **2019**, *62* (19), 8711–8732. DOI: 10.1021/acs.jmedchem.9b01234.

(30) Valant, C.; Sexton, P. M.; Christopoulos, A. Orthosteric/allosteric bitopic ligands: going hybrid at GPCRs. *Molecular interventions* **2009**, *9* (3), 125–135. DOI: 10.1124/mi.9.3.6.

(31) Arnatt, C. K.; Zhang, Y. Bivalent ligands targeting chemokine receptor dimerization: molecular design and functional studies. *Current topics in medicinal chemistry* **2014**, *14* (13), 1606–1618. DOI: 10.2174/1568026614666140827144752.

(32) Xu, W.; Wang, X.; Tocker, A. M.; Huang, P.; Reith, M. E. A.; Liu-Chen, L.-Y.; Smith, A. B.; Kortagere, S. Functional Characterization of a Novel Series of Biased Signaling Dopamine D3 Receptor Agonists. *ACS chemical neuroscience* **2017**, *8* (3), 486–500. DOI: 10.1021/acschemneuro.6b00221.

(33) Littlepage-Saunders, M.; Hochstein, M. J.; Chang, D. S.; Johnson, K. A. G protein-coupled receptor modulation of striatal dopamine transmission: Implications for psychoactive drug effects. *British journal of pharmacology* **2023.** DOI: 10.1111/bph.16151.

(34) Kebabian, J. W. Multiple classes of dopamine receptors in mammalian central nervous system: the involvement of dopamine-sensitive adenylyl cyclase. *Life sciences* **1978**, *23* (5), 479–483. DOI: 10.1016/0024-3205(78)90157-1.

(35) Chakraborty, R.; Ganguli, S.; Chakraborty, H. J.; Datta, A. STRUCTURAL ANALYSIS AND MOLECULAR MODELING OF HUMAN DOPAMINE RECEPTOR 5 (DRD5). *Int J of Bioi Res* **2010**, *2* (2), 96–102. DOI: 10.9735/0975-3087.2.2.96-102.

(36) McDonald, W. M.; Sibley, D. R.; Kilpatrick, B. F.; Caron, M. G. Dopaminergic inhibition of adenylate cyclase correlates with high affinity agonist binding to anterior pituitary D2 dopamine receptors. *Molecular and cellular endocrinology* **1984**, *36* (3), 201–209. DOI: 10.1016/0303-7207(84)90037-6.

(37) Simunovic, F.; Yi, M.; Wang, Y.; Macey, L.; Brown, L. T.; Krichevsky, A. M.; Andersen, S. L.; Stephens, R. M.; Benes, F. M.; Sonntag, K. C. Gene expression profiling of substantia nigra dopamine neurons: further insights into Parkinson's disease pathology. *Brain: a journal of neurology* **2009**, *132* (Pt 7), 1795–1809. DOI: 10.1093/brain/awn323.

(38) Chinta, S. J.; Andersen, J. K. Dopaminergic neurons. *The international journal of biochemistry & cell biology* **2005**, *37* (5), 942–946. DOI: 10.1016/j.biocel.2004.09.009.

(39) Wise, R. A. Dopamine, learning and motivation. *Nature reviews. Neuroscience* **2004**, *5* (6), 483–494. DOI: 10.1038/nrn1406.

(40) Schultz, W. Dopamine neurons and their role in reward mechanisms. *Current opinion in neurobiology* **1997**, *7* (2), 191–197. DOI: 10.1016/S0959-4388(97)80007-4.

(41) Dreyer, J. K.; Herrik, K. F.; Berg, R. W.; Hounsgaard, J. D. Influence of phasic and tonic dopamine release on receptor activation. *The Journal of neuroscience: the official journal of the Society for Neuroscience* **2010**, *30* (42), 14273–14283. DOI: 10.1523/JNEUROSCI.1894-10.2010.

(42) Brisch, R.; Saniotis, A.; Wolf, R.; Bielau, H.; Bernstein, H.-G.; Steiner, J.; Bogerts, B.; Braun, K.; Jankowski, Z.; Kumaratilake, J.; Henneberg, M.; Gos, T. The role of dopamine in schizophrenia from a neurobiological and evolutionary perspective: old fashioned, but still in vogue. *Frontiers in psychiatry* **2014**, *5*, 47. DOI: 10.3389/fpsyt.2014.00047.

(43) Zhou, Z. D.; Yi, L. X.; Wang, D. Q.; Lim, T. M.; Tan, E. K. Role of dopamine in the pathophysiology of Parkinson's disease. *Translational neurodegeneration* **2023**, *12* (1), 44. DOI: 10.1186/s40035-023-00378-6.

(44) Di Chiara, G.; Bassareo, V.; Fenu, S.; Luca, M. A. de; Spina, L.; Cadoni, C.; Acquas, E.; Carboni, E.; Valentini, V.; Lecca, D. Dopamine and drug addiction: the nucleus accumbens shell connection. *Neuropharmacology* **2004**, *47 Suppl 1*, 227–241. DOI: 10.1016/j.neuropharm.2004.06.032.

(45) Ashok, A. H.; Marques, T. R.; Jauhar, S.; Nour, M. M.; Goodwin, G. M.; Young, A. H.; Howes, O. D. The dopamine hypothesis of bipolar affective disorder: the state of the art and implications for treatment. *Molecular psychiatry* **2017**, *22* (5), 666–679. DOI: 10.1038/mp.2017.16.

(46) Bennett, J. P.; Piercey, M. F. Pramipexole--a new dopamine agonist for the treatment of Parkinson's disease. *Journal of the neurological sciences* **1999**, *163* (1), 25–31. DOI: 10.1016/S0022-510X(98)00307-4.

(47) Heinonen, E. H.; Rinne, U. K. Selegiline in the treatment of Parkinson's disease. *Acta neurologica Scandinavica. Supplementum* **1989**, *126*, 103–111. DOI: 10.1111/j.1600-0404.1989.tb01789.x.

(48) The Impact of Treatment with Levodopa on Parkinson's Disease. *QJM: An International Journal of Medicine* **1980.** DOI: 10.1093/oxfordjournals.qjmed.a067623.

(49) Tohen, M.; Zhang, F.; Keck, P. E.; Feldman, P. D.; Risser, R. C.; Tran, P. V.; Breier, A. Olanzapine versus haloperidol in schizoaffective disorder, bipolar type. *Journal of affective disorders* **2001**, *67* (1-3), 133–140. DOI: 10.1016/S0165-0327(00)00303-7.

(50) Marder, S. R.; Meibach, R. C. Risperidone in the treatment of schizophrenia. *The American journal of psychiatry* **1994**, *151* (6), 825–835. DOI: 10.1176/ajp.151.6.825.

(51) Falkai, P.; Vogeley, K. Die Chancen neuer atypischer Substanzen. *Fortschritte der Neurologie-Psychiatrie* **2000**, *68 Suppl 1*, S32-7.

(52) Bhat, L.; Bhat, S. R.; Ramakrishnan, A.; Amirthalingam, M. Brilaroxazine lipogel displays antipsoriatic activity in imiquimod-induced mouse model. *Skin research and technology: official journal of International Society for Bioengineering and the Skin (ISBS) [and] International Society for Digital Imaging of Skin (ISDIS) [and] International Society for Skin Imaging (ISSI)* **2024**, *30* (2), e13606. DOI: 10.1111/srt.13606.

(53) Tsapakis, E. M.; Diakaki, K.; Miliaras, A.; Fountoulakis, K. N. Novel Compounds in the Treatment of Schizophrenia-A Selective Review. *Brain sciences* **2023**, *13* (8). DOI: 10.3390/brainsci13081193.

(54) Oparil, S.; Aronson, S.; Deeb, G. M.; Epstein, M.; Levy, J. H.; Luther, R. R.; Prielipp, R.; Taylor, A. Fenoldopam: a new parenteral antihypertensive: consensus roundtable on the management of perioperative hypertension and hypertensive crises. *American journal of hypertension* **1999**, *12* (7), 653–664. DOI: 10.1016/S0895-7061(99)00059-X.

(55) Haas, H.; Panula, P. The role of histamine and the tuberomamillary nucleus in the nervous system. *Nature reviews. Neuroscience* **2003**, *4* (2), 121–130. DOI: 10.1038/nrn1034.

(56) Haas, H. L.; Sergeeva, O. A.; Selbach, O. Histamine in the nervous system. *Physiological reviews* **2008**, *88* (3), 1183–1241. DOI: 10.1152/physrev.00043.2007.

(57) Zampeli, E.; Tiligada, E. The role of histamine H4 receptor in immune and inflammatory disorders. *British journal of pharmacology* **2009**, *157* (1), 24–33. DOI: 10.1111/j.1476-5381.2009.00151.x.

(58) Zhang, Z.; Kurashima, Y. Two Sides of the Coin: Mast Cells as a Key Regulator of Allergy and Acute/Chronic Inflammation. *Cells* **2021**, *10* (7). DOI: 10.3390/cells10071615.

(59) Tashiro, M.; Mochizuki, H.; Iwabuchi, K.; Sakurada, Y.; Itoh, M.; Watanabe, T.; Yanai, K. Roles of histamine in regulation of arousal and cognition: functional neuroimaging of histamine H1 receptors in human brain. *Life sciences* **2002**, *72* (4-5), 409–414. DOI: 10.1016/S0024-3205(02)02276-2.

(60) Tashiro, M.; Sakurada, Y.; Iwabuchi, K.; Mochizuki, H.; Kato, M.; Aoki, M.; Funaki, Y.; Itoh, M.; Iwata, R.; Wong, D. F.; Yanai, K. Central effects of fexofenadine and cetirizine: measurement of psychomotor performance, subjective sleepiness, and brain histamine H1-receptor occupancy using 11C-doxepin positron emission tomography. *Journal of clinical pharmacology* **2004**, *44* (8), 890–900. DOI: 10.1177/0091270004267590.

(61) Li, J.; Wang, F.; Lv, L.; Xu, L.; Zeng, E.; Tang, X. Histamine H2 antagonists for functional dyspepsia: A protocol for a systematic review and meta-analysis. *Medicine* **2019**, *98* (47), e18128. DOI: 10.1097/MD.0000000000018128.

(62) Howard, J. M.; Chremos, A. N.; Collen, M. J.; McArthur, K. E.; Cherner, J. A.; Maton, P. N.; Ciarleglio, C. A.; Cornelius, M. J.; Gardner, J. D.; Jensen, R. T. Famotidine, a new, potent, long-acting histamine H2-receptor antagonist: comparison with cimetidine and ranitidine in the treatment of Zollinger-Ellison syndrome. *Gastroenterology* **1985**, *88* (4), 1026–1033. DOI: 10.1016/S0016-5085(85)80024-X.

(63) Lamb, Y. N. Pitolisant: A Review in Narcolepsy with or without Cataplexy. *CNS drugs* **2020**, *34* (2), 207–218. DOI: 10.1007/s40263-020-00703-x.

(64) Harwell, V.; Fasinu, P. S. Pitolisant and Other Histamine-3 Receptor Antagonists-An Update on Therapeutic Potentials and Clinical Prospects. *Medicines (Basel, Switzerland)* **2020**, *7* (9). DOI: 10.3390/medicines7090055.

(65) Ohsawa, Y.; Hirasawa, N. The role of histamine H1 and H4 receptors in atopic dermatitis: from basic research to clinical study. *Allergology international: official journal of the Japanese Society of Allergology* **2014**, *63* (4), 533–542. DOI: 10.2332/allergolint.13-RA-0675.

(66) Kollmeier, A.; Francke, K.; Chen, B.; Dunford, P. J.; Greenspan, A. J.; Xia, Y.; Xu, X. L.; Zhou, B.; Thurmond, R. L. The histamine H_4 receptor antagonist, JNJ 39758979, is effective in reducing histamine-induced pruritus in a randomized clinical study in healthy subjects. *The Journal of pharmacology and experimental therapeutics* **2014**, *350* (1), 181–187. DOI: 10.1124/jpet.114.215749.

(67) Murata, Y.; Song, M.; Kikuchi, H.; Hisamichi, K.; Xu, X. L.; Greenspan, A.; Kato, M.; Chiou, C.-F.; Kato, T.; Guzzo, C.; Thurmond, R. L.; Ohtsuki, M.; Furue, M. Phase 2a, randomized, double-blind, placebo-controlled, multicenter, parallel-group study of a H4 R-antagonist (JNJ-39758979) in Japanese adults with moderate atopic dermatitis. *The Journal of dermatology* **2015**, *42* (2), 129–139. DOI: 10.1111/1346-8138.12726.

(68) Mehta, P.; Miszta, P.; Rzodkiewicz, P.; Michalak, O.; Krzeczyński, P.; Filipek, S. Enigmatic Histamine Receptor H4 for Potential Treatment of Multiple Inflammatory, Autoimmune, and Related Diseases. *Life (Basel, Switzerland)* **2020**, *10* (4). DOI: 10.3390/life10040050.

(69) Xia, R.; Shi, S.; Xu, Z.; Vischer, H. F.; Windhorst, A. D.; Qian, Y.; Duan, Y.; Liang, J.; Chen, K.; Zhang, A.; Guo, C.; Leurs, R.; He, Y. Structural basis of ligand recognition and design of antihistamines targeting histamine H4 receptor. *Nature communications* **2024**, *15* (1), 2493. DOI: 10.1038/s41467-024-46840-5.

(70) Grekowitz, E.; Metz, M.; Altrichter, S.; Bauer, A.; Brockow, K.; Heine, G.; Lionnet, L.; Saday, K. K.; Hultsch, T.; Søerensen, O. E.; Maurer, M. Targeting Histamine Receptor 4 in Cholinergic Urticaria with Izuforant (LEO 152020): Results from a Phase 2a, Randomised, Double-Blind, Placebo-Controlled, Multicentre, Crossover trial. *The British journal of dermatology* **2024.** DOI: 10.1093/bjd/ljae038.

(71) Seibel-Ehlert, U.; Plank, N.; Inoue, A.; Bernhardt, G.; Strasser, A. Label-Free Investigations on the G Protein Dependent Signaling Pathways of Histamine Receptors. *International journal of molecular sciences* **2021**, *22* (18). DOI: 10.3390/ijms22189739.

(72) Höring, C.; Seibel, U.; Tropmann, K.; Grätz, L.; Mönnich, D.; Pitzl, S.; Bernhardt, G.; Pockes, S.; Strasser, A. A Dynamic, Split-Luciferase-Based Mini-G Protein Sensor to Functionally Characterize Ligands at All Four Histamine Receptor Subtypes. *International journal of molecular sciences* **2020**, *21* (22). DOI: 10.3390/ijms21228440.

(73) Glukhova, A.; Draper-Joyce, C. J.; Sunahara, R. K.; Christopoulos, A.; Wootten, D.; Sexton, P. M. Rules of Engagement: GPCRs and G Proteins. *ACS pharmacology & translational science* **2018**, *1* (2), 73–83. DOI: 10.1021/acsptsci.8b00026.

(74) Nehmé, R.; Carpenter, B.; Singhal, A.; Strege, A.; Edwards, P. C.; White, C. F.; Du, H.; Grisshammer, R.; Tate, C. G. Mini-G proteins: Novel tools for studying GPCRs in their active conformation. *PloS one* **2017**, *12* (4), e0175642. DOI: 10.1371/journal.pone.0175642.

(75) Carpenter, B.; Tate, C. G. Engineering a minimal G protein to facilitate crystallisation of G protein-coupled receptors in their active conformation. *Protein engineering, design & selection: PEDS* **2016**, *29* (12), 583–594. DOI: 10.1093/protein/gzw049.

(76) Wan, Q.; Okashah, N.; Inoue, A.; Nehmé, R.; Carpenter, B.; Tate, C. G.; Lambert, N. A. Mini G protein probes for active G protein-coupled receptors (GPCRs) in live cells. *The Journal of biological chemistry* **2018**, *293* (19), 7466–7473. DOI: 10.1074/jbc.RA118.001975.

(77) García-Nafría, J.; Lee, Y.; Bai, X.; Carpenter, B.; Tate, C. G. Cryo-EM structure of the adenosine A2A receptor coupled to an engineered heterotrimeric G protein. *eLife* **2018**, *7.* DOI: 10.7554/eLife.35946.

(78) García-Nafría, J.; Nehmé, R.; Edwards, P. C.; Tate, C. G. Cryo-EM structure of the serotonin 5-HT1B receptor coupled to heterotrimeric Go. *Nature* **2018**, *558* (7711), 620–623. DOI: 10.1038/s41586-018-0241-9.

(79) Carpenter, B.; Nehmé, R.; Warne, T.; Leslie, A. G. W.; Tate, C. G. Structure of the adenosine A(2A) receptor bound to an engineered G protein. *Nature* **2016**, *536* (7614), 104–107. DOI: 10.1038/nature18966.

(80) Mönnich, D.; Humphrys, L. J.; Höring, C.; Hoare, B. L.; Forster, L.; Pockes, S. Activation of Multiple G Protein Pathways to Characterize the Five Dopamine Receptor Subtypes Using Bioluminescence Technology. *ACS Pharmacol. Transl. Sci.* **2024.** DOI: 10.1021/acsptsci.3c00339.

(81) van Daele, M.; Kilpatrick, L. E.; Woolard, J.; Hill, S. J. Characterisation of tyrosine kinase inhibitor-receptor interactions at VEGFR2 using sunitinib-red and nanoBRET. *Biochemical pharmacology* **2023**, *214*, 115672. DOI: 10.1016/j.bcp.2023.115672.

(82) Yano, H.; Provasi, D.; Cai, N. S.; Filizola, M.; Ferré, S.; Javitch, J. A. Development of novel biosensors to study receptor-mediated activation of the G-protein α subunits Gs and Golf. *The Journal of biological chemistry* **2017**, *292* (49), 19989–19998. DOI: 10.1074/jbc.M117.800698.

(83) Schihada, H.; Shekhani, R.; Schulte, G. Quantitative assessment of constitutive G protein-coupled receptor activity with BRET-based G protein biosensors. *Science signaling* **2021**, *14* (699), eabf1653. DOI: 10.1126/scisignal.abf1653.

(84) Hohlbein, J.; Craggs, T. D.; Cordes, T. Alternating-laser excitation: single-molecule FRET and beyond. *Chemical Society reviews* **2014**, *43* (4), 1156–1171. DOI: 10.1039/C3CS60233H.

(85) Stoddart, L. A.; White, C. W.; Nguyen, K.; Hill, S. J.; Pfleger, K. D. G. Fluorescence- and bioluminescence-based approaches to study GPCR ligand binding. *British journal of pharmacology* **2016**, *173* (20), 3028–3037. DOI: 10.1111/bph.13316.

(86) Stoddart, L. A.; Kilpatrick, L. E.; Briddon, S. J.; Hill, S. J. Probing the pharmacology of G protein-coupled receptors with fluorescent ligands. *Neuropharmacology* **2015**, *98*, 48–57. DOI: 10.1016/j.neuropharm.2015.04.033.

(87) Piehler, J. New methodologies for measuring protein interactions in vivo and in vitro. *Current opinion in structural biology* **2005**, *15* (1), 4–14. DOI: 10.1016/j.sbi.2005.01.008.

(88) Paulmurugan, R.; Umezawa, Y.; Gambhir, S. S. Noninvasive imaging of protein-protein interactions in living subjects by using reporter protein complementation and reconstitution strategies. *Proceedings of the National Academy of Sciences of the United States of America* **2002**, *99* (24), 15608–15613. DOI: 10.1073/pnas.242594299.

(89) Ozawa, T.; Kaihara, A.; Sato, M.; Tachihara, K.; Umezawa, Y. Split luciferase as an optical probe for detecting protein-protein interactions in mammalian cells based on protein splicing. *Analytical chemistry* **2001**, *73* (11), 2516–2521. DOI: 10.1021/ac0013296.

(90) Villalobos, V.; Naik, S.; Bruinsma, M.; Dothager, R. S.; Pan, M.-H.; Samrakandi, M.; Moss, B.; Elhammali, A.; Piwnica-Worms, D. Dual-color click beetle luciferase heteroprotein fragment complementation assays. *Chemistry & biology* **2010**, *17* (9), 1018–1029. DOI: 10.1016/j.chembiol.2010.06.018.

(91) Littmann, T.; Ozawa, T.; Hoffmann, C.; Buschauer, A.; Bernhardt, G. A split luciferase-based probe for quantitative proximal determination of Gαq signalling in live cells. *Scientific reports* **2018**, *8* (1), 17179. DOI: 10.1038/s41598-018-35615-w.

(92) Rozbeh, R.; Forchhammer, K. Split NanoLuc technology allows quantitation of interactions between PII protein and its receptors with unprecedented sensitivity and reveals transient interactions. *Scientific reports* **2021**, *11* (1), 12535. DOI: 10.1038/s41598-021-91856-2.

(93) Hall, M. P.; Unch, J.; Binkowski, B. F.; Valley, M. P.; Butler, B. L.; Wood, M. G.; Otto, P.; Zimmerman, K.; Vidugiris, G.; Machleidt, T.; Robers, M. B.; Benink, H. A.; Eggers, C. T.; Slater, M. R.; Meisenheimer, P. L.; Klaubert, D. H.; Fan, F.; Encell, L. P.; Wood, K. V. Engineered luciferase reporter from a deep sea shrimp utilizing a novel imidazopyrazinone substrate. *ACS chemical biology* **2012**, *7* (11), 1848–1857. DOI: 10.1021/cb3002478.

(94) Dixon, A. S.; Schwinn, M. K.; Hall, M. P.; Zimmerman, K.; Otto, P.; Lubben, T. H.; Butler, B. L.; Binkowski, B. F.; Machleidt, T.; Kirkland, T. A.; Wood, M. G.; Eggers, C. T.; Encell, L. P.; Wood, K. V. NanoLuc Complementation Reporter Optimized for Accurate Measurement of Protein Interactions in Cells. *ACS chemical biology* **2016**, *11* (2), 400–408. DOI: 10.1021/acschembio.5b00753.

(95) Gaspar, N.; Walker, J. R.; Zambito, G.; Marella-Panth, K.; Lowik, C.; Kirkland, T. A.; Mezzanotte, L. Evaluation of NanoLuc substrates for bioluminescence imaging of transferred cells in mice. *Journal of photochemistry and photobiology. B, Biology* **2021**, *216*, 112128. DOI: 10.1016/j.jphotobiol.2021.112128.

(96) Shimomura, O. Bioluminescence in the sea: photoprotein systems. *Symposia of the Society for Experimental Biology* **1985**, *39*, 351–372.

(97) Xu, X.; Soutto, M.; Xie, Q.; Servick, S.; Subramanian, C.; Arnim, A. G. von; Johnson, C. H. Imaging protein interactions with bioluminescence resonance energy transfer (BRET) in plant and mammalian cells and tissues. *Proceedings of the National Academy of Sciences of the United States of America* **2007**, *104* (24), 10264–10269. DOI: 10.1073/pnas.0701987104.

(98) Borroto-Escuela, D. O.; Ravani, A.; Tarakanov, A. O.; Brito, I.; Narvaez, M.; Romero-Fernandez, W.; Corrales, F.; Agnati, L. F.; Tanganelli, S.; Ferraro, L.; Fuxe, K. Dopamine D2 receptor signaling dynamics of dopamine D2-neurotensin 1 receptor heteromers. *Biochemical and biophysical research communications* **2013**, *435* (1), 140–146. DOI: 10.1016/j.bbrc.2013.04.058.

(99) Plach, M.; Schäfer, T.; Borroto-Escuela, D. O.; Weikert, D.; Gmeiner, P.; Fuxe, K.; Friedland, K. Differential allosteric modulation within dopamine D2R - neurotensin NTS1R and D2R - serotonin 5-HT2AR receptor complexes gives bias to intracellular calcium signalling. *Scientific reports* **2019**, *9* (1), 16312. DOI: 10.1038/s41598-019-52540-8.

(100) El Khamlichi, C.; Cobret, L.; Arrang, J.-M.; Morisset-Lopez, S. BRET Analysis of GPCR Dimers in Neurons and Non-Neuronal Cells: Evidence for Inactive, Agonist, and Constitutive Conformations. *International journal of molecular sciences* **2021**, *22* (19). DOI: 10.3390/ijms221910638.

(101) Charest, P. G.; Terrillon, S.; Bouvier, M. Monitoring agonist-promoted conformational changes of beta-arrestin in living cells by intramolecular BRET. *EMBO reports* **2005**, *6* (4), 334–340. DOI: 10.1038/sj.embor.7400373.

(102) Machleidt, T.; Woodroofe, C. C.; Schwinn, M. K.; Méndez, J.; Robers, M. B.; Zimmerman, K.; Otto, P.; Daniels, D. L.; Kirkland, T. A.; Wood, K. V. NanoBRET--A Novel BRET Platform for the Analysis of Protein-Protein Interactions. *ACS chemical biology* **2015**, *10* (8), 1797–1804. DOI: 10.1021/acschembio.5b00143.

(103) Dale, N. C.; Johnstone, E. K. M.; White, C. W.; Pfleger, K. D. G. NanoBRET: The Bright Future of Proximity-Based Assays. *Frontiers in bioengineering and biotechnology* **2019**, *7*, 56. DOI: 10.3389/fbioe.2019.00056.

(104) De, A.; Ray, P.; Loening, A. M.; Gambhir, S. S. BRET3: a red-shifted bioluminescence resonance energy transfer (BRET)-based integrated platform for imaging protein-protein interactions from single live cells and living animals. *FASEB journal: official publication of the Federation of American Societies for Experimental Biology* **2009**, *23* (8), 2702–2709. DOI: 10.1096/fj.08-118919.

(105) Mezzanotte, L.; van 't Root, M.; Karatas, H.; Goun, E. A.; Löwik, C. W. G. M. In Vivo Molecular Bioluminescence Imaging: New Tools and Applications. *Trends in biotechnology* **2017**, *35* (7), 640–652. DOI: 10.1016/j.tibtech.2017.03.012.

(106) Angers, S.; Salahpour, A.; Joly, E.; Hilairet, S.; Chelsky, D.; Dennis, M.; Bouvier, M. Detection of beta 2-adrenergic receptor dimerization in living cells using bioluminescence resonance energy transfer (BRET). *Proceedings of the National Academy of Sciences of the United States of America* **2000**, *97* (7), 3684–3689. DOI: 10.1073/pnas.97.7.3684.

(107) Stoddart, L. A.; Johnstone, E. K. M.; Wheal, A. J.; Goulding, J.; Robers, M. B.; Machleidt, T.; Wood, K. V.; Hill, S. J.; Pfleger, K. D. G. Application of BRET to monitor ligand binding to GPCRs. *Nature methods* **2015**, *12* (7), 661–663. DOI: 10.1038/nmeth.3398.

(108) Kocan, M.; See, H. B.; Seeber, R. M.; Eidne, K. A.; Pfleger, K. D. G. Demonstration of improvements to the bioluminescence resonance energy transfer (BRET) technology for the monitoring of G protein-coupled receptors in live cells. *Journal of biomolecular screening* **2008**, *13* (9), 888–898. DOI: 10.1177/1087057108324032.

(109) Borroto-Escuela, D. O.; Flajolet, M.; Agnati, L. F.; Greengard, P.; Fuxe, K. Bioluminescence resonance energy transfer methods to study G protein-coupled receptor-receptor tyrosine kinase heteroreceptor complexes. *Methods in cell biology* **2013**, *117*, 141–164. DOI: 10.1016/B978-0-12-408143-7.00008-6.

(110) Kobayashi, H.; Picard, L.-P.; Schönegge, A.-M.; Bouvier, M. Bioluminescence resonance energy transfer-based imaging of protein-protein interactions in living cells. *Nature protocols* **2019**, *14* (4), 1084–1107. DOI: 10.1038/s41596-019-0129-7.

(111) Stoddart, L. A.; Kilpatrick, L. E.; Briddon, S. J.; Hill, S. J. Probing the pharmacology of G protein-coupled receptors with fluorescent ligands. *Neuropharmacology* **2015**, *98*, 48–57. DOI: 10.1016/j.neuropharm.2015.04.033.

(112) Stoddart, L. A.; White, C. W.; Nguyen, K.; Hill, S. J.; Pfleger, K. D. G. Fluorescence- and bioluminescence-based approaches to study GPCR ligand binding. *British journal of pharmacology* **2016**, *173* (20), 3028–3037. DOI: 10.1111/bph.13316.

(113) Olsen, R. H. J.; DiBerto, J. F.; English, J. G.; Glaudin, A. M.; Krumm, B. E.; Slocum, S. T.; Che, T.; Gavin, A. C.; McCorvy, J. D.; Roth, B. L.; Strachan, R. T. TRUPATH, an open-source biosensor platform for interrogating the GPCR transducerome. *Nature chemical biology* **2020**, *16* (8), 841–849. DOI: 10.1038/s41589-020-0535-8.

(114) Ransone, L. J. Detection of protein-protein interactions by coimmunoprecipitation and dimerization. *Methods in enzymology* **1995**, *254*, 491–497. DOI: 10.1016/0076-6879(95)54034-2.

(115) Hebert, T. E.; Moffett, S.; Morello, J. P.; Loisel, T. P.; Bichet, D. G.; Barret, C.; Bouvier, M. A peptide derived from a beta2-adrenergic receptor transmembrane domain inhibits both receptor dimerization and activation. *The Journal of biological chemistry* **1996**, *271* (27), 16384–16392. DOI: 10.1074/jbc.271.27.16384.

(116) Fukushima, Y.; Asano, T.; Saitoh, T.; Anai, M.; Funaki, M.; Ogihara, T.; Katagiri, H.; Matsuhashi, N.; Yazaki, Y.; Sugano, K. Oligomer formation of histamine H2 receptors expressed in Sf9 and COS7 cells. *FEBS letters* **1997**, *409* (2), 283–286. DOI: 10.1016/s0014-5793(97)00531-0.

(117) Jones, K. A.; Borowsky, B.; Tamm, J. A.; Craig, D. A.; Durkin, M. M.; Dai, M.; Yao, W. J.; Johnson, M.; Gunwaldsen, C.; Huang, L. Y.; Tang, C.; Shen, Q.; Salon, J. A.; Morse, K.; Laz, T.; Smith, K. E.; Nagarathnam, D.; Noble, S. A.; Branchek, T. A.; Gerald, C. GABA(B) receptors function as a heteromeric assembly of the subunits GABA(B)R1 and GABA(B)R2. *Nature* **1998**, *396* (6712), 674–679. DOI: 10.1038/25348.

(118) Kaupmann, K.; Malitschek, B.; Schuler, V.; Heid, J.; Froestl, W.; Beck, P.; Mosbacher, J.; Bischoff, S.; Kulik, A.; Shigemoto, R.; Karschin, A.; Bettler, B. GABA(B)-receptor subtypes assemble into functional heteromeric complexes. *Nature* **1998**, *396* (6712), 683–687. DOI: 10.1038/25360.

(119) Nelson, G.; Chandrashekar, J.; Hoon, M. A.; Feng, L.; Zhao, G.; Ryba, N. J. P.; Zuker, C. S. An amino-acid taste receptor. *Nature* **2002**, *416* (6877), 199–202. DOI: 10.1038/nature726.

(120) Rocheville, M.; Lange, D. C.; Kumar, U.; Patel, S. C.; Patel, R. C.; Patel, Y. C. Receptors for dopamine and somatostatin: formation of hetero-oligomers with enhanced functional activity. *Science (New York, N.Y.)* **2000**, *288* (5463), 154–157. DOI: 10.1126/science.288.5463.154.

(121) Taura, J.; Fernández-Dueñas, V.; Ciruela, F. Visualizing G Protein-Coupled Receptor-Receptor Interactions in Brain Using Proximity Ligation In Situ Assay. *Current protocols in cell biology* **2015**, *67*, 17.17.1-17.17.16. DOI: 10.1002/0471143030.cb1717s67.

(122) Terrillon, S.; Bouvier, M. Roles of G-protein-coupled receptor dimerization. *EMBO reports* **2004**, *5* (1), 30–34. DOI: 10.1038/sj.embor.7400052.

(123) Lee, S. P.; O'Dowd, B. F.; George, S. R. Homo- and hetero-oligomerization of G protein-coupled receptors. *Life sciences* **2003**, *74* (2-3), 173–180. DOI: 10.1016/j.lfs.2003.09.028.

(124) Perreault, M. L.; Hasbi, A.; O'Dowd, B. F.; George, S. R. Heteromeric dopamine receptor signaling complexes: emerging neurobiology and disease relevance. *Neuropsychopharmacology: official publication of the American College of Neuropsychopharmacology* **2014**, *39* (1), 156–168. DOI: 10.1038/npp.2013.148.

(125) Albizu, L.; Moreno, J. L.; González-Maeso, J.; Sealfon, S. C. Heteromerization of G protein-coupled receptors: relevance to neurological disorders and neurotherapeutics. *CNS & neurological disorders drug targets* **2010**, *9* (5), 636–650. DOI: 10.2174/187152710793361586.

(126) Wouters, E.; Vasudevan, L.; Ciruela, F.; Saini, D. K.; Stove, C.; van Craenenbroeck, K. Assessing GPCR Dimerization in Living Cells: Comparison of the NanoBiT Assay with Related Bioluminescence- and Fluorescence-Based Approaches. In *Receptor-Receptor Interactions in the Central Nervous System*; Fuxe, K., Borroto-Escuela, D. O., Eds.; Neuromethods; Springer New York, 2018; pp 239–250. DOI: 10.1007/978-1-4939-8576-0_15.

(127) Koschatzky, S.; Tschammer, N.; Gmeiner, P. Cross-receptor interactions between dopamine D2L and neurotensin NTS1 receptors modulate binding affinities of dopaminergics. *ACS chemical neuroscience* **2011**, *2* (6), 308–316. DOI: 10.1021/cn200020y.

(128) Budzinski, J.; Maschauer, S.; Kobayashi, H.; Couvineau, P.; Vogt, H.; Gmeiner, P.; Roggenhofer, A.; Prante, O.; Bouvier, M.; Weikert, D. Bivalent ligands promote endosomal trafficking of the dopamine D3 receptor-neurotensin receptor 1 heterodimer. *Communications biology* **2021**, *4* (1), 1062. DOI: 10.1038/s42003-021-02574-4.

(129) White, J. H.; Wise, A.; Main, M. J.; Green, A.; Fraser, N. J.; Disney, G. H.; Barnes, A. A.; Emson, P.; Foord, S. M.; Marshall, F. H. Heterodimerization is required for the formation of a functional GABA(B) receptor. *Nature* **1998**, *396* (6712), 679–682. DOI: 10.1038/25354.

(130) Nelson, G.; Hoon, M. A.; Chandrashekar, J.; Zhang, Y.; Ryba, N. J.; Zuker, C. S. Mammalian sweet taste receptors. *Cell* **2001**, *106* (3), 381–390. DOI: 10.1016/s0092-8674(01)00451-2.

(131) Hiller, C.; Kühhorn, J.; Gmeiner, P. Class A G-protein-coupled receptor (GPCR) dimers and bivalent ligands. *Journal of medicinal chemistry* **2013**, *56* (17), 6542–6559. DOI: 10.1021/jm4004335.

(132) Franco, R.; Casadó, V.; Mallol, J.; Ferré, S.; Fuxe, K.; Cortés, A.; Ciruela, F.; Lluis, C.; Canela, E. I. Dimer-based model for heptaspanning membrane receptors. *Trends in biochemical sciences* **2005**, *30* (7), 360–366. DOI: 10.1016/j.tibs.2005.05.010.

(133) Albizu, L.; Balestre, M.-N.; Breton, C.; Pin, J.-P.; Manning, M.; Mouillac, B.; Barberis, C.; Durroux, T. Probing the existence of G protein-coupled receptor dimers by positive and negative ligand-dependent cooperative binding. *Molecular pharmacology* **2006**, *70* (5), 1783–1791. DOI: 10.1124/mol.106.025684.

(134) Gomes, I.; Gupta, A.; Filipovska, J.; Szeto, H. H.; Pintar, J. E.; Devi, L. A. A role for heterodimerization of mu and delta opiate receptors in enhancing morphine analgesia. *Proceedings of the National Academy of Sciences of the United States of America* **2004**, *101* (14), 5135–5139. DOI: 10.1073/pnas.0307601101.

(135) Novi, F.; Stanasila, L.; Giorgi, F.; Corsini, G. U.; Cotecchia, S.; Maggio, R. Paired activation of two components within muscarinic M3 receptor dimers is required for recruitment of beta-arrestin-1 to the plasma membrane. *The Journal of biological chemistry* **2005**, *280* (20), 19768–19776. DOI: 10.1074/jbc.M411281200.

(136) Vivo, M.; Lin, H.; Strange, P. G. Investigation of cooperativity in the binding of ligands to the D(2) dopamine receptor. *Molecular pharmacology* **2006**, *69* (1), 226–235. DOI: 10.1124/mol.105.012443.

(137) Ferrada, C.; Ferré, S.; Casadó, V.; Cortés, A.; Justinova, Z.; Barnes, C.; Canela, E. I.; Goldberg, S. R.; Leurs, R.; Lluis, C.; Franco, R. Interactions between histamine H3 and dopamine D2 receptors and the implications for striatal function. *Neuropharmacology* **2008**, *55* (2), 190–197. DOI: 10.1016/j.neuropharm.2008.05.008.

(138) Petersen, J.; Wright, S. C.; Rodríguez, D.; Matricon, P.; Lahav, N.; Vromen, A.; Friedler, A.; Strömqvist, J.; Wennmalm, S.; Carlsson, J.; Schulte, G. Agonist-induced dimer dissociation as a macromolecular step in G protein-coupled receptor signaling. *Nature communications* **2017**, *8* (1), 226. DOI: 10.1038/s41467-017-00253-9.

(139) Wouters, E.; Marín, A. R.; Dalton, J. A. R.; Giraldo, J.; Stove, C. Distinct Dopamine D_2 Receptor Antagonists Differentially Impact D_2 Receptor Oligomerization. *International journal of molecular sciences* **2019**, *20* (7). DOI: 10.3390/ijms20071686.

(140) Portoghese, P. S. From models to molecules: opioid receptor dimers, bivalent ligands, and selective opioid receptor probes. *Journal of medicinal chemistry* **2001**, *44* (14), 2259–2269. DOI: 10.1021/jm010158+.

(141) Soriano, A.; Ventura, R.; Molero, A.; Hoen, R.; Casadó, V.; Cortés, A.; Fanelli, F.; Albericio, F.; Lluís, C.; Franco, R.; Royo, M. Adenosine A2A receptor-antagonist/dopamine D2 receptor-agonist bivalent ligands as pharmacological tools to detect A2A-D2 receptor heteromers. *Journal of medicinal chemistry* **2009**, *52* (18), 5590–5602. DOI: 10.1021/jm900298c.

(142) Valant, C.; Sexton, P. M.; Christopoulos, A. Orthosteric/allosteric bitopic ligands: going hybrid at GPCRs. *Molecular interventions* **2009**, *9* (3), 125–135. DOI: 10.1124/mi.9.3.6.

(143) Waldhoer, M.; Fong, J.; Jones, R. M.; Lunzer, M. M.; Sharma, S. K.; Kostenis, E.; Portoghese, P. S.; Whistler, J. L. A heterodimer-selective agonist shows in vivo relevance of G protein-coupled receptor dimers. *Proceedings of the National Academy of Sciences of the United States of America* **2005**, *102* (25), 9050–9055. DOI: 10.1073/pnas.0501112102.

(144) Pérez-Benito, L.; Henry, A.; Matsoukas, M.-T.; Lopez, L.; Pulido, D.; Royo, M.; Cordomí, A.; Tresadern, G.; Pardo, L. The size matters? A computational tool to design bivalent ligands. *Bioinformatics (Oxford, England)* **2018**, *34* (22), 3857–3863. DOI: 10.1093/bioinformatics/bty422.

(145) Diestler, D. J.; Knapp, E. W. Statistical thermodynamics of the stability of multivalent ligand-receptor complexes. *Physical review letters* **2008**, *100* (17), 178101. DOI: 10.1103/PhysRevLett.100.178101.

(146) Huang, B.; St Onge, C. M.; Ma, H.; Zhang, Y. Design of bivalent ligands targeting putative GPCR dimers. *Drug discovery today* **2021**, *26* (1), 189–199. DOI: 10.1016/j.drudis.2020.10.006.

(147) Ercolani, G. Comment on "Using a Convenient, Quantitative Model for Torsional Entropy To Establish Qualitative Trends for Molecular Processes That Restrict Conformational Freedom". *The Journal of organic chemistry* **1999**, *64* (9), 3350–3353. DOI: 10.1021/jo981986m.

(148) Berque-Bestel, I.; Lezoualc'h, F.; Jockers, R. Bivalent ligands as specific pharmacological tools for G protein-coupled receptor dimers. *Current drug discovery technologies* **2008**, *5* (4), 312–318. DOI: 10.2174/157016308786733591.

(149) Shonberg, J.; Scammells, P. J.; Capuano, B. Design strategies for bivalent ligands targeting GPCRs. *ChemMedChem* **2011**, *6* (6), 963–974. DOI: 10.1002/cmdc.201100101.

(150) Carli, M.; Kolachalam, S.; Aringhieri, S.; Rossi, M.; Giovannini, L.; Maggio, R.; Scarselli, M. Dopamine D2 Receptors Dimers: How can we Pharmacologically Target Them? *Current neuropharmacology* **2018**, *16* (2), 222–230. DOI: 10.2174/1570159X15666170518151127.

(151) Vanhanen, J.; Kinnunen, M.; Nuutinen, S.; Panula, P. Histamine H3 receptor antagonist JNJ-39220675 modulates locomotor responses but not place conditioning by dopaminergic drugs. *Psychopharmacology* **2015**, *232* (6), 1143–1153. DOI: 10.1007/s00213-014-3751-7.

(152) Ferrada, C.; Moreno, E.; Casadó, V.; Bongers, G.; Cortés, A.; Mallol, J.; Canela, E. I.; Leurs, R.; Ferré, S.; Lluís, C.; Franco, R. Marked changes in signal transduction upon heteromerization of dopamine D1 and histamine H3 receptors. *British journal of pharmacology* **2009**, *157* (1), 64–75. DOI: 10.1111/j.1476-5381.2009.00152.x.

(153) Rashid, A. J.; So, C. H.; Kong, M. M. C.; Furtak, T.; El-Ghundi, M.; Cheng, R.; O'Dowd, B. F.; George, S. R. D1-D2 dopamine receptor heterooligomers with unique pharmacology are coupled to rapid activation of Gq/11 in the striatum. *Proceedings of the National Academy of Sciences of the United States of America* **2007**, *104* (2), 654–659. DOI: 10.1073/pnas.0604049104.

(154) Rodríguez-Ruiz, M.; Moreno, E.; Moreno-Delgado, D.; Navarro, G.; Mallol, J.; Cortés, A.; Lluís, C.; Canela, E. I.; Casadó, V.; McCormick, P. J.; Franco, R. Heteroreceptor Complexes Formed by Dopamine D1, Histamine H3, and N-Methyl-D-Aspartate Glutamate Receptors as Targets to Prevent Neuronal Death in Alzheimer's Disease. *Molecular neurobiology* **2017**, *54* (6), 4537–4550. DOI: 10.1007/s12035-016-9995-y.

(155) Moreno-Delgado, D.; Puigdellívol, M.; Moreno, E.; Rodríguez-Ruiz, M.; Botta, J.; Gasperini, P.; Chiarlone, A.; Howell, L. A.; Scarselli, M.; Casadó, V.; Cortés, A.; Ferré, S.; Guzmán, M.; Lluís, C.; Alberch, J.; Canela, E. I.; Ginés, S.; McCormick, P. J. Modulation of dopamine D1 receptors via histamine H3 receptors is a novel therapeutic target for Huntington's disease. *eLife* **2020**, *9.* DOI: 10.7554/eLife.51093.

(156) Yang, K.; Jackson, M. F.; MacDonald, J. F. Recent progress in understanding subtype specific regulation of NMDA receptors by G Protein Coupled Receptors (GPCRs). *International journal of molecular sciences* **2014**, *15* (2), 3003–3024. DOI: 10.3390/ijms15023003.

(157) Moreno, E.; Hoffmann, H.; Gonzalez-Sepúlveda, M.; Navarro, G.; Casadó, V.; Cortés, A.; Mallol, J.; Vignes, M.; McCormick, P. J.; Canela, E. I.; Lluís, C.; Moratalla, R.; Ferré, S.; Ortiz, J.; Franco, R. Dopamine D1-histamine H3 receptor heteromers provide a selective link to MAPK signaling in GABAergic neurons of the direct striatal pathway. *The Journal of biological chemistry* **2011**, *286* (7), 5846–5854. DOI: 10.1074/jbc.M110.161489.

(158) Kotagale, N.; Rahmatkar, S.; Chauragade, S.; Dixit, M.; Umekar, M.; Chopde, C.; Taksande, B. Involvement of hippocampal agmatine in β1-42 amyloid induced memory impairment, neuroinflammation and BDNF signaling disruption in mice. *Neurotoxicology* **2020**, *80*, 1–11. DOI: 10.1016/j.neuro.2020.06.002.

(159) Olajide, O. J.; Chapman, C. A. Amyloid-β (1-42) peptide induces rapid NMDA receptor-dependent alterations at glutamatergic synapses in the entorhinal cortex. *Neurobiology of aging* **2021**, *105*, 296–309. DOI: 10.1016/j.neurobiolaging.2021.05.006.

(160) Liu, J.; Chang, L.; Song, Y.; Li, H.; Wu, Y. The Role of NMDA Receptors in Alzheimer's Disease. *Frontiers in neuroscience* **2019**, *13*, 43. DOI: 10.3389/fnins.2019.00043.

(161) Borovac, J. A. Side effects of a dopamine agonist therapy for Parkinson's disease: a mini-review of clinical pharmacology. *The Yale journal of biology and medicine* **2016**, *89* (1), 37–47.

(162) Xu, J.; Pittenger, C. The histamine H3 receptor modulates dopamine D2 receptor-dependent signaling pathways and mouse behaviors. *The Journal of biological chemistry* **2023**, *299* (4), 104583. DOI: 10.1016/j.jbc.2023.104583.

(163) Casadó-Anguera, V.; Moreno, E.; Mallol, J.; Ferré, S.; Canela, E. I.; Cortés, A.; Casadó, V. Reinterpreting anomalous competitive binding experiments within G protein-coupled receptor homodimers using a dimer receptor model. *Pharmacological research* **2019**, *139*, 337–347. DOI: 10.1016/j.phrs.2018.11.032.

(164) Herrick-Davis, K.; Grinde, E.; Harrigan, T. J.; Mazurkiewicz, J. E. Inhibition of serotonin 5-hydroxytryptamine2c receptor function through heterodimerization: receptor dimers bind two molecules of ligand and one G-protein. *The Journal of biological chemistry* **2005**, *280* (48), 40144–40151. DOI: 10.1074/jbc.M507396200.

2. Activation of Multiple G protein Pathways to Characterize the Five Dopamine Receptor Subtypes using Bioluminescence Technology

Note: Prior to the submission of this thesis, the content of this chapter, except for minor changes, was published in collaborations with partners:

Mönnich, D.*; Humphrys, L. J.*; Höring, C.; Hoare, B. L.; Forster, L.; Pockes, S. Activation of Multiple G Protein Pathways to Characterize the Five Dopamine Receptor Subtypes Using Bioluminescence Technology. *ACS Pharmacol. Transl. Sci.* **2024**. DOI: 10.1021/acsptsci.3c00339. *contributed equally

The following experimental work was performed by co-workers:

Dr. Laura J. Humphrys contributed equally: Generation of plasmids for stable cell lines of HEK293T CAMYEN $D_{1,2l,3,4,5}R$ and equaly experemetal work for the characterization of HEK293T CAMYEN $D_{1,2l,3,4,5}R$ and the G-case assay ELISA and Immunofluorescence experiments.

Dr. Carina Höring: generating of plasmids $pIRES_{puro}$ NLN_mG_s/mG_{si}/mG_q; $pcDNA3.1_{neo}$ $D_{2l}R$_NLC and party of experimental work for the coupling of $mG_{s,i,q}$ proteins with $D_{1,5}R$ with dopamine.

Dr. Lisa Forster: part of experimental work for characterization of HEK293T NLN_miniG_i $D_{2l}R$_NLC.

Please note that, parts of this work were obtained during the master thesis (2019-2020 in-house).

2.1. Introduction

G protein-coupled receptors (GPCRs) are the most studied targets in drug discovery and are the most common transmembrane receptors in the mammalian genome.[1–4] GPCRs are connected to heterotrimeric proteins containing an α,β and γ subunit and can be classified according to their primary coupling behaviour to the Gα subunit, which is divided into α_s-, $\alpha_{i/o}$-, $\alpha_{q/11}$- and $\alpha_{12/13}$-families.[5] The activation of a GPCR subsequently regulates intracellular signaling by engaging heterotrimeric G proteins or β-arrestins, which transfer the signal to further downstream effector proteins or leads to internalization and desensitization of the receptor.[6–8]

The neurotransmitter dopamine acts as an endogenous ligand through five dopamine receptors belonging to the superfamily of class A GPCRs that can be divided into two subtype families. The D_1-like family comprises the D_1 receptor (D_1R) and D_5 receptor (D_5R), which activate the second messenger pathway by stimulating adenylyl cyclase, leading to cyclic adenosine monophospahte (cAMP) production. The D_2 receptor (D_2R), D_3 receptor (D_3R), and D_4 receptor (D_4R) form the D_2-like family and, in contrast, block the cAMP-initiated second messenger cascade.[2,3,9,10] Dopamine receptors are highly expressed in ventral tegmental areas and substantia nigra pars compacta in the CNS and are of great importance in learning processes, motivation, and motorial output.[10–12] Dysregulation of the catecholamine dopamine plays diverse roles in pathogenesis and therapy for different diseases such as schizophrenia, Parkinson's disease (PD), drug addiction and bipolar disorders.[13–15]

In the preceding few decades, several test systems have been developed to characterize binding properties or functionality of ligands concerning either the D_1R or D_2R.[7,16,17] Unfortunately, the other subtypes have not been as much of a focus. Selectivity studies between all 5 dopamine receptors, coupling studies contrary to primary coupling of dopamine receptors, and the monitoring of their functional response all remain under-researched.[14] The three less-targeted receptors (D_3R, D_4R, D_5R) are nevertheless important as they are associated with diseases as potential drug targets independent of the D_1R and D_2R. For example, both the D_4R and D_5R have been implicated to play a role in attention deficit hyperactivity disorder (ADHD), whereas the D_3R receptor is associated with autism spectrum disorder (ASD) and substance abuse disorders.[18–23] Additionally, the coupling profile of all five dopamine receptors is often referred to as 'predominantly coupling' and have been previously researched in other studies to detect the receptors' G protein preferences (the canonical predominant G protein families being G_s for D_1R and D_5R,[24] G_i for $D_{2l}R$ and G_o for D_3R and D_4R[25]). Although predominant, these do not represent exclusive G protein coupling at the dopamine receptors. For example, the D_1R prefers to couple to

the $G\alpha_s$ subunit but can also recruit the $G\alpha_{i1}$, $G\alpha_{i2}$, $G\alpha_o$ and $G\alpha_q$ subunits.[26] There are hints that the D_2R and D_3R can recruit β-arrestins with a ligand-dependent bias that creates new opportunities for dopamine receptor drug discovery.[16,27,28] For example, improving β-arrestin2 recruitment of the D_2R is thought to help with the therapeutic effect of L-DOPA in PD, whereas decreasing β-arrestin2 recruitment at the D_3R and using a G protein biased ligand may help treat dyskinesia.[29,30] Such selectivity profiles may also be possible targeting the different G proteins and their coupling. To address this, we have applied three different, bioluminescence-based assay procedures for functional characterization of all five dopamine receptors in live cells (Figure 2.1). Through these assays, we aim to thoroughly describe and compare the G protein activation profile of the five dopamine receptors with their endogenous and selective ligands.

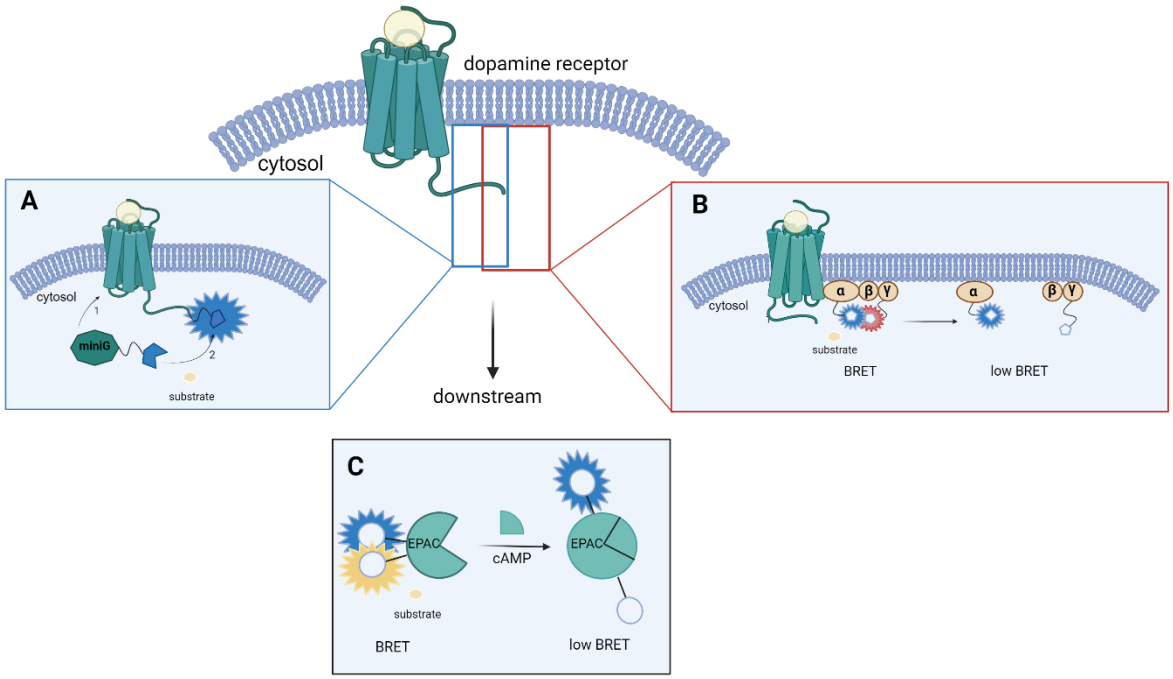

Figure 2.1: Overview of all three testsystems. **A:** Scheme of the miniG recruitment assay with split-NanoLuc technology,[31] where the large fragment (LgBit) is fused N-terminally to the miniG protein and the small fragment (smBit) C-terminally to the human dopamine receptors. After ligand binding, an induced conformational change leads to the recruitment of the respective miniG protein and complementation of the two NanoLuc fragments. Bioluminescence intensity is measured in the presence of a substrate. **B:** Scheme of the G-CASE assay, where the Nanoluc is cloned into the Gα subunit of a G protein trimer, and the cpVenus protein is fused to the N-terminus of the corresponding Gγ subunit. After receptor activation by a ligand, the Gα-NanoLuc donor and cpVenus-Gγ acceptor proteins are spatially displaced, decreasing the BRET ratio and enabling measurement of the specific activation of a chosen Gα subunit. **C:** Principle of CAMYEN BRET-based biosensor. The NanoLuc is fused to the C-terminus of an Epac cAMP binding domain, and mCitrine to the N-terminus. Conformational change of the CAMYEN protein decreases the BRET ratio between the NanoLuc donor and mCitrine fluorescent acceptor when bound to cAMP. Created with BioRender.com.

2.2. Materials and Methods

2.2.1. Materials

The cDNA for the human (h)$D_{2long}R$ ($D_{2l}R$; NM_000795.4) and hD_3R (D_3R; NM_000796.5) were kindly provided by Harald Hübner (Friedrich-Alexander-University, Erlangen, Germany), and cDNA of the hD_1R (D_1R; NM_000794.5), hD_5R (D_5R; NM_000798.5) and h$D_{4.4}R$ (D_4R; NM_000797.4) were purchased from the cDNA Resource Center (Rolla, MO, USA). Molecular biology enzymes and reagents were from New England Biolabs (NEB; Frankfurt am Main, Germany), unless otherwise described. G-CASE plasmids for G_{i1}, G_{i2}, G_{i3}, G_{o1}, G_s, G_q, and G_{13} sensors were a kind gift from Gunnar Schulte (available on Addgene[32]), and the G_z-CASE was made and verified previously in house.[33]

Dulbecco's modified Eagle's medium high glucose (DMEM) and HEPES (1 M in distilled (d)H_2O, pH = 7.4, sterilized and stored at 4 °C) were from Sigma (Taufkirchen, Germany). Leibovitz's L-15 medium without phenol red (L-15) was from Gibco (Taufkirchen, Germany). Fetal calf serum (FCS), trypsin (0.05% trypsin, 0.02% EDTA in PBS) and geneticin (G418) were from Merck (Darmstadt, Germany). Puromycin and zeocin were obtained from Invivogen (Toulouse, France). The NanoLuciferase substrate Furimazine (Nano-Glo®) was from Promega (Walldorf, Germany), and Coelenterazine h (CZH; 5 mM in methanol, stored at -80 °C) was from BioSynth s.r.o (Bratislava, Slovakia). HEK293T cells (RRID:CVCL_0063) were a kind gift from Wulf Schneider (Institute for Medical Microbiology and Hygiene, Regensburg, Germany).

Depending on their physicochemical properties, when possible, ligands were dissolved in dH_2O; otherwise DMSO (Merck) was used as a solvent. Dopamine dihydrochloride (Dopa), (+)-butaclamol hydrochloride (Buta), pramipexole dihydrochloride (Prami), and (+)-SCH-23390 hydrochloride (SCH) were purchased from Sigma (Taufkirchen, Germany). Haloperidol (Halo) was from TCI Deutschland GmbH (Eschborn, Germany). *R*-(-)-apomorphine (Apo) (+)-SKF-81297 hydrobromide (SKF), spiperone hydrochloride (Spip), nemonapride (Nemo), and (-)-quinpirole hydrochloride (Quin) were obtained from TOCRIS (Bristol, UK). The radioligands [^{3}H]*N*-methyl-spiperone (77 Ci/mmol) and [^{3}H]SCH-23390 (81 Ci/mmol) were purchased from Novandi Chemistry AB (Södertälje, Sweden).

2.2.2. Molecular Cloning

Plasmids for the split NanoLuc (also known as NanoBiT[31]) miniG protein assay were generated by standard PCR amplification and restriction enzyme techniques. The cDNA of the miniG_s (miniG_s_393; mG_s), mini$G_{s/i}$ (m$G_{s/i}$_43; mG_{i1}), mini$G_{s/q}$ (m$G_{s/q}$_71; mG_q) and miniG_{o1} (miniG_{o1}_12;

mG_{o1}) were a customized gene-synthesis from Eurofins Genomics, according to the published protein sequence of Nehmé et al. 2017[34] as described by Höring et al. 2020[35] for the $miniG_s$, $miniG_{i1}$, and $miniG_q$, the $miniG_{o1}$ protein was cloned within a $pIRES_{puro}3$ vector backbone that encodes the large fragment of split NanoLuc (NlucN; MVFTLEDFVGDWEQTAAYNLDQVLEQGGVSSLLQNLAVSVTPIQRIVRSGENALKIDIHVIIPYEGLSAD QMAQIEEVFKVVYPVDDHHFKVILPYGTLVIDGVTPNMLNYFGRPYEGIAVFDGKKITVTGTLWNGNKII DERLITPDGSMLFRVTINS; also known as LgBiT[31]) C-terminally fused via a flexible glycine-serine-linker (-GSSGGGGSGGGGSS-) downstream of the inserted cDNA sequence. The fusion of the human dopamine receptors $D_{2l}R$, D_3R and D_4R with the small fragment of the split NanoLuc (NlucC; VTGYRLFEEIL; also known as smBiT[31]) was facilitated by PCR, restriction enzyme digest and ligation. The receptors were subcloned into a vector backbone of $pcDNA3.1_{neo}$ NlucC between restriction enzymes *Hind*III and *Xba*I, allowing for fusion of NlucC on the receptor C-terminus. For D_1R and D_5R, Gibson assembly reactions were performed to subclone the gene of interest into the $pcDNA3.1_{neo}$ vector backbone. Therefore, overlaps of 25 base pairs (bp) matching the vector backbone were attached to the receptor cDNA by PCR using following primers, where receptor complimentary bases are underlined:

D_1R fw: CAAGCTGGCTAGTTAagcttccaccATGAGGACTCTGAACACCTC

D_1R rv: cgccacctccaTCTAGACtcgagccGGTTGGGTGCTGACCGTTT

D_5R fw: CAAGCTGGCTAGTTAagcttccaccATGCTGCCGCCAGGCAG

D_5R rv: cgccacctccaTCTAGACtcgagccATGGAATCCATTCGGGGTGA.

For use with the CAMYEN and G-CASE assays, whose biosensor expression were both neomycin resistant, dopamine receptor cDNA was cloned into a $pcDNA3.1_{zeo}$ 5-HT_{3A}-FLAG-SacB vector backbone, made in house. This vector contained zeocin antibiotic resistance, with the murine 5-HT_{3A} signal peptide (5-HT_{3A}; MRLCIPQVLLALFLSMLTGPGEGSR; to improve plasma membrane targeting and expression)[31,36] and FLAG tag (DYKDDDDK; to detect receptor expression) for N-terminal fusion to the receptor. The SacB gene was used as a counter-selection gene to the receptor cDNA.[31,37] For D_1R, $D_{2l}R$, D_4R and D_5R, the receptor cDNA was cloned into the vector using standard PCR, restriction digest and ligation techniques between *Bam*HI and *Xho*I restriction sites. For the D_3R, Gibson assembly was used with an NEOBuilder reaction for 1hr at 50 °C, using the following primers for the PCR:

D_3R fw: acgatgacgacaagggatcc*aagctt*GCATCTCTGAGCCAGCTG

D_3R rv:cctctagaggtaccctcgagTCAGCAAGACAGGATCTTG.

A *Hind*III site was added upstream of the receptor sequence and two silent mutations from the original sequence were found (T873C, G897A).

Positive bacterial colonies were first extracted in a mini-prep from overnight cultures (Miniprep Kit, Nippon Genetics, Düren, Germany) and then maxi-prepped for use in mammalian cells (Maxiprep Kit, Qiagen, Hilden, Germany). All plasmids were quantified by UV-Vis absorbance using a NanoDrop spectrophotometer (ThermoFisher, Braunschweig, Germany) and sequences were confirmed by custom DNA sequencing from Eurofins Genomics (Ebersberg, Germany).

The well characterized cAMP sensor called "CAMYEL" (cAMP sensor using YFP-Epac-RLuc) was improved by replacing Renilla luciferase (Rluc) with the much brighter Nanoluciferase (Nluc).[38] This was achieved by PCR amplification of the DNA encoding Nluc and insertion into the CAMYEL plasmid (a kind gift from Alastair Keen) via Gibson Assembly as described above. We named the resulting construct "CAMYEN" (cAMP sensor using YFP-Epac-Nluc).

2.2.3. Cell Culture

HEK293T cells were cultured in DMEM supplemented with 10% FCS and 2 mM L-glutamine at 37 °C, 5% CO_2 in a H_2O saturated atmosphere. Cells were periodically inspected for mycoplasma contamination by Venor GeM Mycoplasma Detection Kit (Minerva Biolabs, Berlin, Germany) or by costumer service of Eurofins Genomics (Ebersberg, Germany).

2.2.4. Generation of Stable HEK293T Cell Lines

For biosensors requiring stable expression, HEK293T cells (passage 10 - 15) were seeded on a sterile 6 well dish at a cell density of 300,000 cells/ml in DMEM supplemented with 10% FCS and 2 mM L-glutamine. The next day, cells were transfected with 2 µg cDNA of $pIRES_{puro}$ NlucN-miniG_{o1}, pcDNA3 L-His-CAMYEN or G_s-CASE using the transfection reagent XtremeGene HP (Merk) according to the supplier's protocol (1:3 cDNA (µg):XtremeGene (µl) ratio). After an incubation period of 48 hours, cells were detached by using trypsin and seeded in a 25 cm^3 or 175 cm^3 cell culture flask with 5 ml or 25 ml DMEM supplemented with 10% FCS, respectively. Cells were allowed to attach and thereafter treated with the antibiotic puromycin (miniG_{o1}; 3 µg/ml) or G418 (CAMYEN and G_s-CASE; 1,000 µg/ml) to achieve stable expression. The media was refreshed every three days, and puromycin/G418 levels were dropped to 1 µg/mL/600 µg/ml for continued selection pressure in later passages.

HEK293T cells stably expressing the miniG_s, miniG_{i1}, or miniG_{o1} protein with N-terminal NlucN were then stably transfected in the same manner with the dopamine receptor-NlucC plasmids to generate the stable cell lines miniG_s_D_1R, miniG_s_ D_5R, miniG_{o1}_D_3R, miniG_{o1}_D_4R and miniG_{si1}_D_{2l}R.

These cells then underwent continued antibiotic selection pressure through passages with 1 µg/ml puromycin and 600 µg/ml G418. HEK293T-CAMYEN cells were also stably transfected with XtremeGene HP using the same protocol to insert the pcDNA3.1$_{zeo}$-5HT$_{3A}$-FLAG-D_1R, D_{2l}R, D_3R, D_4R or D_5R plasmids. All five cell lines generated were selected using 300 µg/ml zeocin and thereafter cultured using DMEM containing 100 µg/ml zeocin and 600 µg/ml G418.

2.2.5. MiniG Protein Recruitment Assay

HEK293T cells stably expressing the miniG protein of interest and corresponding dopamine receptor tagged by the split NanoLuc fragments were seeded in a 75 cm^3 flask in DMEM supplemented with 10% FCS and 2 mM L-glutamine and allowed to grow until 80% confluence was reached. After trypsinization, cells were suspended in Leibovitz' L-15 media (with 5% FCS and 10 mM HEPES) and centrifuged at 700 rpm for 5 minutes. After discarding the supernatant, the cells were re-suspended in L-15 media supplemented with 5% FCS and 10 mM HEPES and the cell density was adjusted at $1.25*10^6$ cells/ml. 80 µl of the cell suspension was transferred to each well of a white 96 well plate (BRANDplates® cellGrade 781965, VWR) and incubated at 37 °C overnight in a humidified atmosphere.

The miniG protein recruitment assay was performed as described before by Höring et al. 2020[35] at 37 °C with an EnSpire plate reader (PerkinElmer, Baesweiler, Germany) or CLARIOstar Plus plate reader (BMG LABTECH, Ortenberg, Germany) to characterize agonists (agonist mode). The dilution of the substrate and samples were prepared in Leibovitz's L-15 media supplemented with 10 mM HEPES prior to the experiment. The basal luminescence was recorded immediately after adding 10 µl of the substrate to each well for 33 plate repeats (CLARIOstar Plus, 13 plate repeats), with an integration time of 100 ms per well (CLARIOstar Plus, 0.5 s). 10 µl of every concentration of the ligand dilution series were added in triplicate, and the final luminescence measurement was performed for a further 100 plate repeats (CLARIOstar Plus, 39 plate repeats).

A similar procedure was performed for the characterization of antagonists (antagonist mode). Here, a further 33 plate repeats were recorded (CLARIOstar Plus, 13 plate repeats) after the addition of the antagonist ligand dilutions to evaluate possible inverse agonist effects, followed by the final measurement of 100 cycles (CLARIOstar Plus, 39 plate repeats) after adding 10 µL of the endogenous agonist dopamine at an EC_{80} concentration of 100 nM for D_1R and D_5R, 100 nM dopamine, 1 µM pramipexole in the case of D_2R and D_3R or 1 µM (-)-quinpirole for the D_4R. For normalization of the data, the negative control (solvent) and positive control (maximum level of

10 µM dopamine for D_1R and D_5R, 10 µM /100 µM pramipexole for $D_{2l}R$ / D_3R, and 10 µM (-)-quinpirole for D_4R) were included on every plate. The resulting pK_b values were determined according to the Cheng-Prusoff equation.[39]

In the case of miniG_{o1} with the D_4R, HEK293T cells were seeded on a sterile 6 well dish at a cell density of 300,000 cells/ml in DMEM supplemented with 10% FCS and 2 mM L-glutamine (2 ml/well). The next day, cells were transfected with 1 µg cDNA of pIRES$_{puro}$-NlucN-miniG_{o1} and pcDNA3.1$_{neo}$-D_4R-NlucC using the Transporter 5 PEI transfection reagent (Polyscience, Inc., Warrington, USA) according to the supplier's protocol (1:5 cDNA (µg): PEI (µL) ratio) in 200 µL unsupplemented DMEM, after 20 min incubation at room temperature. After an incubation period of 48 hours, cells were trypsinated and 80 µl of the adjusted cell suspension of 1.25*10^6 cells/ml were transferred to each well of a white 96 well plate (BRANDplates® cellGrade 781965, VWR, Darmstadt, Germany) and incubated at 37 °C overnight in a humidified atmosphere. For luminescence measurements, a Tecan Infinite® Lumi (Tecan, Männedorf, Switzerland) plate reader was used with 33 plate repeats for baseline recording and 66 plate repeats after the addition of the ligands, with an integration time of 200 ms.

The same procedure was used for transient experiments probing the selectivity of miniG protein coupling to dopamine receptors, except HEK293T cells were seeded on a sterile 24 well dish at a cell density of 70,000 cells/ml in DMEM supplemented with 10% FCS and 2 mM L-glutamine (500 µl/well) and transfected with 250 ng respective plasmid DNA. After 48 h incubation period, 40 µL/well of the cell suspension were seeded in a 384 well plate (LUMITRAC™ medium binding, Greiner Bio-One, 781075, UV sterilized prior to experiment). For luminescence measurements, a Tecan Infinite® Lumi plate reader was used with 6 plate repeats for baseline recording and 19 plate repeats after the addition of the ligands, with an integration time of 200 ms.

2.2.6. G-CASE assay

To measure the specificity of dopamine receptor G protein activation, the BRET-based G-CASE sensors were used. After trypsinisation and centrifugation (1,000 rpm for 5 min), HEK293T or HEK-G_s-CASE cell lines were seeded on a sterile 24 well plate at a cell density of 300,000 cells/ml in DMEM supplemented with 10% FCS (500 µl/well). The next day, cells in each well were transfected with 500 ng of pcDNA (negative control) or dopamine receptor plasmid (pcDNA3.1$_{zeo}$-$5HT_{3A}$-FLAG-D_1R, $D_{2l}R$, D_3R, D_4R or D_5R) plus 500 ng of the G-CASE plasmid (G_{i1}, G_{i2}, G_{i3}, G_{o1}, G_z, G_q, G_{13}, or pcDNA for the G_s-CASE cell line) using linear polyethylenimine (PEI 1 mg/l, 5µl) in 100 µl unsupplemented DMEM, after 15 min incubation at room temperature. All 46 variants were left for 48 hours, then trypsinized and centrifuged. Cells were then plated onto white, opaque 384 well plates (LUMITRAC™ medium binding or BRANDplates® 781981; VWR, Darmstadt, Germany) in

L-15 media supplemented with 5% FCS and 10 mM HEPES at 40 µl/well (24 wells of the 384-well plate from a single 24 well) and left overnight at 37 °C in a humidified atmosphere. On the day of the experiment, 5 µl of 50 µM CZH in L-15 with 10 mM HEPES (final concentration 5 µM) was added to each well and the baseline was read for 3 cycles (35 min) at 200 ms integration time for both 'Blue' (< 470nm) and 'Green' (520-580nm) filter wavelengths on a Tecan Infinite® Lumi. Prediluted ligands to 10x final concentration or negative solvent control in L-15 + 10 mM HEPES were then added in triplicate at 5 µl per well and the plate was read with the same parameters for 6 cycles (75 min). The BRET ratio for each timepoint was calculated by dividing the Green filtered light emission by the blue filtered light emission.

2.2.7. CAMYEN cAMP assay

HEK-CAMYEN_D_1R, D_{2l}R, D_3R, D_4R or D_5R cells were trypsinized and centrifuged (1,000 rpm for 5 min) and resuspended in L-15 media supplemented with 5% FCS and 10 mM HEPES. After adjusting the cell count to 600,000 cells/ml, the cell suspension was added to a sterile, white 96 well plate (BRANDplates® cellGrade 781965) at 80 µl per well. Plates were incubated overnight at 37 °C in a humidified environment. On the day of the experiment, 10 µl furimazine 200x diluted in L-15 with 10 mM HEPES with either 100 µM forskolin (D_2-like receptors) or 1 mM 3-isobutyl-1-methylxanthine (IBMX; D_1-like receptors) was added to each well (final assay concentrations; furimazine 2000x diluted with 100 µM IBMX or 10 µM forskolin), and the baseline luminescence was taken for both 'Blue' (< 470nm) and 'Green' (520-580nm) filter wavelengths on a Tecan Infinite® Lumi (Tecan, Männedorf, Switzerland) at an integration time of 100 ms for 11 cycles (30 min). Ligands diluted to 10x final concentration in Leibovitz' L-15 media with 10 mM HEPES were added in triplicate at 10 µl/well. The luminescence response was then measured for a further 23 cycles (1 h) and the raw BRET ratio was calculated for each timepoint by dividing the Green filtered light emission by the Blue filtered light emission.

2.2.8. Calcium mobilisation assay

HEK293A cells (passage 20 - 30, kindly gifted from Asuka Inoue) were plated at 300,000 cells/well in 6 well plates in DMEM with 5% fetal bovine serum (FBS) and transiently transfected the following day using PEI Max (MW 40,000; Polysciences Asia Pacific, Taipei, Taiwan) at a 1:5 DNA (µg):PEI Max (µl) ratio. The variables tested used the following cDNA amounts per well: 1 µg dopamine receptor plasmid plus 1 µg empty vector; 2 µg empty vector; 1 µg wildtype $G\alpha_q$ (#GNA0Q00000, cDNA Resource Centre) with 1 µg dopamine receptor plasmid, or 1 µg wildtype $G_{\alpha q}$ with 1 µg empty vector. Cells were detached with versene (PBS with 0.5 mM EDTA, pH = 7.4),

and then plated onto black walled, clear bottom 96 well plates (PerkinElmer) in 100 µL/well DMEM with 5% FBS the day before the experiment. On the day of the experiment the plates were washed once with calcium imaging buffer (150 mM NaCl, 2.6 mM KCl, 1.18 mM $MgCl_2$, 10 mM D-Glucose, 10 mM HEPES, 2.2 mM $CaCl_2$, 0.5% (w/v) bovine serum albumin, 4 mM probenecid, pH = 7.4) and media was aspirated before addition of 90 µL/well calcium imaging buffer with 1 µM Fluo-8-AM dye (1 mM stock made up in DMSO; AAT Bioquest, Pleasanton, CA, USA) and 1 µM propranolol ((*S*)-(-)-propranolol hydrochloride, 10 mM in dH_2O, Sigma). Plates were then incubated at 37°C for 45 min – 1 h before reading on the FDSS/µCELL kinetic plate imager (#C13299, Hamamatsu Photonics, Hamamatsu, Shizuoka, Japan). Prior to read, dopamine serial dilutions and ionomycin control (1 µM final concentration) were prepared at 10 x final concentration in a v-bottom 96 well plate using the calcium buffer. Calcium mobilization via Fluo-8-AM fluorescence intensity (ex/em = 490/520 nm, K_d = 389 nM) was simultaneously measured in all wells every second at 37°C for 30 s baseline. The drug dilutions were then automatically pipetted from the 96 well compound plate, and the fluorescence was read for a further 4.5 min after ligand addition.

2.2.9. Radioligand Binding Assay

In order to measure the receptor density for the stably expressed dopamine receptor cell lines (HEK-miniG_x_D_yR and HEK-CAMYEN_D_yR), radioligand binding assays were performed. The cell density was adjusted to 80,000 cells/well after counting in a "Neubauer" haemocytometer, followed by seeding 80 µl of the cell suspension in binding buffer (50 mM Tris – HCl, 1 mM EDTA, 5 mM $MgCl_2$ * 6 H_2O and 100 µg/ml bacitracin, pH = 7.4) in each well of a 96 well plate (mircoplate PP, U-shape, Greiner Bio-One, Kremsmünster, Germany) The radioligand for D_1-like receptors was [^{3}H]SCH-23390 (81 Ci/mmol, Novandi Chemistry AB, Södertälje, Sweden; K_d=0.2 nM D_1R/ 0.3 nM D_5R[16,40,41]) and [^{3}H] *N*-methyl-spiperone (77 Ci/mmol, Novandi Chemistry AB, Södertälje, Sweden; K_d= 0.014 nM D_2R/ 0.026 nM D_3R/ 0.078 nM D_4R –[16]) was used for D_2-like receptors, both with increasing concentrations in the range of approximately 1/10 K_d -10 K_d. Total binding was determined in the absence of any competitor and non-specific binding was measured by incubating the cell suspension in the presence of radioligand and (+)-butaclamol in a 2,000-fold excess with a total volume of 100 µl per well. Incubation periods of 1 hour for D_2-like receptors or 1.5 h for D_1-like receptors were terminated by separating bound and free radioligand with an automated cell harvester (Brandel, Gaithersburg, USA) utilizing rapid filtration through Whatman GF/C filters precoated with 0.3% polyethylenimine. Filters were transferred to flexible 96-well sample plates (Perkin Elmer, Rodgau, Germany) and incubated with scintillation cocktail for at least 5 h before radioactivity was measured using a MicroBeta^2 1450 scintillation counter (Perkin

Elmer, Rodgau, Germany). Data were analyzed using Prism 9 and 10 (GraphPad, La Jolla, CA, USA) and, after subtracting nonspecific binding, K_i values were determined from IC_{50} values according to the Cheng-Prusoff-equation.[39]

2.2.10. ELISA and Immunofluorescence

ELISA and immunofluorescence were used to assess relative amounts and localization of dopamine receptors, miniG and G-CASE components in their transient expression. Clear 96-well plates (Cellstar®, 655180, Greiner Bio-one) were coated with 0.5% gelatine, crosslinked using 2.5% glutaraldehyde, and washed 10x with distilled H_2O. Cells were transiently transfected with PEI using the same amounts and ratios as the G-CASE and miniG coupling selectivity assays. After passaging, cells were diluted to a density of 600,000 cells/ml, then 500 µl of cells were added to the 100 µl of cDNA and PEI, and 100 µl of this mix was seeded per well. Following overnight incubation at 37 °C, 5% CO_2, all steps were conducted at room temperature. The next day, cells were washed 1x with PBS and fixed with 4% paraformaldehyde in PBS (Alfa Aesar) for 10 min, washed 3x with PBS, and then permeabilized using 0.1% Triton X-100 for 10 min. After washing 3x with PBS, 1 hour incubation with 0.5% bovine serum albumin (BSA) in PBS was used to block unspecific sites. Primary antibodies for either the FLAG protein (1:500; DYKDDDDK monoclonal antibody from mouse; #MA1-91878, LOT #SLCD3524, Invitrogen), fused to the N-terminus of the dopamine receptors, or NanoLuc (2 µg/ml; monoclonal antibody from mouse; #MAB10026, LOT CLUG0221101, RnD systems), internally expressed within the G-CASE G_α subunit or targeting the NlucN-miniG, were dissolved in 1% BSA in PBS and incubated with cells for 1 h. Cells were then washed 3x with 0.5% BSA in PBS and either horseradish peroxidase-conjugated (ELISA, 1:3000, #31430, LOT #077M4820V, Thermo Fisher Scientific) or Cy3-conjugated (immunofluorescence, 1:1000, #AP124C, Merk) goat anti-mouse polyclonal antibodies were diluted using 1% BSA in PBS and incubated with cells for 1 h. Cells were then washed 3x with PBS. For the ELISA, cells were incubated in 50µl/well 3,3',5,5'-Tetramethylbenzidine (Sigma) for 20 min, then 50 µl 2 M HCl was added. The 450 nm absorbance was measured on an EnSpire plate reader (PerkinElmer, Rodgau, Germany) at 37°C. For immunofluorescence, DAPI (1:50 in PBS) was used to stain cell nuclei after 10 min incubation, and then washed 3x with PBS. Images were taken on a widefield Eclipse Ts2-FL inverted microscope (Nikon Europe, Amstelveen, The Netherlands) using a 10x/0.25 Ph1 ADL WD 6.2 objective. For each variable, three fluorescent images were taken; DAPI (385 nm filter cube) for nuclei, with 30 ms exposure, Cy3 (525 nm filter cube) for antibody-tagged proteins, with 1 s exposure, and cpVenus (470 nm filter cube) for tagged G_γ subunits, with 400 ms exposure.

2.3. Data Analysis

The luminescence or raw BRET ratio traces were recorded for each ligand addition in a time-resolved manner, averaged between the well repeats, and corrected to the baseline measurements. Area under the curve (AUC) was calculated and used in concentration-response curves for all assays (time period of 1 hr for CAMYEN and G-CASE assays, 45 min for the miniG protein recruitment assay, and 4.5 min for the calcium assay). Finally, the CAMYEN assay data were normalized to the 1 μM dopamine response for each receptor. For the miniG recruitment assay the data were normalized to the highest concentration of either the endogenous agonist dopamine (10 μM, D_1R and D_5R), pramipexole (10 μM $D_{2l}R$ and 100 μM D_3R) or (-)-quinpirole (10 μM, D_4R), and for the calcium assay data were normalized to 1 μM ionomycin response. G-CASE assay data for efficacy (E_{max}) were normalized to the dopamine response as a reference ligand for each G protein subunit. All calculations were conducted using Prism 9 or 10 (GraphPad, La Jolla, CA, USA).

For comparison of assay responses where receptor and sensor levels varied, the $\Delta\log(E_{max}/EC_{50})$ was calculated using EC_{50} values and E_{max} percentage responses from the concentration-response curves best fit in Prism. Only drug responses with both an $E_{max} \geq 5$ % and $pEC_{50} > 4.50$ (miniG) or > 6.00 (G-CASE) were considered true responses. A three-parameter fit was used for all assays. These values were then referenced to the sensor with the highest response with dopamine as a reference ligand (G_s-CASE for $D_{1,5}Rs$, G_z-CASE for $D_{2l,3,4}Rs$).

For statistical analysis, data were first tested for normal Gaussian distribution using the Shapiro-Wilk test and, when confirmed, one-way analysis of variation (ANOVA) with Šídák's multiple comparisons test was used (calcium response data). Statistical analysis was only performed on data where $N = 5$ from different experiments on different days (achieved with all primary experiments).

Data are expressed as mean ± SEM, unless otherwise specified.

2.4. Results

2.4.1. Characterisation of Canonical miniG Coupling by Dopamine Receptors

The miniG protein recruitment assay combined with split NanoLuc technology is an excellent tool for the functional characterization of ligands and investigation of different G protein coupling behaviors of GPCRs in live cells.[1] Upon activation by a ligand, a conformational change of the receptor is induced and recruitment of the miniG protein occurs with concomitant complementation of the split luciferase fragments. The resulting bioluminescence is measured under the presence of the NanoLuc substrate and recruitment of the specific miniG protein upon receptor activation can be monitored in a concentration dependent manner of the ligand in real-time. An additional advantage is the ability of the miniG protein to bind to the receptor in the absence of a ligand for monitoring of inverse agonism.

In accordance with the canonical signaling pathways of dopamine receptors the miniG$_s$ was used with D$_{1,5}$Rs, miniG$_{i1}$ with the D$_{2l}$R, and miniG$_{o1}$ with D$_{3,4}$Rs in our assays. To examine the influence of receptor modification (C-terminus NlucC fusion) and receptor expression in all stable NlucN-miniG$_x$_D$_y$R-NlucC cell lines, radioligand saturation binding experiments were performed with the radiolabeled antagonist [^{3}H]SCH-23390 for the D$_1$-like and [^{3}H]*N*-methylspiperone ([^{3}H]NMSP) for the D$_2$-like family constructs (Appendix, Figure 7.1). Although the D$_{1,2l,3,5}$R-NlucCs expressed at a similar level, the D$_4$R-NlucC expressed poorly (roughly 5-fold lower). We performed an additional experiment to investigate the impact of varying the plasmid cDNA, therefore changing receptor expression in our system (Appendix, Figure 7.30). The D$_{2l}$R-NlucC was chosen as a representative receptor due to its varied expression levels between the miniG and CAMYEN assays (Appendix, Figure 7.1 and 7.2). The D$_{2l}$R-NlucC was transfected in differing amounts (0.125 – 1 µg) using an equivalent amount of the NlucN-mG$_{i1}$ sensor (1 µg) and made up to 2 µg with empty vector cDNA when required. Upon (-)-quinpirole stimulation, no difference in potency was observed for differing D$_{2l}$R amounts.

Sensor expression was determined using an ELISA with an anti-NanoLuc antibody against the NlucN (Appendix, Figure 7.10).The mG$_s$_D$_1$R expressed the highest, followed by a modest reduction in sensor expression for mG$_{i1}$_D$_{2l}$R and mG$_s$_D$_5$R. The mG$_o$ sensor in conjunction with the D$_{3,4}$Rs expressed the lowest in our system (about 50% of mG$_s$_D$_1$R).

We tested dopamine as the endogenous ligand, (+)-SKF-81297 and (+)-SCH-23390 as D$_1$R-like ligands and pramipexole and (-)-quinpirole as D$_2$-like ligands at all five dopamine receptors. Additionally, we tested (-)-apomorphine, (+)-butaclamol, haloperidol, spiperone, and nemonapride for selected dopamine receptors. For an accurate differentiation between the

selected standard ligands, we used an agonist mode, where ligands are added after reaching baseline, and antagonist mode, where an extra incubation step with an antagonist was added before the agonist.

2.4.2. Canonical miniG Coupling with Dopamine Receptor Agonists

We have obtained potencies and efficacies of a broad range, which were comparable with literature data (Table 2.1). Dopamine was characterized as full agonist at all receptors except the $D_4R\_mG_{o1}$ (Figure 2.2 and 2.3). At the $D_3R\_mG_{o1}$, the potency of dopamine was lower than expected (pEC_{50} = 5.78 ± 0.35) compared to a published radioligand binding assay (pK_i = 7.74[42]). (+)-SKF-81297, which is described as either D_1-like partial agonist[43,44] or full agonist,[45,46] was confirmed to be a full agonist for D_1-like receptors in this assay (E_{max}: $D_1R\_mG_s$ = 105 ± 3%, $D_5R\_mG_s$ = 104 ± 2% dopamine response) and showed high potency at the $D_1R\_mG_s$ (pEC_{50} = 7.89 ± 0.12) and $D_5R\_mG_s$ (pEC_{50} = 7.33 ± 0.10). The selective D_2-like ligand pramipexole was a full, potent agonist at the D_2-like receptors $D_{2l}R\_mG_{i1}$ (pEC_{50} = 7.69 ± 0.06) and $D_3R\_mG_{o1}$ (pEC_{50} = 8.08 ± 0.07), but not the $D_4R\_mG_{o1}$, where no activation of the receptor was observed.

2.4.3. Canonical miniG Coupling with Dopamine Receptor Antagonists

The reported antagonists (+)-SCH-23390, (+)-butaclamol and spiperone were successfully characterized in the miniG protein recruitment assay as competitive antagonists. By taking advantage of the constitutive activity in the miniG assay, the three ligands were also tested in the agonist mode and showed an additional partial (inverse) signal. Inverse or partial agonistic effects were also observed in the antagonist mode, lowering the signal under the baseline in the highest concentrations ((+)-butaclamol at $D_{1,3,5}R$ and spiperone at D_3R; Figure 2.2 and 2.3), or by an incomplete displacement of dopamine by (+)-SCH-23390 to an efficacy of approx. 40% ($D_1R\_mG_s$) and 20% ($D_5R\_mG_s$; Figure 2.2).

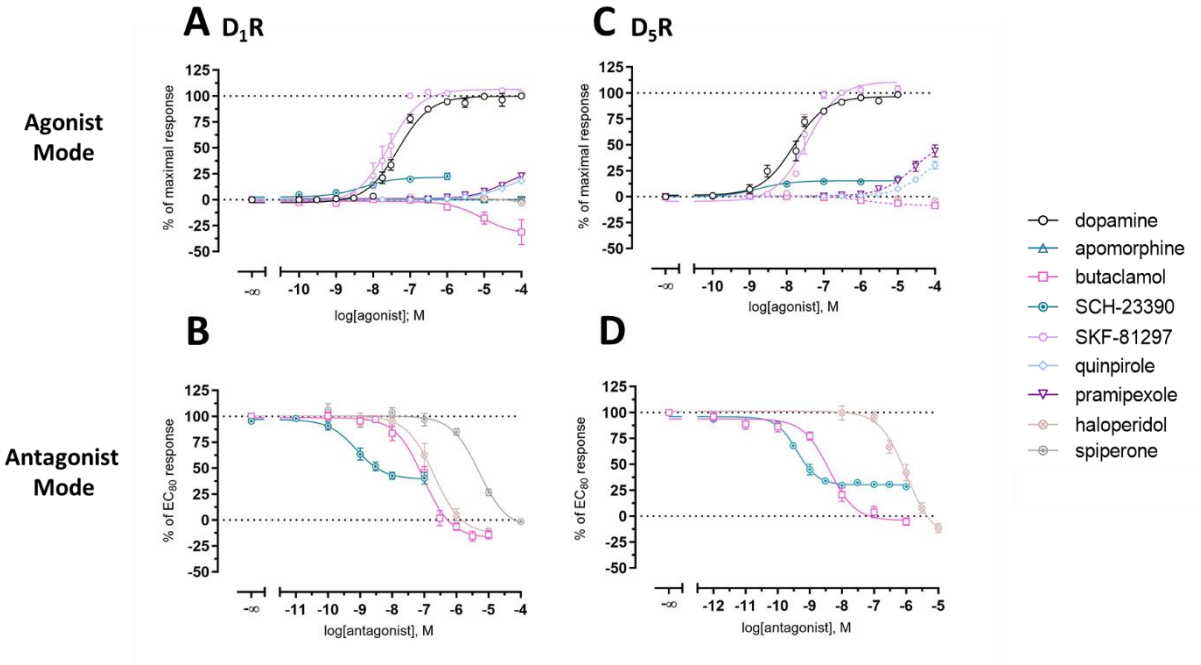

Figure 2.2: Concentration-response curves of standard ligands at the D_1-like receptors obtained in the miniG$_s$ protein recruitment assay using agonist mode and antagonist mode. **A, C:** Agonist mode for the D_1R and D_5R, respectively. **B, D:** The antagonist mode was performed in the presence of the agonist dopamine (100 nM) for D_1R and D_5R, respectively. All experiments were performed using whole cells stably expressing the NlucN-miniG$_s$ and the respective dopamine receptor-NlucC. Dashed lines represent incomplete or flat curve fits. Data are expressed as mean ± SEM, of $N \geq 5$ independent experiments, each performed in triplicate.

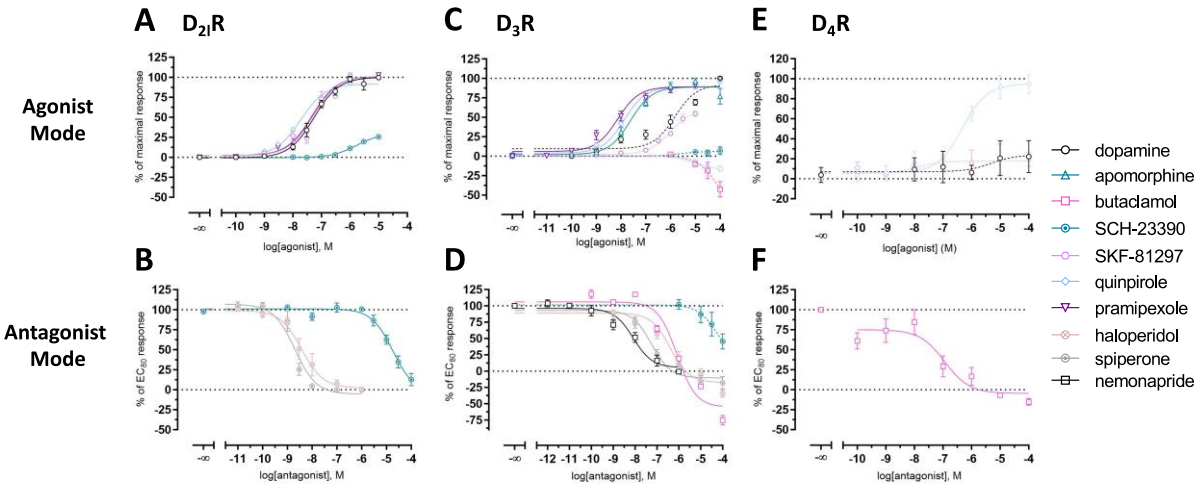

Figure 2.3: Concentration-response curves of standard ligands at the D_2-like receptors obtained in the miniG protein recruitment assay using agonist mode and antagonist mode. **A:** Agonist mode of standard ligands for the D_{2l}R_mG$_{i1}$. **B:** Antagonist mode was performed in the presence of the agonist pramipexole (10 µM) for the D_{2l}R_mG$_{i1}$. **C:** Agonist mode for the D_3R_mG$_{o1}$. **D:** Antagonist mode was performed in the presence of the agonist pramipexole (1 µM) for the D_3R_mG$_{o1}$. **E:** Agonist mode for the D_4R_mG$_{o1}$. **F:** Antagonist mode was performed in the presence of 1 µM (-)-quinpirole for the D_4R_mG$_{o1}$. All experiments were performed on whole cells stably expressing the NlucN-miniG$_{s/i1/o1}$ and the respective dopamine receptor-NlucC, except in the case of D_4R. HEK293T cells were transiently transfected with 1 µg of plasmid DNA of NlucN-miniG$_{o1}$ and D_4R-NlucC. Dashed lines represent incomplete or flat curve fits. Data are expressed as mean ± SEM, of $N \geq 5$ independent experiments, each performed in triplicate.

2.4.4. CAMYEN measured cAMP Response at the Five Dopamine Receptor Subtypes

To compare miniG coupling with downstream effects, cAMP responses of the five dopamine receptors were investigated. Relative accumulation of intracellular cAMP was measured in real-time using the CAMYEN BRET-based biosensor with stably expressed dopamine receptors. As with the miniG protein recruitment assay, receptor expression was evaluated using radioligand binding, where the $D_{1,3,5}$Rs expressed at a similar level, the D_{2l}R about 10-fold lower, and the D_4R 6-fold higher (Table 2.1, Appendix, Figure 7.2). Compared to the NlucC tagged receptors, receptor densities were comparable for the $D_{1,3,5}$Rs. The D_{2l}R expressed about 10-fold lower than the D_{2l}R-NlucC, and the D_4R had a 25-fold increase in receptor density than the D_4R-NlucC.

Concentration-response curves using area under the curve of the BRET ratio after 1 h were generated for the five dopamine receptors with seven different ligands (dopamine, (-)-apomorphine, (+)-butaclamol, (+)-SCH-23390, (+)-SKF-81297, pramipexole, and (-)-quinpirole), normalized to 1 µM dopamine (100%) and either 10 µM forskolin (D_2-like, 0%) or buffer (D_1-like, 0%; Figure 2.4). Kinetic traces for each ligand at each receptor and the CAMYEN response to ligands without transfected receptors are provided in the Appendix (Appendix, Figure 7.3 - 7.9).

2.4.5. Dopamine receptor agonist cAMP responses

In general, pEC_{50} values were increased in the CAMYEN cAMP assay compared with the miniG recruitment assay, typically by 1–1.5 log units (Figure 2.4 and Table 2.1) Dopamine produced similar potency responses at the five receptor subtypes, with EC_{50} values ranging from 0.8–6.0 nM (pEC_{50} = 9.09–8.22). Comparably, (-)-apomorphine was also a potent full agonist at all receptors with EC_{50} values between 0.8–17.4 nM (pEC_{50} = 9.09–7.76). The D_1-like selective compound (+)-SKF-81297 had sub-nanomolar potency at $D_{1,5}$Rs and, unlike miniG recruitment, was only a partial agonist for cAMP production at the D_1R (84% dopamine response). At the D_2-like receptors, (+)-SKF-81297 had a low potency inverse agonist effect at the D_3R, but had a partial agonistic cAMP response via the D_4R (pEC_{50} = 6.19, E_{max} = 61%) and D_{2l}R (pEC_{50} = 6.87, E_{max} = 22%). Both D_2-like selective agonists, (-)-quinpirole and pramipexole, were unable to produce full concentration response curves for $D_{1,5}$Rs up to 10 µM (Figure 2.4). D_2-like receptors however had comparable cAMP potencies for (-)-quinpirole and pramipexole, ranging from 0.3–1.4 nM (pEC_{50} = 9.49–8.86), and were always full agonists.

2.4.6. Dopamine Receptor Antagonist cAMP Response

In agreement with the miniG protein recruitment, the antagonist (+)-butaclamol produced an inverse agonistic effect on cAMP production (E_{max}: D_1R = -43%, $D_{2l}R$ = -44%, D_3R = -32%, D_4R = -43%, and D_5R = -37% dopamine response), and the other antagonist (+)-SCH-23982 acted as a partial agonist at all subtypes except D_3R (E_{max}: D_1R = 56%, $D_{2l}R$ = 58%, D_4R = 83%, and D_5R = 54% dopamine response).

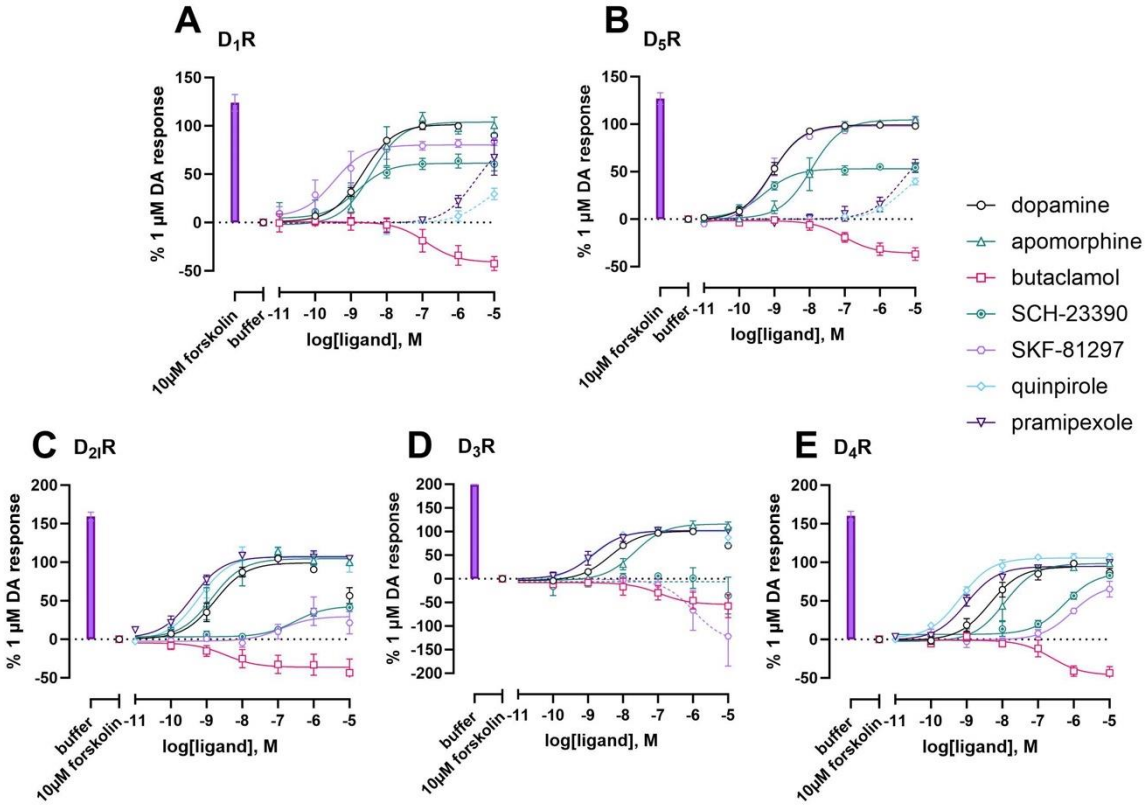

Figure 2.4: Ligand-induced changes of cAMP in HEK293T cells stably expressing the CAMYEN biosensor with the five dopamine receptors. Concentration response curves were generated using area under the curve of the BRET ratio/buffer control trace over 1 h. D_1-like receptor cAMP production in **A:** D_1R and **B:** D_5R were measured using 100 µM IBMX (30 min preincubation) and normalized to buffer (0%) and 1 µM dopamine (DA; 100%) responses. D_2-like receptor cAMP inhibition in **C:** $D_{2l}R$, **D:** D_3R and **E:** D_4R were taken with 10 µM forskolin (30 min preincubation) and normalized to 10 µM forskolin (0%) and 1 µM dopamine (DA; 100%) responses. For all graphs, the purple bar represents either 10 µM forskolin cAMP response (D_1-like) or the baseline CAMYEN read in buffer (D_2-like) to show the dynamic range of the sensor in each stable cell line. Ligands include agonists dopamine and (-)-apomorphine, antagonists (+)-butaclamol and (+)-SCH-23390, D_1-like selective agonist (+)-SKF-81297, and D_2-like selective agonists quinpirole and pramipexole. Dashed lines represent incomplete or flat curve fits. Data are expressed as mean ± S.E.M., of N = 5 independent experiments, each performed in triplicate.

Table 2.1: Ligand potencies at dopamine receptors in the miniG Protein Recruitment Assay and CAMYEN cAMP assay compared to literature data of pK_i values or cAMP stimulation (D_1-like)/inhibition (D_2-like) in HEK293 cells.

D_xR	Cpd.	MiniG Protein Recruitment					CAMYEN cAMP			
		pEC_{50}	E_{max} [%]	pK_b	*N*	Ref. pK_i	pEC_{50}	E_{max} [%]	*N*	Ref. pEC_{50}
D_1R				$miniG_s$						
	Dopa	7.45 ± 0.10	100	n.d.	8	8.25[47]	8.68 ± 0.06	100	6	8.49[45]
	Prami	< 5[≠]	65 ± 2	n.d.	5	< 5[≠,48]	5.54 ± 0.19	67 ± 16	5	n.a.[≠,42]
	Quin	< 5[≠]	47 ± 3	n.d.	5	< 5[≠,43]	< 5	30 ± 5	5	< 5[49]
	SKF	7.63 ± 0.15	102 ± 2	n.d.	9	8.55[43]	9.53 ± 0.43	84 ± 4	6	8.70[*,45]
	Apo	n.d.	n.d.	n.d.		-	8.44 ± 0.22	101 ± 8	5	8.42[39,48,50]
	Buta	<5[≠]	-9 ± 1	7.96 ± 0.17	5[a] /7[b]	7.57[47]	7.32 ± 0.46	-43 ± 7	5	9.20[51]
	SCH	8.56 ± 0.11	16 ± 1	9.69 ± 0.17	5[a] /5[b]	9.96[11]	8.02 ± 0.95	56 ± 6	5	8.80[#,52]
	Halo	n.a.	n.a.	7.39 ± 0.16	5[a] /8[b]	7.57[11]	n.d.	n.d.		-
	Spip	n.d.	n.d.	5.80 ± 0.04	0[a] /3[b]	6.45[11]	n.d.	n.d.		-
$D_{2l}R$				$miniG_{si1}$						
	Dopa	7.43 ± 0.16	99 ± 2	n.d.	8	7.05[53]	8.77 ± 0.18	100	6	7.55[42]
	Prami	7.51 ± 0.1	100	n.d.	5	5.77[48]	9.49 ± 0.18	67 ± 16	5	9.04[54]
	Quin	7.36 ± 0.06	103 ± 2	n.d.	8	7.11[55]	9.20 ± 0.18	30 ± 5	5	8.77[56]
	SKF	5.81 ± 0.1	33 ± 1	n.d.	5	5.97[57]	6.87 ± 0.20	22 ± 11	5	n.a.[†,≠,58]
	Apo	7.28 ± 0.09	100 ± 2	n.d.	7	7.48[16]	9.09 ± 0.25	101 ± 8	5	8.80[50]
	Buta	n.d.	n.d.	n.d.		-	8.04 ± 0.56	-44 ± 8	5	8.29[16]
	SCH	n.d.	n.d.	5.82 ± 0.10	5	5.92[57]	7.22 ± 0.53	58 ± 5	5	5.96[$,40]
	Halo	n.d.	n.d.	10.1 ± 0.35	5	8.89[16]	n.d.	n.d.		-
	Spip	n.d.	n.d.	10.5 ± 0.13	6	9.49[11]	n.d.	n.d.		-

	Nemo	n.d.	n.d.	10.9 ± 0.11	5	9.76[16]	n.d.	n.d.		-
D_3R			$miniG_{o1}$							
	Dopa	5.78 ± 0.35	94 ± 4	n.d.	5	7.74[42]	8.36 ± 0.06	100	5	8.80[42]
	Prami	8.18 ± 0.28	100	n.d.	6	7.98[48]	8.86 ± 0.17	103 ± 6	5	9.52[42]
	Quin	7.85 ± 0.15	98 ± 1	n.d.	6	7.39[48]	8.92 ± 0.03	89 ± 10	5	10.0[59]
	SKF	6.02 ± 0.12	55 ± 3	n.d.	6	< 5[57]	5.84 ± 0.22	-122 ± 56	5	5.96†,[58]
	Apo	7.55 ± 0.11	93 ± 3	n.d.	5	7.59[48]	7.76 ± 0.15	118 ± 4	5	8.1†,[49]
	Buta	< 4≠	-43 ± 9	8.31 ± 0.13	5[a] /5[b]	8.59[16]	6.83 ± 0.36	-32± 2	5	6.49[60]
	SCH	n.a.≠	n.a.	< 4≠	5[a] /5[b]	< 5[57]	< 5≠	n.a.≠	5	-
	Halo	n.d.	n.d.	8.79 ± 0.24	0[a] /6[b]	8.90[16]	n.d.	n.d.		-
	Spip	< 4≠	-16 ± 3	9.28 ± 0.21	5[a] /6[b]	9.49[11]	n.d.	n.d.		-
	Nemo	n.d.	n.d.	10.5 ± 0.19	0[a] /6[b]	9.20[61]	n.d.	n.d.		-
D_4R				$miniG_{o1}$						
	Dopa	6.15 ± 0.49	23 ± 6	n.d.	5	6.32[11]	8.22 ± 0.28	100	6	8.52[62]
	Prami	n.a.≠	n.a.	n.d.	5	6.86[63]	9.00 ± 0.11	100 ± 2	5	-
	Quin	6.24 ± 0.16	100	n.d.	5	7.47[48]	9.06 ± 0.19	108 ± 5	6	9.70[62]
	SKF	n.a.≠	n.a.≠	n.d.	5	-	6.19 ± 0.19	61 ± 9	6	n.a.†,≠,[58]
	Apo	n.d.	n.d.	n.d.		-	8.02 ± 0.23	99 ± 1	5	8.22†,[64]
	Buta	n.d.	n.d.	8.23 ± 0.23	5	7.42[11]	6.69 ± 0.14	-43 ± 7	5	-
	SCH	n.d.	n.d.	n.d.		-	6.20 ± 0.10	83 ± 3	5	-
D_5R				$miniG_s$						
	Dopa	8.00 ± 0.11	100	n.d.	8	7.85[47]	9.09 ± 0.11	100	6	6.73[45]
	Prami	< 5≠	44 ± 1	n.d.	5	< 5≠,[48]	< 5≠	56 ± 6	5	< 5[43]
	Quin	< 5≠	29 ± 3	n.d.	5	< 5≠,[48]	5.36 ± 0.14	40 ± 3	5	-

SKF	7.33 ± 0.10	104 ± 2	n.d.	6	-	9.07 ± 0.11	104 ± 4	5	-
Apo	n.d.	n.d.	n.d.		-	7.95 ± 0.18	106 ± 3	5	-
Buta	5.81 ± 0.19	-10 ± 2	9.32 ± 0.13	6[a] /5[b]	8.30[11]	7.79 ± 0.37	-37 ± 6	5	-
SCH	8.71 ± 0.08	17 ± 2	11.2 ± 0.79	5[a] /5[b]	9.52[11]	9.42 ± 0.17	54 ± 4	5	-
Halo	n.a.[≠]	n.a.[≠]	7.09 ± 0.06	5[a] /5[b]	7.32[11]	n.d.	n.d.		-

[≠]No non-linear fit possible. *racemic mixture; [#]SCH-23390 non-iodinated analogue; [†]FLIPR assay. [$]p$K_i$ value. Data represent means ± SEM of at least three independent experiments ($N \geq 5$), each performed in triplicate. Dopa = dopamine, Prami = pramipexole, Quin = quinpirole, SKF = (+)-SKF-81297, Apo = (-)-apomorphine, Buta = (+)-butaclamol, SCH = (+)-SCH-23390, Halo = haloperidol, Spip = spiperone, n.a. = not active, n.d. = not determined. [a]Independent experiments in Agonist mode. [b]Independent experiments in Antagonist mode.

2.4.7. Selectivity of miniG Protein Coupling by Dopamine Receptors

To investigate the selectivity of miniG protein coupling by dopamine receptors, HEK293T cells were transiently transfected with 1 µg of dopamine receptor plasmid cDNA ($D_{1\text{-}5}$R-NlucC) and one of the four miniG proteins (NLucN-$mG_{s/i1/q/o1}$). For characterisation we have used dopamine, (+)-SKF-81297 as a D_1-like selective ligand, and pramipexole as a D_2-like selective ligand. For evaluation of the data, the $\Delta\log(E_{max}/EC_{50})$ was calculated and normalized to the canonical coupling of the respective dopamine receptor activated by dopamine. The canonical signalling was set to '0.00', whereby a negative value shows a decreased selectivity and a positive value increased selectivity.

2.4.8. D_1-like Receptor miniG Protein Selectivity

Within the D_1-like family, both receptors showed preference in their selectivity of miniG protein coupling and also exhibit the ability to couple with other subtypes (Figure 2.5). Additional to the canonical coupling with mG_s, the D_1R-NlucC recruited mG_{i1} through dopamine and (+)-SKF-81297 activation ($\Delta\log(E_{max}/EC_{50})$: dopamine = -0.13 / (+)-SKF-81297 = -0.15) with a high efficacy, but lower potency compared to mG_s. The D_5R-NlucC was also able to recruit mG_{i1} ($\Delta\log(E_{max}/EC_{50})$: dopamine = -0.11 / (+)-SKF-81297 = -0.14), however, both ligands had 10-fold lower efficacy compared to mG_s coupling. The D_1R-NlucC recruited mG_q upon binding any of the three ligands, where, surprisingly, the activation profile was pramipexole > dopamine > (+)-SKF-81297 ($\Delta\log(E_{max}/EC_{50})$: -0.008 > -0.29 > -0.48). Though, in the case of efficacy the selectivity changed to (+)-SKF-81297 > dopamine > pramipexole. The D_5R-NlucC failed to recruit mG_q, and neither receptor recruited mG_{o1} with the compounds tested.

2.4.9. D_2-like Receptor miniG Protein Selectivity

In the D_2-like family, the D_3R-NlucC and D_4R-NlucC were both selective for $mG_{i1/o1}$ (Figure 2.6). Only the D_3R-NlucC coupled to mG_{o1} with all three ligands ($\Delta\log(E_{max}/EC_{50})$: dopamine = 0.00 / pramipexole = 0.29 / (+)-SKF-81297 = -3), but with low potency for dopamine and pramipexole. The mG_{o1} protein was recruited to the D_4R-NlucC after being activated by dopamine ($\Delta\log(E_{max}/EC_{50})$: -0.06) and (-)-quinpirole, with low potency and efficacy for dopamine and surprisingly low potency for (-)-quinpirole. In the case of the D_{2l}R-NlucC, dopamine coupled the receptor to mG_q additional to its canonical coupling (mG_{i1} and mG_{o1}), with very low efficacy. Interestingly, (+)-SKF-81297 and pramipexole were not able to couple D_{2l}R-NlucC to the mG_q, but recruited both mG_{i1} and mG_{o1} ($\Delta\log(E_{max}/EC_{50})$: mG_{i1} dopamine = 0.00 / (+)-SKF-81297 = 0.22 / pramipexole = 0.15; mG_{o1} dopamine = -0.05 / (+)-SKF-81297 = -0.29 / pramipexole =

-0.06). Concentration responses for all ligand/receptor pairs are shown in the Appendix (Figure 7.21 and 7.22).

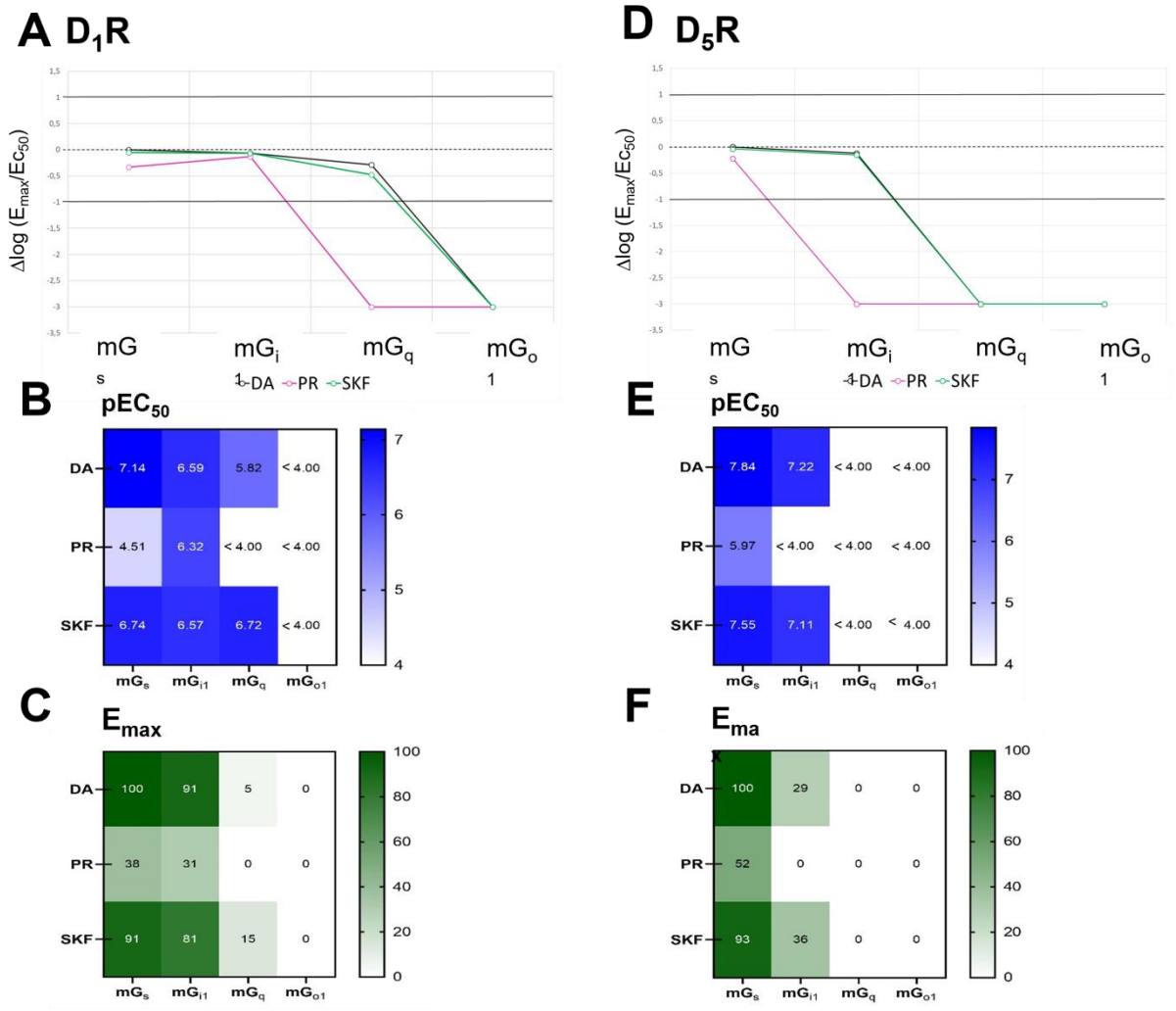

Figure 2.5: Selectivity profile of miniG protein recruitment at D_1-like receptors. **A:** Selectivity for the recruitment of four different miniG proteins ($miniG_{s/i1/q/o1}$) at the D_1R using the $\Delta\log(E_{max}/EC_{50})$ normalized to the dopamine/mG_s response. The pEC_{50} **B:** and E_{max} **C:** are shown separately as heatmaps, where the 100% E_{max} is taken as the mG_s response to dopamine. **D:** Selectivity for the recruitment of four different miniG proteins ($miniG_{s/i1/q/o1}$) at the D_5R using the $\Delta\log(E_{max}/EC_{50})$ normalized to the dopamine/mG_s response. The pEC_{50} **E:** and E_{max} **F:** are shown separately as heatmaps, where the 100% E_{max} is taken as the mG_s response to dopamine. Data are expressed as the means of $N \geq 3$ independent experiments, each performed in triplicate. DA = dopamine, PR = pramipexole, SKF = (+)-SKF-81297.

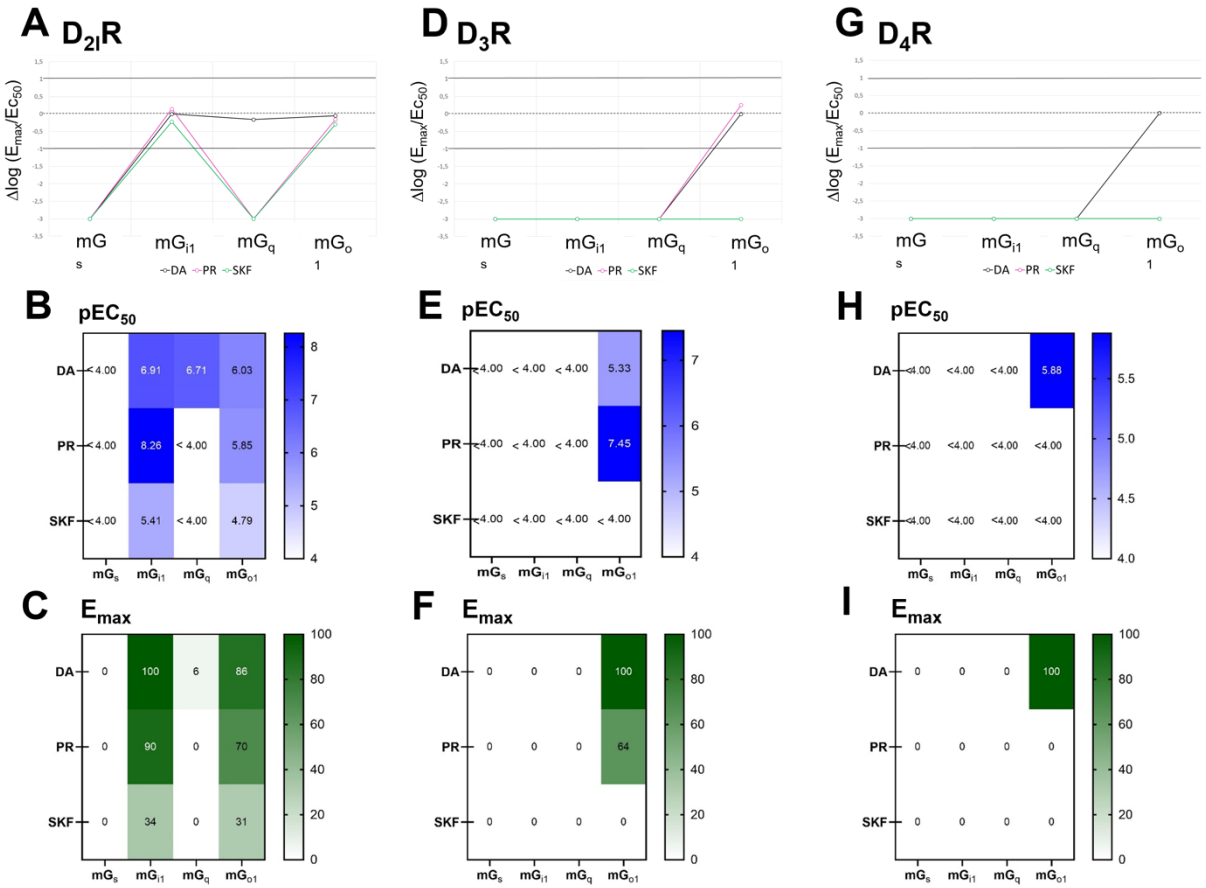

Figure 2.6: Selectivity profile of miniG protein recruitment at D_2-like receptors. **A:** Selectivity for the recruitment of four different miniG proteins (mini$G_{s/i1/q/o1}$) at the D_2R using the $\Delta\log(E_{max}/EC_{50})$ normalized to the dopamine/mG_{i1} response. The pEC_{50} **B:** and E_{max} **C:** are shown separately as heatmaps, where the 100% E_{max} is taken as the mG_{i1} response to dopamine. **D:** Selectivity for the recruitment of four different miniG proteins (mini$G_{s/i1/q/o1}$) at the D_3R using the $\Delta\log(E_{max}/EC_{50})$ normalized to the pramipexole/mG_{o1} response. The pEC_{50} **E:** and E_{max} **F:** are shown separately as heatmaps, where the 100% E_{max} is taken as the mG_{o1} response to pramipexole. **G:** Selectivity for the recruitment of four different miniG proteins (mini$G_{s/i1/q/o1}$) at the D_4R using the $\Delta\log(E_{max}/EC_{50})$ normalized to the (-)-quinpirole/mG_{o1} response. The pEC_{50} **H:** and E_{max} **I:** are shown separately as heatmaps, where the 100% E_{max} is taken as the mG_{o1} response to (-)-quinpirole. Data are expressed as the means of $N \geq 3$ independent experiments, each performed in triplicate. DA = dopamine, PR = pramipexole, SKF = (+)-SKF-81297; Quin = (-)-quinpirole.

2.4.10. Activation of G Proteins by the Five Dopamine Receptor Subtypes using G-CASE Sensors

In order to expand on the selectivity observations seen with the miniG protein recruitment, the five dopamine receptors were transiently transfected with eight different G-CASE sensors (G_{i1}, G_{i2}, G_{i3}, G_{o1}, G_z, G_q, and G_{13}; G_s-CASE was used as a stable cell line) into HEK293T cells to measure ligand-dependent G protein activation. Receptor expressions were consistent between the G-CASE sensors, with D_3R and D_5R usually expressing the lowest, although showed some variation between experiments, and dopamine receptor co-expression had no effect on sensor expression (ELISA and immunofluorescence, Figure 7.11 - 7.20). As with the miniG assay, ligands were selected for checking subtype and endogenous activity; endogenous ligand dopamine, D_1-like selective (+)-SKF-81297, and D_2-like selective pramipexole.

The endogenous ligand dopamine was used as the reference ligand for sensor selectivity measurements. G_{13} was not activated by any receptor/ligand combination. Concentration responses for all ligand/receptor/sensor combinations are shown in the Supporting Information, along with negative control ligand responses in wild type HEK293T cells expressing only the G-CASE sensor (Appendix, Figure 7.23 - 7.28).

2.4.11. D_1-like Receptor non-canonical G protein Activation

For the D_1-like receptors, G_s-CASE was used as the canonical reference sensor. The D_1R was the most selective for G protein activation, limited to $G_{s,z,o1,q}$-CASE (Figure 2.7). The selectivity profile for dopamine was $G_s > G_q > G_{o1} > G_z$ ($\Delta\log(E_{max}/EC_{50})$: 0.00, -1.18, -1.29, -1.86, respectively). (+)-SKF-81297 produced a 20-fold greater G_s-CASE response at the D_1R with a selectivity profile for $G_s > G_{o1} > G_q > G_z$ ($\Delta\log(E_{max}/EC_{50})$: 1.47, 0.92, -0.11, -0.85, respectively), whereas pramipexole could only produce weak $G_{i2,q,z}$-CASE activation. E_{max} and therefore $\Delta\log(E_{max}/EC_{50})$ could not be calculated for the G_{i2} sensor as the reference ligand, dopamine, did not activate G_{i2}-CASE up to the 10 μM tested.

When bound to dopamine, the D_5R could activate all $G_{s,i/o/z,q}$ subtypes, with a selectivity for $G_s > G_{i1/z} > G_{i2/o1} > G_{q/i3}$ (G_s 4–40-fold over $G_{z/i1}$-$G_{q/i3}$, respectively, Figure 2.7). Pramipexole concentrations up to 10 μM could not activate G_q-CASE, G_{i2}-CASE or G_s-CASE at the D_5R, however similar potencies and efficacies to dopamine were seen for $G_{i1,i3,o1,z}$-CASE. Similarly, (+)-SKF-81297 could not produce $G_{i1,q}$-CASE responses through D_5R, however the D_1-selective compound had a 5-fold greater G_s response than dopamine, and a 40-fold decrease in G_z activation ($\Delta\log(E_{max}/EC_{50})$ G_s = 0.48; G_z = -1.64).

2.4.12. D_2-like Receptor non-canonical G protein Activation

G_z-CASE was used as the reference sensor for $D_{2l,3,4}$Rs as this sensor produced the highest potency response to dopamine. Dopamine could activate all $G_{i/o/z}$-CASE subtypes at the D_2-like receptors, with a preference for G_z, followed by G_{o1} (Figure 2.8). For the G_i subtypes, D_3R and D_4R both showed selectivity for $G_{i3} > G_{i2} > G_{i1}$ ($\Delta\log(E_{max}/EC_{50})$ D_3R = 0.11, -0.60, -0.96, D_4R = -0.77, -0.79, -1.19, respectively), whereas $D_{2l}R$ had a greater response for $G_{i1} > G_{i2} > G_{i3}$ ($\Delta\log(E_{max}/EC_{50})$ $D_{2l}R$ = -0.47, -0.57, -1.15, respectively). Dopamine could activate G_q-CASE at all three receptors. G_s-CASE activation by dopamine was weak at $D_{2l}R$ and D_4R, and not detectable at the D_3R up to 10 µM ($\Delta\log(E_{max}/EC_{50})$: -2.08, -2.14, respectively). The selective ligand pramipexole could not activate G_s at any of the D_2-like receptors, but produced an increase in $\Delta\log(E_{max}/EC_{50})$ compared to dopamine for most $G_{i/o/z}$ subtypes (around 5-fold increase, excluding $G_{o1,i1}$ for D_3R and $G_{z,i3}$ for D_4R; Figure 2.8). (+)-SKF-81297 could activate G_s-CASE, G_{o1}-CASE and G_z-CASE for all D_2-like receptors, although no $\Delta\log(E_{max}/EC_{50})$ value could be calculated for the G_s-CASE with D_3R as the reference ligand dopamine did not produce a response up to 10 µM. At the $D_{2l}R$, there was activation of $G_{i1,i2,q}$-CASE using (+)-SKF-81297 that was unique between the D_2-like receptors.

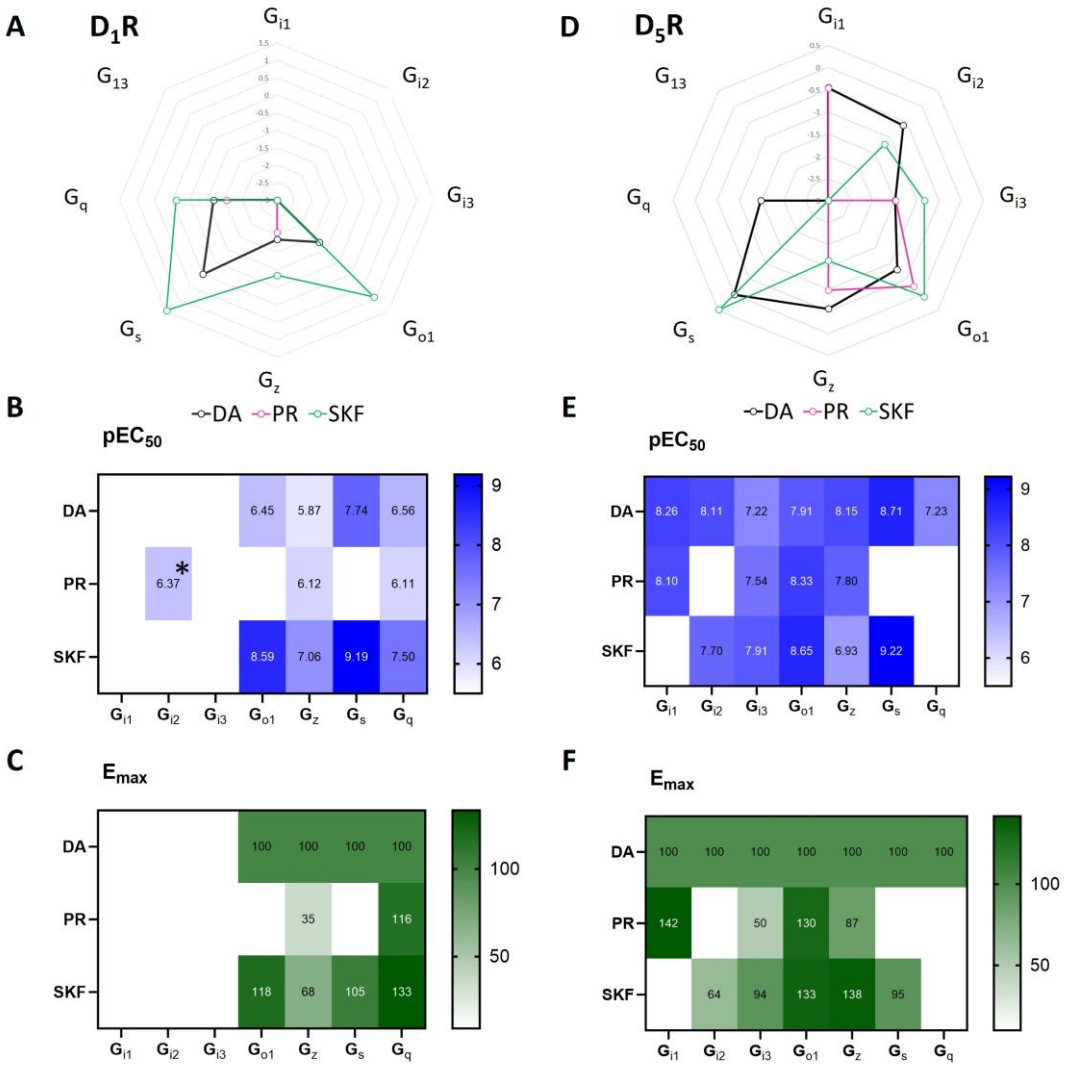

Figure 2.7: G protein selectivity profile of D_1-like receptors determined by the G-CASE assay. The endogenous ligand dopamine, D_2-like selective pramipexole and D_1-like selective (+)-SKF-8129 are assessed for ligand induced G protein selectivity. **A:** web of selectivity at D_1R for the eight different G-CASE constructs (G_{i1}, G_{i2}, G_{i3}, G_{o1}, G_z, G_s, G_q, G_{13}) using the $\Delta\log(E_{max}/EC_{50})$ referenced to the dopamine/G_s response. The pEC_{50} **B:** and E_{max} **C:** are shown separately as heatmaps, where the 100% E_{max} is taken as the response to dopamine for each sensor. **D:** web of selectivity at D_5R for the eight different G-CASE constructs (G_{i1}, G_{i2}, G_{i3}, G_{o1}, G_z, G_s, G_q, G_{13}) using the $\Delta\log(E_{max}/EC_{50})$ referenced to the dopamine/G_s response. The pEC_{50} **E:** and E_{max} **F:** are shown separately as heatmaps, where the 100% E_{max} is taken as the response to dopamine for each sensor. Data are expressed as the means of N = 5 independent experiments, each performed in triplicate. DA = dopamine, PR = pramipexole, SKF = (+)-SKF-81297. Note the logarithmic scale of the web axes. White spaces without numbers in the heatmaps indicate no measureable response up to 10 µM ligand, apart from *no E_{max} could be caculated for the G_{i2} sensor with pramipexole at the D_1R due to no response to dopamine up to 10 µM.

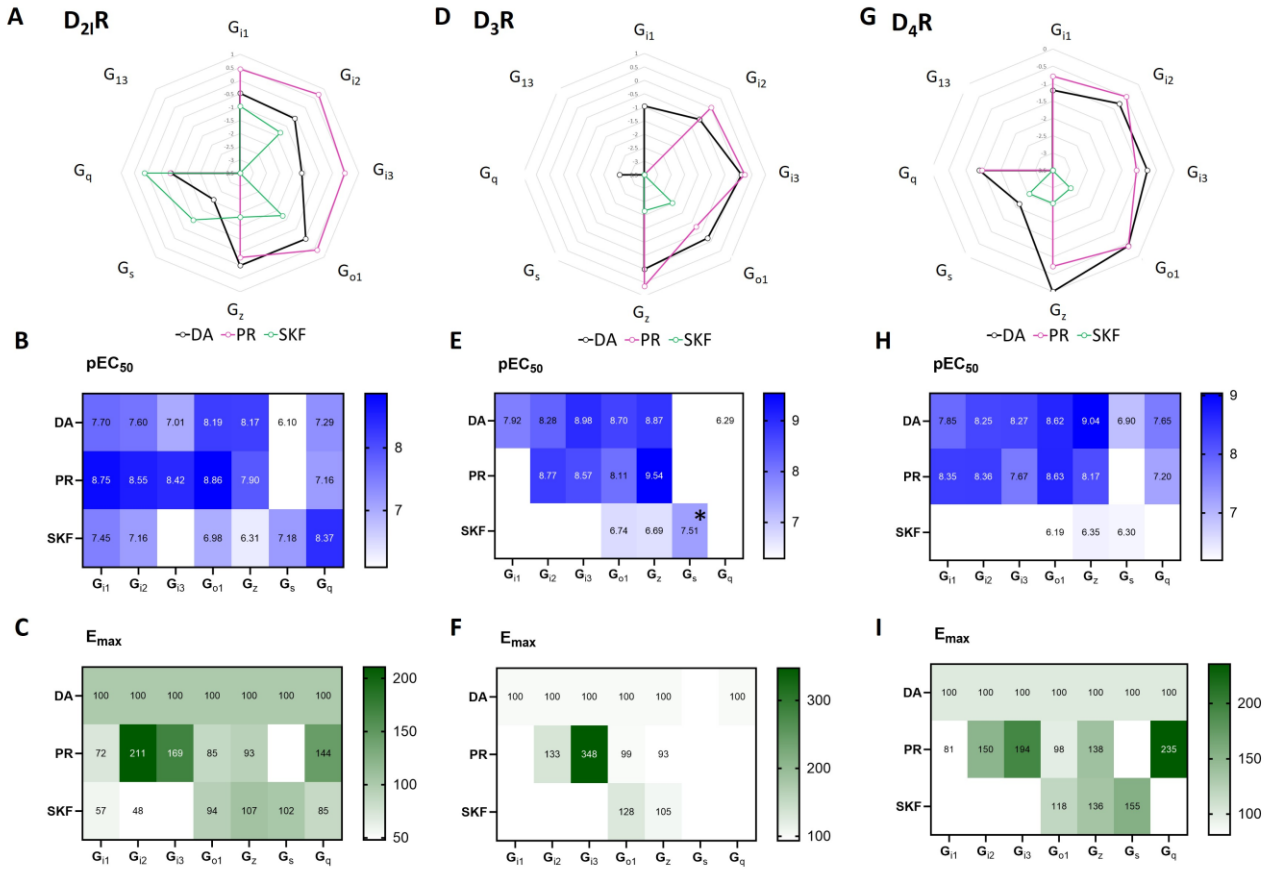

Figure 2.8: G protein selectivity profile of D_2-like receptors determined by the G-CASE assay. The endogenous ligand dopamine, D_2-like selective pramipexole and D_1-like selective (+)-SKF-8129 are assessed for ligand induced G protein selectivity. **A:** web of selectivity at $D_{2l}R$ for the eight different G-CASE constructs (G_{i1}, G_{i2}, G_{i3}, G_{o1}, G_z, G_s, G_q, G_{13}) using the $\Delta\log(E_{max}/EC_{50})$ relative to the dopamine/G_z response. The pEC_{50} **B:** and E_{max} **C:** are shown separately as heatmaps, where the 100% E_{max} is taken as the response to dopamine for each sensor. **D:** web of selectivity at D_3R for the eight different G-CASE constructs (G_{i1}, G_{i2}, G_{i3}, G_{o1}, G_z, G_s, G_q, G_{13}) using the $\Delta\log(E_{max}/EC_{50})$ relative to the dopamine/G_z response The pEC_{50} **E:** and E_{max} **F:** are shown separately as heatmaps, where the 100% E_{max} is taken as the response to dopamine. **G:** web of selectivity at D_4R for the eight different G-CASE constructs (G_{i1}, G_{i2}, G_{i3}, G_{o1}, G_z, G_s, G_q, G_{13}) using the $\Delta\log(E_{max}/EC_{50})$ relative to the dopamine/G_z response. The pEC_{50} **H:** and E_{max} **I:** are shown separately as heatmaps, where the 100% E_{max} is taken as the response to dopamine for each sensor. Data are expressed as the means of $N = 5$ independent experiments, each performed in triplicate. DA = dopamine, PR = pramipexole, SKF = (+)-SKF-81297. Note the logarithmic scale of the web axes. White spaces without numbers in the heatmaps indicate no measureable response up to 10 µM ligand, apart from *no E_{max} could be caculated for the G_s sensor with (+)-SKF-8129 at the D_3R due to no response to dopamine up to 10 µM.

2.4.13. Calcium mobilization of dopamine receptors

The coupling of mG_q to the D_1R-NlucC and $D_{2l}R$-NlucC and dissociation of G_q-CASE with all subtypes prompted the investigation of the downstream calcium ion mobilization of the five dopamine receptors with the endogenous agonist dopamine. HEK293A cells were transiently transfected with the wildtype dopamine receptor constructs used in the CAMYEN cAMP assay, with or without the overexpression of $G\alpha_q$, and loaded with 1 µM Fluo-8 AM calcium dye, which increases in fluorescence intensity when bound to calcium ions. To selectively block native adrenoceptors and serotonin receptors that should be present in the cells and may bind dopamine, 1 µM propranolol was added at the same time as the dye and remained throughout the experiment.

Concentration-dependent calcium responses to dopamine were detected with D_1R and D_5R, both with and without overexpression of the $G\alpha_q$ subunit (Figure 2.9). The $D_{2l}R$ could only produce an influx of calcium in response to dopamine activation when the $G_{\alpha q}$ subunit was also overexpressed in the HEK cells. For the D_3R and D_4R, the efficacy of calcium mobilization was similar to wildtype cells without dopamine receptor expression. Coupling and activation of G_s can cause a downstream calcium response, therefore the statistical significance of the addition of overexpressed $G\alpha_q$ was tested for both the E_{max} and pEC_{50} generated in each calcium experiment to determine the impact of $G\alpha_q$ expression in the system (Figure 2.9). Both the D_1R and $D_{2l}R$ caused a significant increase in the efficacy of the calcium response detected in the cells when $G\alpha_q$ was overexpressed, suggesting that coupling to the G_q is at least partly responsible for the calcium mobilization with dopamine for these receptors in HEK293A cells. No change in pEC_{50} was discovered for any receptor. Kinetic response curves are provided in the appendix (Figure 7.29)

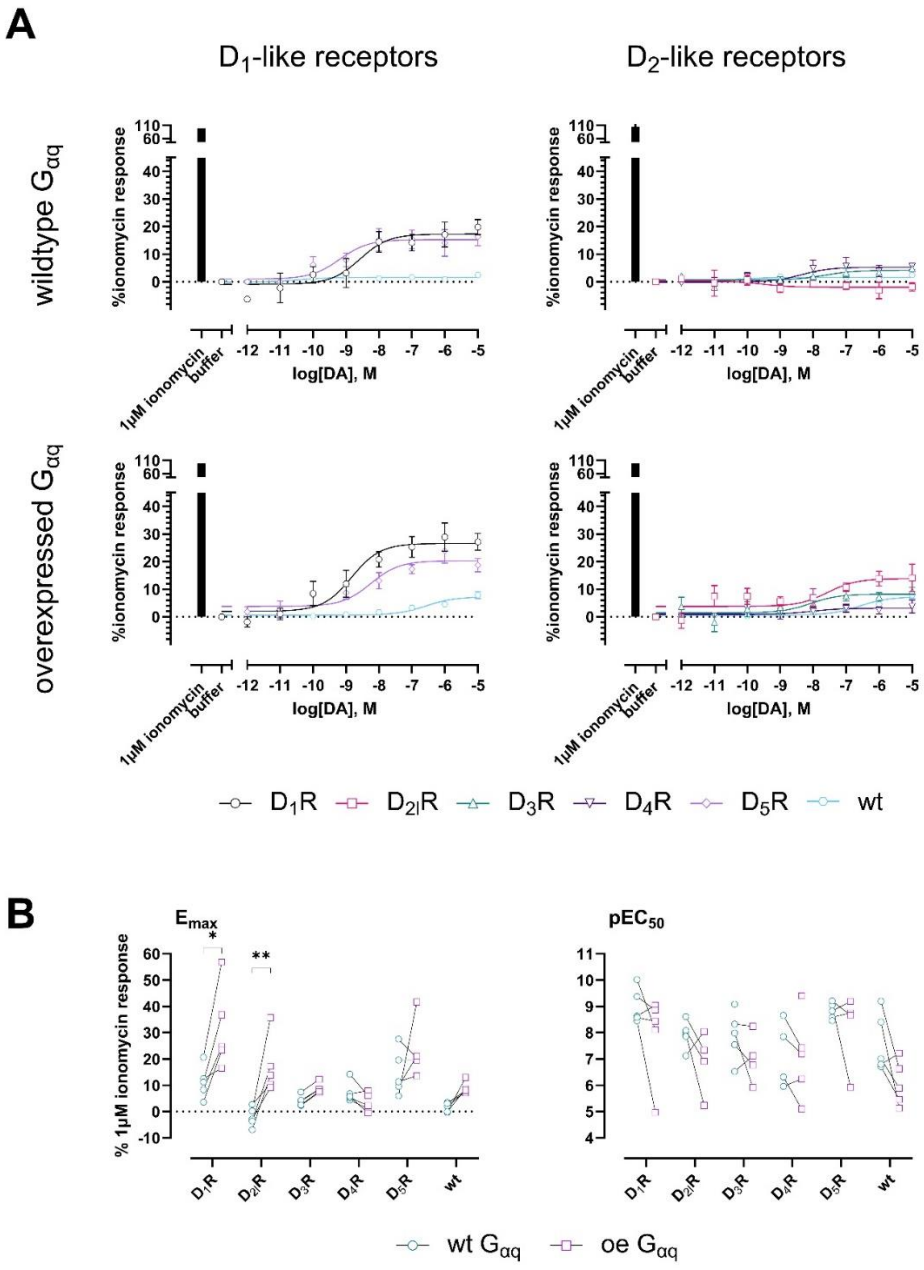

Figure 2.9: Calcium mobilisation of the five dopamine receptors in HEK293A cells. HEK293A cells were transiently transfected with dopamine receptor or empty plasmid vector with or without $G\alpha_q$. **A:** Concentration response curves of calcium ion influx for the D_1-like and D_2-like receptors with wildtype or overexpressed $G\alpha_q$. The bar on the left represents the 1 µM ionomycin response (100%) used to normalise the data. **B:** E_{max} and pEC_{50} values from each individual expreiment used to create the response curves in (A), with differential $G\alpha_q$ expression paired by the experimental day/transfection. Repeated measures one-way ANOVA was used to determine if E_{max} ($F(11, 44) = 8.42$, $p < 0.0001$) or pEC_{50} values ($F(11, 44) = 1.63$, $p = 0.12$) significantly differed between wildtype and overexpressed $G\alpha_q$. Šídák's multiple comparisons test concluded that overexpression of $G\alpha_q$ increased the E_{max} of the calcium response for D_1R (*$p = 0.0005$) and $D_{2l}R$ (**$p = 0.0009$). $N = 5$ individual experiments from different transfections on different days, carried out in triplicate. DA = dopamine, wt = wildtype, oe = overexpressed.

2.5. Discussion

2.5.1. Canonical G protein signaling

The three bioluminescence-based assays used in this study have highlighted important pharmacological responses of the five dopamine receptor subtypes. Functional characterisation of the dopamine receptors through their canonical pathways was performed using the CAMYEN cAMP assay and miniG protein recruitment. All agonists (dopamine, pramipexole, (+)-SKF-81297, (-)-apomorphine, and (-)-quinpirole) were sucessfully characterised for both acute receptor activation with the cannonical miniG proteins and downstream cAMP response. The assays are suitable for detecting ligand potency, efficacy and selectivity. Either methodology can be used for basic functional characterization of dopamine ligands.

2.5.1.1. Antagonist canonical response

As expected, haloperidol, (+)-SCH-23390 and (+)-butaclamol acted as antagonists at all dopamine receptors in the miniG recruitment assay. (+)-butaclamol acted as an inverse agonist in agonist mode and for cAMP production. Confirming our results, (+)-butaclamol has previously been reported to reverse the $D_{1,5}$Rs confirmation from the active to inactive form,[52,65] and has shown to be an efficacious inverse agonist at the D_2-like receptors.[52,66] (+)-SCH-23390 is known as a selective D_1-like receptor antagonist. Intriguingly, (+)-SCH-23390 could act as a partial agonist by itself at the $D_{1,2l,4,5}$Rs and was unable to completely block miniG_s coupling in antagonist mode, noted before in other assays.[52,65] Affinity of (+)-SCH-23390 for 5-HT_{2A} receptors could cause G_q responses,[57] reflecting the cAMP increase by D_1-like receptors, however this would not account for the agonist effect of (+)-SCH-23390 at the $D_{2l,4}$Rs in our cAMP assay. We therefore hypothesize that (+)-SCH-23390 acts as a partial agonist at the $D_{1,2l,4,5}$Rs, but not the D_3R, creating an interesting prospect for selective drug design.

2.5.1.2. Comparison between cAMP generation and canonical G protein recruitment

Between the assays, higher potencies were always observed in the CAMYEN assay than with miniG protein recruitment due to the more proximal position of G protein recruitment to ligand binding than the cAMP response further downstream in the signaling cascade.[1,35] Of interest, while (+)-SKF-81297 produced a partial response at the D_1R in the cAMP and G_s-CASE assays, there was a full agonist response with the miniG_s. This partial response could be due to a potent β-arrestin recruitment by (+)-SKF-81297, measured in previous studies, causing internalization and reducing G protein activation at the membrane and when the receptor is recycled.[45,67] The miniG_s recruitment was perhaps not affected because of the higher affinity of miniG_s, lowering the turn-

over of the sensor when tightly bound to the receptor and obstructing arrestin interaction.[1] Our theory represents only one postulation, and indeed other factors such as G protein subunit promiscuity and off target effects may also be involved in the difference between the assay results. Compared to the CAMYEN assay and literature-reported values, reduced dopamine responses were seen with the $D_{3,4}$Rs in the miniG recruitment assay. With the D_3R, this was unexpected as the D_{2l}R_miniG with dopamine, D_3R_mG_{o1} with all other agonists, and the cAMP responses with dopamine at the D_3R produced values comparable to literature data. We theorize that the NlucC fusion on the C-terminus of the D_3R is impacting the receptor activation in a way that is ligand- and receptor-dependent. Currently, there is no structure of the D_3R with dopamine bound, making it difficult to hypothesize the exact structural significance of these data. For the D_4R, where all ligands except quinpirole failed to produce full agonist responses, we propose the low dopamine response is because the D_4R-NlucC had a 25-fold lower expression than the non-modified receptors (radioligand saturation, Appendix, Figure 7.1 and Table 7.1). Speculatively, the NlucC fragment on the C-terminus could interfere with D_4R trafficking and cell membrane expression, but not the similar D_{2l}R. Palmitoylation of both the D_3R and D_4R C terminus regions has been shown to be more extensive and crucial than the D_{2l}R.[68–70] The D_3R has also been shown to interact with the GPCR regulating protein GIPC via the C-terminus regions,[59] protecting the receptor from degradation. There may also be other factors involved in the differing dopamine activity with C-terminus modification of the D_3R-NlucC and D_4R-NlucC, such as a decreased/enhanced ability for miniG binding that could be ligand-dependent. Lower responses for both these receptors could also be compounded by the reduced presence of the mG_{o1} sensor (ELISA, Appendix Figure 7.10). To the best of our knowledge, this is the first report of C-terminus modifications for an assay affecting the dopamine response at the $D_{3,4}$Rs, and the importance of the C-terminus in their signaling and expression is of interest for future studies.

2.5.1.3. Comparison of individual dopamine receptor G protein subunit coupling

Aside from canonical coupling, patterns of G protein recruitment are important even within sub-families of Gα subunits where the downstream messenger is the same, as subtle differences in the effectors and kinetics of the response cascade are present.[71–73] Targeting G protein selectivity in drug development can therefore lead to useful physiological responses.[25,74–76] To investigate dopamine receptor selectivity of G protein subunits, the miniG recruitment assay was used in combination with the G-CASE G protein activation assay. G-CASE α and γ subunits showed no difference in expression level, however direct comparison between the assay sensors is not possible due to inherent differences in signal windows for the different constructs due to small spatial changes in the position of the Nluc tag within the α subunit and differences in the γ subunits used within each sensor (Figure 7.23-7.28).

2.5.2. G protein selectivity of the endogenous ligand dopamine

2.5.2.1. G_z and dopamine

Dopamine coupled to various G protein subtypes in our miniG and G-CASE assays. Of the inhibitory G protein subunits, G_z-CASE had both the highest potency and efficacy when activated by dopamine binding of all five receptors. G_z couples to both D_2-like[77–81] and D_1-like[76,80,82] families, making it an interesting drug target. Abundantly expressed in the brain, but elsewhere limited to platelets and pancreatic islet cells,[83] G_z protein activation is thought to be involved with the response to psychoactive drugs, circadian rhythm, brain development and reward systems, although the subunit remains under-researched.[84–86] G_z activation has been described before in G protein selectivity with the $D_{2l}R$ and D_3R, though these previous experiments have reported a higher activity of the receptors with G_o proteins.[81,87] This discrepancy is likely due to the difference in kinetics between the G_z and G_o proteins, as G_z is much slower in GTPase catalytic activity than other inhibitory G protein subunits.[88]

2.5.2.2. G_s and $G_{i/o}$ coupling by non-cannonical dopamine innervation

As well as G_z, dopamine could recruit and activate inhibatory subunits at D_1-like receptors. D_5R has been previously shown to recruit the G_z protein[27] and D_1R with the G_o proteins.[89] The inhibitory G protein coupling may therefore have physiological relevance, such as in renal proximal tubules.[90] Conversely, for D_2-like receptors, while there was no indication of coupling between G_s and D_3R for miniG_s or G_s-CASE up to 10 μM, the $D_{2l,4}$Rs showed a low potency activation of the G_s-CASE. To the best of our knowledge, there is no known cell type or physiological relevance known for the impact of this coupling. Recently published bias studies by Hauser and Inoue have shown no coupling between G_s and D_2-like receptors.[26,80]

2.5.2.3. Possible G_q activation and calcium mobilisation by dopamine

G_q coupling (mG_q) and/or dissociation (G_q-CASE) was also detected at all dopamine receptors. Our calcium mobilization assay successfully linked overexpressed $G\alpha_q$ with increased dopamine receptor calcium influx efficacy for D_1R and $D_{2l}R$. In agreement with our findings, D_1-like receptors have been known to couple to G_q subunits.inou[26,27,91–93] This coupling appears to be important in both the cerebral cortex and striatum, although the exact impact of this activation remains unclear. For the $D_{2l}R$, this is in contrast to results using a different G protein BRET-based assay where no G_q activation was reported, potentially due to a change in βγ subunit expression compared to our G-CASE assay.[81,87,94] Physiologically, studies looking at heterodimers of D_1R and D_2R or astrocytic D_2Rs have also seen calcium influx and potential G_q coupling.[95,96] Although not

proved in this study, there is still the potential that the other dopamine receptors may produce a downstream response through G_q as calcium responses were detected, if not significantly altered by $G\alpha_q$ overexpression or different to wild type HEK293A cells. Indeed, D_3R has also been previously reported to show coupling with G_q in some cell types.[93,97,98] Further assays with knock-out ΔGα cells, G protein inhibitors, initisol-1-phosphate detection and potentially other cell types would be required to confirm this. Investigation into the potential for ligand-based selectivity of G_q would also be interesting, as pramipexole appears to decrease G_q activation in D_1-like receptors and increase in D_2-like receptors in relation to dopamine in our G-CASE assay.

2.5.3. Native G protein and Dopamine Receptor Expression

To understand the impact of the G protein coupling profiles with the endogenous ligand dopamine, it is important to consider the expression and abundance of the subunits and receptors in different cell populations. Of the G proteins subunits used in our assays, the $G\alpha_s$, $G\alpha_{i3}$, $G\alpha_q$ and $G_{\alpha 13}$ are thought to be ubiquitous, with the $G\alpha_{i1}$ and $G\alpha_{i2}$ also widely spread.[99] Both $G\alpha_z$ and $G\alpha_{o1}$ are found primarily neuronal tissue, and $G\alpha_z$ can also be found in platelets and pancreatic islet cells.[100] Dopamine receptor expression of all five subtypes is highest in the brain, particularly in the basal ganglia.[101] The basal ganglia similarly expresses all G protein subunits investigated in this paper. However, the expression level of these G protein subunits will vary when compared to another area of the brain, such as the hypothalamus, or body, such as the stomach (where the D_5R is expressed at a high level), or cell type, where $G\alpha_q$ has higher expression in astrocytes than neurons, for example (Table 7.2). Specialized studies into the abundance of receptor and G protein at a single cell level would be of great value to help understand the impact of promiscuous G protein coupling of the dopamine receptors.

2.5.4. G protein coupling of selective ligands

The D_1-like receptor agonist (+)-SKF-81297 produced some interesting new insights into G protein specificity. For D_1-like receptors, (+)-SKF-81297 activated/recruited the same subunits as dopamine, except for $G_{q,i1}$-CASE at the D_5R. With the D_2-like receptors, (+)-SKF-81297 at the $D_{2l,3}Rs$ activated G_s-CASE at a higher potency than dopamine (shown previously possible for D_3R with G_s in CHO and COS-7 cell lines[77,102]), although they both failed to recruit the mG_s. Along with an increase in G_s activation, the $D_{2l}R$ also retains some potency for the $G_{i/o/z}$-CASE and $mG_{i1/o1}$ with (+)-SKF-81297, hence creating a low-efficacy agonistic cAMP response in the CAMYEN assay. Alternatively, (+)-SKF-81297 does not activate G_i subunits at the D_3R nor recruit the $mG_{i1/o1}$, and only weakly activated the $G_{z/o1}$-CASE. Therefore, the result in the cAMP assay where no agonist response was detected could be due to a more dominant G_s recruitment. Future studies could

assess the impact of this through knock-out cells and G protein inhibitors to tease out the G_s response. D_4R did not couple to G_i in any assay in response to (+)-SKF-81297 activation and displayed a partial, low-potency agonistic cAMP decrease, likely via the recruitment of $G_{z/o1}$, as detected with G-CASE.

While (+)-SKF-81297 increased G_s-CASE activation at all receptors (except D_4R), the D_2-like receptor agonist pramipexole recruited and activated $G_{i/o/z}$ proteins. These data suggest that the selective dopamine ligands show an inherent bias in G protein recruitment, although the exact structural mechanism is speculative. Structural insights into the D_1R and D_2R were investigated by Zhuang et al. 2021.[67] The steric clash between the D_2R transmembrane helix 6 (TM6) and α5 helix in the G_s protein impairs G_s protein recruitment. However, interacting residues with (+)-SKF-81297 in the TM5 are conserved between the receptors (Figure 2.10). It is therefore feasible that (+)-SKF-81297 could induce enough conformational change in the TM domains to overcome the steric hindrance of TM6 and accommodate G_s binding. The position of interacting residue $His^{6.55}$ in the D_4R is also altered compared to the $D_{2,3}Rs$ due to the change of $Tyr^{7.35}$ to $Val^{7.35}$, perhaps explaining why there is reduced G_s activity at D_4R with (+)-SKF-81297 compared to the $D_{2,3}Rs$.[103] For pramipexole, G_i protein binding was facilitated through the gap between TM3 and TM5/6 in the D_3R,[103] therefore binding of pramipexole to TM3 in $D_{1,5}Rs$ could help with this interaction, causing the increase in $G_{i/o/z}$ subunit recruitment and activation (Figure 2.10). In summary, structural studies into these phenomena would be of interest to understand the apparent ligand-induced selectivity of G protein binding at the dopamine receptors.

2.5.5. G-CASE vs. miniG recruitment results

There were several differences between the miniG recruitment and G-CASE activation. One hypothesis that this is due to the loss of the GTPase region in the miniG proteins. Recently, Jang et al. 2022[104] described a model whereby the GTPase activity of the G protein is a critical determinant of its coupling selectivity, perhaps more than the structural compatibility between the GPCR and the G protein. However, it has also been shown that some apparent subunit 'dissociation' in G_{12} BRET assays similar to the G-CASE shown here are in fact not effective to downstream signaling and may simply be subtle movements of Gα relative to Gγ.[105] Tagging positions of the Gα subunits are also different between the sensors, which may change the true sensor dissociation range; for example, when the Gα-Gβγ interface opens under ligand stimulation of the receptor but only rotates the Gα subunit, not causing full dissociation.[106]

We therefore suggest that subunit dissociation, G protein recruitment and secondary messengers are important to assess the receptor-ligand response as no method alone produces a full profile of G protein responses.

2.5.6. Study limitations

Although we have been thorough in our characterization of the five dopamine receptors with these assays, some G_{α} subtypes and common receptor isoforms were not included in this study due to time constraints. Responses to G_{olaf}, G_{oB}, other G_q family subunits, $G_{11/14/15}$, and the $D_{2short}R$ or known D_4R isoforms would be of great interest. As well as investigating G protein activation of ligands specific for the two different subclasses ((+)-SKF-81297 for D_1-like and pramipexole for D_2-like), it would also be advisable to use selective compounds for the individual receptors, although it is particularly difficult to find subtype-selective ligands for the D_2-like receptors (D_2R, D_3R and D_4R). Nevertheless, it would certainly be interesting to investigate compounds such as benperidol, 7-OH-DPAT and aripriprazole.[107–109] Future studies could also investigate the impacts of natively expressed G proteins in the recombinant cells by using CRISPR/Cas9 knockout cell lines and G protein inhibitors with even more downstream assays. For our cell systems, receptor expression was comparable but not identical, which may alter the potencies and signal windows of our bioluminescent assays. As discussed, the C-terminus modification of a fused NlucC protein used in the miniG recruitment assay could also have an impact on the dopamine receptor expression, binding and signaling in subtle ways that will require further examination. It is also necessary to confirm findings first discovered in overexpressed recombinant systems, such as the HEK293T cells used here, with endogenous protein expression, primary cells and animal models to aid with translational efforts.

2.6. Conclusion

In conclusion, this study has successfully characterized the five dopamine receptors with both canonical and selective G protein activation. We have demonstrated that it is important to undertake full ligand pharmacological characterization to understand the acute and downstream effects. G protein selectivity by dopamine receptors is a complex and interesting target for drug discovery, for which our assay systems represent valuable and important tools.

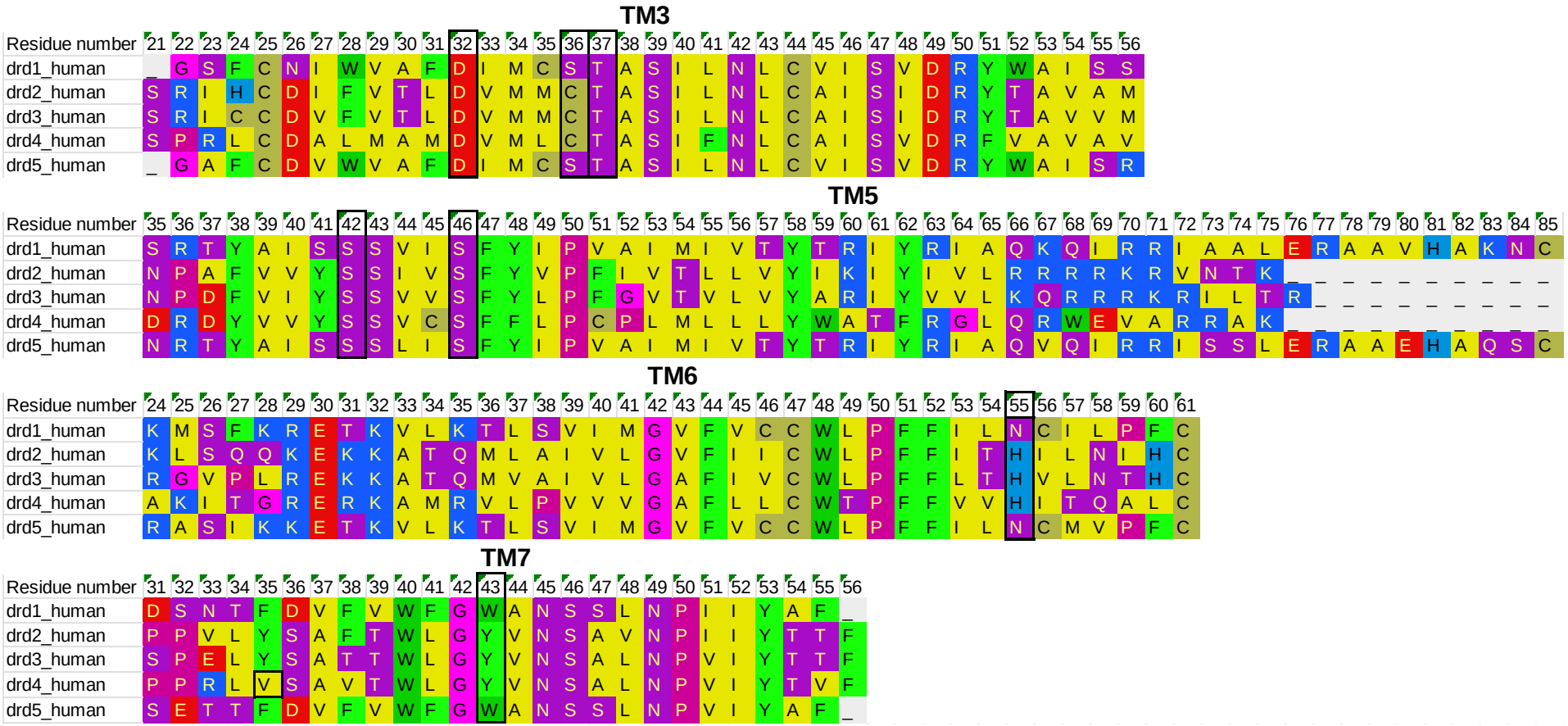

Figure 2.10: Interacting residues between the dopamine receptors and (+)-SKF-81297 or pramipexole. Important transmembrane helix residues are outlined in bold. For (+)-SKF-81297, interacting residues in the TM5 are conserved between the receptors ($Ser^{5.42}$ and $Ser^{5.46}$), $Trp^{7.43}$ in TM7 of the $D_{1,5}Rs$ is changed for a similar bulky residue, $Tyr^{7.43}$, in the $D_{2,3,4}Rs$, and the TM6 interacting residue $Asn^{6.55}$ in the D_1R is replaced with $His^{6.55}$ in the $D_{2,3,4}Rs$, still allowing for hydrogen bonding with the ligand. $Tyr^{7.35}$ becomes $Val^{7.35}$ in the D_4R, changing availability for $His^{6.55}$. Pramipexole also interacts with $His^{6.55}$ and the three interacting residues in TM3, $Asp^{3.32}$, $Cys/Ser^{3.36}$ and $Thr^{3.37}$, are all conserved between receptor subtypes. Sequence alignment was performed using GPCRdb.[110,111]

2.7 References

(1) Wan, Q.; Okashah, N.; Inoue, A.; Nehmé, R.; Carpenter, B.; Tate, C. G.; Lambert, N. A. Mini G protein probes for active G protein-coupled receptors (GPCRs) in live cells. *The Journal of biological chemistry* **2018**, *293* (19), 7466–7473. DOI: 10.1074/jbc.RA118.001975.

(2) Dal Prà, I.; Armato, U.; Chiarini, A. Family C G-Protein-Coupled Receptors in Alzheimer's Disease and Therapeutic Implications. *Frontiers in pharmacology* **2019**, *10*, 1282. DOI: 10.3389/fphar.2019.01282.

(3) Fredriksson, R.; Lagerström, M. C.; Lundin, L.-G.; Schiöth, H. B. The G-protein-coupled receptors in the human genome form five main families. Phylogenetic analysis, paralogon groups, and fingerprints. *Molecular pharmacology* **2003**, *63* (6), 1256–1272. DOI: 10.1124/mol.63.6.1256.

(4) Hilger, D.; Kumar, K. K.; Hu, H.; Pedersen, M. F.; O'Brien, E. S.; Giehm, L.; Jennings, C.; Eskici, G.; Inoue, A.; Lerch, M.; Mathiesen, J. M.; Skiniotis, G.; Kobilka, B. K. Structural insights into differences in G protein activation by family A and family B GPCRs. *Science (New York, N.Y.)* **2020**, *369* (6503). DOI: 10.1126/science.aba3373.

(5) Neves, S. R.; Ram, P. T.; Iyengar, R. G protein pathways. *Science (New York, N.Y.)* **2002**, *296* (5573), 1636–1639. DOI: 10.1126/science.1071550.

(6) Vargas, G. A.; Zastrow, M. von. Identification of a novel endocytic recycling signal in the D1 dopamine receptor. *The Journal of biological chemistry* **2004**, *279* (36), 37461–37469. DOI: 10.1074/jbc.M401034200.

(7) Jiang, N.; Ou-Yang, K.; Cai, S.; Hu, Y.; Xu, Z. Identification of human dopamine D1-like receptor agonist using a cell-based functional assay. *Acta pharmacologica Sinica* **2005**, *26* (10), 1181–1186. DOI: 10.1111/j.1745-7254.2005.00199.x.

(8) Carpenter, B. Current applications of mini G proteins to study the structure and function of G protein-coupled receptors. *AIMS Bioengineering* **2018**, *5* (4), 209–225. DOI: 10.3934/bioeng.2018.4.209.

(9) Kebabian, J. W. Multiple classes of dopamine receptors in mammalian central nervous system: the involvement of dopamine-sensitive adenylyl cyclase. *Life sciences* **1978**, *23* (5), 479–483. DOI: 10.1016/0024-3205(78)90157-1.

(10) Missale, C.; Nash, S. R.; Robinson, S. W.; Jaber, M.; Caron, M. G. Dopamine receptors: from structure to function. *Physiological reviews* **1998**, *78* (1), 189–225. DOI: 10.1152/physrev.1998.78.1.189.

(11) Vallone, D.; Picetti, R.; Borrelli, E. Structure and function of dopamine receptors. *Neuroscience and biobehavioral reviews* **2000**, *24* (1), 125–132. DOI: 10.1016/s0149-7634(99)00063-9.

(12) Dreyer, J. K.; Herrik, K. F.; Berg, R. W.; Hounsgaard, J. D. Influence of phasic and tonic dopamine release on receptor activation. *The Journal of neuroscience : the official journal of the Society for Neuroscience* **2010**, *30* (42), 14273–14283. DOI: 10.1523/JNEUROSCI.1894-10.2010.

(13) Di Chiara, G. Drug addiction as dopamine-dependent associative learning disorder. *European journal of pharmacology* **1999**, *375* (1-3), 13–30. DOI: 10.1016/S0014-2999(99)00372-6.

(14) Wang, Q.; Jolly, J. P.; Surmeier, J. D.; Mullah, B. M.; Lidow, M. S.; Bergson, C. M.; Robishaw, J. D. Differential dependence of the D1 and D5 dopamine receptors on the G protein gamma 7 subunit for activation of adenylylcyclase. *The Journal of biological chemistry* **2001**, *276* (42), 39386–39393. DOI: 10.1074/jbc.M104981200.

(15) Di Chiara, G.; Bassareo, V.; Fenu, S.; Luca, M. A. de; Spina, L.; Cadoni, C.; Acquas, E.; Carboni, E.; Valentini, V.; Lecca, D. Dopamine and drug addiction: the nucleus accumbens shell connection. *Neuropharmacology* **2004**, *47 Suppl 1*, 227–241. DOI: 10.1016/j.neuropharm.2004.06.032.

(16) Forster, L.; Grätz, L.; Mönnich, D.; Bernhardt, G.; Pockes, S. A Split Luciferase Complementation Assay for the Quantification of β-Arrestin2 Recruitment to Dopamine D2-Like Receptors. *International journal of molecular sciences* **2020**, *21* (17). DOI: 10.3390/ijms21176103.

(17) Forster, L.; Pockes, S. Investigating the ligand agonism and antagonism at the D2long receptor by dynamic mass redistribution. *Scientific reports* **2022**, *12* (1), 9637. DOI: 10.1038/s41598-022-14311-w.

(18) Lowe, N.; Kirley, A.; Hawi, Z.; Sham, P.; Wickham, H.; Kratochvil, C. J.; Smith, S. D.; Lee, S. Y.; Levy, F.; Kent, L.; Middle, F.; Rohde, L. A.; Roman, T.; Tahir, E.; Yazgan, Y.; Asherson, P.; Mill, J.; Thapar, A.; Payton, A.; Todd, R. D.; Stephens, T.; Ebstein, R. P.; Manor, I.; Barr, C. L.; Wigg, K. G.; Sinke, R. J.; Buitelaar, J. K.; Smalley, S. L.; Nelson, S. F.; Biederman, J.; Faraone, S. V.; Gill, M. Joint analysis of the DRD5 marker concludes association with attention-deficit/hyperactivity disorder confined to the predominantly inattentive and combined subtypes. *American journal of human genetics* **2004**, *74* (2), 348–356. DOI: 10.1086/381561.

(19) Krom, M. de; Staal, W. G.; Ophoff, R. A.; Hendriks, J.; Buitelaar, J.; Franke, B.; Jonge, M. V. de; Bolton, P.; Collier, D.; Curran, S.; van Engeland, H.; van Ree, J. M. A common variant in DRD3 receptor is associated with autism spectrum disorder. *Biological psychiatry* **2009**, *65* (7), 625–630. DOI: 10.1016/j.biopsych.2008.09.035.

(20) Gabriela, M.-L.; John, D.-G.; Magdalena, B.-V.; Ariadna, G.-S.; La Francisco, D. P.-O.; Liz, S.-M.; Lino, P.-C.; Josefina, R.-G.; Ernesto, R.-Z.; Carlos, C.-F. Genetic interaction analysis for DRD4 and DAT1 genes in a group of Mexican ADHD patients. *Neuroscience letters* **2009**, *451* (3), 257–260. DOI: 10.1016/j.neulet.2009.01.004.

(21) Martel, M. M.; Nikolas, M.; Jernigan, K.; Friderici, K.; Waldman, I.; Nigg, J. T. The dopamine receptor D4 gene (DRD4) moderates family environmental effects on ADHD. *Journal of abnormal child psychology* **2011**, *39* (1), 1–10. DOI: 10.1007/s10802-010-9439-5.

(22) Staal, W. G. Autism, DRD3 and repetitive and stereotyped behavior, an overview of the current knowledge. *European neuropsychopharmacology: the journal of the European College of Neuropsychopharmacology* **2015**, *25* (9), 1421–1426. DOI: 10.1016/j.euroneuro.2014.08.011.

(23) Galaj, E.; Newman, A. H.; Xi, Z.-X. Dopamine D3 receptor-based medication development for the treatment of opioid use disorder: Rationale, progress, and challenges. *Neuroscience and biobehavioral reviews* **2020**, *114*, 38–52. DOI: 10.1016/j.neubiorev.2020.04.024.

(24) Yano, H.; Cai, N.-S.; Xu, M.; Verma, R. K.; Rea, W.; Hoffman, A. F.; Shi, L.; Javitch, J. A.; Bonci, A.; Ferré, S. Gs- versus Golf-dependent functional selectivity mediated by the dopamine D1 receptor. *Nature communications* **2018**, *9* (1), 486. DOI: 10.1038/s41467-017-02606-w.

(25) Lane, J. R.; Powney, B.; Wise, A.; Rees, S.; Milligan, G. Protean agonism at the dopamine D2 receptor: (S)-3-(3-hydroxyphenyl)-N-propylpiperidine is an agonist for activation of Go1 but an antagonist/inverse agonist for Gi1,Gi2, and Gi3. *Molecular pharmacology* **2007**, *71* (5), 1349–1359. DOI: 10.1124/mol.106.032722.

(26) Inoue, A.; Raimondi, F.; Kadji, F. M. N.; Singh, G.; Kishi, T.; Uwamizu, A.; Ono, Y.; Shinjo, Y.; Ishida, S.; Arang, N.; Kawakami, K.; Gutkind, J. S.; Aoki, J.; Russell, R. B. Illuminating G-Protein-Coupling Selectivity of GPCRs. *Cell* **2019**, *177* (7), 1933-1947.e25. DOI: 10.1016/j.cell.2019.04.044.

(27) Sidhu, A.; Niznik, H. B. Coupling of dopamine receptor subtypes to multiple and diverse G proteins. *International journal of developmental neuroscience: the official journal of the International Society for Developmental Neuroscience* **2000**, *18* (7), 669–677. DOI: 10.1016/s0736-5748(00)00033-2.

(28) Beaulieu, J.-M.; Espinoza, S.; Gainetdinov, R. R. Dopamine receptors - IUPHAR Review 13. *British journal of pharmacology* **2015**, *172* (1), 1–23. DOI: 10.1111/bph.12906.

(29) Männel, B.; Dengler, D.; Shonberg, J.; Hübner, H.; Möller, D.; Gmeiner, P. Hydroxy-Substituted Heteroarylpiperazines: Novel Scaffolds for β-Arrestin-Biased D2R Agonists. *Journal of medicinal chemistry* **2017**, *60* (11), 4693–4713. DOI: 10.1021/acs.jmedchem.7b00363.

(30) Simms, S. L.; Huettner, D. P.; Kortagere, S. In vivo characterization of a novel dopamine D3 receptor agonist to treat motor symptoms of Parkinson's disease. *Neuropharmacology* **2016**, *100*, 106–115. DOI: 10.1016/j.neuropharm.2015.04.004.

(31) Rozbeh, R.; Forchhammer, K. Split NanoLuc technology allows quantitation of interactions between PII protein and its receptors with unprecedented sensitivity and reveals transient interactions. *Scientific reports* **2021**, *11* (1), 12535. DOI: 10.1038/s41598-021-91856-2.

(32) Schihada, H.; Shekhani, R.; Schulte, G. Quantitative assessment of constitutive G protein-coupled receptor activity with BRET-based G protein biosensors. *Science signaling* **2021**, *14* (699), eabf1653. DOI: 10.1126/scisignal.abf1653.

(33) Schihada, H.; Klompstra, T. M.; Humphrys, L. J.; Cervenka, I.; Dadvar, S.; Kolb, P.; Ruas, J. L.; Schulte, G. Isoforms of GPR35 have distinct extracellular N-termini that allosterically modify receptor-transducer coupling and mediate intracellular pathway bias. *The Journal of biological chemistry* **2022**, *298* (9), 102328. DOI: 10.1016/j.jbc.2022.102328.

(34) Nehmé, R.; Carpenter, B.; Singhal, A.; Strege, A.; Edwards, P. C.; White, C. F.; Du, H.; Grisshammer, R.; Tate, C. G. Mini-G proteins: Novel tools for studying GPCRs in their active conformation. *PloS one* **2017**, *12* (4), e0175642. DOI: 10.1371/journal.pone.0175642.

(35) Höring, C.; Seibel, U.; Tropmann, K.; Grätz, L.; Mönnich, D.; Pitzl, S.; Bernhardt, G.; Pockes, S.; Strasser, A. A Dynamic, Split-Luciferase-Based Mini-G Protein Sensor to Functionally Characterize Ligands at All Four Histamine Receptor Subtypes. *International journal of molecular sciences* **2020**, *21* (22). DOI: 10.3390/ijms21228440.

(36) Shepard, B. D.; Natarajan, N.; Protzko, R. J.; Acres, O. W.; Pluznick, J. L. A cleavable N-terminal signal peptide promotes widespread olfactory receptor surface expression in HEK293T cells. *PloS one* **2013**, *8* (7), e68758. DOI: 10.1371/journal.pone.0068758.

(37) Gay, P.; Le Coq, D.; Steinmetz, M.; Berkelman, T.; Kado, C. I. Positive selection procedure for entrapment of insertion sequence elements in gram-negative bacteria. *Journal of bacteriology* **1985**, *164* (2), 918–921. DOI: 10.1128/jb.164.2.918-921.1985.

(38) Jiang, L. I.; Collins, J.; Davis, R.; Lin, K.-M.; DeCamp, D.; Roach, T.; Hsueh, R.; Rebres, R. A.; Ross, E. M.; Taussig, R.; Fraser, I.; Sternweis, P. C. Use of a cAMP BRET sensor to characterize a novel regulation of cAMP by the sphingosine 1-phosphate/G13 pathway. *The Journal of biological chemistry* **2007**, *282* (14), 10576–10584. DOI: 10.1074/jbc.M609695200.

(39) Cheng, Y.; Prusoff, W. H. [Duplikat] Relationship between the inhibition constant (K1) and the concentration of inhibitor which causes 50 per cent inhibition (I50) of an enzymatic reaction. *Biochemical pharmacology* **1973**, *22* (23), 3099–3108. DOI: 10.1016/0006-2952(73)90196-2.

(40) Bourne, J. A. SCH 23390: the first selective dopamine D1-like receptor antagonist. *CNS drug reviews* **2001**, *7* (4), 399–414. DOI: 10.1111/j.1527-3458.2001.tb00207.x.

(41) Kirillova, G. P.; Hrutkay, R. J.; Shurin, M. R.; Shurin, G. V.; Tourkova, I. L.; Vanyukov, M. M. Dopamine receptors in human lymphocytes: radioligand binding and quantitative RT-PCR assays. *Journal of neuroscience methods* **2008**, *174* (2), 272–280. DOI: 10.1016/j.jneumeth.2008.07.018.

(42) Perachon, S.; Schwartz, J. C.; Sokoloff, P. Functional potencies of new antiparkinsonian drugs at recombinant human dopamine D1, D2 and D3 receptors. *European journal of pharmacology* **1999**, *366* (2-3), 293–300. DOI: 10.1016/s0014-2999(98)00896-6.

(43) Andersen, P. H.; Jansen, J. A. Dopamine receptor agonists: selectivity and dopamine D1 receptor efficacy. *European journal of pharmacology* **1990**, *188* (6), 335–347. DOI: 10.1016/0922-4106(90)90194-3.

(44) Ryman-Rasmussen, J. P.; Nichols, D. E.; Mailman, R. B. Differential activation of adenylate cyclase and receptor internalization by novel dopamine D1 receptor agonists. *Molecular pharmacology* **2005**, *68* (4), 1039–1048. DOI: 10.1124/mol.105.012153.

(45) Conroy, J. L.; Free, R. B.; Sibley, D. R. Identification of G protein-biased agonists that fail to recruit β-arrestin or promote internalization of the D1 dopamine receptor. *ACS chemical neuroscience* **2015**, *6* (4), 681–692. DOI: 10.1021/acschemneuro.5b00020.

(46) Dixon, A. S.; Schwinn, M. K.; Hall, M. P.; Zimmerman, K.; Otto, P.; Lubben, T. H.; Butler, B. L.; Binkowski, B. F.; Machleidt, T.; Kirkland, T. A.; Wood, M. G.; Eggers, C. T.; Encell, L. P.; Wood, K. V. NanoLuc Complementation Reporter Optimized for Accurate Measurement of Protein Interactions in Cells. *ACS chemical biology* **2016**, *11* (2), 400–408. DOI: 10.1021/acschembio.5b00753.

(47) Sunahara, R. K.; Guan, H. C.; O'Dowd, B. F.; Seeman, P.; Laurier, L. G.; Ng, G.; George, S. R.; Torchia, J.; van Tol, H. H.; Niznik, H. B. Cloning of the gene for a human dopamine D5 receptor with higher affinity for dopamine than D1. *Nature* **1991**, *350* (6319), 614–619. DOI: 10.1038/350614a0.

(48) Millan, M. J.; Maiofiss, L.; Cussac, D.; Audinot, V.; Boutin, J.-A.; Newman-Tancredi, A. Differential actions of antiparkinson agents at multiple classes of monoaminergic receptor. I. A multivariate analysis of the binding profiles of 14 drugs at 21 native and cloned human receptor subtypes. *The Journal of pharmacology and experimental therapeutics* **2002**, *303* (2), 791–804. DOI: 10.1124/jpet.102.039867.

(49) Wood, M.; Dubois, V.; Scheller, D.; Gillard, M. Rotigotine is a potent agonist at dopamine D1 receptors as well as at dopamine D2 and D3 receptors. *British journal of pharmacology* **2015**, *172* (4), 1124–1135. DOI: 10.1111/bph.12988.

(50) Park, H.; Urs, A. N.; Zimmerman, J.; Liu, C.; Wang, Q.; Urs, N. M. Structure-Functional-Selectivity Relationship Studies of Novel Apomorphine Analogs to Develop D1R/D2R Biased Ligands. *ACS medicinal chemistry letters* **2020**, *11* (3), 385–392. DOI: 10.1021/acsmedchemlett.9b00575.

(51) Cai, G.; Gurdal, H.; Smith, C.; Wang, H. Y.; Friedman, E. Inverse agonist properties of dopaminergic antagonists at the D(1A) dopamine receptor: uncoupling of the D(1A) dopamine receptor from G(s) protein. *Molecular pharmacology* **1999**, *56* (5), 989–996. DOI: 10.1124/mol.56.5.989.

(52) Al-Fulaij, M. A.; Ren, Y.; Beinborn, M.; Kopin, A. S. Pharmacological analysis of human D1 AND D2 dopamine receptor missense variants. *Journal of molecular neuroscience: MN* **2008**, *34* (3), 211–223. DOI: 10.1007/s12031-007-9030-x.

(53) Free, R. B.; Chun, L. S.; Moritz, A. E.; Miller, B. N.; Doyle, T. B.; Conroy, J. L.; Padron, A.; Meade, J. A.; Xiao, J.; Hu, X.; Dulcey, A. E.; Han, Y.; Duan, L.; Titus, S.; Bryant-Genevier, M.; Barnaeva, E.; Ferrer, M.; Javitch, J. A.; Beuming, T.; Shi, L.; Southall, N. T.; Marugan, J. J.; Sibley, D. R. Discovery and characterization of a G protein-biased agonist that inhibits β-arrestin recruitment to the D2 dopamine receptor. *Molecular pharmacology* **2014**, *86* (1), 96–105. DOI: 10.1124/mol.113.090563.

(54) Brust, T. F.; Hayes, M. P.; Roman, D. L.; Watts, V. J. New functional activity of aripiprazole revealed: Robust antagonism of D2 dopamine receptor-stimulated Gβγ signaling. *Biochemical pharmacology* **2015**, *93* (1), 85–91. DOI: 10.1016/j.bcp.2014.10.014.

(55) Song, Y. B.; Park, C. O.; Jeong, J.-Y.; Huh, W.-K. Monitoring G protein-coupled receptor activation using an adenovirus-based β-arrestin bimolecular fluorescence complementation assay. *Analytical biochemistry* **2014**, *449*, 32–41. DOI: 10.1016/j.ab.2013.12.017.

(56) Chen, X.; McCorvy, J. D.; Fischer, M. G.; Butler, K. V.; Shen, Y.; Roth, B. L.; Jin, J. Discovery of G Protein-Biased D2 Dopamine Receptor Partial Agonists. *Journal of medicinal chemistry* **2016**, *59* (23), 10601–10618. DOI: 10.1021/acs.jmedchem.6b01208.

(57) Neumeyer, J. L.; Kula, N. S.; Bergman, J.; Baldessarini, R. J. Receptor affinities of dopamine D1 receptor-selective novel phenylbenzazepines. *European journal of pharmacology* **2003**, *474* (2-3), 137–140. DOI: 10.1016/s0014-2999(03)02008-9.

(58) Moreland, R. B.; Nakane, M.; Donnelly-Roberts, D. L.; Miller, L. N.; Chang, R.; Uchic, M. E.; Terranova, M. A.; Gubbins, E. J.; Helfrich, R. J.; Namovic, M. T.; El-Kouhen, O. F.; Masters, J. N.; Brioni, J. D. Comparative pharmacology of human dopamine D(2)-like receptor stable cell lines coupled to calcium flux through Galpha(qo5). *Biochemical pharmacology* **2004**, *68* (4), 761–772. DOI: 10.1016/j.bcp.2004.05.019.

(59) Jeanneteau, F.; Diaz, J.; Sokoloff, P.; Griffon, N. Interactions of GIPC with dopamine D2, D3 but not D4 receptors define a novel mode of regulation of G protein-coupled receptors. *Molecular biology of the cell* **2004**, *15* (2), 696–705. DOI: 10.1091/mbc.e03-05-0293.

(60) Troppmann, B.; Balfanz, S.; Krach, C.; Baumann, A.; Blenau, W. Characterization of an invertebrate-type dopamine receptor of the American cockroach, Periplaneta americana. *International journal of molecular sciences* **2014**, *15* (1), 629–653. DOI: 10.3390/ijms15010629.

(61) MacKenzie, R. G.; VanLeeuwen, D.; Pugsley, T. A.; Shih, Y. H.; Demattos, S.; Tang, L.; Todd, R. D.; O'Malley, K. L. Characterization of the human dopamine D3 receptor expressed in transfected cell lines. *European journal of pharmacology* **1994**, *266* (1), 79–85. DOI: 10.1016/0922-4106(94)90212-7.

(62) Chemel, B. R.; Roth, B. L.; Armbruster, B.; Watts, V. J.; Nichols, D. E. WAY-100635 is a potent dopamine D4 receptor agonist. *Psychopharmacology* **2006**, *188* (2), 244–251. DOI: 10.1007/s00213-006-0490-4.

(63) Mierau, J.; Schneider, F. J.; Ensinger, H. A.; Chio, C. L.; Lajiness, M. E.; Huff, R. M. Pramipexole binding and activation of cloned and expressed dopamine D2, D3 and D4 receptors. *European journal of pharmacology* **1995**, *290* (1), 29–36. DOI: 10.1016/0922-4106(95)90013-6.

(64) Gopalakrishnan, S. M.; Moreland, R. B.; Kofron, J. L.; Helfrich, R. J.; Gubbins, E.; McGowen, J.; Masters, J. N.; Donnelly-Roberts, D.; Brioni, J. D.; Burns, D. J.; Warrior, U. A cell-based microarrayed compound screening format for identifying agonists of G-protein-coupled receptors. *Analytical biochemistry* **2003**, *321* (2), 192–201. DOI: 10.1016/s0003-2697(03)00425-1.

(65) Tiberi, M.; Caron, M. G. High agonist-independent activity is a distinguishing feature of the dopamine D1B receptor subtype. *The Journal of biological chemistry* **1994**, *269* (45), 27925–27931.

(66) Roberts, D. J.; Strange, P. G. Mechanisms of inverse agonist action at D2 dopamine receptors. *British journal of pharmacology* **2005**, *145* (1), 34–42. DOI: 10.1038/sj.bjp.0706073.

(67) Zhuang, Y.; Xu, P.; Mao, C.; Wang, L.; Krumm, B.; Zhou, X. E.; Huang, S.; Liu, H.; Cheng, X.; Huang, X.-P.; Shen, D.-D.; Xu, T.; Liu, Y.-F.; Wang, Y.; Guo, J.; Jiang, Y.; Jiang, H.; Melcher, K.; Roth, B. L.; Zhang, Y.; Zhang, C.; Xu, H. E. Structural insights into the human D1 and D2 dopamine receptor signaling complexes. *Cell* **2021**, *184* (4), 931-942.e18. DOI: 10.1016/j.cell.2021.01.027.

(68) Ebersole, B.; Petko, J.; Woll, M.; Murakami, S.; Sokolina, K.; Wong, V.; Stagljar, I.; Lüscher, B.; Levenson, R. Effect of C-Terminal S-Palmitoylation on D2 Dopamine Receptor Trafficking and Stability. *PloS one* **2015**, *10* (11), e0140661. DOI: 10.1371/journal.pone.0140661.

(69) Zhang, X.; Kim, K.-M. Palmitoylation of the carboxyl-terminal tail of dopamine D4 receptor is required for surface expression, endocytosis, and signaling. *Biochemical and biophysical research communications* **2016**, *479* (2), 398–403. DOI: 10.1016/j.bbrc.2016.09.094.

(70) Zhang, X.; Le, H. T.; Zhang, X.; Zheng, M.; Choi, B.-G.; Kim, K.-M. Palmitoylation on the carboxyl terminus tail is required for the selective regulation of dopamine D2 versus D3 receptors. *Biochimica et biophysica acta* **2016**, *1858* (9), 2152–2162. DOI: 10.1016/j.bbamem.2016.06.021.

(71) van den Buuse, M.; Martin, S.; Brosda, J.; Leck, K. J.; Matthaei, K. I.; Hendry, I. Enhanced effect of dopaminergic stimulation on prepulse inhibition in mice deficient in the alpha subunit of G(z). *Psychopharmacology* **2005**, *183* (3), 358–367. DOI: 10.1007/s00213-005-0181-6.

(72) Anderson, A.; Masuho, I.; Marron Fernandez de Velasco, E.; Nakano, A.; Birnbaumer, L.; Martemyanov, K. A.; Wickman, K. GPCR-dependent biasing of GIRK channel signaling dynamics by RGS6 in mouse sinoatrial nodal cells. *Proceedings of the National Academy of Sciences of the United States of America* **2020**, *117* (25), 14522–14531. DOI: 10.1073/pnas.2001270117.

(73) Lukasheva, V.; Devost, D.; Le Gouill, C.; Namkung, Y.; Martin, R. D.; Longpré, J.-M.; Amraei, M.; Shinjo, Y.; Hogue, M.; Lagacé, M.; Breton, B.; Aoki, J.; Tanny, J. C.; Laporte, S. A.; Pineyro, G.; Inoue, A.; Bouvier, M.; Hébert, T. E. Signal profiling of the β1AR reveals coupling to novel signalling pathways and distinct phenotypic responses mediated by β1AR and β2AR. *Scientific reports* **2020**, *10* (1), 8779. DOI: 10.1038/s41598-020-65636-3.

(74) Busnelli, M.; Saulière, A.; Manning, M.; Bouvier, M.; Galés, C.; Chini, B. Functional selective oxytocin-derived agonists discriminate between individual G protein family subtypes. *The Journal of biological chemistry* **2012**, *287* (6), 3617–3629. DOI: 10.1074/jbc.M111.277178.

(75) Seyedabadi, M.; Ghahremani, M. H.; Albert, P. R. Biased signaling of G protein coupled receptors (GPCRs): Molecular determinants of GPCR/transducer selectivity and therapeutic potential. *Pharmacology & therapeutics* **2019**, *200*, 148–178. DOI: 10.1016/j.pharmthera.2019.05.006.

(76) Preto, A. J.; Barreto, C. A. V.; Baptista, S. J.; Almeida, J. G. de; Lemos, A.; Melo, A.; Cordeiro, M. N. D. S.; Kurkcuoglu, Z.; Melo, R.; Moreira, I. S. Understanding the Binding Specificity of G-Protein Coupled Receptors toward G-Proteins and Arrestins: Application to the Dopamine Receptor Family. *Journal of chemical information and modeling* **2020**, *60* (8), 3969–3984. DOI: 10.1021/acs.jcim.0c00371.

(77) Obadiah, J.; Avidor-Reiss, T.; Fishburn, C. S.; Carmon, S.; Bayewitch, M.; Vogel, Z.; Fuchs, S.; Levavi-Sivan, B. Adenylyl cyclase interaction with the D2 dopamine receptor family; differential coupling to Gi, Gz, and Gs. *Cellular and molecular neurobiology* **1999**, *19* (5), 653–664. DOI: 10.1023/a:1006988603199.

(78) Leck, K. J.; Blaha, C. D.; Matthaei, K. I.; Forster, G. L.; Holgate, J.; Hendry, I. A. Gz proteins are functionally coupled to dopamine D2-like receptors in vivo. *Neuropharmacology* **2006**, *51* (3), 597–605. DOI: 10.1016/j.neuropharm.2006.05.002.

(79) Klein Herenbrink, C.; Sykes, D. A.; Donthamsetti, P.; Canals, M.; Coudrat, T.; Shonberg, J.; Scammells, P. J.; Capuano, B.; Sexton, P. M.; Charlton, S. J.; Javitch, J. A.; Christopoulos, A.; Lane, J. R. The role of kinetic context in apparent biased agonism at GPCRs. *Nature communications* **2016**, *7*, 10842. DOI: 10.1038/ncomms10842. Published Online: Feb. 24, 2016.

(80) Hauser, A. S.; Avet, C.; Normand, C.; Mancini, A.; Inoue, A.; Bouvier, M.; Gloriam, D. E. Common coupling map advances GPCR-G protein selectivity. *eLife* **2022**, *11.* DOI: 10.7554/eLife.74107.

(81) Moo, E. von; Harpsøe, K.; Hauser, A. S.; Masuho, I.; Bräuner-Osborne, H.; Gloriam, D. E.; Martemyanov, K. A. Ligand-directed bias of G protein signaling at the dopamine D2 receptor. *Cell chemical biology* **2022**, *29* (2), 226-238.e4. DOI: 10.1016/j.chembiol.2021.07.004.

(82) Sidhu, A.; Kimura, K.; Uh, M.; White, B. H.; Patel, S. Multiple coupling of human D5 dopamine receptors to guanine nucleotide binding proteins Gs and Gz. *Journal of neurochemistry* **1998**, *70* (6), 2459–2467. DOI: 10.1046/j.1471-4159.1998.70062459.x.

(83) Fenske, R. J.; Cadena, M. T.; Harenda, Q. E.; Wienkes, H. N.; Carbajal, K.; Schaid, M. D.; Laundre, E.; Brill, A. L.; Truchan, N. A.; Brar, H.; Wisinski, J.; Cai, J.; Graham, T. E.; Engin, F.; Kimple, M. E. The Inhibitory G Protein α-Subunit, Gαz, Promotes Type 1 Diabetes-Like Pathophysiology in NOD Mice. *Endocrinology* **2017**, *158* (6), 1645–1658. DOI: 10.1210/en.2016-1700.

(84) Yang, J.; Wu, J.; Kowalska, M. A.; Dalvi, A.; Prevost, N.; O'Brien, P. J.; Manning, D.; Poncz, M.; Lucki, I.; Blendy, J. A.; Brass, L. F. Loss of signaling through the G protein, Gz, results in abnormal platelet activation and altered responses to psychoactive drugs. *Proceedings of the National Academy of Sciences of the United States of America* **2000**, *97* (18), 9984–9989. DOI: 10.1073/pnas.180194597.

(85) Ho, M. K.; Wong, Y. H. G(z) signaling: emerging divergence from G(i) signaling. *Oncogene* **2001**, *20* (13), 1615–1625. DOI: 10.1038/sj.onc.1204190.

(86) Doi, M.; Murai, I.; Kunisue, S.; Setsu, G.; Uchio, N.; Tanaka, R.; Kobayashi, S.; Shimatani, H.; Hayashi, H.; Chao, H.-W.; Nakagawa, Y.; Takahashi, Y.; Hotta, Y.; Yasunaga, J.; Matsuoka, M.; Hastings, M. H.; Kiyonari, H.; Okamura, H. Gpr176 is a Gz-linked orphan G-protein-coupled receptor that sets the pace of circadian behaviour. *Nature communications* **2016**, *7*, 10583. DOI: 10.1038/ncomms10583.

(87) Masuho, I.; Ostrovskaya, O.; Kramer, G. M.; Jones, C. D.; Xie, K.; Martemyanov, K. A. Distinct profiles of functional discrimination among G proteins determine the actions of G protein-coupled receptors. *Science signaling* **2015**, *8* (405), ra123. DOI: 10.1126/scisignal.aab4068.

(88) Casey, P. J.; Fong, H. K.; Simon, M. I.; Gilman, A. G. Gz, a guanine nucleotide-binding protein with unique biochemical properties. *The Journal of biological chemistry* **1990**, *265* (4), 2383–2390.

(89) Kimura, K.; White, B. H.; Sidhu, A. Coupling of human D-1 dopamine receptors to different guanine nucleotide binding proteins. Evidence that D-1 dopamine receptors can couple to both Gs and G(o). *The Journal of biological chemistry* **1995**, *270* (24), 14672–14678. DOI: 10.1074/jbc.270.24.14672.

(90) Uh, M.; White, B. H.; Sidhu, A. Alteration of association of agonist-activated renal D1(A) dopamine receptors with G proteins in proximal tubules of the spontaneously hypertensive rat. *Journal of hypertension* **1998**, *16* (9), 1307–1313. DOI: 10.1097/00004872-199816090-00012.

(91) La Mannoury Cour, C.; Vidal, S.; Pasteau, V.; Cussac, D.; Millan, M. J. Dopamine D1 receptor coupling to Gs/olf and Gq in rat striatum and cortex: a scintillation proximity assay (SPA)/antibody-capture characterization of benzazepine agonists. *Neuropharmacology* **2007**, *52* (3), 1003–1014. DOI: 10.1016/j.neuropharm.2006.10.021.

(92) Rashid, A. J.; O'Dowd, B. F.; Verma, V.; George, S. R. Neuronal Gq/11-coupled dopamine receptors: an uncharted role for dopamine. *Trends in pharmacological sciences* **2007**, *28* (11), 551–555. DOI: 10.1016/j.tips.2007.10.001.

(93) Odagaki, Y.; Kinoshita, M.; Ota, T. Dopamine-induced functional activation of Gαq mediated by dopamine D1-like receptor in rat cerebral cortical membranes. *Journal of receptor and signal transduction research* **2019**, *39* (1), 9–17. DOI: 10.1080/10799893.2018.1562470.

(94) Masuho, I.; Martemyanov, K. A.; Lambert, N. A. Monitoring G Protein Activation in Cells with BRET. *Methods in molecular biology (Clifton, N.J.)* **2015**, *1335*, 107–113. DOI: 10.1007/978-1-4939-2914-6_8.

(95) Kim, S.; Kwon, J.; Park, M. G.; Lee, C. J. Dopamine-induced astrocytic Ca2+ signaling in mPFC is mediated by MAO-B in young mice, but by dopamine receptors in adult mice. *Molecular brain* **2022**, *15* (1), 90. DOI: 10.1186/s13041-022-00977-w.

(96) Uefune, F.; Aonishi, T.; Kitaguchi, T.; Takahashi, H.; Seino, S.; Sakano, D.; Kume, S. Dopamine Negatively Regulates Insulin Secretion Through Activation of D1-D2 Receptor Heteromer. *Diabetes* **2022**, *71* (9), 1946–1961. DOI: 10.2337/db21-0644.

(97) Newman-Tancredi, A.; Cussac, D.; Audinot, V.; Pasteau, V.; Gavaudan, S.; Millan, M. J. G protein activation by human dopamine D3 receptors in high-expressing Chinese hamster ovary cells: A guanosine-5'-O-(3-35Sthio)- triphosphate binding and antibody study. *Molecular pharmacology* **1999**, *55* (3), 564–574.

(98) Jose, P. A.; Soares-da-Silva, P.; Eisner, G. M.; Felder, R. A. Dopamine and G protein-coupled receptor kinase 4 in the kidney: role in blood pressure regulation. *Biochimica et biophysica acta* **2010**, *1802* (12), 1259–1267. DOI: 10.1016/j.bbadis.2010.02.004.

(99) Syrovatkina, V.; Alegre, K. O.; Dey, R.; Huang, X.-Y. Regulation, Signaling, and Physiological Functions of G-Proteins. *Journal of molecular biology* **2016**, *428* (19), 3850–3868. DOI: 10.1016/j.jmb.2016.08.002.

(100) Kimple, M. E.; Hultman, R. C.; Casey, P. J. Signaling Through Gz. In *Handbook of Cell Signaling*; Elsevier, 2010; pp 1649–1653. DOI: 10.1016/B978-0-12-374145-5.00202-3.

(101) Uhlén, M.; Fagerberg, L.; Hallström, B. M.; Lindskog, C.; Oksvold, P.; Mardinoglu, A.; Sivertsson, Å.; Kampf, C.; Sjöstedt, E.; Asplund, A.; Olsson, I.; Edlund, K.; Lundberg, E.; Navani, S.; Szigyarto, C. A.-K.; Odeberg, J.; Djureinovic, D.; Takanen, J. O.; Hober, S.; Alm, T.; Edqvist, P.-H.; Berling, H.; Tegel, H.; Mulder, J.; Rockberg, J.; Nilsson, P.; Schwenk, J. M.; Hamsten, M.; Feilitzen, K. von; Forsberg, M.; Persson, L.; Johansson, F.; Zwahlen, M.; Heijne, G. von; Nielsen, J.; Pontén, F. Proteomics. Tissue-based map of the human proteome. *Science (New York, N.Y.)* **2015**, *347* (6220), 1260419. DOI: 10.1126/science.1260419.

(102) Ilani, T.; Fishburn, C. S.; Levavi-Sivan, B.; Carmon, S.; Raveh, L.; Fuchs, S. Coupling of dopamine receptors to G proteins: studies with chimeric D2/D3 dopamine receptors. *Cellular and molecular neurobiology* **2002**, *22* (1), 47–56. DOI: 10.1023/a:1015341712166.

(103) Xu, P.; Huang, S.; Mao, C.; Krumm, B. E.; Zhou, X. E.; Tan, Y.; Huang, X.-P.; Liu, Y.; Shen, D.-D.; Jiang, Y.; Yu, X.; Jiang, H.; Melcher, K.; Roth, B. L.; Cheng, X.; Zhang, Y.; Xu, H. E. Structures of the human dopamine D3 receptor-Gi complexes. *Molecular cell* **2021**, *81* (6), 1147-1159.e4. DOI: 10.1016/j.molcel.2021.01.003.

(104) Jang, W.; Lu, S.; Lambert, N. A. *Nucleotide-decoupled G proteins reveal the role of G protein conformation in receptor-G protein selectivity*, 2022. DOI: 10.1101/2022.05.25.493498.

(105) Okashah, N.; Wright, S. C.; Kawakami, K.; Mathiasen, S.; Zhou, J.; Lu, S.; Javitch, J. A.; Inoue, A.; Bouvier, M.; Lambert, N. A. Agonist-induced formation of unproductive receptor-G12 complexes. *Proceedings of the National Academy of Sciences of the United States of America* **2020**, *117* (35), 21723–21730. DOI: 10.1073/pnas.2003787117.

(106) Galés, C.; van Durm, J. J. J.; Schaak, S.; Pontier, S.; Percherancier, Y.; Audet, M.; Paris, H.; Bouvier, M. Probing the activation-promoted structural rearrangements in preassembled receptor-G protein complexes. *Nature structural & molecular biology* **2006**, *13* (9), 778–786. DOI: 10.1038/nsmb1134.

(107) Seeman, P.; Tallerico, T. Antipsychotic drugs which elicit little or no parkinsonism bind more loosely than dopamine to brain D2 receptors, yet occupy high levels of these receptors. *Molecular psychiatry* **1998**, *3* (2), 123–134. DOI: 10.1038/sj.mp.4000336.

(108) Sautel, F.; Griffon, N.; Lévesque, D.; Pilon, C.; Schwartz, J. C.; Sokoloff, P. A functional test identifies dopamine agonists selective for D3 versus D2 receptors. *Neuroreport* **1995**, *6* (2), 329–332. DOI: 10.1097/00001756-199501000-00026.

(109) Schetz, J. A.; Benjamin, P. S.; Sibley, D. R. Nonconserved residues in the second transmembrane-spanning domain of the D(4) dopamine receptor are molecular determinants of D(4)-selective pharmacology. *Molecular pharmacology* **2000**, *57* (1), 144–152.

(110) Isberg, V.; Graaf, C. de; Bortolato, A.; Cherezov, V.; Katritch, V.; Marshall, F. H.; Mordalski, S.; Pin, J.-P.; Stevens, R. C.; Vriend, G.; Gloriam, D. E. Generic GPCR residue numbers - aligning topology maps while minding the gaps. *Trends in pharmacological sciences* **2015**, *36* (1), 22–31. DOI: 10.1016/j.tips.2014.11.001.

(111) Pándy-Szekeres, G.; Munk, C.; Tsonkov, T. M.; Mordalski, S.; Harpsøe, K.; Hauser, A. S.; Bojarski, A. J.; Gloriam, D. E. GPCRdb in 2018: adding GPCR structure models and ligands. *Nucleic acids research* **2018**, *46* (D1), D440-D446. DOI: 10.1093/nar/gkx1109.

3. Discovery of a High-Affinity and Selective Radioligand for the Histamine H_3 Receptor

Note: Prior to the submission of this thesis, the content of this chapter, except for minor changes, was published in collaborations with partners:

Mönnich, D.*; Nagl, M.*; Forster, L.; Rosier, N.; Igel, P.; Pockes, S. Discovery of a Tritiated Radioligand with High Affinity and Selectivity for the Histamine H3 Receptor. *ACS medicinal chemistry letters* **2023,** 14 (11), 1589–1595. DOI: 10.1021/acsmedchemlett.3c00413. *contributed equally

The following work was performed by co-workers:

Dr. Martin Nagl contributed equally: Synthesis, analytical characterization and radiolabeling of the radioligand [^{3}H]UR-MN259 (not shown).

Ulla Seibel-Ehlert: Generation of stable HEK293T SP-Flag-hH_1R / hH_2R / hH_3R and hH_4R cell lines.

3.1. Introduction

The histamine H_3 receptor (H_3R) represents one of four members of the histamine receptor family, which belong to class A of the superfamily of G-protein-coupled receptors (GPCRs).[1] The H_3R conveys its signaling primarily through G_i proteins[2,3] and is predominantly found in the brain,[1,4–6] making it a target of interest in multiple central nervous system disorders, including Parkinson's,[7] Huntington's,[8,9] and Alzheimer's diesease,[10] as well as tic disorders.[11] The 2016 commercial launch of the inverse H_3R agonist pitolisant for the treatment of narcolepsy has demonstrated that the H_3R is druggable, making it of greatest interest for the central nervous system (CNS) disorders described above.[12] In order to perform more advanced studies in cell-based assays or human and animal tissues to further explore the biological role of the H_3R, the use of pharmacological tools like radioligands with strong selectivity for the corresponding receptor is of paramount importance. Especially for the H_3R, this issue plays a major role due to the high sequence homology to the H_4R, since many H_3R ligands also have a considerable affinity at the H_4R.[13] Taking a look at the tritium-labeled radioligands used so far, the partial agonist [^{3}H]UR-PI294 reveals a compound that exhibits exactly these properties, namely an almost equal affinity for both receptors, the H_3R and H_4R.[14] The previously used radioligands [^{3}H](*R*)-α-methylhistamine[15] and [^{3}H]N^{α}-methylhistamine[16,17] entail long known problems as full agonists, such as receptor internalization in cell-based systems, and are therefore similarly unsuitable.[18]

3.2. Materials and Methods

3.2.1. Materials

Dulbecco's modified Eagle's medium high glucose (DMEM) and HEPES (1 M in distilled (d)H_2O, pH = 7.4, sterilized and stored at 4 °C) were from Sigma (Taufkirchen, Germany). Leibovitz's L-15 medium without phenol red (L-15) was from Gibco (Taufkirchen, Germany). Fetal calf serum (FCS), trypsin (0.05% trypsin, 0.02% EDTA in PBS) and geneticin (G418) were from Merck (Darmstadt, Germany). The NanoLuciferase substrate furimazine (Nano-Glo®) was from Promega (Walldorf, Germany). HEK293T cells (RRID:CVCL_0063) were a kind gift from Wulf Schneider (Institute for Medical Microbiology and Hygiene, Regensburg, Germany) and stable cell lines HEK293T SP-Flag-h$H_{1/2/3/4}$R was generated from Ulla Seibel – Ehlert (Institute of Chemistry and Pharmacy, Medicinal and Pharmaceutical Chemistry II, University of Regensburg).

Depending on their physicochemical properties, when possible, ligands were dissolved in dH_2O; otherwise DMSO (Merck) was used as a solvent. Pitolisant (pito), clobenpropit (clo), JNJ-5207852 (JNJ), thioperamide (thio), histamine (his), imetit (imet) ,(*R*) – α- methylhistamine (RAMH); (*S*) – α- methylhistamine (SAMH).

3.2.2. NanoBRET competition binding experiments at the NLuc-hH$_3$R

NanoBRET competition binding experiments were performed as described by Grätz et al. 2020 and Rosier et al. 2021 at 37° C using a CLARIOstar Plus plate reader (BMG LABTECH, Ortenberg, Germany) and furimazine as a substrate (Promega, Mannheim).[19,20] Cells were seeded at a density of 1.25 x 10^6 cells/ml in Leibovitz's L-15 media supplemented with 10 mM HEPES and 5% FCS 16 h befor the experiemtns in a white 96-well plate (BRANDplates® cellGrade 781965, VWR) and incubated at 37 °C overnight in a humidified atmosphere. The dilution of the substrate (furimazine), fluorescence ligand UR-NR266 (c = 500 pM) and samples were prepared in Leibovitz's L-15 media supplemented with 10 mM HEPES and 1% BSA prior to the experiment. After the addition of 10 µl of the substrate and pre-diluted samples cells were incubatet for 5 min, follwed by the addition of 10 µl of the fluorescent ligand. The luminscence was read for 20 cycles at 1 s integration time for both 'Blue' (< 470nm) and 'Red' (> 610nM) filter wavelengths. The BRET ratio for each timepoint was calculated by dividing the Red filtered light emission by the Blue filtered light emission.

3.2.3. Radioligand Binding Experiments

Radioligand competition binding experiments and generation of the stable HEK293T SP-FLAG-hH$_1$R, HEK293T SP-FLAG-hH$_2$R, HEK293T SP-FLAG-hH$_3$R K16, and HEK293T SP-FLAG-hH$_4$R cell lines were performed as previously described.[20–22] Bartole Ligand dilutions were prepared 10-fold concentrated in binding buffer supplemented with 5 mg/mL bacitracin and 10 µL/well was transferred to a flat-bottom polypropylene 96-well microtiter plate (Greiner Bio-One, Frickenhausen, Germany), as well as 10 µL/well of the respective radioligand [H$_1$R: [^{3}H]mepyramine (c = 5 nM, K_d = 5.05 nM); H$_2$R: [^{3}H]UR-KAT479 (c = 25 nM, K_d = 25.00 nM); H$_3$R: [^{3}H]**2.1** ([^{3}H]UR-MN259, c = 0.5 nM, K_d = 0.558 nM); H$_4$R: [^{3}H]histamine (c = 40 nM, K_d = 47.50 nM)]. The cells were adjusted to a density of 1.00 × 10^6 cells/mL for H$_1$R, H$_2$R, and H$_4$R and in case of the H$_3$R to 300,000 cells/mL, and 80 µL of the cell suspension was added to each well (total volume of 100 µL). After 60 min the incubation was stopped by using rapid filtration through Whatman GF/C filters precoated with 0.3% polyethyleneimine with an automated cell harvester (Brandel, Gaithersburg, USA).

Radioligand saturation binding and kinetic binding experiments were performed and analyzed as described by Tropmann et al.[23] and Forster et al.[24] In saturation binding experiments, non-specific binding was determined in the presence of clobenpropit in a 1,000-fold excess of the radioligand. Association and dissociation studies were performed with live HEK293T Flag-hH$_3$R-K16 cells in binding buffer supplemented with 5 mg/mL bacitracin. For association experiments radioligand [^{3}H]**2.1** ([^{3}H]UR-MN259) was added at different time points in a final concentration of 500 pM. Non-specific binding was determined in the presence of clobenpropit in a 1,000-fold excess of the

radioligand. After 60 min the incubation was stopped using rapid filtration through Whatman GF/C filters precoated with 0.3% Polyethylenimine with an automated cell harvester (Brandel, Gaithersburg, USA). For dissociation studies HEK293T- Flag-hH_3R cells were incubated with [^{3}H]**2.1** (c = 500 pM) for 30 min. Afterwards 500 nM clobenpropit (1,000-fold excess) was added at different time points and after 60 min reaction was terminated using a cell harvester as described above. For all experiments, radioactivity was measured using a MicroBeta2 1450 scintillation counter (PerkinElmer, Rodgau, Germany).

All data were analyzed using GraphPad Prism10 software (San Diego, CA, USA). The normalized competition binding curves were fitted with a four-parameter logistic fit yielding pIC_{50}-values. These were transformed into pK_i values using the Cheng-Prusoff equation.[25] Specific-binding data (dpm) from saturation binding experiments were plotted against the free radioligand concentration (nM) and analyzed by nonlinear regression (one site-specific-binding equation) to obtain pK_d and B_{max} values. Nonspecific-binding data were fitted by linear regression. The specific-binding data (dpm) from association experiments were fitted by a one-phase equation (one-phase association) to a maximum to obtain k_{obs} (observed association rate constant) and specifically bound radioligand, which is plotted against time. Specifically bound radioligand from dissociation experiments were plotted against time and were analyzed by a three-parameter equation (one-phase decay).

3.2.4. MiniG Recruitment Assay

The miniG recruitment Assay was performed on stable HEK293T-hH_3R-NlucC-NlucN-miniG_{si} cells as described by Höring et al. 2022 at 37 °C with a CLARIOstar Plus plate reader (BMG LABTECH, Ortenberg, Germany) to characterize **2.1** in both modes, agonist and antagonist mode) using furimazine as a substrate (Promega, Mannheim).[26] One day before the experiments, cells were seeded at a density of 1.25 x 10^6 cells/mL in Leibovitz's L-15 media supplemented with 10 mM HEPES and 5% FCS in a white 96-well plate (BRANDplates® cellGrade 781965, VWR) and incubated at 37 °C overnight in a humidified atmosphere. The dilution of the substrate (furimazine) and samples were prepared in Leibovitz's L-15 media supplemented with 10 mM HEPES prior to the experiment. The basal luminescence was recorded immediately after adding 10 µL of the substrate to each well for 13 plate repeats with an integration time of 0.5 s per well. 10 µL of every concentration of the ligand dilution series were added in triplicate, and the final luminescence measurement was performed for further 39 plate repeats. A similar procedure was performed for the characterization of **2.1** in the antagonist mode. Further 13 plate repeats were recorded after the addition of the serial dilutions of **2.1**, followed by the final measurement of 39 cycles after adding 10 µL of 1 µM histamine as the endogenous agonist at the EC_{80} concentration. For the normalization of the data, the negative control (solvent control) and positive control (maximum level of 100 µM histamine in agonist mode and 1 µM histamine in antagonist mode)

were included on every assay plate. The resulting pK_b values were all determined according to the Cheng-Prusoff equation.[25]

3.3. Results

For the synthesis of a new H_3R radioligand, the H_3R antagonist JNJ-5207852 (Appendix, Figure 7.31) seemed to be a suitable scaffold due to its high affinity and selectivity to the target receptor.[20,27] The synthetic accessibility and the fact that this lead structure has been recently and very successfully used as a fluorescent ligand for NanoBRET studies (a technique that has been successfully established in our group[19,20]) and single-molecule microscopy, makes this motif an excellent pharmacophore for a radioligand.[20] The para position of the benzylic piperidine moiety showed high tolerance in structure-activity relationships with respect to structural changes of the ligand, so this position of the molecule was chosen for the implementation of a primary amine.[28] This functionality now allows the commercially available tritiated propionyl residue to be introduced via nucleophilic substitution reaction using *N*-succinimidyl [2,3-^{3}H]propionate under standard laboratory conditions.[14,23,29]

In order to evaluate the suitability of compound **2.1** as a potential radioligand, binding to the human H_3R was first tested in our standard NanoBRET binding assay in a competition with fluorescent ligand UR-NR266.[20] We observed a dose-dependent concentration-response curve (CRC) with sub-nanomolar affinity to the hH_3R (pK_i = 9.56, Figure 3.1 A, Table 3.1), which was to be expected given the present pharmacophore. The extent to which propionylation affects selectivity within the histamine receptor family was also of great interest, which is why radioligand binding studies were performed at the H_1R, H_2R, and H_4R. Hardly any displacement of the corresponding radioligands was observed, up to a concentration of 100 µM (Figure 3.1 B), indicating compound **2.1** to be highly selective for the H_3R (> 100,000-fold, Table 3.1). Furthermore, the mode of action of compound **2.1** at the H_3R was investigated using the miniG recruitment assay (H_3R-NlucC/NlucN-mG_{si}) to exclude the disadvantages of agonistic compounds mentioned above. As expected, compound **2.1** showed no agonistic activity up to a concentration of 10 µM (cf. Figure 3.1 C) and gave a pK_b value of 9.39 in the antagonist mode (full displacement of the 1 µM histamine effect, Figure 3.1, D), which is in very good agreement with the NanoBRET binding data (Table 3.1). These data were convincing that compound **2.1** would be an excellent radioligand at the H_3R, leading to the decision to prepare **2.1** as a tritium-labeled compound.

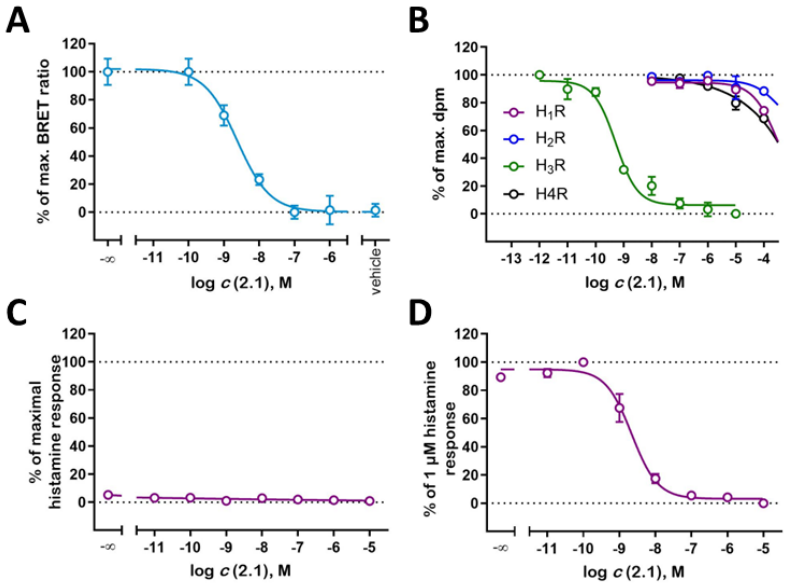

Figure 3.1: A: Representative displacement curve from BRET competition binding experiments of the fluorescent ligand UR-NR266 (c = 500 pM) and 2.1 at HEK293T cells, stably expressing the NLuc-hH$_3$R. "Vehicle" denotes the condition where the cells were not incubated with UR-NR266. B: Displacement curves from radioligand competition binding experiments performed with compound 2.1 and the respective radioligands at H$_{1\text{-}4}$Rs (cf. Table 3.1 footnotes). C/D: Concentration response curves obtained in the mini-G protein recruitment assay (H$_3$R-NlucC/NlucN-mG$_{si}$) using 2.1 in the agonist mode (C) and antagonist mode in competition with 1 µM histamine (D).

Table 3.1: Binding and functional data of **2.1** on human histamine receptor subtypes.

	NanoBRET binding UR-NR266[a]		Radioligand competition binding[b]								H$_3$R selectivity	miniG protein recruitment[c]	
	pK_i		pK_i								K_i (H$_{1,2,4}$R) / K_i (H$_3$R)	pK_b	
Cpd.	hH$_3$R[d]	*N*	hH$_1$R[e]	*N*	hH$_2$R[f]	*N*	hH$_3$R[g]	*N*	hH$_4$R[h]	*N*	hH$_{1,2,4}$R	hH$_3$R[i]	*N*
2.1	9.56 ± 0.18	4	< 4	3	< 4	3	9.55 ± 0.17	4	< 4	3	> 100.000	9.39 ± 0.09	3

[a]NanoBRET competition binding assay at live HEK293T cells stably expressing the NLuc-hH$_3$R. [b]Radioligand competition binding assay at HEK293T-SP-FLAG-hH$_1$R, HEK293T-SP-FLAG-hH$_2$R, HEK293T-SP-FLAG-hH$_3$R or HEK293T-SP-FLAG-hH$_4$R cells. [c]Competition binding experiment at HEK293T cells stably co-expressing a combination of the H$_3$R-NlucC/NlucN-mG$_{si}$ constructs.[26] [d]Displacement of 500 pM UR-NR266[20] (K_d = 158 pM). [e]Displacement of 5 nM [^{3}H]mepyramine (K_d = 5.05 nM). [f]Displacement of 25 nM [^{3}H]UR-KAT479[23,30] (K_d = 25.00 nM). [g]Displacement of 0.5 nM [^{3}H]UR-MN259 ([^{3}H]**2.1**) (K_d = 0.558 nM). [h]Displacement of 40 nM [^{3}H]histamine (K_d = 47.50 nM). [i]Displacement of 1 µM histamine (EC$_{50}$ = 0.331 µM). Data shown are mean values ± SEM of *N* independent experiments, each performed in triplicate. Data were analyzed by nonlinear regression and were best fitted to sigmoidal concentration-response curves (variable slope). Displacement curves are presented in Figure 3.1.

The radioligand was first characterized in saturation binding experiments at wild-type hH_3R stably expressed in HEK293T cells (HEK293T SP-FLAG-hH_3R) analogous to previous studies.[23,24] The specific binding of [^{3}H]**2.1** was best fitted by nonlinear regression to a one-site binding model and the non-specific binding by linear regression. In a concentration range of 0.05-5 nM, [^{3}H]**2.1** showed moderate to low non-specific binding in the presence of 1,000-fold excess of clobenpropit and bound to the hH_3R in a saturable manner revealing a pK_d of 9.25 (Figure 3.2, Table 3.2) with a B_{max} of 1,668 dpm, which is corresponding to 89,430 receptor sites/cell. We performed kinetic binding experiments at the hH_3R to further characterize [^{3}H]**2.1** with association and dissociation curves shown in Figure 3.2. Ligand binding of the radioligand (c = 500 pM) was rapid, saturated after about 15 minutes (τ_{ass} = 6.11 min) and could be described by a monophasic fit with an association rate constant k_{on} of 0.22 min^{-1} nM^{-1} and k_{obs} of 0.18 min^{-1} (cf. Figure 3.2 B, Table 3.2). Dissociation of [^{3}H]**2.1** (hH_3R: c = 500 pM, 30 min preincubation) was performed upon addition of clobenpropit (c = 500 nM) with full dissociation from the receptor after about 60 minutes and a dissociation rate constant k_{off} of 0.07 min^{-1} (τ_{diss} = 14.48 min) (cf. Figure 3.2 C, Table 3.2). The data obtained indicate reversible binding and the pK_d value calculated from kinetics (9.49, Table 3.2) was in good agreement with the pK_d value from saturation binding experiments (9.25, Table 3.2). All kinetic parameters describing the binding of **2.1** in the presented study are listed in Table 3.2.

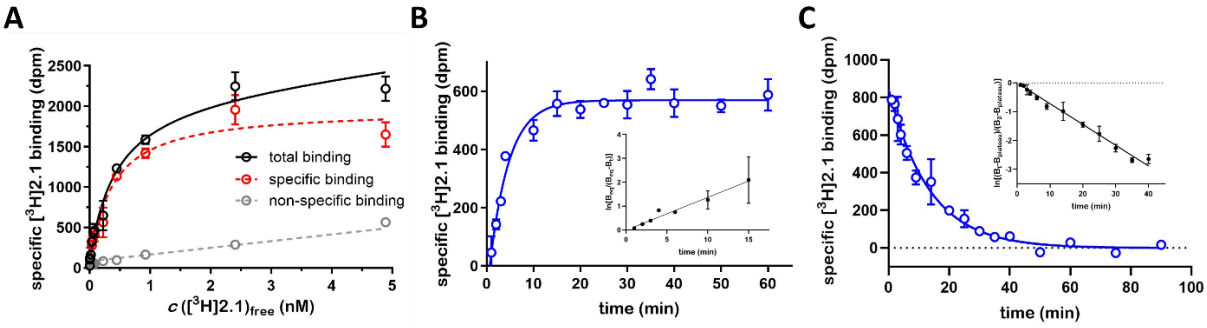

Figure 3.2: Representative data from saturation and kinetic binding experiments with [^{3}H]**2.1** at the hH_3R stably expressed in HEK293T cells. **A:** Saturation of [^{3}H]**2.1** to the hH_3R. Non-specific binding was determined in the presence of 1,000-fold excess of clobenpropit. **B:** Association of [^{3}H]**2.1** (c = 500 pM) to the hH_3R. C: Dissociation of [^{3}H]**2.1** (c = 500 pM, 30 min preincubation) induced by addition of clobenpropit (c = 500 nM, 1,000-fold excess).

Table 3.2: Thermodynamic and kinetic binding constants of **2.1** at the wild-type hH_3R in radioligand binding studies.

Cpd.	pK_d (sat)[a]	k_{obs}[b] / min^{-1}	τ_{ass}[c] / min	k_{off}[b] / min^{-1}	τ_{diss}[d] / min	k_{on}[e] / min^{-1} nM^{-1}	pK_d (kin)[f]
2.1	9.25 ± 0.09	0.18 ± 0.04	6.11 ± 2.41	0.07 ± 0.01	14.48 ± 1.84	0.22 ± 0.07	9.49 ± 0.46

[a]Data represent mean values ± SEM from five independent experiments each performed in triplicate. Radioligand binding measurements were performed at HEK293T-SP-FLAG-hH_3R (wild-type hH_3R) cells. [b]Data represent mean values ± SEM from three independent experiments. [c]Association time constant: $\tau_{ass} = 1/k_{obs}$. [d]Dissociation time constant: $\tau_{diss} = 1/k_{off}$. [c,d]Data represent mean values ± CI (95%). [e]Association rate constant: $k_{on} = (k_{obs}-k_{off})/c$ (**2.1**). [f]K_d (kin) = k_{off}/k_{on}; pK_d (kin) = -log K_d (kin).[e,f]Indicated errors were calculated according to the Gaussian law of error propagation.

The total reversibility of receptor binding makes radioligand [^{3}H]**2.1** a suitable tool for the application in competition binding studies. For this purpose, we made a selection of standard H_3R agonists and antagonists and performed the corresponding experiments (see structures in Appendix, Figure 7.31). We chose histamine (his),[31] imetit (imet),[32] (*R*)-(-)-α-methylhistamine (RAMH),[15] and (*S*)-(+)-α-methylhistamine (SAMH)[15] as agonists and clobenpropit (clob),[33] thioperamide (thio),[15] pitolisant (pito),[34] and JNJ-5207852 (JNJ)[27] as inverse agonists/antagonists. Additionally, we tested unlabeled **2.1** for comparison. For all ligands, total displacement could be observed with Hill slopes around 1 (Figure 3.3). The values obtained were in good agreement with literature data, only the affinities for RAMH and SAMH were reversed in their order (Table 3.3). The displacement of the radioligand with its "cold" form, compound **2.1**, was also complete (Figure 3.3) and resulted in a pK_i value of 9.55 (cf. Table 3.1 and 3.3). The determined affinity of **2.1** thus confirms, as expected, the affinity of **2.1** from the NanoBRET binding experiment (pK_i = 9.56, Figure 3.1 A, Table 3.1) and correspondingly also the exceptionally high selectivity within the histamine receptor family (> 100,000, Table 3.1).

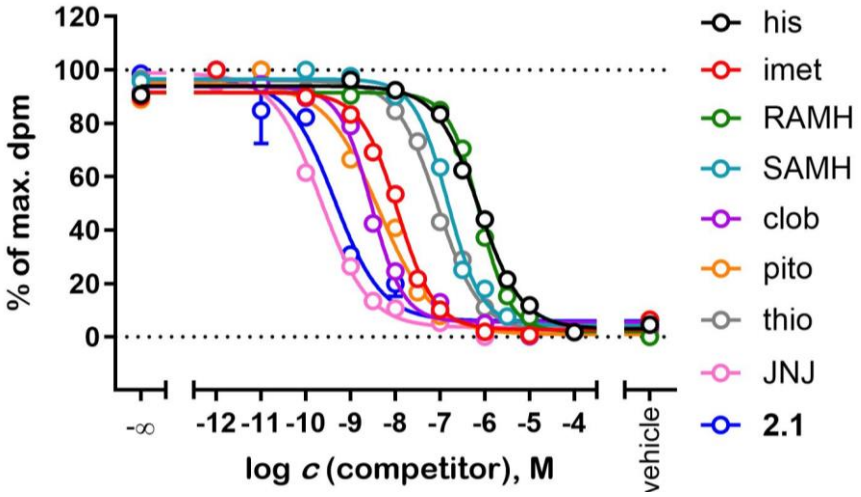

Figure 3.3: Displacement curves from radioligand competition binding experiments of radioligand [^{3}H]**2.1** (c = 500 pM) and reported H_3 receptor ligands at HEK293T cells stably expressing the hH_3R. "Vehicle" denotes the condition where the cells were incubated with [^{3}H]**2.1** in the presence of 500 nM clobenpropit. Abbreviations used: histamine (his), imetit (imet), (*R*)-(−)-α-methylhistamine (RAMH), (*S*)-(+)-α-methylhistamine (SAMH), clobenpropit (clob), pitolisant (pito), thioperamide (thio), and JNJ-5207852 (JNJ).

Table 3.3: Binding data (pK_i values) of standard H_3R ligands and **2.1** determined at the human H_3R in the radioligand competition binding assay using [^{3}H]**2.1** as a radioligand.[a]

compound	RLB using [^{3}H]2.1		references
	pK_i	*N*	pK_i
his	6.41 ± 0.06	4	6.2[20]; 6.3[35]; 6.5[21]; 7.6[36]; 8.0[37]
imet	8.24 ± 0.12	4	7.9[20]; 8.3[35]; 8.8[37]
RAMH	6.37 ± 0.12	5	7.2[20]; 8.4[38]; 8.2[37]; 8.3[39]
SAMH	7.12 ± 0.18	3	5.8[20]; 6.4[35]; 7.6[38]; 7.2[37]; 7.3[39]
clob	8.84 ± 0.25	4	9.3[20]; 9.6[35]; 9.5[21]; 8.6[37]
thio	7.38 ± 0.14	3	7.3[20]; 7.3[35]; 7.4[21]; 7.3[37]
pito	8.81 ± 0.27	3	9.0[20]; 8.6[35]; 8.6[34]
JNJ	9.98 ± 0.06	3	10.2[20]; 9.2[19]
2.1	9.55 ± 0.17	4	-

[a]Data represent mean values ± SEM from *N* independent experiments, each performed in triplicate. Radioligand binding experiments were performed at HEK293T-SP-FLAG-hH_3R (wild-type hH_3R) cells as described in the Experimental Section. The standard H_3R ligands used are depicted in Figure 7.31 in the Appendix. Abbreviations used: histamine (his), imetit (imet), (*R*)-(−)-α-methylhistamine (RAMH), (*S*)-(+)-α-methylhistamine (SAMH), clobenpropit (clob), thioperamide (thio), pitolisant (pito), and JNJ-5207852 (JNJ).

3.4. Summary and Conclusion

In this study, we have synthesized and characterized a new radioligand for the human histamine H_3 receptor, [^{3}H]**2.1** ([^{3}H]UR-MN259), by derivatizing amino-functionalized precursors, structurally related to JNJ-5207852. [^{3}H]UR-MN259 turned out to be a high-affinity hH_3R antagonist (pK_i (NanoBRET) = 9.56; pK_i (RLB) = 9.55) with an outstanding selectivity profile (> 100,000-fold selective) within the histamine receptor family. Radiosynthesis was successful using commercially available *N*-succinimidyl [2,3-3H]propionate resulting in [^{3}H]**2.1** with a radiochemical yield of 40%, specific activity of 105 Ci/mmol and high (radio)chemical purity (> 99% each) and stability (> 99% each) over 7 months. Saturation binding experiments were best described by a one-site binding model and resulted in sub-nanomolar affinity to the hH_3R (pK_d = 9.25) with moderate to low non-specific binding. Kinetic experiments exhibited fast association of [^{3}H]**2.1** to the receptor (τass = 6.11 min) and full dissociation from the receptor (τdiss = 14.48 min). The resulting dissociations constants from kinetic studies were in good agreement with the pK_d determined in saturation binding experiments. The determined binding constants of the standard H_3R ligands in competition binding experiments were in agreement with the data published in the literature (Figure 3.4).

Since the radioligand is highly selective for the H_3R, it is ideally suited for studies in whole primary cells at the endogenous level in addition to the application in recombinant systems, in which only the H_3R is expressed. The high selectivity of the JNJ pharmacophore in extensive off-target studies described by Apodaca et al. (> 50 receptors and ion channels) and Rosier et al. (14 GPCRs) also suggests high selectivity/specificity toward other target proteins. Therefore, [^{3}H]UR-MN259 is a promising pharmacological tool to further explore the role of the hH_3R in the CNS and other tissues.

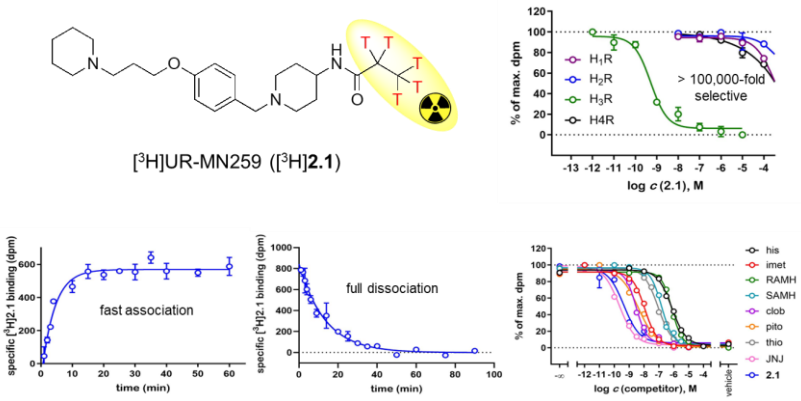

Figure 3.4: Summery of characterization results for the novel radioligand [^{3}H]UR-MN259 ([^{3}H]**2.1**).

3.5. References

(1) Clark, E. A.; Hill, S. J. Sensitivity of histamine H3 receptor agonist-stimulated 35SGTP gammaS binding to pertussis toxin. *European journal of pharmacology* **1996**, *296* (2), 223–225. DOI: 10.1016/0014-2999(95)00800-4.

(2) Arrang, J. M.; Garbarg, M.; Schwartz, J. C. Auto-inhibition of brain histamine release mediated by a novel class (H3) of histamine receptor. *Nature* **1983**, *302* (5911), 832–837. DOI: 10.1038/302832a0.

(3) Takeshita, Y.; Watanabe, T.; Sakata, T.; Munakata, M.; Ishibashi, H.; Akaike, N. Histamine modulates high-voltage-activated calcium channels in neurons dissociated from the rat tuberomammillary nucleus. *Neuroscience* **1998**, *87* (4), 797–805. DOI: 10.1016/S0306-4522(98)00152-3.

(4) Arrang, J. M.; Devaux, B.; Chodkiewicz, J. P.; Schwartz, J. C. H3-receptors control histamine release in human brain. *Journal of neurochemistry* **1988**, *51* (1), 105–108. DOI: 10.1111/j.1471-4159.1988.tb04841.x.

(5) Lovenberg, T. W.; Roland, B. L.; Wilson, S. J.; Jiang, X.; Pyati, J.; Huvar, A.; Jackson, M. R.; Erlander, M. G. Cloning and functional expression of the human histamine H3 receptor. *Molecular pharmacology* **1999**, *55* (6), 1101–1107.

(6) Rapanelli, M. The magnificent two: histamine and the H3 receptor as key modulators of striatal circuitry. *Progress in neuro-psychopharmacology & biological psychiatry* **2017**, *73*, 36–40. DOI: 10.1016/j.pnpbp.2016.10.002.

(7) Ferrada, C.; Ferré, S.; Casadó, V.; Cortés, A.; Justinova, Z.; Barnes, C.; Canela, E. I.; Goldberg, S. R.; Leurs, R.; Lluis, C.; Franco, R. Interactions between histamine H3 and dopamine D2 receptors and the implications for striatal function. *Neuropharmacology* **2008**, *55* (2), 190–197. DOI: 10.1016/j.neuropharm.2008.05.008.

(8) Goodchild, R. E.; Court, J. A.; Hobson, I.; Piggott, M. A.; Perry, R. H.; Ince, P.; Jaros, E.; Perry, E. K. Distribution of histamine H3-receptor binding in the normal human basal ganglia: comparison with Huntington's and Parkinson's disease cases. *The European journal of neuroscience* **1999**, *11* (2), 449–456. DOI: 10.1046/j.1460-9568.1999.00453.x.

(9) Moreno-Delgado, D.; Puigdellívol, M.; Moreno, E.; Rodríguez-Ruiz, M.; Botta, J.; Gasperini, P.; Chiarlone, A.; Howell, L. A.; Scarselli, M.; Casadó, V.; Cortés, A.; Ferré, S.; Guzmán, M.; Lluís, C.; Alberch, J.; Canela, E. I.; Ginés, S.; McCormick, P. J. Modulation of dopamine D1 receptors via histamine H3 receptors is a novel therapeutic target for Huntington's disease. *eLife* **2020**, *9.* DOI: 10.7554/eLife.51093.

(10) Rodríguez-Ruiz, M.; Moreno, E.; Moreno-Delgado, D.; Navarro, G.; Mallol, J.; Cortés, A.; Lluís, C.; Canela, E. I.; Casadó, V.; McCormick, P. J.; Franco, R. Heteroreceptor Complexes Formed by Dopamine D1, Histamine H3, and N-Methyl-D-Aspartate Glutamate Receptors as Targets to Prevent Neuronal Death in Alzheimer's Disease. *Molecular neurobiology* **2017**, *54* (6), 4537–4550. DOI: 10.1007/s12035-016-9995-y. 5127

(11) Rapanelli, M.; Frick, L.; Pogorelov, V.; Ohtsu, H.; Bito, H.; Pittenger, C. Histamine H3R receptor activation in the dorsal striatum triggers stereotypies in a mouse model of tic disorders. *Translational psychiatry* **2017**, *7* (1), e1013. DOI: 10.1038/tp.2016.290.

(12) Syed, Y. Y. Pitolisant: First Global Approval. *Drugs* **2016**, *76* (13), 1313–1318. DOI: 10.1007/s40265-016-0620-1.

(13) Esch, I. J. P. de; Thurmond, R. L.; Jongejan, A.; Leurs, R. The histamine H4 receptor as a new therapeutic target for inflammation. *Trends in pharmacological sciences* **2005**, *26* (9), 462–469. DOI: 10.1016/j.tips.2005.07.002.

(14) Igel, P.; Schnell, D.; Bernhardt, G.; Seifert, R.; Buschauer, A. Tritium-labeled N(1)-3-(1H-imidazol-4-yl)propyl-N(2)-propionylguanidine ((3)HUR-PI294), a high-affinity histamine H(3) and H(4) receptor radioligand. *ChemMedChem* **2009**, *4* (2), 225–231. DOI: 10.1002/cmdc.200800349.

(15) Arrang, J. M.; Garbarg, M.; Lancelot, J. C.; Lecomte, J. M.; Pollard, H.; Robba, M.; Schunack, W.; Schwartz, J. C. Highly potent and selective ligands for histamine H3-receptors. *Nature* **1987**, *327* (6118), 117–123. DOI: 10.1038/327117a0.

(16) Korte, A.; Myers, J.; Shih, N. Y.; Egan, R. W.; Clark, M. A. Characterization and tissue distribution of H3 histamine receptors in guinea pigs by N alpha-methylhistamine. *Biochemical and biophysical research communications* **1990**, *168* (3), 979–986. DOI: 10.1016/0006-291x(90)91125-c.

(17) West, R. E.; Zweig, A.; Shih, N. Y.; Siegel, M. I.; Egan, R. W.; Clark, M. A. Identification of two H3-histamine receptor subtypes. *Molecular pharmacology* **1990**, *38* (5), 610–613.

(18) Osorio-Espinoza, A.; Escamilla-Sánchez, J.; Aquino-Jarquin, G.; Arias-Montaño, J.-A. Homologous desensitization of human histamine H_3 receptors expressed in CHO-K1 cells. *Neuropharmacology* **2014**, *77*, 387–397. DOI: 10.1016/j.neuropharm.2013.09.011.

(19) Grätz, L.; Tropmann, K.; Bresinsky, M.; Müller, C.; Bernhardt, G.; Pockes, S. NanoBRET binding assay for histamine H2 receptor ligands using live recombinant HEK293T cells. *Scientific reports* **2020**, *10* (1), 13288. DOI: 10.1038/s41598-020-70332-3.

(20) Rosier, N.; Grätz, L.; Schihada, H.; Möller, J.; Işbilir, A.; Humphrys, L. J.; Nagl, M.; Seibel, U.; Lohse, M. J.; Pockes, S. A Versatile Sub-Nanomolar Fluorescent Ligand Enables NanoBRET Binding Studies and Single-Molecule Microscopy at the Histamine H3 Receptor. *Journal of medicinal chemistry* **2021**, *64* (15), 11695–11708. DOI: 10.1021/acs.jmedchem.1c01089.

(21) Bartole, E.; Grätz, L.; Littmann, T.; Wifling, D.; Seibel, U.; Buschauer, A.; Bernhardt, G. UR-DEBa242: A Py-5-Labeled Fluorescent Multipurpose Probe for Investigations on the Histamine H3 and H4 Receptors. *Journal of medicinal chemistry* **2020**, *63* (10), 5297–5311. DOI: 10.1021/acs.jmedchem.0c00160.

(22) Seibel-Ehlert, U.; Plank, N.; Inoue, A.; Bernhardt, G.; Strasser, A. Label-Free Investigations on the G Protein Dependent Signaling Pathways of Histamine Receptors. *International journal of molecular sciences* **2021**, *22* (18). DOI: 10.3390/ijms22189739.

(23) Tropmann, K.; Höring, C.; Plank, N.; Pockes, S. Discovery of a G Protein-Biased Radioligand for the Histamine H2 Receptor with Reversible Binding Properties. *Journal of medicinal chemistry* **2020**, *63* (21), 13090–13102. DOI: 10.1021/acs.jmedchem.0c01494.

(24) Forster, L.; Grätz, L.; Mönnich, D.; Bernhardt, G.; Pockes, S. A Split Luciferase Complementation Assay for the Quantification of β-Arrestin2 Recruitment to Dopamine D2-Like Receptors. *International journal of molecular sciences* **2020**, *21* (17). DOI: 10.3390/ijms21176103.

(25) Cheng, Y.; Prusoff, W. H. Relationship between the inhibition constant (K1) and the concentration of inhibitor which causes 50 per cent inhibition (I50) of an enzymatic reaction. *Biochemical pharmacology* **1973**, *22* (23), 3099–3108. DOI: 10.1016/0006-2952(73)90196-2.

(26) Höring, C.; Seibel, U.; Tropmann, K.; Grätz, L.; Mönnich, D.; Pitzl, S.; Bernhardt, G.; Pockes, S.; Strasser, A. A Dynamic, Split-Luciferase-Based Mini-G Protein Sensor to Functionally Characterize Ligands at All Four Histamine Receptor Subtypes. *International journal of molecular sciences* **2020**, *21* (22). DOI: 10.3390/ijms21228440.

(27) Apodaca, R.; Dvorak, C. A.; Xiao, W.; Barbier, A. J.; Boggs, J. D.; Wilson, S. J.; Lovenberg, T. W.; Carruthers, N. I. A new class of diamine-based human histamine H3 receptor antagonists: 4-(aminoalkoxy)benzylamines. *Journal of medicinal chemistry* **2003**, *46* (18), 3938–3944. DOI: 10.1021/jm030185v.

(28) Wingen, K.; Schwed, J. S.; Isensee, K.; Weizel, L.; Zivković, A.; Odadzic, D.; Stark, H. Benzylpiperidine variations on histamine H3 receptor ligands for improved drug-likeness. *Bioorganic & medicinal chemistry letters* **2014**, *24* (10), 2236–2239. DOI: 10.1016/j.bmcl.2014.03.098.

(29) Keller, M.; Pop, N.; Hutzler, C.; Beck-Sickinger, A. G.; Bernhardt, G.; Buschauer, A. Guanidine-acylguanidine bioisosteric approach in the design of radioligands: synthesis of a tritium-labeled N(G)-propionylargininamide (3H-UR-MK114) as a highly potent and selective neuropeptide Y Y1 receptor antagonist. *Journal of medicinal chemistry* **2008**, *51* (24), 8168–8172. DOI: 10.1021/jm801018u.

(30) Pockes, S.; Tropmann, K. Histamine H2 receptor radioligands: triumphs and challenges. *Future medicinal chemistry* **2021**, *13* (12), 1073–1081. DOI: 10.4155/fmc-2021-0058.

(31) Windaus, A., Vogt, W. Synthesis of Imidazolylethylamine. *Berichte der Deutschen Chemischen Gesellschaft* **1907** (40), 3685–3691.

(32) Garbarg, M.; Arrang, J. M.; Rouleau, A.; Ligneau, X.; Tuong, M. D.; Schwartz, J. C.; Ganellin, C. R. S-2-(4-imidazolyl)ethylisothiourea, a highly specific and potent histamine H3 receptor agonist. *The Journal of pharmacology and experimental therapeutics* **1992**, *263* (1), 304–310.

(33) van der Goot, H.; Schepers, M. J.; Sterk, G. J.; Timmerman, H. Isothiourea analogues of histamine as potent agonists or antagonists of the histamine H3-receptor. *European journal of medicinal chemistry* **1992**, *27* (5), 511–517. DOI: 10.1016/0223-5234(92)90185-4.

(34) Ligneau, X.; Perrin, D.; Landais, L.; Camelin, J.-C.; Calmels, T. P. G.; Berrebi-Bertrand, I.; Lecomte, J.-M.; Parmentier, R.; Anaclet, C.; Lin, J.-S.; Bertaina-Anglade, V.; La Rochelle, C. D.; d'Aniello, F.; Rouleau, A.; Gbahou, F.; Arrang, J.-M.; Ganellin, C. R.; Stark, H.; Schunack, W.; Schwartz, J.-C. BF2.649 1-{3-3-(4-Chlorophenyl)propoxypropyl}piperidine, hydrochloride, a nonimidazole inverse agonist/antagonist at the human histamine H3 receptor: Preclinical pharmacology. *The Journal of pharmacology and experimental therapeutics* **2007**, *320* (1), 365–375. DOI: 10.1124/jpet.106.111039.

(35) Mocking, T. A. M.; Verweij, E. W. E.; Vischer, H. F.; Leurs, R. Homogeneous, Real-Time NanoBRET Binding Assays for the Histamine H3 and H4 Receptors on Living Cells. *Molecular pharmacology* **2018**, *94* (6), 1371–1381. DOI: 10.1124/mol.118.113373.

(36) Pockes, S.; Wifling, D.; Keller, M.; Buschauer, A.; Elz, S. Highly Potent, Stable, and Selective Dimeric Hetarylpropylguanidine-Type Histamine H2 Receptor Agonists. *ACS omega* **2018**, *3* (3), 2865–2882. DOI: 10.1021/acsomega.8b00128.

(37) Lim, H. D.; van Rijn, R. M.; Ling, P.; Bakker, R. A.; Thurmond, R. L.; Leurs, R. Evaluation of histamine H1-, H2-, and H3-receptor ligands at the human histamine H4 receptor: identification of 4-methylhistamine as the first potent and selective H4 receptor agonist. *The Journal of pharmacology and experimental therapeutics* **2005**, *314* (3), 1310–1321. DOI: 10.1124/jpet.105.087965.

(38) Wulff, B. S.; Hastrup, S.; Rimvall, K. Characteristics of recombinantly expressed rat and human histamine H3 receptors. *European journal of pharmacology* **2002**, *453* (1), 33–41. DOI: 10.1016/S0014-2999(02)02382-8.

(39) Schihada, H.; Ma, X.; Zabel, U.; Vischer, H. F.; Schulte, G.; Leurs, R.; Pockes, S.; Lohse, M. J. Development of a Conformational Histamine H3 Receptor Biosensor for the Synchronous Screening of Agonists and Inverse Agonists. *ACS sensors* **2020**, *5* (6), 1734–1742. DOI: 10.1021/acssensors.0c00397.

4. Investigation of Binding and Functional Characteristics of the D_1R-H_3R and $D_{2l}R$-H_3R Heteromers

Co-workers performed the following experimental work:

Dr. Niklas Rosier: Synthesis and analytical characterization of bivalent ligand NR330 (not shown).

Dr. Martin Nagl: Synthesis and analytical characterization of bivalent ligands MN075, MN209, and MN240 (not shown).

Ulla Seibel-Ehlert: Generation of stable cell line HEK293T FLAG-hH_3R.

Dr. Lisa Forster: One radioligand competition binding experiment, shown in Chapter 7.

4.1. Introduction

G protein-coupled receptors (GPCRs) are seven transmembrane receptors, connected through three extracellular loops (ECL) and intracellular loops (ICL), divided into six subclasses (class A – class F).[1–3] They are targeted by 30% - 40% of all current drugs and therefore an evolution in the understanding of signaling pathways and binding properties of GPCRs is constantly required.[4,5] Currently, the theory that receptors of the class A family can exist, besides monomers, as homo-, heterodimers, or higher order oligomers is widely regarded as probable.[6–8] With the development of techniques like bioluminescence and fluorescence resonance energy transfer,[9–11] protein complementation,[12,13] and imaging[14,15], the existence of oligomers is supported. The formation of homo- or heteromers is not necessary for the functionality of the receptors, unlike the class C family of GPCRs,[16,17] and is not always a steady state,[18,19] like in Huntington's disease, where the D_1R-H_3R heteromer is only present in a certain stage of the disease.[20] Thus, it is important to understand if the formation of the homo- or heteromer has advantages or disadvantages in binding or signal properties compared to the monomers.[21]

As mentioned, one known representative of receptor heteromerization is the D_1R-H_3R heteromer which occurs in the striatal tissue of the human brain.[22] Both the D_1R and H_3R belong to the class A family of GPCRs. It has been shown that those receptors can form heterodimers and oligomeric complexes containing the D_1R, H_3R and N-methyl-D-aspartate (NMDA)-receptor subunits.[23,24] Inhibition of this complex leads to reduced dopamine, NMDA and $\beta_{1\text{-}42}$-amyloid induced cell death, demonstrating its potential as a target for neurodegenerative diseases, such as Alzheimer's disease.[25,26] Therefore bivalent ligands were a novel approach in drug design, consisting of two pharmacophores for the respective receptors, coupled through a linker with different lengths and properties. [27–29] In contrast to bitopic ligands, bivalent ligands target two orthosteric binding sites in a homomer or heteromer,[30] instead of one orthosteric binding site and an adjacent allosteric binding pocket. [31,32] Likewise, the $D_{2l}R$-H_3R heteromer, comprising two protomers of class A GPCRs, occurs in the striatal tissue of the human brain – as shown by Ferrada et al. 2009 in BRET studies.[33] Furthermore, the working group demonstrated a H_3R-mediated negative modulation of the $D_{2l}R$ function as a new possibility for therapeutic targets against Parkinson's disease[34] that could be addressed by novel bivalent ligands.

In previous studies for the adenosine A_1R-D_1R or A_2R–D_2R heteromer, radioligand competition binding experiments for the respective homo- or heteromers were developed to characterize those novel bivalent ligands in co-expressing cell systems in the presence of two specific radioligands for each protomer.[35,36] The bivalent ligands obtained biphasic curves with $pK_{i,low}$ and $pK_{i,high}$ values, where the $pK_{i,low}$ value represents the affinity of the bivalent ligand bound with only one pharmacophore or on expressed monomers The $pK_{i,high}$ value represents the affinity to the

heteromer when both pharmacophores are bound to the two orthosteric binding sites.[36–38] Moreover, functional assays for homo- or heteromers measuring cyclic adenosine monophosphate (cAMP) accumulation were formerly developed for a complete characterization of the newly synthesized bivalent ligands.[35,39]

To address this, the aim of this project was the development of a radioligand binding assay for the D_1R-H_3R and $D_{2L}R$-H_3R heteromers using different receptor ratios in transient co-expressing cell systems or stable cell lines. The receptor ratio of 1:2 is predicted to result in functional complexes *in vitro* for class A GPCRs and was set as aim ratio for both heteromers. Nevertheless, other stoichiometric receptor ratios were considered. Thus, to characterize the generated heteromeric system in co-expressing cells, saturation binding experiments were performed to validate the receptor expression of each protomer, followed by the calculation of the stoichiometric receptor ratio. In addition, competition binding experiments were performed with the novel bivalent ligands NR330 at the D_1R-H_3R heteromer, and MN079, MN209, and MN240 at the $D_{2l}R$-H_3R heteromer, both in co-expressing HEK293T cells (Figure 4.1). For every test compound, binding affinities with either the D_1R, $D_{2l}R$, or H_3R were compared with mono expressing HEK293T cells to the respective co-expressing HEK293T cell line.

For the investigation of negative or positive cooperativity or modulation at the $D_{2l}R$-H_3R heteromer, a miniG protein recruitment assay combined with split NanoLuc technology was designed.[40] The 'small bit' (SmBiT) was C-terminally linked to the H_3R receptor, whereas the $D_{2l}R$ was connected to the 'large bit' (LgBiT) of the spilt nano luciferase through linkers, followed by the $miniG_{si}$ protein. Upon activation by a ligand, a conformational change of the respective receptor is induced and recruitment of the $miniG_{si}$ protein occurs with concomitant complementation of the split luciferase fragments. The resulting bioluminescence is measured in the presence of the NanoLuc substrate and recruitment of the specific $miniG_{si}$ protein upon receptor activation can be monitored in a concentration-dependent manner of the ligand in real-time (Figure 4.2). For characterization, literature-known D_2-like standard ligands, H_3R standard ligands and bivalent ligands for the $D_{2l}R$-H_3R heteromer were tested.

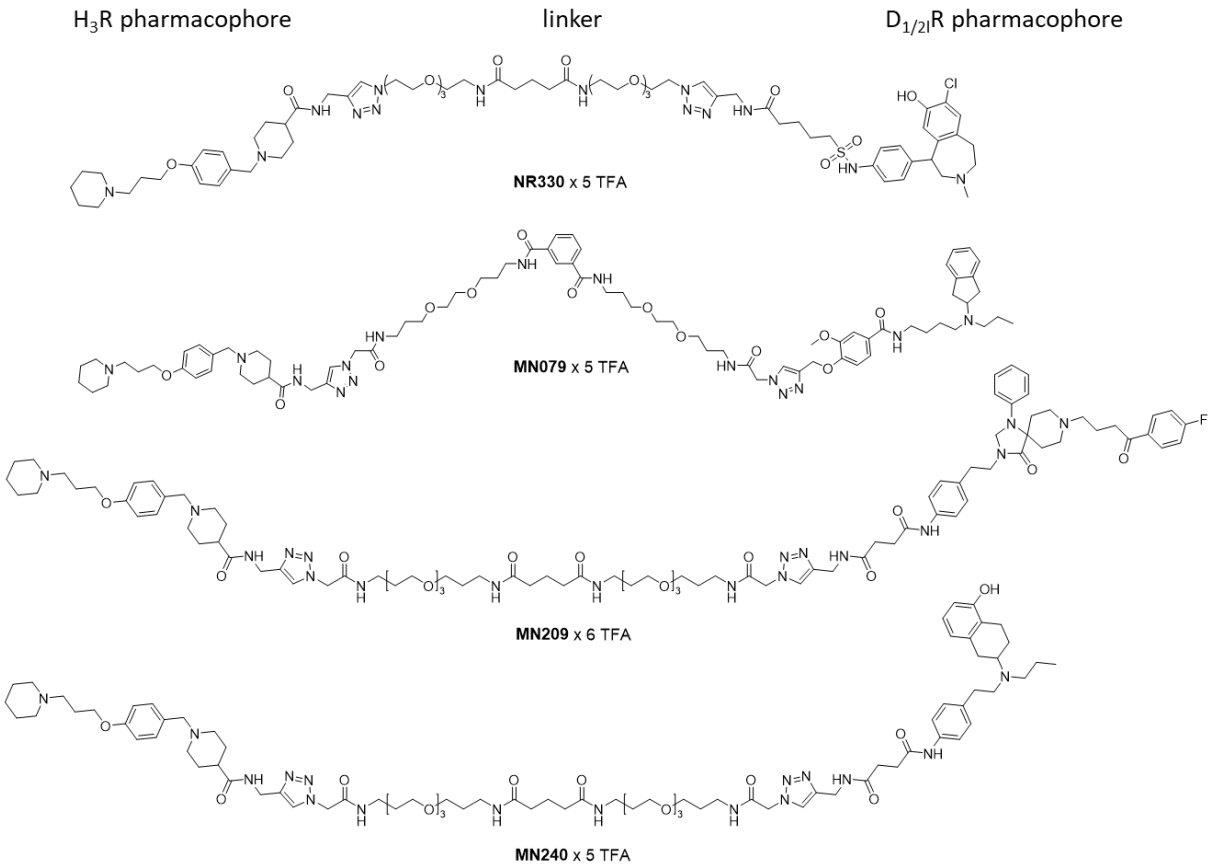

Figure 4.1: Structures of investigated bivalent ligands for the D_1R-H_3R and $D_{2l}R$-H_3R heteromer. The bivalent ligand NR330 was used for the D_1R-H_3R, whereas MN079, MN209 and MN240 were used for the characterization of the $D_{2l}R$-H_3R co-expressing HEK293T cells in radioligand binding experiments or the functional split luciferase-based miniG protein recruitment assay.

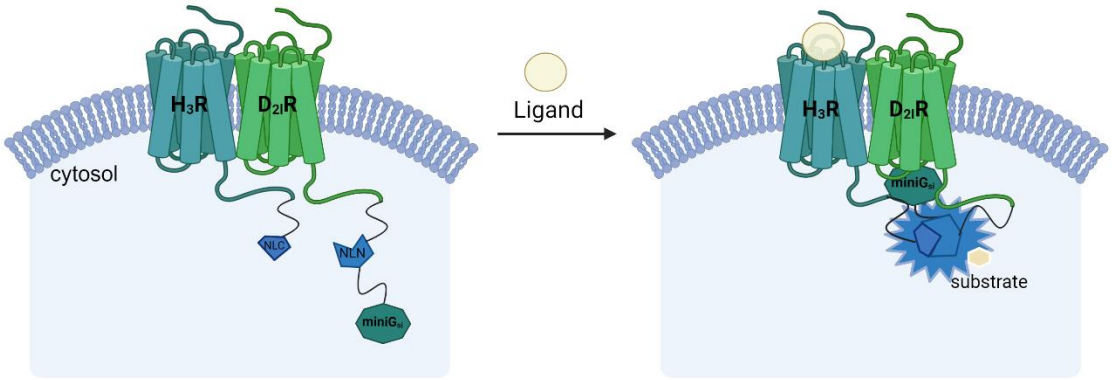

Figure 4.2: Scheme of the split nano luciferase-based miniG protein recruitment assay for the $D_{2l}R$-H_3R heterodimer in HEK293T wild type cells. After activation of the $D_{2l}R$-H_3R heteromer by a ligand, the complementation of the split luciferase fragments occurs and in presence of a substrate Furimazine bioluminescence is measurable at λ = 480 nM in the presence of a substrate. Created with BioRender.com

4.2. Materials and Methods

4.2.1. Materials

Dulbecco's modified Eagle's medium high glucose (DMEM) and HEPES (1 M in distilled (d)H_2O, pH = 7.4, sterilized and stored at 4 °C) were obtained from Sigma (Taufkirchen, Germany). Leibovitz's L-15 medium without phenol red (L-15) was from Gibco (Taufkirchen, Germany). Fetal calf serum (FCS), trypsin (0.05% trypsin, 0.02% EDTA in dH_2O) and geneticin (G418) were from Merck (Darmstadt, Germany). The NanoLuciferase substrate furimazine (Nano-Glo®) was from Promega (Walldorf, Germany). HEK293T cells (RRID:CVCL_0063) were a kind gift of Wulf Schneider (Institute for Medical Microbiology and Hygiene, Regensburg, Germany). HEK293T Flag-hH_3R were kindly provided by Ulla Seibel—Ehlert (Institute of Chemistry and Pharmacy, Medicinal und Pharmaceutical Chemistry II, Universität Regensburg). The pcDNA3.1$_{neo}$ vector was from Thermo Scientific (Nidderau, Germany). The pcDNA5 vector, as well as the HEK293T-FlipIn cells were a kind gift from Dr. Laura J. Humphrys (Institute of Chemistry and Pharmacy, Medicinal und Pharmaceutical Chemistry II, Universität Regensburg). The pIRES$_{puro}$ vector was a kind gift from Dr. Carina Höring (Institute of Chemistry and Pharmacy, Medicinal und Pharmaceutical Chemistry II, Universität Regensburg). The cDNA of the dopamine receptors and the histamine H_3R were purchased from the cDNA Resource Center (Rolla, MO, USA). The restriction enzymes *Bam*HI and *Apa*I, were purchased from New England Biolabs (Frankfurt am Main, Germany).

Depending on their physicochemical properties, if possible, ligands were dissolved in dH_2O; otherwise DMSO (Merck) was used as solvent. Dopamine dihydrochloride (dopa), (+)-butaclamol hydrochloride (buta), and pramipexole dihydrochloride (prami) were purchased from Sigma (Taufkirchen, Germany). Haloperidol (halo), JNJ-5207852 and SCH-23390 were obtained from TCI Deutschland GmbH (Eschborn, Germany). (-)-Quinpirole hydrochloride (quin), (*S*)-(-)-sulpiride (sulp), and spiperone hydrochloride (spip) were obtained from TOCRIS (Bristol, UK). All bivalent ligands NR330, MN075, MN085, MN209, and MN240 were kindly provided by Dr. Niklas Rosier and Dr. Martin Nagl (Institute of Chemistry and Pharmacy, Medicinal und Pharmaceutical Chemistry I, Universität Regensburg).

4.2.2. Methods

The cDNA of the human D_1R and H_3R were purchased from the cDNA Resource Center (Rolla, MO, USA). The sequences of the D_1R and H_3R were amplified by standard PCR to introduce a P2A site (ATNFSLLKQAGDVEENPGP) fused to the D_1R C-terminus and overlapping sites to the vector. The dopamine receptor with the P2A site and the H_3R was afterwards cloned into the digested pcDNA5 vector backbone using Gibson assembly, forming pcDNA5 D_1R-P2A-H_3R.

For the functional split nano luciferase-based miniG protein recruitment assay, the cDNA of the human $D_{2l}R$ was purchased from the cDNA Resource Center (Rolla, MO, USA). The sequences of the $D_{2l}R$ were amplified by standard PCR by introducing an overlap of base pairs for a Gibson assembly. The linker, consisting of 42 base pairs (-GSSGGGGSGGGGSS-), was purchased from Eurofins Genomics (Eurofins Genomics LLC, Ebersberg, Germany). The dopamine $D_{2l}R$ and the linker were cloned with a Gibson assembly into a $pIRES_{puro}$ vector backbone containing the LgBiT of the Nano luciferase N-terminally fused to the $miniG_{si}$ protein sequence.[40] After the ligation step, the sequence of the $D_{2l}R$ and the 42 base pair linker are N-terminally connected to the NLucN-$miniG_{si}$ protein sequence. Positive bacterial colonies were first extracted in a mini-prep from overnight cultures (Miniprep Kit, Nippon Genetics, Düren, Germany) and then maxi-prepped for use in mammalian cells (Maxiprep Kit, Qiagen, Hilden, Germany). All plasmid DNA was quantified by UV-VIS absorbance using a NanoDrop spectrophotometer (ThermoFisher, Braunschweig, Germany) and sequences were verified by sequencing performed by Eurofins Genomics (Eurofins Genomics LLC, Ebersberg, Germany).

4.2.3. Cell Culture

HEK293T cells were cultured in DMEM supplemented with 10% FCS and 2 mM L-glutamine at 37 °C, 5% CO_2 in a H_2O saturated atmosphere. Cells were periodically inspected for mycoplasma contamination by Eurofins Genomics (Eurofins Genomics LLC, Ebersberg, Germany).

4.2.4. Generation of Stable Cell Lines

Stable HEK293T Flip-In cells were seeded on a sterile 6-well dish at a cell density of 300,000 cells/ml in DMEM supplemented with 10% FCS and 2 mM L-glutamine. The next day, cells were transfected with 2 µg cDNA of $pcDNA5_{zeo}$ D_1R-P2A-H_3R using the transfection reagent XtremeGene HP (Merk, Darmstadt, Deutschland) according to supplier's protocol (1:3 cDNA (µg): XtremeGene (µl) ratio). After an incubation period of 48 h, cells were detached by using trypsin and seeded in a 175 cm^3 cell culture flask with 25 ml DMEM supplemented with 10% FCS, respectively. Cells were allowed to attach and thereafter treated with the antibiotic zeocin (300 µg/ml) to achieve stable expression. The media was refreshed every three days, and the zeocin level was dropped to 100 µg/ml for continued selection pressure in later passages.

4.2.5. Generation of Frozen Cell Aliquots

HEK293T Flag-hH_3R cells were seeded on a sterile 100 cm^2 dish at a cell density of 500,000 cells/ml in DMEM supplemented with 10% FCS and 2 mM L-glutamine. The next day, cells were transfected with different amounts of $pcDNA3.1_{neo}$ D_1R-myc (5 µg – 12 µg) or $pcDNA3.1_{neo}$ $D_{2l}R$-myc (5 µg) by using the transfection reagent transporter 5 PEI (Polysciences, Warrington, PA,

USA) according to supplier's protocol (1:5 pcDNA3.1$_{neo}$ $D_{1,2l}R$-myc (µg): PEI (µl) ratio). DMEM medium supplemented with 10% FCS and 2 mM L-glutamine was changed for 4 h to DMEM without supplements during transfection. After 48 h, cells were detached by trypsinization, and the density was adjusted to 1.1 x 10^6 cells/ml (D_1R-H_3R) or 300,000 cells/ml ($D_{2l}R$-H_3R) after counting in a "Neubauer" hemocytometer. Cells were aliquoted in DMEM medium supplemented with 10% FCS, 2 mM L-glutamine and 10% DMSO and frozen at -80 °C in cryo-vials.

4.2.6. Radioligand Binding Experiment

To measure the receptor density in either the stable cell lines HEK293T FlipIn-D_1R-P2A-H_3R or frozen cell aliquots of transient co-expressing HEK293T cells for the D_1R-H_3R or $D_{2l}R$-H_3R heteromers, saturation radioligand binding experiments were performed as previously described, with minor changes.[41] The frozen co-expressing HEK293T cell aliquots were thawed, resuspended and centrifugated at 4°C, 700 rpm for 4 min. For the stable cell lines, the cell density was adjusted to 80,000 cells/well after counting in a "Neubauer" hemocytometer in binding buffer (BB; 50 mM Tris HCl, 1 mM EDTA, 5 mM $MgCl_2$ * 6 H_2O, supplemented with 100 µg/ml bacitracin, pH = 7.4). Frozen cells (already adjusted to 1.1 x10^6 cells/ml per aliquot) were resuspended in 9.5 ml of BB, followed by seeding 160 µl of the stable or frozen cells in each well of a 96-well plate (clear, u-bottom 96-well plate, Greiner Bio-One, Kremsmünster, Austria). The radioligands [^{3}H]SCH-23390 for D_1R (81 Ci/mmol, Novandi Chemistry AB, Södertälje, Sweden; K_d = 0.2 nM)[42], [^{3}H] *N*-methyl-spiperone (77 Ci/mmol, Novandi Chemistry AB, Södertälje, Sweden; K_d = 0.014 nM)[41] for the $D_{2l}R$ and [^{3}H]UR-PI294 (93.3 Ci/mmol, Universität Regensburg, Germany, K_d = 1.1 nM)[43] or [^{3}H]UR-MN259 (105 Ci/mmol, Universität Regensburg, Germany, K_d = 0.55 nM)[44] for the H_3R were used with increasing concentrations in the range of approx. 1/10 K_d -10 K_d. Total binding was determined in the absence of any competitor. Non-specific binding was measured by incubating the co-expressing cell suspension in the presence of the respective radioligand and (+)-butaclamol (D_1R), haloperidol ($D_{2l}R$) in a 2,000-fold excess or clobenpropit (H_3R) in 1,000-fold excess, with a total volume of 200 µl per well. Incubation periods of 1.5 h were terminated by separating bound and free radioligand with an automated cell harvester (Brandel, Gaithersburg, USA) utilizing rapid filtration through Whatman GF/C filters precoated with 0.3% polyethyleneimine. Filters were transferred to flexible 96-well sample plates (Perkin Elmer, Rodgau, Germany) and incubated with scintillation cocktail for at least 5 h before radioactivity was measured using a MicroBeta^2 1450 scintillation counter (Perkin Elmer, Rodgau, Germany).

For competition binding experiments, dilutions of the competitors and radioligands were accomplished in the respective buffer (BB; Leibovitz's L-15 media; BB supplemented with 100 mM or 140 mM NaCl). For the D_1R [^{3}H]SCH-23390 (c = 0.4 nM), $D_{2l}R$ [^{3}H]*N*-methylspiperone (c = 0.02 nM), and H_3R [^{3}H]UR-MN259 (c = 0.5 nM) were used as radioligands. For non-specific

binding, (+)-butaclamol (D_1R), (+)-haloperidol ($D_{2l}R$), and clobenpropit (H_3R) were diluted to 1,000-fold access compared to the respective radioligand. For allosteric experiments, the radioligand [^{3}H]UR-MN259 in a concentration of 0.15 nM was chosen. The frozen co-expressing cells were handled as described above. Mono-expressing cells for the D_1R, $D_{2l}R$ and H_3R were adjusted to 80,000 cells/well after counting in the respective buffer, either in BB, Leibovitz's L-15 media, BB supplemented with 100 mM NaCl or 140 mM, followed by seeding 70 µl (competition binding experiments with two competitors per well) or 80 µl (normal competition binding) of the respective cells in each well of a 96-well plate (clear, u-bottom 96-well plate, Greiner Bio-One, Kremsmünster, Austria). Incubation of the specific radioligand in the presence of either the competitors or non-specific binding was terminated after 1 h for the mono-expressing cells and 1.5 h for the co-expressing cells using an automated cell harvester. For normalization, a total binding (buffer with the respective radioligand as 100 % value) and non-specific binding (0% value) were always included.

Data were analyzed using Prism10 (GraphPad, La Jolla, CA, USA). After subtracting non-specific binding, specific binding and the resulting K_d were determined in saturation binding experiments. In competition binding experiments curves were fitted with either a one-site fit, or a two-site fit after analysis with the compared function of Prism10. A two-site fit was chosen, when the respective *p*-value was < 0.05 and null hypothesis was rejected. The determined *p*-values were always indicated under the respective figures and tables. The K_i values were calculated from IC_{50} values, after normalization, according to the Cheng-Prusoff-equation.[45]

4.2.7. Functional miniG$_{si}$ Assay for the $D_{2l}R$-H_3R Heteromer

The miniG recruitment assay was performed using transiently transfected HEK293Tcells with plasmid DNA of pcDNA3.1$_{neo}$ hH_3R-NlucC and pIRES$_{puro}$ $D_{2l}R$-NlucN-L42bp-miniG$_{si}$ as described by Höring et al. 2020[46]. The miniG$_{si}$ denotes the chimeric miniG protein and the term L42bp imply the flexible serin linker consisting of 42 base pairs. All experiments were performed at 37 °C with a CLARIOstar Plus plate reader (BMG LABTECH, Ortenberg, Germany) to characterize different H_3R-like, D_2R-like standard ligands, and bivalent ligands (MN209 and MN240) in both modes, (agonist and antagonist mode) using furimazine as substrate (Promega, Mannheim). HEK293T cells were seeded on a sterile 6-well dish at a cell density of 300,000 cells/ml in DMEM supplemented with 10% FCS and 2 mM L-glutamine (2 ml/well). The next day, cells were transfected with 1 µg cDNA of pIRES$_{puro}$-$D_{2l}R$-NlucN-L42bp-miniG$_{si}$ and pcDNA3.1$_{neo}$$H_3R$-NlucC using the Transporter 5 PEI transfection reagent (Polyscience, Inc., Warrington, PA, USA) according to supplier's protocol (1:5 cDNA (µg): PEI (µL) ratio) in 200 µL sodium-free DMEM, after 20 min incubation at room temperature. After an incubation period of 48 h, cells were seeded at a density of 1.25 x 10^6 cells/mL in Leibovitz's L-15 media supplemented with 10 mM HEPES

and 5% FCS in a white 96-well plate (BRANDplates® cellGrade 781965, VWR) and incubated at 37 °C overnight in a humidified atmosphere. The dilution of the substrate (furimazine) and samples were prepared in Leibovitz's L-15 media supplemented with 10 mM HEPES prior to the experiment. The basal luminescence was recorded immediately after adding 10 µL of the substrate to each well for 13 plate repeats (or 15.5 min) with an integration time of 0.5 s per well. 10 µL of every concentration of the ligand dilution series were added in triplicate, and the final luminescence measurement was performed for further 39 plate repeats (equal to 46.5 min). A similar procedure was performed for the characterization of the different ligands in the antagonist mode. Further 13 plate repeats (equal to 15.5 min) were recorded after the addition of the serial dilutions of the ligands, followed by the final measurement of 39 cycles (equal to 46.4 min) after adding 10 µL of 100 µM dopamine ($D_{2l}R$) or 1 µM histamine (H_3R) as the endogenous agonist at the EC_{80} concentration. For normalization of the data, the negative control (solvent control) and positive control (maximum level of 100 µM histamine in agonist mode and 1 µM histamine in antagonist mode) were included on every assay plate. After the addition of the substrate and the ligands, the luminescence traces were recorded for each addition in a time-resolved manner, followed by a baseline and an inter-well correction, and the area under the curve (AUC) was calculated and transferred to concentration-response curves. Finally, the data were normalized to the highest concentration of the agonist histamine, dependent on agonist or antagonist mode. The resulting pK_b values were all determined according to the Cheng-Prusoff equation.[45]

4.3. Results and Discussion

4.3.1. D_1R-H_3R Heterodimer

4.3.1.1. Generation of a Stable Cell Line Expressing D_1R-H_3R Using a P2A Site

To generate a stable co-expressing D_1R-H_3R cell line, a 2A-peptide analogue was used. The self-cleavage protein was from a porcine teschovirus-1 2A (P2A)[47] and is an oligopeptide consisting of 19 amino acids.[48] Self-cleavage of P2A occurs during translation, targeted at the last C-terminally located glycine and the first proline of the 2B downstream protein in the respective cell. Thus, the protein sequence was cloned in a $pcDNA_{zeo}5$ vector backbone between the D_1R and H_3R sequence (refer Chapter 4.2.2.) with the intention of producing equal expression of both receptors in a stoichiometric ratio of 1:1 because both genes were under the same promoter.[48] To verify the expression of both receptors and the stoichiometry of the two receptors in the co-expressing HEK293T FlipIn-D_1R-P2A-H_3R cells, radioligand saturation binding experiments were performed in the presence of [^{3}H]SCH-23390 for the D_1R protomer and [^{3}H]UR-PI294 for the H_3R protomer. The obtained signal-to-noise ratio of the specific binding for both receptors was very low and no reliable dissociation constants (K_d) or maximum binding capacity (B_{max}) were calculated (Appendix, Figure 7.32).

Due to an insufficient signal-to-noise ratio and receptor ratio, no further studies, such as competition binding experiments or kinetic experiments, were performed. Thus, for the following experiments transient co-expressing D_1R-H_3R cells were generated.

4.3.1.2. Characterization of Bivalent Ligands on Transient Transfectants of The D_1R-H_3R Heteromer

HEK293T wild-type cells were transiently transfected with different amounts of plasmid DNA of $pcDNA3.1_{neo}$ D_1R-myc (1 µg – 3 µg) and $pcDNA3.1_{neo}$ H_3R-myc (1 µg – 5 µg) to validate the optimal amount of each receptor to observe a sufficient signal-to-noise ratio. Saturation binding experiments were performed on these cells in the presence of either [^{3}H]SCH-23390 (D_1R, c = 0.4 nM) or [^{3}H]UR-PI294 (H_3R, c = 6 nM). In all transiently transfected plasmid DNA ratios, the expression of the H_3R was insufficient (Appendix, Figure 7.33). The ratio of the plasmid DNA was not equal to the expressed receptor ratio and the expression of the H_3R was consistently very low, with no option for further increased plasmid DNA amounts. Therefore, HEK293T wild-type cells stably expressing the H_3R (HEK293T Flag-hH_3R) were used for transfection with plasmid DNA of $pcDNA3.1_{neo}$ D_1R-myc (5 µg – 12 µg for each 100 cm^2 dish). To get a sufficient number of cells with equal expression, the transient transfected cells were pooled and frozen in aliquots for each batch at -80 °C, where no remarkable difference between pre-frozen and living cells were

observed.[49–51] Afterwards, radioligand saturation binding experiments were performed to verify the receptor ratio and investigate the impact by varying the cDNA amount (Appendix, Figure 7.34, Table 7.4 - 7.7). The best result was achieved with 12 µg of plasmid DNA of pcDNA3.1.$_{neo}$ D_1R-myc (batch 10, Appendix Figure 7.35). Under consideration of the B_{max} at the D_1R (2549 dpm), at the H_3R (6232 dpm) and taking into account the specific activity of each radioligand (D_1R: [^{3}H]SCH-23390: 3.00 TBq/mmol, H_3R: [^{3}H]UR-MN259: 3.89 TBq/mmol) the receptor expression per cell was calculated and thus, a stoichiometric receptor ratio of 1:2 for the transient co-expressing D_1R-H_3R HEK293T cells (Table 4.1). The calculated pK_d value for the H_3R (pK_d = 9.11) was in good agreement with literature data, while it was remarkably lower for the D_1R (pK_d = 8.85), compared to literature data on the D_1R monomer. We assume, due the co-overexpression of both receptors and the potential for heteromerization the binding properties of the receptors were affected.[52] The achieved stoichiometric receptor ratio was previously reported for class A GPCRs for the formation of functional heteromers *in vitro*,[53] as well as in BRET-based experiments for the D_1R-H_3R heteromer.[22] Nevertheless, the investigation of other stoichiometric ratios should be aimed to complete the establishment of the heteromerization of these class A receptors.

Table 4.1: Equilibrium dissociation constants (pK_d values), receptor expression (B_{max}), and receptor ratio obtained from radioligand saturation binding experiments on transient co-expressing D_1R-H_3R HEK293T cells (batch 10). As specific radioligands [^{3}H]SCH-23390 for the D_1R and [^{3}H]UR-MN259 for H_3R were used For the determination of non-specific binding (+)-butaclamol was used for the D_1R and for the H_3R clobenpropit was applied, both in a 1,000-fold excess. Data are shown from one experiment, performed in duplicate.

receptor	pK_d	B_{max}/ dpm	receptors per cell	ratio (D_1R:H_3R)	Ref.
D_1R protomer	8.85	2549	1,07E+05	1: 2	9.40[54]
H_3R protomer	9.11	6232	2,01E+05		9.26[55]

Moreover, competition binding experiments with the D_1R antagonist SCH-23390 (SCH), the antagonistic H_3R standard ligand JNJ-5207852 (JNJ), and the bivalent ligand NR330 were performed on co-expressing D_1R-H_3R cells with a receptor ratio of 1:2 with aliquots of batch 10 (Figure 4.3). The bivalent ligand NR330 is composed of a SCH-23390 analogue as D_1R pharmacophore coupled trough a linker to a JNJ-5207852 analogue as H_3R pharmacophore, whereas the linker consists of two polyethylene glycol (PEG) moieties (12 C-atoms each) connected through a glutaric acid amide. Experiments with NR330 in the presence of the D_1R radioligand [^{3}H]SCH-23390 (c = 0.4 nM), referred to as D_1R mode, or in the presence of the H_3R radioligand [^{3}H]UR-MN259 (c = 0.5 nM) as H_3R mode. As NR330 consists of both a SCH-23390 analogue and a JNJ-5207852 analogue as pharmacophores, both standard ligands were included as controls. Thus, it is assumed, that bivalent ligands show biphasic curves on functional heteromers, while monovalent ligands obtain monophasic curves, due to its ability to bind with

one or both pharmacophores to the heteromer and to expressed monomers .[56,57] For analysis of the obtained data, the one-site fit was compared with two-site fit and the calculated *p*-value was always indicated in the respective figure captions and table footnotes.

The bivalent ligand for the D_1R-H_3R heteromer NR330 yielded a biphasic curve ($p < 0.001$) in both modes using co-expressing D_1-H_3R cells (ratio 1:2), whereas the standard ligands SCH and JNJ achieved monophasic curves (SCH: $p = 0.18$, JNJ: $p = 0.16$) in the respective D_1R mode (Figure 4.3, A) or H_3R mode. (Figure 4.3, B), which supported the assumption of NR300 as true bivalent ligand and the ability of NR330 to bind in different binding-modes to the respective monomer or heteromer. In the D_1R mode the specific radioligand [^{3}H]SCH-23390 was incubated with either the bivalent ligand or the standard ligand SCH and in the H_3R mode NR330 or JNJ in the presence of [^{3}H]UR-MN259. In the case of the D_1R mode, the bivalent ligand yielded a p$K_{i,low}$ value in the micromolar range (p$K_{i,low}$ = 5.61 ± 0.13) and a right-shifted p$K_{i,high}$ value of 8.86 ± 0.04, which was lower compared to the standard ligand SCH (pK_i = 9.29 ± 0.20) (Table 4.2). In the H_3R-mode, NR330 achieved a p$K_{i,low}$ of 5.94 ± 0.04 and an additional p$K_{i,high}$ value of 9.83 ± 0.05, which were comparable with the pK_i of JNJ (pK_i = 9.57 ± 0.09) (Table 4.3). In both cases, the bivalent ligand showed no higher affinity to the D_1-H_3R heteromer compared to the protomer and the respective standard ligands. Nevertheless, the pK_i values for both standard ligands were in good agreement with the literature data.

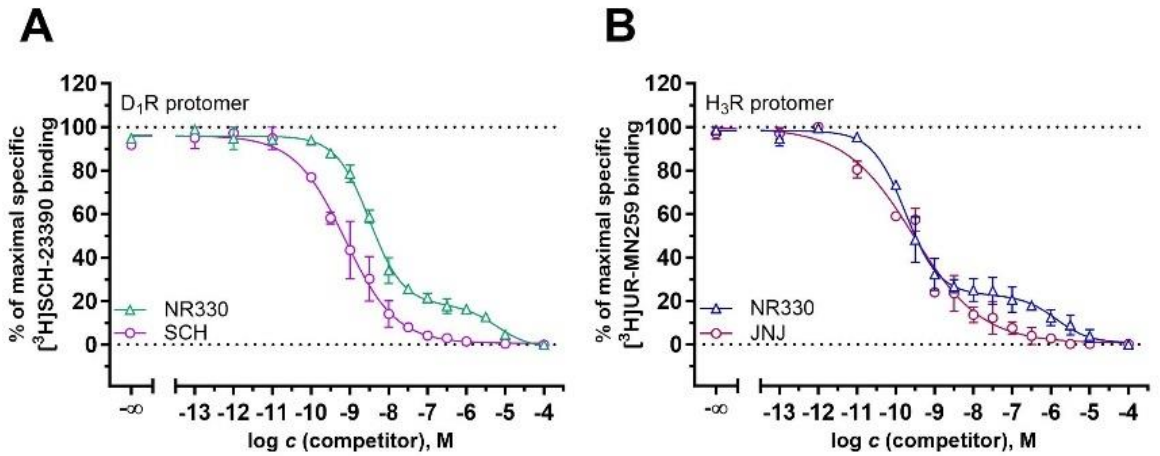

Figure 4.3: Representative radioligand competition binding experiments on co-expressing HEK293T D_1R-H_3R cells with a ratio of 1:2. **A:** Radioligand competition binding curve of the D_1R standard ligand SCH-23390 (SCH) (purple)† and the bivalent ligand NR330 (green)*** in the presence of [^{3}H]SCH-23390. To determine non-specific binding (+)-butaclamol was used in a 1,000-fold excess. **B:** Representative radioligand competition binding curve of the H_3R standard ligand JNJ-5207852 (JNJ) (dark red)† and the bivalent ligand NR330 (dark blue)*** in the presence of [^{3}H]UR-MN259. To determine non-specific binding clobenpropit was used in a 1,000-fold excess. Data are shown as means ± SEM from two independent experiments, each performed in triplicate. $^{***}p < 0.001$. $^{\dagger}p > 0.05$.

Table 4.2: Binding affinities (pK_i values) of the bivalent ligand NR330 and the D_1R standard ligand SCH-23390 (SCH) in radioligand competition binding experiments on cells co-expressing D_1R-H_3R HEK293T cells with a ratio of 1:2. Data are shown as means ± SEM from two independent experiments, each performed in triplicate.

Cpd.	HEK293T D_1R-H_3R (H_3R mode)					
	pK_i ± SEM	$pK_{i,low}$ ± SEM	$pK_{i,high}$ ± SEM	*N*	curve-fit	Ref.
NR330		5.61 ± 0.13	8.86 ± 0.04	2	two-site***	
SCH	9.29 ± 0.20			2	one-site†	9.96[58]

***$p < 0.001$. †$p > 0.05$.

Table 4.3: Binding affinities (pK_i values) of the bivalent ligand NR330 and H_3R standard ligand JNJ-5207852 (JNJ) in radioligand competition binding experiments on co-expressing D_1R-H_3R HEK293T cells with a ratio of 1:2. Data are shown as means ± SEM from two independent experiments, each performed in triplicate.

Cpd.	HEK293T D_1R-H_3R (H_3R mode)					
	pK_i ± SEM	$pK_{i,low}$ ± SEM	$pK_{i,high}$ ± SEM	*N*	curve-fit	Ref.
NR330	-	5.94 ± 0.04	9.83 ± 0.05	2	two-site***	-
JNJ	9.57 ± 0.09			2	one-site†	9.20[59]

***$p < 0.001$. †$p > 0.05$.

A higher binding affinity is not necessarily implemented by addressing dimers with bivalent ligands. For the binding of a bivalent ligand the gain in entropic energy or the stabilization of the heteromeric complex are important factors.[60] On the one hand, due to the binding of both pharmacophores to the respective orthosteric binding pocket, the linker loses in degrees of freedom, which should be considered for entropic contribution to the Gibbs energy and could have a negative impact on the affinity.[61] On the other hand, the formation of a receptor dimer and the binding of one pharmacophore can eventually lead to a conformational change and a decrease of binding affinity for the second pharmacophore of the bivalent ligand.[62]

In order to test whether the biphasic curve can be transformed to a monophasic curve by blocking one receptor protomer of the D_1-H_3R heteromer, radioligand competition binding experiments with NR330 in both modes were performed in the presence of an additional competitor. In the D_1R-mode JNJ (c = 10 µM) was used as H_3R standard ligand and for the H_3R mode SCH (c = 10 µM) as D_1R standard ligand. The respective concentration was chosen to be capable of sufficiently blocking the receptor protomer. In the presence of each standard ligand, SCH or JNJ, the specific binding of the NR330 dropped to approximately 35% in the D_1R mode and to approximately 20% in the H_3R mode. However, the biphasic curve of NR330 in the presence of either 10 µM SCH or 10 µM JNJ turned into a monophasic curve in both modes (Figure 4.4, A and B). The results confirm a biphasic binding mode of the bivalent ligand, which is reversible in the present of a second competitor. The pK_i value in the D_1R mode of the monophasic curve (pK_i = 7.45) was two orders of magnitude lower compared to the $pK_{i,low}$ value of NR330 additional competitor ($pK_{i,low}$ = 5.61 ± 0.13) co-expressing the D_1R-H_3R. In contrast, the pK_i of NR330 obtained from experiments with

cell homogenates of HEK293T cells expressing only the D_1R, was one order of magnitude higher ($pK_i = 8.67 \pm 0.10$) (Figure 4.4, A). The same result was observed in the H_3R mode of NR330 in the presence of the competitor SCH (c = 10 µM), even though the pK_i value of the monophasic curve was right shifted and yielded a higher pK_i value ($pK_i = 6.29$) compared at the H_3R monomer receptor stably expressed by HEK293T Flag-hH_3R cells ($pK_i = 5.61 \pm 0.13$) (Figure 4.4, B).

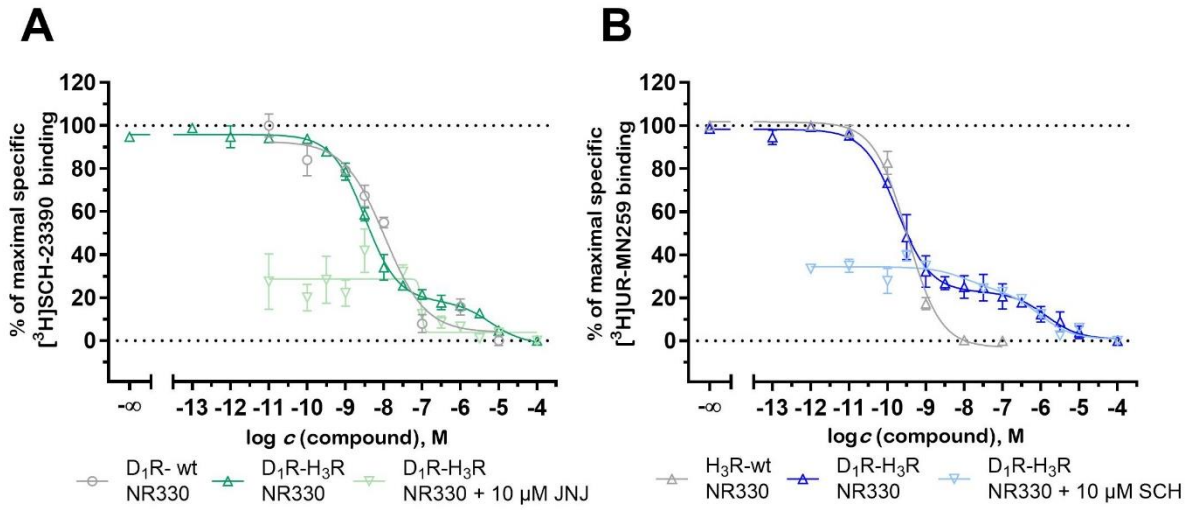

Figure 4.4: Representative radioligand competition binding experiments of NR330 in the presence of the respective radioligand and an additional competitor on co-expressing D_1R-H_3R HEK293T cells. **A:** D_1R mode: Radioligand competition binding curve of NR330 in the presence of [^{3}H]SCH-23390 and 10 µM of the H_3R standard antagonist JNJ-5207852 (JNJ) (light green)†. Competition binding curves of NR330 without additional competitor on co-expressing D_1R-H_3R HEK293T cells (dark green)*** and on homogenates of HEK293T D_1R-CreLuc2P cells (grey)† are shown. For determination of non-specific binding (+)-butaclamol was used in a 1,000-fold excess. **B:** H_3R mode: Radioligand competition binding curve of NR330 in the presence of [^{3}H]UR-MN259 and 10 µM of the D_1R standard antagonist SCH-23390 (light blue)†. As non-specific binding clobenpropit in 1,000-fold excess was used. Competition binding curves of NR330 without additional competitor (dark blue)*** and NR330 on HEK293T Flag-hH_3R cells (grey)† are shown. Data are shown as means ± SEM from one to three independent experiments, each performed in triplicate. $^{***}p < 0.001$. $^{\dagger}p > 0.05$.

Table 4.4: Binding affinities (pK_i values) of the bivalent ligand NR330 alone and in presence of 10 µM JNJ-5207852 (JNJ) in the D_1R-mode determined in radioligand competition binding experiments on co-expressing D_1R-H_3R HEK293T cells with a ratio of 1:2 and HEK293T D_1R-CRELuc2P homogenates (wt receptor). Data are shown as means ± SEM from one to three independent experiments ($N \geq 1$), each performed in triplicate.

Cpd.	HEK293T D_1R-CRELuc2P (wt receptor)		HEK293T D_1R-H_3R (D_1R mode)				
	pK_i ± SEM	N	pK_i ± SEM	$pK_{i,low}$ ± SEM	$pK_{i,high}$ ± SEM	curve-fit	N
NR330	8.67 ± 0.10[a]	3		5.61 ± 0.13	8.86 ± 0.04	two-site***	2
NR330 + 10 µM JNJ			7.54			one-site†	1

[a] performed by Dr. Niklas Rosier. $^{***}p < 0.001$. $^{\dagger}p > 0.05$.

Table 4.5: Binding affinities (pK_i values) of the bivalent ligand NR330 alone and in presence of 10 µM SCH-23390 (SCH) in the H_3R-mode determined in radioligand competition binding experiments on transient co-expressing D_1R-H_3R HEK293T cells with a ratio of 1:2 and stable HEK293T Flag-hH_3R cells (wt receptor). Data are shown as means ± SEM from one to three independent experiments ($N \geq 1$), each performed in triplicate.

Cpd.	HEK293T Flag-hH_3R (wt receptor)		HEK293T D_1R-H_3R (H_3R mode)				
	pK_i ± SEM	*N*	pK_i ± SEM	p$K_{i,low}$ ± SEM	p$K_{i,high}$ ± SEM	curve-fit	*N*
NR330	10.3 ± 0.01	3		5.94 ± 0.04	9.83 ± 0.05	two-site***	2
NR330 + 10 µM SCH			6.29			one-site†	1

***$p < 0.001$. †$p > 0.05$.

We suspect that the decrease in specific radioligand binding was induced by the binding of both standard ligands (SCH and JNJ) to the respective other protomer of the D_1R-H_3R heteromer, making them unsuitable for this competition binding experiments. Unfortunately, the experiment was only performed once, because the transient transfection of the stable HEK293T Flag-hH_3R with the same amount of plasmid DNA of pcDNA3.1$_{neo}$ D_1R-myc (12 µg) was not reproducible (except in batch 8) within the given time frame (Appendix, Figure 7.34). However, to verify this hypothesis and the possible impact of JNJ on binding affinities of known D_1R standard ligands, radioligand competition binding experiments with JNJ alone or in the present of literature known D_1R standard ligands and the bivalent ligand NR330 were performed on whole stable HEK293T D_1R-CREluc2P cells. Furthermore, the cold ligand MN259 was included. In addition, the same competition radioligand experiments with SCH alone or in the presence of literature known H_3R standard ligands and the bivalent ligand NR330 on stable HEK293T Flag-hH_3R were conducted.

4.3.1.3. Investigation of Binding Properties of Standard Ligands on D_1R and H_3R Monomers

<u>D_1R Wild-type Receptor</u>

To examine the binding affinities of the antagonistic H_3R ligands JNJ and MN259, or the bivalent ligand NR330 to the D_1R, radioligand competition binding experiments on stable HEK293T D_1R-CREluc2P cells were performed. Additionally, the D_1R standard ligands SCH-23390 (SCH) and (+)-butaclamol (buta) were tested as controls and in the presence of these H_3R ligands to investigate the impact on the binding properties to the D_1R (Figure 4.5, A and B). Regardless of whether a one-site fit (monophasic curve) or a two-site fit (biphasic curve) was accepted, both fits were compared by performing the F-test with Prism10, and the calculated *p*-value was always indicated in the respective figure captions and table footnotes. The K_i values were calculated from IC_{50} values with the K_d value for the respective buffer (sodium-free BB, Leibovitz's L-15 media or BB supplemented with 140 mM NaCl, Appendix Figure 7.36 and Table 7.11), after normalization, according to the Cheng-Prusoff-equation.[45]

The bivalent ligand NR330 (consisting of a SCH analogue as D_1R pharmacophore and a JNJ analogue as H_3R pharmacophore) resulted a right-shifted monophasic curve (p = 0.25) at the D_1R monomer receptor with an affinity in the nanomolar range (pK_i = 8.52 ± 0.02), compared to the standard ligand SCH (pK_i = 9.23 ± 0.11) (Figure 4.5 and Table 4.6). In contrast, the affinity of NR330 to the mono-expressing cells was equal to the $pK_{i,high}$ value in the D_1R mode on D_1R- H_3R co-expressing HEK293T cells (pK_i = 8.86 ± 0.04) (Table 4.4). Remarkably, the combination of the two bivalent ligand pharmacophores (SCH + 10 µM JNJ) led to a monophasic curve (p = 0.98) and a decrease in specific binding of the radioligand [^{3}H]SCH-23390 to approximately 30%. The calculated pK_i of 7.58 ± 0.31 was 44-fold lower, compared to SCH alone (pK_i = 9.23 ± 0.11), which implies a negative modulation of SCH by JNJ. Likewise, SCH in the presence of 10 µM of the H_3R ligand MN259 showed a monophasic curve (p = 0.91) and achieved a comparable pK_i value of 8.84 ± 0.18, but the specific binding of the radioligand [^{3}H]SCH-23390 decreased to approximately 80% (Figure 4.5, A). A depression in the binding signal was also observed with the D_1R standard ligand buta in the presence of either 10 µM MN259 or 10 µM JNJ, whereas specific binding of the radioligand dropped to approximately 65% and 45% (Figure 4.5, B). Both H_3R ligands, MN259 and JNJ, showed no affinity to the D_1R monomer but they produced a negative ligand-dependent impact on the binding of D_1R standard ligands (Figure 4.5, A and B). Moreover, the pK_i value of buta was left shifted to the nanomolar or sub-nanomolar range in the presence of the H_3R ligands (buta + 10 µM JNJ: pK_i = 9.25 ± 0.15, buta + 10 µM MN259: pK_i =8.76 ± 0.31), compared to buta on mono-expressing D_1R HEK293T cells (pK_i = 8.25 ± 0.25) (Figure 4.5, B and Table 4.6).

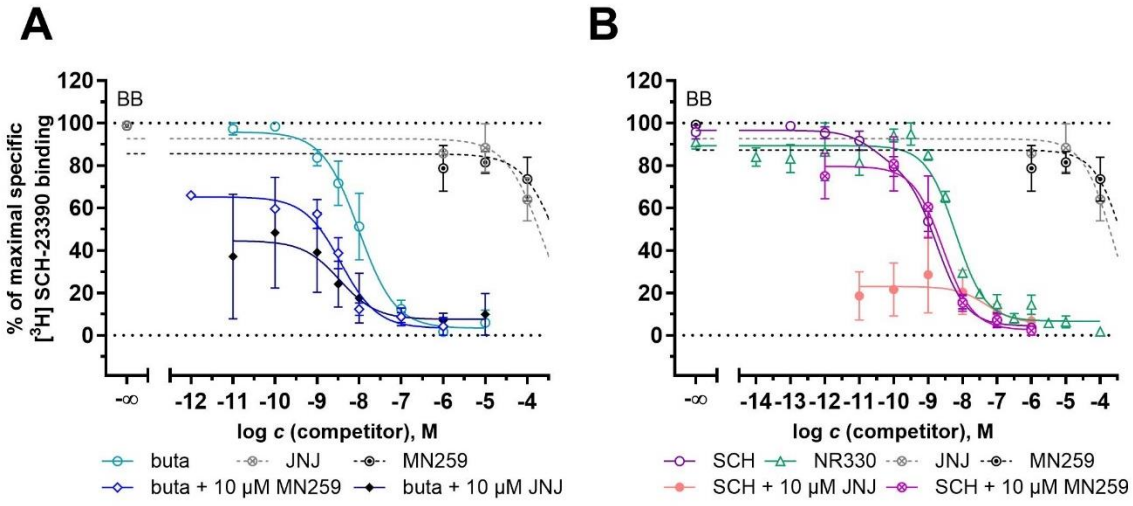

Figure 4.5: Radioligand displacement curves of [^{3}H]SCH-23390 in the presence of **A:** SCH-23390 (SCH) alone (purple)† or in combination with JNJ-5207852 (JNJ) (rose)† or 10 µM MN259 (pink)†, the H_3R ligand MN259 or the bivalent ligand NR330 (dark green)† and **B:** (+)-butaclamol (buta) alone (petrol)† or in the present of 10 µM MN259 (blue)† or JNJ (dark blue)† and the H_3R ligand MN259 (grey) and JNJ (black) on stable HEK293T D_1R-CRELuc2P cells. To determine non-specific binding (+)-butaclamol in 1,000-fold excess was used and BB without supplements as buffer. Dashed lines mark incomplete curves. Data are shown as means ± SEM from three to five independent experiments, each performed in triplicate. †p > 0.05.

Table 4.6: Binding affinities (pK_i values) of D_1R standard ligands SCH-23390 (SCH) or (+)-butaclamol (buta) alone or in the presence of either 10 µM JNJ-5207852 (JNJ) or 10 µM MN259, the bivalent ligand NR330, and these H_3R standard ligands alone in radioligand competition binding experiments on stable HEK293T D_1R-CRELuc2P cells. Sodium-free BB was used as buffer. Data are shown as means ± SEM from three to five independent experiments, each performed in triplicate.

Cpd.	pK_i ± SEM	% max. spec. bdg. [^{3}H]SCH-23390	curve-fit	*N*	Ref.
buta	8.52 ± 0.25	100	one-site †	5	8.52[63]
buta + 10 µM JNJ	9.25 ± 0.15	45	one-site †	3	n.a.
buta + 10 µM MN259	8.76 ± 0.31	65	one-site †	4	n.a.
JNJ	<4.0	70	n.a.	3	<4[a,64]
MN259	<4.5	100	n.a.	3	n.a.
NR330	8.52 ± 0.02	100	one-site †	3	n.a.
SCH	9.23 ± 0.11	100	one-site †	5	9.96[58]
SCH + 10 µM JNJ	7.58 ± 0.31	30	one-site †	3	n.a.
SCH + 10 µM MN259	8.84 ± 0.18	80	one-site †	3	n.a.

n.a. not applicable. [a]NanoBRET. †$p > 0.05$.

The negative modulation of the H_3R ligands to the antagonist SCH implements an allosteric effect, whether JNJ or MN259 are able to bind to a distinct binding pocket except for the orthosteric one. The induced conformational change after binding of the H_3R ligands can lead to a lowered affinity of SCH. An allosteric binding pocket for the D_1R was previously described by Hong et al. 2019, as well as, the positive allosteric modulator (PAM) LY3154207.[65] Further investigations are necessary to validate an allosteric impact of either JNJ or MN259 on the D_1R. Also for consideration, all experiments were performed in BB without sodium, and the sodium-dependent impact on the binding properties of specific ligands to other dopamine receptors (D_2R and D_3R) is known but, so far not the D_1R.[66–68] In the literature, different buffers containing/without sodium are described for radioligand binding experiments on whole cells.[46,69–72] Therefore, several experiments were performed with two other buffers. First, the BB was exchanged for Leibovitz's L-15 media, a sodium-containing medium supplemented with different amino acids, followed by BB supplemented with 140 mM NaCl, which is equal with the sodium concentration of Leibovitz's L-15 media. The term 'sodium-dependent effect' is used in this study to describe results which occur or are demised in the presence of sodium.

All tested ligands yielded monophasic curves with a *p*-value for buta + 10 µM JNJ of 0.19, SCH + 10 µM JNJ of 0.47, SCH + 10 µM MN259 of 0.45, and NR330 of 0.27 (Figure 4.6, A and B). The previously observed signal-depression for SCH + 10 µM MN259 / JNJ and buta + 10 µM JNJ in BB no longer occurred in Leibovitz's L-15 media. The calculated pK_i values for all combinations were in good agreement with the respective ligand within the experiments in Leibovitz's L-15 media (Table 4.7). In contrast, the binding affinity of buta +10 µM JNJ in BB (pK_i = 9.25 ± 0.15), the pK_i

value was right-shifted compared to the result in Leibovitz's L-15 media (pK_i = 8.25 ± 0.02). Interestingly, the specific binding of the radioligand [^{3}H]SCH-23390 increased to 120% in the presence of buta alone. For buta + 10 µM JNJ the specific binding of [^{3}H]SCH-23390 dropped to approximately 85%. This was comparable to the observed results in BB without supplement and implies no sodium-dependent effect. Despite this, the binding affinity for cold SCH increased in the presence of both H_3R ligands compared to the ones observed in BB (BB; p$K_{i,SCH+\ 10\ \mu M\ JNJ}$ = 7.58 ± 0.31, p$K_{i,SCH+\ 10\ \mu M\ MN}$ = 8.84 ± 0.18; L15: p$K_{i,SCH+\ 10\ \mu M\ JNJ}$ = 9.20 ± 0.05, p$K_{i,SCH+\ 10\ \mu M\ MN}$ = 9.11 ± 0.10), and therefore, no trend could be observed. Moreover, the affinity of NR330 was lower in the sodium-containing buffer (pK_i =7.80 ± 0.06) compared to the BB without sodium (pK_i = 8.52 ± 0.02) (Table 4.7).

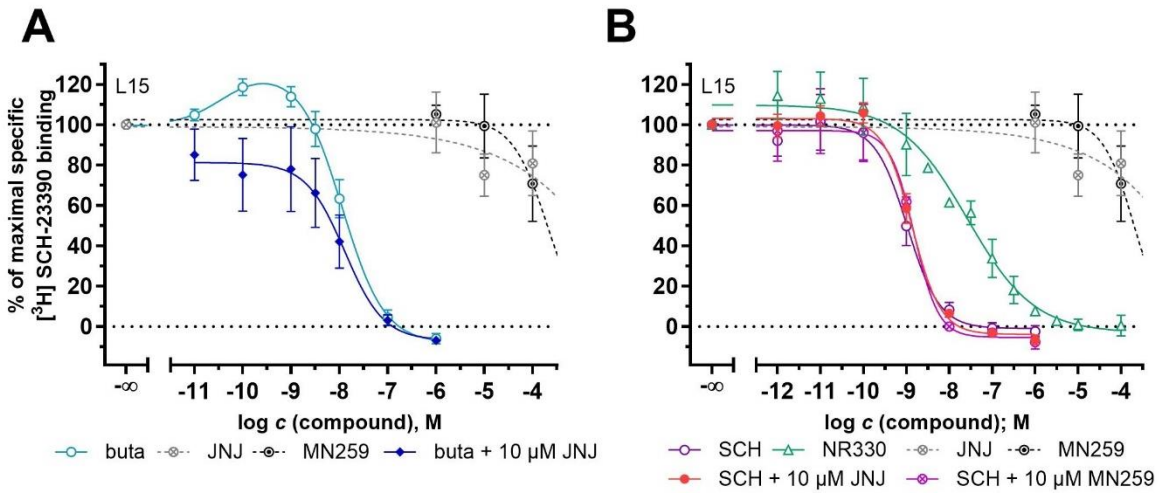

Figure 4.6: Radioligand competition binding curves performed in Leibovitz's L-15 media in the presence of the D_1R specific radioligand [^{3}H]SCH-23390 on stable HEK293T D_1R-CRELuc2P cells. **A:** SCH-23390 (SCH) (purple) †, in the presence of 10 µM MN259 (pink)† or JNJ-5207852 (JNJ) (orange)†, the H_3R ligands MN259 and JNJ or the bivalent ligand NR330† or **B:** of (+)-butaclamol (buta) (alone or in the presence of JNJ†), MN259 or JNJ. (+)-Butaclamol in 1,000-fold access was used to determine non-specific binding. Dashed lines mark incomplete curves. Data are shown as means ± SEM from three to five independent experiments, each performed in triplicate. †p > 0.05.

Table 4.7: Binding affinities (pK_i values) of D_1R standard ligands SCH-23390 (SCH) or (+)-butaclamol (buta) alone or in the presence of either 10 µM JNJ or 10 µM MN259, the bivalent ligand NR330, and these H_3R standard ligands alone in radioligand competition binding experiments on stable HEK293T D_1R-CRELuc2P cells. Leibovitz's L-15 media was used as buffer Data are shown as means ± SEM from three to five independent experiments, each performed in triplicate.

Cpd.	pK_i ± SEM	% max. spec. bdg. [^{3}H]SCH-23390	curve-fit	*N*	Ref.
buta	8.36 ± 0.10	120	one-site¥	4	8.52[63]
buta + 10 µM JNJ	8.40 ± 0.02	80	one-site †	3	n.a.
JNJ	<4.5	100	n.a.	5	<4[a,64]
MN259	<4.0	100	n.a.	3	n.a.
NR330	7.94 ± 0.06	100	one-site †	3	n.a.
SCH	9.45 ± 0.08	100	one-site ¥	4	9.96[58]
SCH + 10 µM JNJ	9.34 ± 0.06	100	one-site †	4	n.a.
SCH + 10 µM MN259	9.27 ± 0.9	100	one-site †	3	n.a.

n.a. not applicable. ¥ simpler model (Prism 10). †p > 0.05.

We suspect that the sodium in Leibovitz's L-15 media was responsible that no shift of binding affinity of either buta or SCH in the presence of JNJ or MN259 was observed. Thus, to verify a sodium-dependent effect, radioligand competition binding experiments were performed with BB supplemented with 140 mM NaCl.

By changing the buffer from Leibovitz's L-15 media to BB supplemented with 140 mM NaCl, no significant changes in binding mode or shift of pK_i values for NR330, SCH, SCH + 10 µM JNJ or + 10 µM MN259 were observed (Figure 4.7, A and B, Table 4.8). The ligands achieved all monophasic curves with *p*-values for NR330 of 0.20, SCH + 10 µM JNJ of 0.78 and SCH + 10 µM MN259 of 0.20 (Figure 4.7, A and B). We were able to vanish the negative modulation of SCH by JNJ and MN by the addition of sodium and proofed no differences in results between the Leibovitz's L-15 media and BB supplemented with 140 mM NaCl. In contrast, buta without or in the presence of 10 µM JNJ obtained a monophasic curve as well (buta: $p = 0.91$, buta + 10 µM JNJ: $p = 0.09$), and showed no increase or decrease in the total binding of the radioligand [^{3}H]SCH-23390. Moreover, the calculated pK_i values were in good agreement with values generated with Leibovitz's L-15 media (Table 4.8). We suspect, that the Leibovitz's L-15 media's extra supplements, like amino acids that are important for protein folding and receptor stabilization, could also have had a further impact on binding affinities.[73–75]

Nevertheless, we confirmed a sodium-dependent effect on the binding affinities for all tested ligands at the D_1R monomer receptor in the presence of JNJ and MN259. In the presence of sodium, the negative modulation of SCH by JNJ and MN was no longer observed.

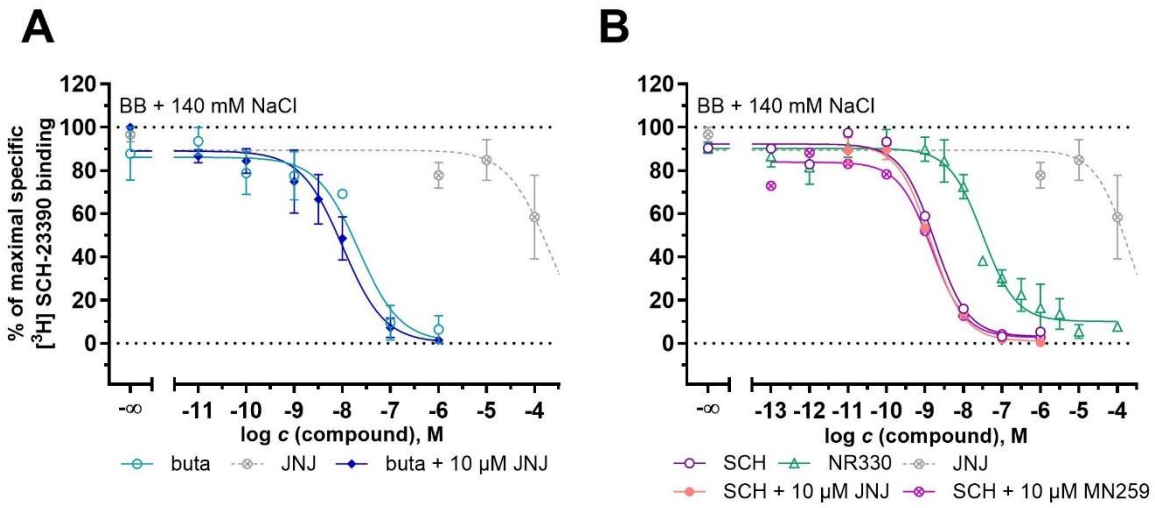

Figure 4.7: Curves obtained in BB supplemented with 140 mM NaCl for radioligand binding experiments in the presence of the D_1R specific radioligand [^{3}H]SCH-23390 on stable HEK293T D_1R-CRELuc2P cells. **A:** SCH-23390 (SCH) alone (purple)† or in the presence of 10 µM MN259 (pink)† or JNJ-5207820 (JNJ) (orange)†, the bivalent ligand NR330† or the H^3R ligand JNJ (grey)† or **B:** (+)-butaclamol (buta) (alone or in the presence of JNJ†), and JNJ alone. (+)-butaclamol in 1,000-fold access was used to determine non-specific binding. Dashed lines mark incomplete curves. Data are shown as means ± SEM from two to five independent experiments (N ≥ 2), each performed in triplicate. †$p > 0.05$.

Table 4.8: Binding affinities (pK_i values) of D_1R standard ligands alone or in the presence of either 10 µM JNJ or 10 µM MN259 and H_3R ligands JNJ or MN259 in radioligand competition binding experiments on stable HEK293T D_1R-CRELuc2P cells. BB supplemented with 140 mM NaCl was used as buffer. Data are shown as means ± SEM from two to five independent experiments ($N \geq 2$), each performed at least in duplicate.

Cpd.	pK_i ± SEM	% max. spec. bdg. [^{3}H]SCH-23390	curve-fit	N	Ref.
buta	8.18 ± 0.41	100	one-site†	2	8.52[63]
buta + 10 µM JNJ	8.41 ± 0.36	100	one-site†	4	n.a.
JNJ	<4.5	90	n.a.	3	<4.0[a,64]
NR330	7.65 ± 0.14	100	one-site†	3	n.a.
SCH	9.12 ± 0.11	100	one-site¥	5	9.96[58]
SCH + 10 µM MN259	9.06 ± 0.02	100	one-site†	3	n.a.
SCH + 10 µM JNJ	9.05 ± 0.03	100	one-site†	3	n.a.

n.a. not applicable. ¥simpler model (Prism). †$p > 0.05$.

The D_1R monomer radioligand competition binding experiments with the respective competitors in three different buffers (sodium-free BB, Leibovitz's L-15 media and BB supplemented with 140 mM NaCl) were performed in the presence of the specific radioligand [^{3}H]SCH-23390. The bivalent ligand NR330 achieved different results in sodium-containing buffer and a sodium-free BB. The affinity of NR330 was decreased in sodium-containing buffers: $pK_{i,140\ mM\ NaCl} = 7.65 \pm 0.14 < pK_{i,L15} = 7.96 \pm 0.06 < pK_{i,BB} = 8.52 \pm 0.06$. Likewise, the combination of the two pharmacophores without the spacer (SCH-23390 and JNJ-5207852) was affected by the change to sodium-containing buffers; in contrast to NR330, however, the pK_i values were increased by using sodium-

containing buffers: $pK_{i,BB}$ = 7.58 ± 0.31 < $pK_{i,140\ mM\ NaCl}$ = 9.05 ± 0.03 < $pK_{i,L15}$ = 9.34 ± 0.06 and the depression of the specific binding of [^{3}H]SCH-23390 in the presence of SCH + 10 µM JNJ also vanished in buffers supplemented with sodium. Moreover, the calculated pK_i values were comparable with the pK_i of SCH alone in the sodium-containing media and buffer, respectively ($pK_{i,BB}$ = 9.23 ± 0.11, $pK_{i,L15}$ = 9.31 ± 0.08, $pK_{i,140\ mM\ NaCl}$ = 9.12 ± 0.11). Thus, we hypothesize that sodium influences the binding kinetics of the D_1R – and therefore the binding affinities of the respective ligands – and is important to be included in radioligand binding experiments.[76,77]

H_3R Wild-type Receptor

In previous radioligand competition binding experiments using the bivalent ligand NR330 in the presence of 10 µM SCH-23390 (SCH) at the D_1R-H_3R heteromer (H_3R-mode), a depression of the specific binding of the radioligand [^{3}H]UR-MN259 and a transition of the biphasic to a monophasic curve was observed. Therefore, radioligand competition binding experiments with the bivalent ligand NR330, the H_3R ligands JNJ-5207852 (JNJ) and MN259 alone or in presence of 10 µM SCH and (+)-butaclamol (buta), and the D_1R standard ligands alone (SCH and buta) were performed to verify the binding affinities and the sodium impact of the chosen buffer on HEK293T Flag-hH_3R HEK293T cells. For choosing between the one-site fit (monophasic curve, $p > 0.05$) or the two-site fit (biphasic curve, $p < 0.05$) the compare function of Prism10 was used and the calculated p-value was always indicated in the respective figure captions and table footnotes. The K_i values were calculated from IC_{50} values with the K_d value for the respective buffer (sodium-free BB, Leibovitz's L-15 media or BB supplemented with 140 mM NaCl, Appendix Figure 7.37and Table 7.12), after normalization, according to the Cheng-Prusoff-equation.[45]

The combination of SCH and JNJ on the H_3R monomer receptor achieved a monophasic curve (p = 0.28) with a depression of the specific binding of the radioligand [^{3}H]UR-MN259 to approximately 70% (Figure 4.8, A). The calculated pK_i value for SCH + JNJ (pK_i = 9.05 ± 0.25) was one order of magnitude lower compared to the pK_i value of JNJ alone (pK_i = 9.98 ± 0.06)[55] (Table 4.9). Thus, the impact of SCH as a negative modulator for the binding affinity of JNJ on the H_3R was high with an observed depression of approximately 50% (Figure 4.8, A). In the presence of SCH with MN259 a monophasic curve was resulted (p = 0.34) with a calculated pK_i of 8.71 ± 0.30, which was 7-fold lower compared to literature data (pK_i = 9.55 ± 0.17).[55] Moreover, a depression in the signal of the radioligand [^{3}H]UR-MN259 (60%) was observed. In the presence of 10 µM buta the affinity for JNJ (pK_i = 9.95 ± 0.03) and for MN259 (pK_i = 9.26 ± 0.21) was comparable to the respective ligands alone and no depression in signal was observed in sodium-free BB at the H_3R monomer (Table 4.9). The D_1R ligand buta did not bind to the H_3R monomer (pK_i < 4), as expected, but in contrast, SCH produced a biphasic curve (p = 0.009) with a $pK_{i,low}$ of 5.51 ± 0.16 and $pK_{i,high}$ of 8.77 ± 0.68 (Figure 4.8, A and B), but the maximum of specific binding of the radioligand [^{3}H]UR-MN259 in

the latter case was approximately 70-90 %. This result implies that SCH binds to the H_3R and is not a D_1R-selective ligand but further investigations are still necessary. However, all experiments were performed in sodium-free BB, and, because of presence of a sodium binding pocket adjacent to the orthosteric binding pocket of the H_3R, we hypothesized a negative modulatory effect on the binding affinity of SCH would be induced by the addition of sodium.[78,79]

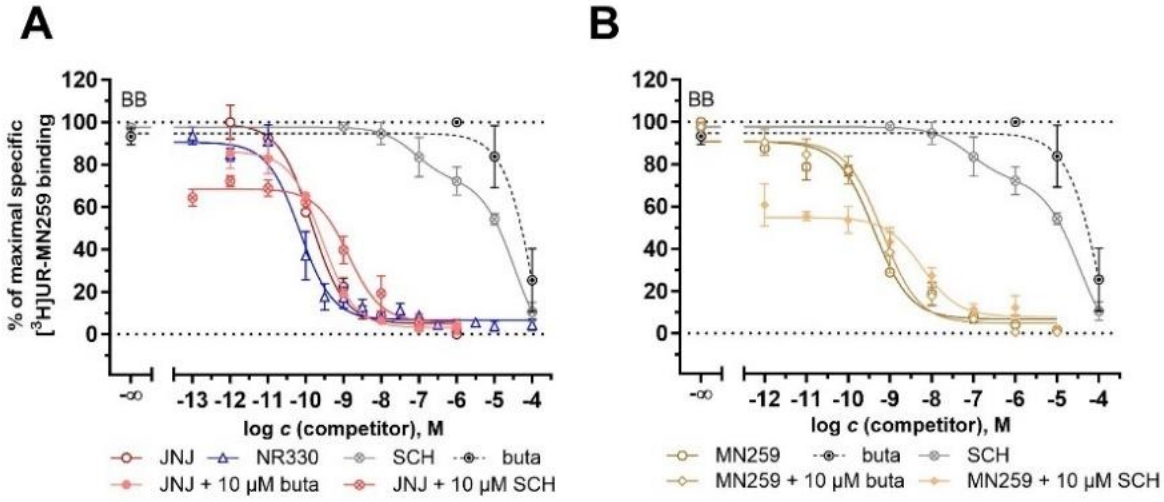

Figure 4.8: Radioligand competition binding curves in the presence of the H_3R specific radioligand [^{3}H]UR-MN259 on stable HEK293T Flag-hH_3R cells in sodium-free BB. **A:** JNJ-5207852 (JNJ) with 10 µM SCH-23390 (SCH) (red)† or (+)-butaclamol (buta) (rose)† or without competitor (dark red)†, the D_1R standard ligands SCH (grey)*** and buta (black) and the bivalent ligand NR330† **B:** of MN259 alone (brown) † or in the presence of 10 µM SCH (beige) † and 10 µM buta (ochre) † and the D_1R standard ligands SCH (grey)*** and buta (black) alone. clobenpropit in 1,000-fold access was used to determine non-specific binding. Dashed lines mark incomplete curves. Data are shown as means ± SEM from three to five independent experiments, each performed in duplicate. ***$p < 0.01$. †$p > 0.05$.

Table 4.9: Binding affinities (pK_i values) of H_3R ligands alone or in the presence of either 10 µM SCH-23390 (SCH) or 10 µM (+)-butaclamol (buta) and of D_1R standard ligands SCH and buta diluted in BB without supplements in radioligand competition binding experiments on stable HEK293T Flag-hH_3R cells. Data are shown as means ± SEM from three to five independent experiments ($N \geq 3$), each performed at least in duplicate.

Cpd.	pK_i ± SEM	p$K_{i,low}$ ± SEM	p$K_{i,high}$ ± SEM	% max. spec. bdg. [^{3}H]UR-MN259	curve-fit	N
buta	<4.5			100	n.a.	4
JNJ	9.98 ± 0.06			100	one-site†	4
JNJ + 10 µM buta	9.95 ± 0.03			90	one-site†	4
JNJ + 10 µM SCH	9.05 ± 0.25			70	one-site†	5
MN259	9.55 ± 0.17			100	one-site†	4
MN259 + 10 µM buta	9.26 ± 0.21			90	one-site†	3
MN259 + 10 µM SCH	8.71 ± 0.30			50	one-site†	4
NR330	10.3 ± 0.01			100	one-site†	3
SCH		5.11 ± 0.15	8.77 ± 0.67[a]	100	two-site***	3

n.a. not applicable. [a]% spec. binding [^{3}H]SCH-23390 90% - 70 %.***$p < 0.01$. †$p > 0.05$.

We assume that the unexpected result of the D_1R standard ligand SCH and the previous finding in this chapter for the D_1R, that a negative modulation can be affected by sodium and that the biphasic binding mode of SCH can possibly be modulated by sodium likewise. Furthermore, it is known, that the H_3R contains a sodium binding pocket adjacent to the orthostatic binding pocket. Thus, the buffer was changed to sodium-containing buffers as Leibovitz's L-15 media and BB supplemented with either 100 mM or 140 mM NaCl to verify a possible sodium-dependent effect. The sodium concentration of 100 mM NaCl was chosen due to previous work by Wittman et al. 2014[78] and 140 mM NaCl represented the identical sodium concentration with respect to Leibovitz's L-15 media.

In Leibovitz's L-15 media, the previously observed biphasic curve of SCH in sodium-free BB turned into a monophasic curve (p = 0.85) and the binding affinity decreased (pK_i < 4.5) (Figure 4.9, A), which confirmed the sodium-dependent impact on the binding affinities for certain ligands at the H_3R. Further radioligand competition binding experiments should be performed with sodium-containing BB to verify the sodium-dependent effect. Besides that, using MN259 in combination with SCH, the pK_i value was shifted into a high nanomolar range (7.74 ± 0.25) and the depression of the signal of the specific binding of the radioligand [^{3}H]UR-MN259 was still present (Table 4.10). We therefore hypothesized that there were probably further binding interactions between MN259 and SCH.

For the bivalent ligand NR330, it was not possible to evaluate a statistically correct fit (Figure 4.9, C). In two replicates, a monophasic curve was obtained (p = 0.91) with a calculated pK_i of 11.0 ± 0.13, which was 10-fold higher compared to the calculated pK_i value in sodium-free BB. In this case, the sodium increased the binding affinity of NR330 at the H_3R monomer. Additionally, for two other experiments, a biphasic binding mode was determined (p = 0.004) with a $pK_{i,low}$ value of 6.03 ± 0.16 and a $pK_{i,high}$ value of 10.5 ± 0.28 (Table 4.10). In a comparison to NR330 on D_1R-H_3R co-expressing HEK293T cells with non-supplemented BB ($pK_{i,low}$ = 5.61 ± 0.13, $pK_{i,high}$ = 9.83 ± 0.05), the observed $pK_{i,low}$ and $pK_{i,high}$ value at the H_3R monomer were left-shifted (Figure 4.9, C and Table 4.10). Furthermore, the observed plateau within the biphasic curve of NR330 in the mono expressing H_3R test system was not identical with the curve of NR330 resulted on the co-expressing D_1R-H_3R HEK293T cells. Therefore, we assume a true bivalent binding mode for NR330 with the co-expressing D_1R-H_3R HEK293T cells so far but further investigations and optimization are necessary. Ideally, the impact of sodium-containing buffer on radioligand binding of D_1R-H_3R co-expressing HEK293T cells needs to be further investigated.

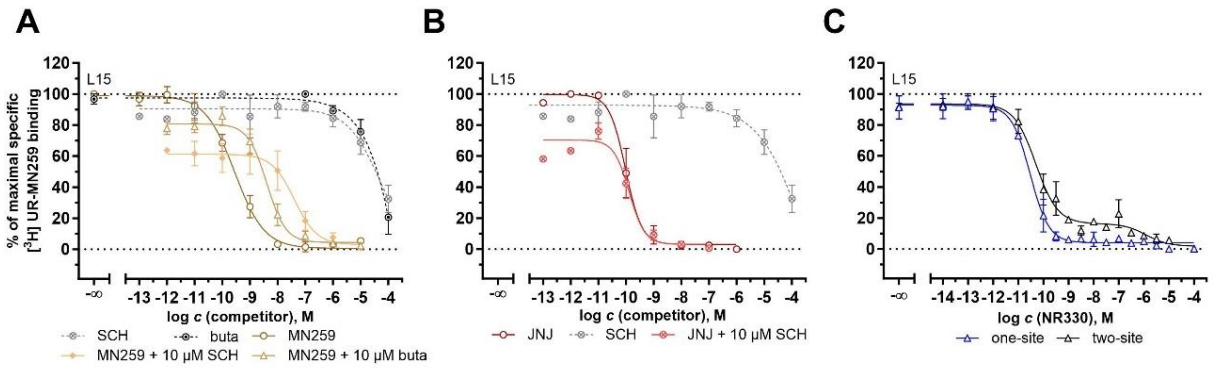

Figure 4.9: Radioligand competition binding curves in the presence of the specific radioligand [^{3}H]UR-MN259 on stable HEK293T Flag-hH_3R cells obtained in Leibovitz's L-15 media **A:** D_1R standard ligands SCH-23390 (SCH) (grey)†, (+)-butaclamol (buta) (black)† and both in combination with MN259 (beige)† or (ochre)† and MN259 alone (brown)†, **B:** D_1R standard ligand SCH-23390 (SCH) (grey)†, JNJ (copper) and JNJ + 10 µM SCH (dark red)†, **C:** of the bivalent ligand NR330 with two different curve fits: one-site fit (blue)†, or two-site fit (black)***. To determine non-specific binding, clobenpropit in 1,000-fold access was used. Data are shown as means ± SEM from two to six independent experiments (N ≥ 2), each performed at least in duplicate. ***$p < 0.005$. †$p > 0.05$.

Table 4.10: Binding affinities (pK_i values) of H_3R ligands alone or in the presence of either 10 µM SCH-23390 (SCH) or 10 µM (+)-butaclamol (buta), the bivalent ligand NR330 and D_1R standard ligands SCH and buta diluted in Leibovitz's L-15 media in radioligand competition binding experiments on stable HEK293T Flag-hH_3R cells. Data are shown as means ± SEM from two to six independent experiments ($N \geq 2$), each performed at least in duplicate.

Cpd.	pK_i ± SEM	p$K_{i,low}$ ± SEM	p$K_{i,high}$ ± SEM	% max. spec. bdg. [^{3}H]UR-MN259	curve-fit	N
buta	<4.5			100	n.a.	6
JNJ	10.22 ± 0.08			100	one-site†	2
JNJ+ 10 µM SCH	10.15 ± 0.08			70	one-site†	3
MN259	9.54 ± 0.08			100	one-site†	5
MN259 + 10 µM buta	8.62 ± 0.25			85	one-site†	4
MN259 + 10 µM SCH	7.74 ± 0.25			60	one-site†	4
NR330	11.0 ± 0.13			100	one-site†	2
NR330		6.03 ± 0.16	10.50 ± 0.28	100	two-site***	2
SCH	<4.5			100	n.a.	6

n.a. not applicable. ***$p < 0.005$. †$p > 0.05$.

Furthermore, radioligand competition experiments were also performed in BB supplemented with 100 mM or 140 mM NaCl in order to investigate the sodium concentration-dependent impact on the binding affinities of the different ligands to the H_3R.

The H_3R ligand MN259 in the presence of 10 µM SCH showed a similar behavior in sodium-containing buffer with NaCl concentrations. The pK_i values were comparable with MN259 alone, but a depression of the radioligand [^{3}H]UR-MN259 binding was observed to approximately 40% for 100 mM NaCl and approximately 70% for 140 mM NaCl (Figure 4.10, A and B). Furthermore,

the depression was less in buffer with higher sodium concentration and was comparable with the observed depression in Leibovitz's L-15 media, although the pK_i values of the cold MN259 were two orders of magnitude higher in BB supplemented with 140 mM NaCl (pK_i = 9.51 ± 0.12) (Figure 4.10, C, Table 4.12). For the bivalent ligand NR330 a monophasic curve was observed with a pK_i value of 9.97 ± 0.32 in BB supplemented with 100 mM NaCl, which was more than one order of magnitude lower compared to the calculated pK_i value in Leibovitz's L-15 media (pK_i = 11.0 ± 013) (Figure 4.10, B, Table 4.11). In contrast, it was not possible to implement a reliable fit for NR330 in BB supplemented with 140 mM NaCl (Figure 4.10, D). For two experiments, a one-site fit was achieved (p = 0.58) with a pK_i value of 9.48 ± 0.03 and in two different experiments a two-site fit (p = 0.04) was obtained with a p$K_{i,low}$ value of 6.48 ± 0.11 and a p$K_{i,high}$ value of 9.64 ± 0.26 (Table 4.12). Due to the low signal-to-noise ratio in this concentration range the comparison-function of Prism10 is limited. We hypothesize the biphasic curve was induced due to the binding of both the JNJ- and SCH- pharmacophores of NR330 to the H_3R receptor, where the observed effect was dependent of the signal-to-noise ratio of the assay and not due to a biphasic binding mode. In both sodium containing buffers, the D_1R ligand SCH produced a monophasic curve at the H_3R monomer receptor (100 mM NaCl: p = 0.37, 140 mM NaCl: p = 0.29) but with different affinities (Figure 4.10, A and C). In BB supplemented with 100 mM NaCl, a calculated pK_i of 7.79 ± 0.46 was observed, whereas in BB supplemented with 140 mM NaCl, a pK_i of 5.58 ± 0.46 was obtained, which underlines the sodium-dependent binding affinity of this ligand to the H_3R (Table 4.11 and Table 4.12). In comparison with the low binding of SCH in Leibovitz's L-15 media, the pK_i value achieved in the same sodium concentration but with BB media was left-shifted, which confirmed that SCH to H_3R binding is not only a sodium-dependent phenomenon. Again, we hypothesized that amino acids present in L-15 impact the ligand binding, as these are important for protein folding and stabilization of the receptor in its active state.[73–75] These should be further investigated in the future.

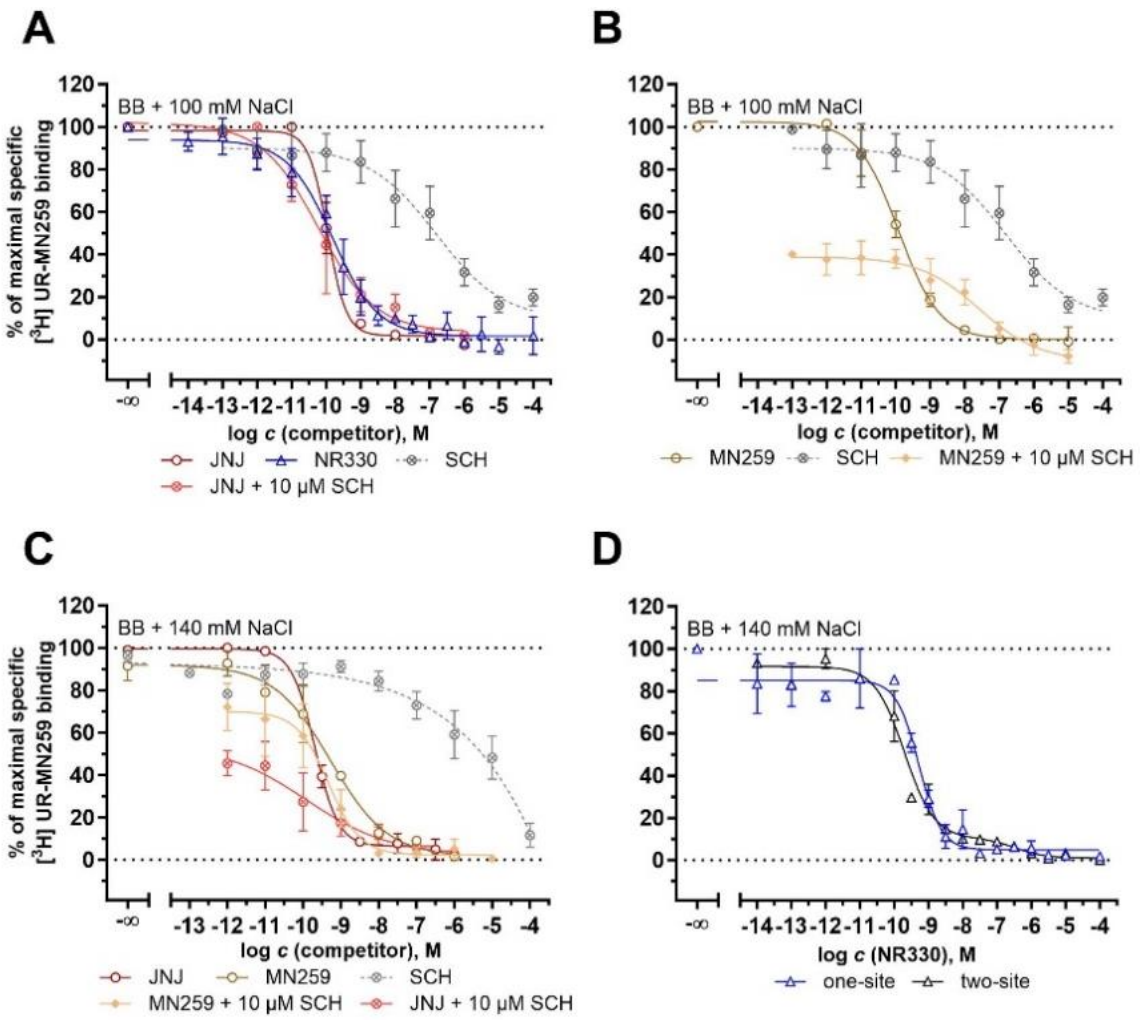

Figure 4.10: Displacement curves obtained in radioligand competition binding experiments in BB supplemented with 100 mM NaCl of **A:** the D_1R standard ligand SCH-23390 (SCH)† alone (grey)†, in combination with JNJ (rose), JNJ alone (red) and NR330 (blue) and **B:** of SCH alone (grey)†, in combination with MN259 (beige)† and MN259 alone (brown)†. **C:** Radioligand competition binding curves performed in BB supplemented with 140 mM NaCl of JNJ alone (red)† or in the presence of 10 µM SCH (rose)†, MN259 alone (brown)† or likewise, in combination with 10 µM SCH (beige)†. **D:** Same radioligand-based experiments with identical buffer for the bivalent ligand NR330 with two different curve fits: one-site (blue)†, and two-site (black)***. All experiments were performed in the presence of [^{3}H]UR-MN259 and on stable HEK239T Flag-hH_3R cells. To determine non-specific binding clobenpropit in 1,000-fold excess was used. Data are shown as means ± SEM from two to five independent experiments (N ≥ 2), each performed at least in duplicate. ***$p < 0.005$. †$p > 0.05$.

Table 4.11: Binding affinities (pK_i values) of H_3R ligands alone or in the presence of either 10 µM SCH-23390 (SCH), of the bivalent ligand NR330 and of D_1R standard ligands SCH diluted in BB supplemented with 100 mM NaCl in radioligand competition binding experiments on stable HEK293T Flag-hH_3R cells. Data are shown as means ± SEM from two to five independent experiments ($N \geq 2$), each performed at least in duplicate.

Cpd.	pK_i ± SEM	p$K_{i,low}$ ± SEM	p$K_{i,high}$ ± SEM	% max. spec. bdg. [^{3}H]UR-MN259	curve-fit	N
JNJ	10.09 ± 0.08	-	-	100	one-site†	2
JNJ + 10 µM SCH	10.25 ± 0.41	-	-	100	one-site†	3
MN259	10.18 ± 0.15	-	-	100	one-site†	4
MN259 + 10 µM SCH	8.04 ± 0.27	-	-	40	one-site†	5
NR330	9.97 ± 0.32	-	-	100	one-site†	4
SCH	7.79 ± 0.46	-	-	95	one-site†	5

$^{***}p < 0.005$. $^{\dagger}p > 0.05$

Table 4.12: Binding affinities (pK_i values) of H_3R ligands alone or in the presence of either 10 µM SCH-23390 (SCH), of the bivalent ligand NR330 and of D_1R standard ligands SCH diluted in BB supplemented with 140 mM NaCl in radioligand competition binding experiments on stable HEK293T Flag-hH_3R cells. Data are shown as means ± SEM from two to four independent experiments ($N \geq 2$), each performed at least in duplicate.

Cpd.	pK_i ± SEM	p$K_{i,low}$ ± SEM	p$K_{i,high}$ ± SEM	% max. spec. bdg. [^{3}H]UR-MN259	curve-fit	N
JNJ	9.31 ± 0.02	-	-	100	one-site†	2
JNJ + 10 µM SCH	10.13 ± 0.83	-	-	50	one-site†	3
MN259	9.51 ± 0.12	-	-	100	one-site†	3
MN259 + 10 µM SCH	9.47 ± 0.09	-	-	70	one-site†	3
NR330	9.48 ± 0.03	-	-	100	one-site†	2
NR330	-	6.48 ± 0.11	9.64 ± 0.26	100	two-site***	2
SCH	5.58 ± 0.46	-	-	90	one-site†	4

$^{***}p < 0.005$. $^{\dagger}p > 0.05$.

Moreover, the two highest concentrations of SCH in BB with 100 mM NaCl revealed higher values compared to the 0% value (non-specific binding). The 20 % difference in specific binding affinity of the radioligand [^{3}H]UR-MN259 implies an allosteric binding of SCH at the H_3R, as described for the structurally related benzodiazepines, which are known to be allosteric modulators on class C GPCRs.[80] Combined, our results indicate that SCH binds possibly allosterically to the sodium binding pocket of the H_3R and acts as a positive modulator for SCH itself, by binding simultaneously to both pockets and as negative modulator for the H_3R ligands. In sodium-containing buffer, the allosteric binding pocket gets blocked, which leads to a reduction of SCH binding. The sodium concentration in BB supplemented with 100 mM NaCl is not high enough to

fully displace SCH-23390 from the sodium binding pocket. Nonetheless, this hypothesis does not explain all observed shifts and depressions of the signal.

To confirm the hypothesis, radioligand competition binding experiments with lower concentration of the radioligand [^{3}H]UR-MN259 (c = 0.15 nM) according to Ehlert et al. 1985[81] were performed in order to show a lower impact of the allosteric modulator. Additionally, an obtained whole monophasic curve between the 0% value (non-specific binding) and 100% value (total binding of the radioligand in the respective buffer) supposed to be observed. The concentration was chosen taking into account the equation of [A*]/K_d, where [A*] described the free radioligand concentration and the K_d represented the dissociation constant of the respective radioligand. Using 0.5 nM for [A*] as previously used in all competition binding experiments and the respective K_d values (Appendix Figure 7.37, A-D) the following values of [A*]/K_d for each buffer were calculated. ([A*]/$K_{d\ BB}$ = 1, [A*]/$K_{d\ L15}$ = 1, [A*]/$K_{d\ BB,100\ mM\ NaCl}$= 0.48, [A*]/$K_{d\ BB,140\ mM\ NaCl}$= 0.55). For the following allosteric experiments, the [A*]/K_d was set to the recommended value of < 0.5.[81] Thus, for the investigation of the possible allosteric modulator SCH and if this modulation is sodium-dependent the concentration of the radioligand [^{3}H]UR-MN259 was set to 0.15 nM.

The curve of SCH was unexpectedly right shifted in all buffers except for Leibovitz's L-15 media (Appendix, Figure 7.38, A-D). Moreover, the previously observed biphasic binding mode of SCH in sodium-free BB transformed to a monophasic binding curve by reducing the radioligand concentration (Figure 7.38, A). Concerning the minimum specific binding of the radioligand in BB supplemented with 100 mM NaCl, no increase of the expected plateau was observed. Despite that, as expected, no difference in the competition binding curves were observed for Leibovitz's L-15 media or BB supplemented with 140 mM NaCl, with the lower radioligand concentration of 0.15 nM.

Unfortunately, these results by themselves did not reliably confirm the allosteric modulator theory. In the future, an experiment to study the dissociation constant of the specific radioligand in the absence and presence of SCH would be recommended.[82] To categorize SCH as an allosteric modulator – i.e. positive allosteric modulator (PAM), negative allosteric modulator (NAM), agonistic PAM, agonistic NAM, antagonistic PAM or antagonistic NAM – functional assays would also be required.[83]

4.3.1.4. Conclusion D_1R-H_3R Heteromer Studies

The development of a radioligand-based test system for the characterization of novel bivalent ligands for the D_1R-H_3R heteromer on either a stable or transient HEK293T cell line was not finalized in this study. The generation of a stable HEK293T cell line with an induced P2A site between the respective receptors was not successful to evaluate the formation of functional D_1R-H_3R heteromers *in vitro*. Thus, radioligand binding experiments using stable HEK293T Flag-hH_3R cells transiently transfected with plasmid DNA of the D_1R (12 µg) were performed. All results were generated with co-expressing D_1R-H_3R HEK293T cells with a stoichiometric receptor ratio of 1:2, determined from saturation binding experiments under consideration of the respective B_{max} value of each protomer and the specific activity constant of the respective radioligand. The achieved 1:2 receptor ratio was the predicted to form functional heteromers *in vitro*.[22]

With the bivalent ligand NR330, consisting of an SCH-23390 (SCH) analogue as D_1R pharmacophore and a JNJ-5207852 (JNJ) analogue as H_3R pharmacophore coupled through a flexible PEG linker, radioligand competition binding experiments on D_1R-H_3R co-expressing HEK293T cells were performed. In the D_1R mode [^{3}H]SCH-23390 (c = 0.4 nM) were used as specific radioligand and in the H_3R mode [^{3}H]UR-MN259 (c = 0.5 nM). NR330 resulted a biphasic curve in both modes in binding buffer (BB) without supplements, while the pharmacophoric ligands alone (SCH and JNJ) achieved a monomeric binding curve, as expected. This underlined the bivalent binding mode of NR330 as true bivalent ligand. In order to confirm the observed biphasic binding mode, radioligand competition binding experiments in the presence of an additional H_3R competitor (10 µM JNJ) in the D_1R mode or a D_1R competitor (10 µM SCH) in the H_3R mode were performed to generate a monophasic curve by blocking one protomer. In both cases, the biphasic turned into a monophasic curve with a calculated pK_i value of 7.54 at the D_1R protomer (D_1R-mode) and a pK_i of 6.29 at the H_3R protomer (H_3R mode). These were comparable to the respective p$K_{i,low}$ values of NR330 in both modes on co-expressing D_1R-H_3 HEK293T cells. Furthermore, an unexpected depression in the signal of the specific binding of either [^{3}H]SCH-23390 (D_1R-mode) or [^{3}H]UR-MN25 9(H_3R mode) to approximately 35% and 20% was observed. We assumed a possible binding affinity of SCH to the H_3R and of JNJ to the D_1R. Therefore, radioligand competition binding experiments with JNJ and MN259 (as cold version of the radioligand) alone or in the present of literature known D_1R standard ligands and with the bivalent ligand NR330 were performed on stable HEK293T D_1R-CREluc2P cells. In addition, the same competition radioligand experiments with SCH and butaclamol (buta) alone or in the presence of literature known H_3R ligands and the bivalent ligand NR330 on stable HEK293T Flag-hH_3R were conducted.

As expected, the antagonistic H_3R ligands JNJ and MN259 had no binding affinity to the D_1R monomer on whole HEK293T D_1R-CREluc2P cells. However, it was nevertheless a drop in signal

of the radioligand [^{3}H]SCH-23390 observed to approximately 20% for SCH in the presence of 10 µM JNJ, likewise as for the bivalent ligand NR330 on D_1R-H_3R co-expressing HEK293T cells. Moreover, the affinity of SCH in the presence of 10 µM JNJ was right shifted to a nanomolar range (pK_i = 7.58 ± 0.31) implementing a negative modulation of SCH by JNJ. However, all experiments were performed in a sodium-free buffer. A sodium-dependent impact on binding properties of specific ligands is known for the D_2R or D_3R of the dopamine receptor family, but not for the D_1R so far.[66–68] For further investigations of a sodium- dependent impact to the binding affinity of D_1R ligands in the presence of JNJ or MN259 at the D_1R, Leibovitz's L-15 media and BB supplemented with 140 mM NaCl, both with equally sodium concentrations, were used in further radioligand binding experiments. For both buffers, a monophasic curve for SCH + 10 µM JNJ was observed without a right shift of the binding affinity of SCH (p$K_{i,L15}$ = 9.20 ± 0.05, p$K_{i,BB,140mM\ NaCl}$ = 9.21 ± 0.02) or a depression in the specific binding of [^{3}H]SCH-23390. This result confirmed the hypothesis, that the observed negative modulation only occurs in sodium-free buffer and thus, is a sodium-dependent effect, which supposed to be considered in further radioligand binding experiments.

On stable mono-expressing HEK293T Flag-hH_3R cells, the D_1R standard ligands SCH and buta alone or in combination with the H_3R ligands JNJ and MN259, and the bivalent ligand NR330 were characterized. Interestingly, SCH alone obtained a biphasic curve at the H_3R (p$K_{i,low}$ of 5.51 ± 0.16, p$K_{i,high}$ of 8.77 ± 0.68) in BB without supplements, leading to the assumption that SCH possibly binds to the H_3R with two binding modes somehow. But it needs to be considered, that the specific binding of the radioligand [^{3}H]SCH-23390 was between 90% and 70% at the p$K_{i,high}$ value. In addition, a negative modulation of the binding affinity of JNJ in the presence of 10 µM SCH to a low nanomolar range was observed (pK_i = 9.05 ± 0.25), compared to JNJ alone (pK_i = 9.98 ± 0.06). As well as for the D_1R all experiments were performed in sodium-free BB. We assumed likewise, a sodium-free-dependent effect, especially due to a known sodium binding pocket of the H_3R adjacent to the orthosteric binding pocket.[78,79,84] To confirm our hypothesis, three different sodium-containing buffers (Leibovitz's L-15 media and BB supplemented with either 100 mM or 140 mM NaCl) were used in further radioligand competition binding experiments. In all sodium-containing buffers, SCH resulted a monophasic curve, but different binding affinities from micromolar (Leibovitz's L15 media, BB with 140 mM NaCl) to high nanomolar range (BB with 100 mM NaCl). Furthermore, the observed monophasic curves of SCH was over the whole concentration range in BB with 100 mM NaCl, but without full displacement of the radioligand [^{3}H]UR-MN259. We hypothesize, that SCH acts possibly as an allosteric modulator, but only in sodium-free BB or in buffer with a sodium concentration below 140 mM NaCl. Therefore, radioligand competition binding experiments with a lower radioligand concentration (c = 0.15 nM) according to Ehlert et al. 1985 were performed.[81] Surprisingly, the binding affinity of

SCH in all buffer was right shifted except for Leibovitz's L15 media. Moreover, SCH resulted monophasic curve without a visible plateau in the highest concentrations in BB with 100 mM NaCl, as expected. In summary, these results were inconclusive to confirm or reject the hypothesis of an allosteric modulator and further investigations with more radioligand concentrations are necessary. Further potential experiments would be the determination of radioligand k_{off} values in kinetic studies or a Schild-analysis, each in the presence of different concentrations of SCH.[85]

In order to verify a possible sodium-dependent effect to the binding affinity or binding mode of bivalent ligand NR330 at the H_3R, radioligand competition binding experiments with sodium-free and sodium-containing buffers were performed. The resulted monophasic curves in sodium-free BB and supplemented with 100 mM NaCl were comparable with respect to the binding affinities ($pK_{i,BB}$= 10.03 ± 0.01, $pK_{i,100mM\ NaCl}$ = 9.97 ± 0.32), implying in this case no sodium-dependent effect. In contrast, for Leibovitz's L-15 media and BB supplemented with 140 mM NaCl, it was not possible to validate the real binding mode of the bivalent ligand NR330 and both binding modes (monophasic binding mode or biphasic binding mode) were considered. To evaluate the question of a bivalent binding mode of NR330 at the monomeric H_3R, compared to the co-expressed D_1R-H_3R test system, the resulted plateau of the biphasic curves by radioligand displacement needs to be considered. In the case of BB with 140 mM NaCl we hypothesize the biphasic curve was induced due to the binding of both pharmacophores of NR330 (JNJ and SCH) to the H_3R receptor, where the observed effect was dependent of the signal-to-noise ratio of the assay and not due to a biphasic binding mode. In Leibovitz's L-15 media the observed plateau within the biphasic curve of NR330 in the mono expressing H_3R test system was not identical with the curve of NR330 resulted on the co-expressing D_1R-H_3R HEK293T cells. Therefore, we assume a true bivalent binding mode for NR330 on the co-expressing D_1R-H_3R HEK293T cells so far, but further investigations and optimization are necessary.

In conclusion, the development of a radioligand binding assay for the D_1R-H_3R heteromer on transient co-expressing cells needs to be further investigated by kinetic studies, like association and dissociation experiments of the radioligand and moreover, competition binding experiments with different receptor ratios, besides the 1:2 ratio. For the biphasic curves of the bivalent ligand NR330 in the D_1R mode and H_3R mode, more replicates are necessary, as well as for the competition binding experiments in the presence of an additional competitor in each mode (D_1R mode and H_3R mode) on co-expressing D_1R-H_3R HEK293T cells with a receptor ratio of 1:2. Furthermore in this set-up, the competitors should be changed due to observed binding affinities or modulations on the two monomeric receptors. In the H_3R mode SCH is supposed to be replaced by (+)-butaclamol and JNJ by GSK33449 in the case of the D_1R mode to obtain monophasic curves of the bivalent ligand by blocking one protomer without a decreasing signal-to-noise ratio. Additionally, the end-capped ligands, consisting of only one pharmacophore and the linker, should

be included as further controls as they are available from the PhD projects of Dr. Rosier and Dr. Nagl, respectively. For all following studies on the D_1R-H_3R heteromer, the buffer needs to be changed to a sodium-containing buffer, like Leibovitz's L-15 media. Therefore, all previously obtained experiments with the bivalent ligand with or without an additional competitor need to be performed in this buffer again for complete and sufficient characterization.

4.3.2. $D_{2l}R$-H_3R Heterodimer

4.3.2.1. Radioligand binding experiments on $D_{2l}R$-H_3R co-expressing cells

For the first batch of $D_{2l}R$-H_3R co-expressing cells, HEK293T Flag-hH_3R cells were transfected with 5 µg of plasmid DNA of pcDNA3.1$_{neo}$ $D_{2l}R$-myc (batch 1). In the D_2R-mode for radioligand saturation binding experiments, the pK_d value was comparable to literature data at the $D_{2l}R$ monomer (Figure 4.11, Table 4.13).[41] In contrast, the affinity of the specific H_3R radioligand [^{3}H]UR-PI294 was eight-fold lower, compared to the H_3R monomer, which can be attributed to dimerization. Utilizing the generated B_{max} in both modes, a stoichiometric ratio of 1:1.8 was calculated.

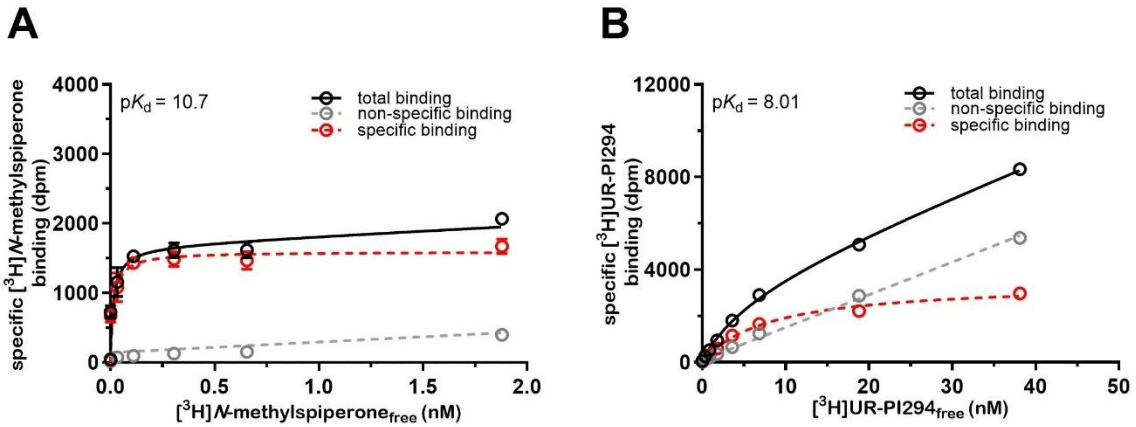

Figure 4.11: Radioligand saturation binding curves with co-expressing $D_{2l}R$-H_3R HEK293T cells. **A**: Saturation binding experiment in the D_2R mode in the presence of different dilutions of the radioligand [^{3}H]*N*-methylspiperone. Haloperidol in 1,000-fold access to the corresponding radioligand concentration was used to determine non-specific binding. **B:** Saturation binding experiment in the H_3R mode in the presence of different dilutions of the radioligand [^{3}H]UR-PI294. Thioperamide in 1,000-fold access to the corresponding radioligand concentration was used for non-specific binding. Data are shown of one experiment, performed in triplicate.

Table 4.13: Obtained dissociation constant (pK_d values) and receptor expression (B_{max}) in radioligand saturation binding experiments on HEK293T $D_{2l}R$-H_3R co-expressing HEK293T cells with a ratio of 1:1.8. Data are shown of one experiment, performed in triplicate.

protomer	pK_d	B_{max}/ dpm	receptors per cell	ratio ($D_{2l}R$:H_3R)	Ref.
$D_{2l}R$	10.7	1592	7.01E+04	1: 1.8	10.6[41]
H_3R	8.01	3455	1.26E+05		8.96[43]

Radioligand competition binding experiments in the presence of [^{3}H]*N*-methylspiperone (D_2R-mode) or [^{3}H]UR-PI294 (H_3R-mode) were performed on $D_{2l}R$-H_3R co-expressing HEK293T cells with a receptor ratio of 1:1.8 to characterize the bivalent ligand MN079, consisting of an agonistic D_2R pharmacophore (*N*-propylaminoindane) and a JNJ-5207852 (JNJ) analogue as an antagonistic H_3R pharmacophore. Both are linked through two PEG linker moieties (eight C-atoms) that are

connected through an isophthalic acid. Additionally, MN209 with the identical H_3R pharmacophore (JNJ) linked to a spiperone analogue as the antagonistic D_2R pharmacophore was tested. Both affinities were then compared to the respective receptor monomers. For analysis, the compare function of Prism10 was used in order to verify a monophasic curve (one-site fit) or biphasic curve (two-site fit). The calculated *p*-value was always indicated in the respective figure captions and table footnotes. The K_i values were calculated from IC_{50} values with the respective K_d value (Appendix Figure 7.39, A-C and Table 7.14 - 7.16), after normalization, according to the Cheng-Prusoff-equation.[45]

The bivalent ligand MN079 produced a monophasic curve (*p*-value = 0.04) in the H_3R mode with a pK_i of 7.65 (Figure 4.12, B, Table 4.14). In comparison with the calculated pK_i value at the H_3R monomer (pK_i = 9.64), a two orders of magnitude rightward shift were observed (Table 4.14). Moreover, in the D_2R mode, an incomplete curve on $D_{2l}R$-H_3R co-expressing HEK293T cells were obtained, including a loss in affinity compared to the binding affinity of MN079 to the $D_{2l}R$ monomer (Figure 4.12, A, Table 4.15). The investigation of the second bivalent ligand MN209 revealed a monophasic curve ($p = 0.63$) in the D_2R mode, whereas a biphasic curve was identified in the H_3R mode ($p < 0.05$). In both modes, no higher affinity of the bivalent ligand was verified to the heteromer. which was observed in a previous publication about bivalent ligand binding to the respective heteromer.[27] Nevertheless, the achieved biphasic curve for the bivalent ligand MN209 in the H_3R mode is a hint that it is a true bivalent ligand for the $D_{2l}R$-H_3R heteromer and needs to be further investigated. It was assumed that the expression level of the respective receptor was insufficient for the formation of functional $D_{2l}R$-H_3R heteromers in both modes.

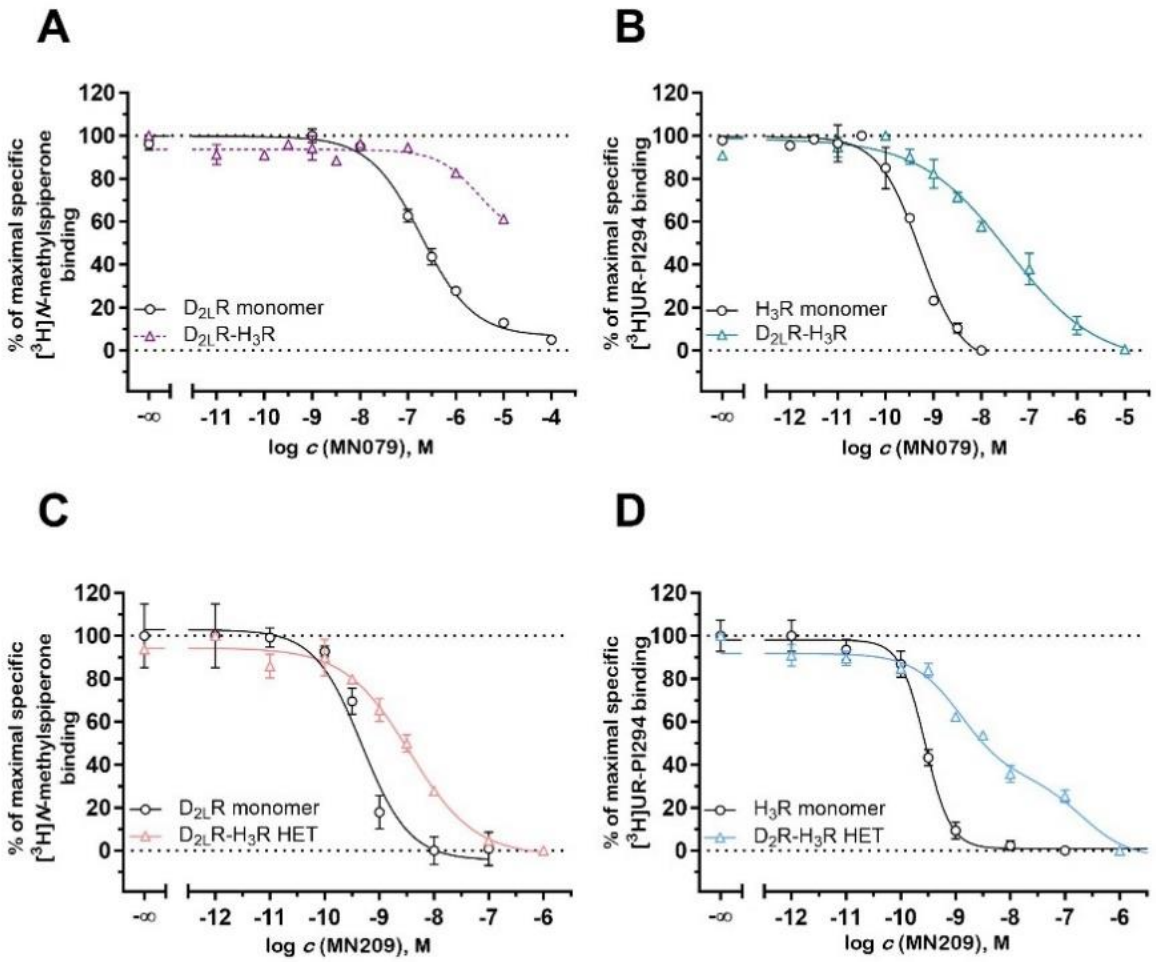

Figure 4.12: Radioligand displacement curves of bivalent ligands in the presence of the specific radioligand [^{3}H]*N*-methylspiperone with **A:** MN079(purple)† or **C:** MN209 (rose)† on $D_{2l}R$-H_3R co-expressing HEK293T cells (receptor ratio 1:1.8) and HEK293T $D_{2l}R$-CRELuc2P wild-type homogenates (black)† or **B:** [^{3}H]UR-PI294 with MN079 (turquoise)† or **D:** MN209 (blue)*** on $D_{2l}R$-H_3R co-expressing HEK293Tcells (receptor ratio 1:1.8) and HEK293T Flag-hH_3R wild-type cells (black) †. As non-specific binding haloperidol in the case of the D_2R mode and in H_3R mode clobenpropit each in 1,000-fold excess was used for determination. Dashed lines mark incomplete curves. Data are shown as mean ± SEM from one to three experiments, all performed in triplicate. ***$p < 0.01$. †$p > 0.05$.

Table 4.14: Calculated binding affinities (pK_i values) of the bivalent Ligand MN079 on either HEK293T $D_{2l}R$-CRELuc2P homogenates or $D_{2l}R$-H_3R co-expressing HEK293T cells (receptor ratio 1:1.8). Data are shown as mean ± SEM from one to three experiments, all performed in triplicate.

Cpd.	HEK293T $D_{2l}R$-CRELuc2P (wt receptor)		HEK293T $D_{2l}R$-H_3R ($D_{2l}R$ mode)		
	pK_i ± SEM	*N*	pK_i ± SEM	curve-fit	*N*
MN079	7.30 ± 0.06[a]	3	< 5.0	n.a.	1
MN209	9.58 ± 0.04[a]	3	9.57	one-site†	1

n.a. – not applicable. [a]unpublished data from Dr. M. Nagl. †$p > 0.05$.

Table 4.15: Calculated binding affinities (pK_i values) of the bivalent ligand MN079 on either HEK293T Flag-hH_3R wild-type cells or D_{2l}R-H_3R co-expressing HEK293T cells (receptor ratio 1:1.8). Data are shown as mean ± SEM from one to three experiments, all performed in triplicate.

Cpd.	HEK293T Flag-hH_3R (wt receptor)		HEK293T D_{2l}R-H_3R (H_3R mode)				
	pK_i ± SEM	*N*	pK_i ± SEM	p$K_{i,low}$ ± SEM	p$K_{i,high}$ ± SEM	curve-fit	*N*
MN079	9.26 ± 0.04[a]	3	7.65			one-site[†]	1
MN209	9.83 ± 0.05[a]	3		6.89	9.11	two-site[***]	1

[a]unpublished data performed by Dr. M. Nagl. ***$p < 0.01$. †$p > 0.05$.

Therefore, we hypothesized that the achieved stoichiometric receptor ratio of 1:1.8 was not sufficient for the characterization of the bivalent ligands, although from previous results it was assumed that in general for the dimerization of class A GPCRs a stoichiometric receptor ratio of 1:2 leads to functional cross-interactions.[53] Thus, the transfected amount of plasmid DNA was changed for the next batch to verify the optimal stoichiometric receptor ratio. Unfortunately, this was not successful, (Appendix, Figure 7.39, Table 7.17) and due to time limitations no further experiments could be conducted.

4.3.2.2. Development of a miniG Protein-Based Functional Assay for the D_{2l}R-H_3R Heteromer

In order to adequately characterize the pharmacological properties of bivalent ligands, consisting of binding affinities (pEC_{50}) and functional efficacies (E_{max}) at the respective target, the development of functional test systems is required. In a previous functional assay the two receptor protomers of the rhodopsin heteromer were synthetically linked together.[86] A possible disadvantage of the set-up is that may the ligand binding and thus, receptor activation may be affected.[87] Another method is the measurement of cAMP accumulation with a cyclic AMP (^{3}H) Assay System (Amersham Biosciences, Uppsala, Sweden), which is time-consuming and produce a high increase of costs due to radioactive waste disposal.[33] To overcome these drawbacks, a miniG protein-based assay was designed, where the small bit (SmBiT, NLC)[88] of the split NanoLuc was fused C-terminally to the H_3R and the large bit (LgBiT, NLN)[88] between the C-terminus of the D_{2l}R and the miniG_{si} protein through flexible linkers (based on Frederick et al. 2015 with changes).[89] After activation by a ligand, the mini G_{si} protein is recruited by one of the activated protomers and the complementation of the full luciferase takes place. The specific substrate Furimazine is oxidized by the complete luciferase and the resulting bioluminescent signal is measurable as the emission of blue light (λ = 460 nm) (Figure 4.13, A). Furthermore, with this set-up the pharmacological effects due to dimerization can be elucidated.

The validation of the miniG protein-based assay was performed on HEK293T cells by the transient transfection with both DNA plasmids of pcDNA3.1$_{neo}$ H_3R-NLC and pIRES$_{puro}$ D_{2l}R-NLN-mG_{si}.

Agonists were chosen based on being well-characterized ligands for the H_3R and D_2R with varied potencies (pEC_{50}) and efficacies (E_{max}) for agonists (histamine (his), imetit, dopamine (dopa), pramipexole (prami) and sufficient pK_b values for antagonists (JNJ-5207852 (JNJ, thioperamide (thio)), and finally the bivalent ligand MN240, consisting of a D_2R agonistic pharmacophore (8-OH-DPAT) and a JNJ analogue as the H_3R pharmacophore for the $D_{2l}R$-H_3R heterodimer. The characterization always included a reference agonist that was able to maximally activate the receptor (defined as 100%). As a control, both DNA plasmids of $pcDNA3.1_{neo}$ H_3R-NLC and $pIRES_{puro}$ $D_{2l}R$-NLN-mG_{si} were transfected alone and tested with different standard ligands, to demonstrate the bioluminescence results only by complementation of both split nano luciferase parts in the presence of the substrate (Appendix, Figure 7.40).

Remarkedly, the observed luminescent traces for histamine after the activation of the $D_{2l}R$-H_3R heteromer differ from the traces detected at the monomeric H_3R in previously performed experiments (Figure 4.13, B and C). For the $D_{2l}R$-H_3R heteromer, the bioluminescence led into a plateau right after the rapid activation (Figure 4.13, C). However, at the H_3R monomer a sharp peak was observed, that slowly decreased and ended in a lower plateau (Figure 4.13, C). This could be a hint for receptor dimerization. Nevertheless, the miniG recruitment signaling could also be affected by other molecular processes, like ligand binding, split luciferase complementation and substrate oxidation (Figure 4.13, A).[46]

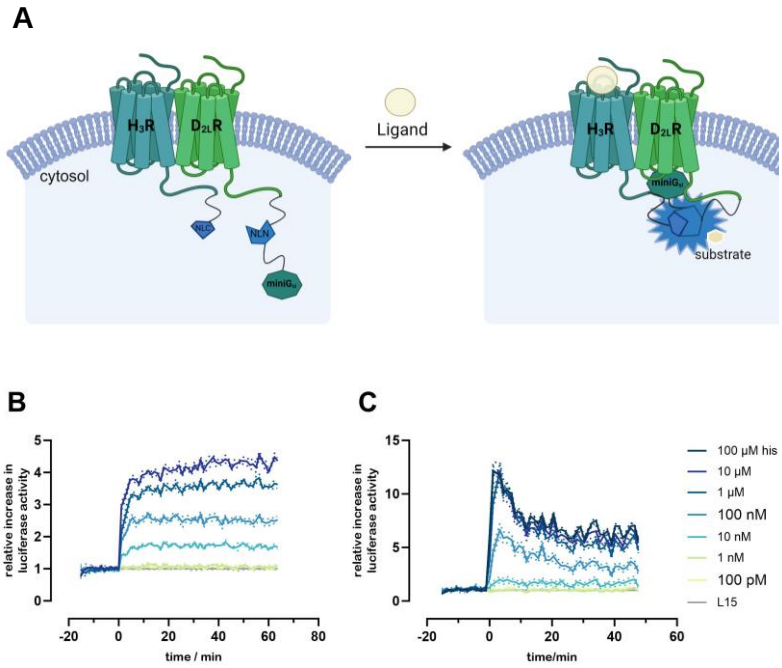

Figure 4.13: A: Scheme of the $miniG_{si}$ protein recruitment assay for the $D_{2l}R$-H_3R heteromer. **B:** Baseline and inter-well corrected luminescent traces of the recruitment of the $miniG_{si}$ protein to the $D_{2l}R$-H_3R heteromer and **C:** H_3R monomer in a concentration-dependent manner of histamine as H_3R ligand.

All analyzed ligands gave robust concentration-response-curves. The agonists histamine, imetit, and pramipexole were analyzed in the so-called agonist mode. On the $D_{2l}R$-H_3R heteromer, histamine acted as a full agonist and the calculated potency (pEC_{50} = 7.17 ± 0.15) was eight-fold higher, compared to the $miniG_{si}$ H_3R monomer assay (pEC_{50} = 6.40 ± 0.04).[46] Furthermore, imetit was confirmed as a partial agonist with an increased potency of one order of magnitude at the H_3R

(pEC_{50} = 7.85 ± 0.26) compared to literature data (Figure 4.14, A and Table 4.16).[46,90] In contrast, the D_2R standard agonists pramipexole and dopamine were not able to induce a functional signal at the $D_{2l}R$-H_3R heteromer (Figure 4.14, A) leading to the assumption of a potential negative cooperativity to the $D_{2l}R$ protomer by dimerization. Another possibility is the asymmetric $miniG_{si}$ recruitment, resulting in a non-measurable response for the $D_{2l}R$ activation. This can occur when both protomers are able to recruit the same G protein and the accessibility is limited.[91,92]

In the so-called antagonist mode thioperamide (thio), JNJ and MN240 were characterized as antagonists in the presence of 1 µM histamine (EC_{80}). The signal of MN240 and JNJ dropped under the baseline, which was a hint for inverse agonism (Figure 4.14, B). In the case of thioperamide (thio) the signal could not reach to the 100% value in the presence of 1 µM histamine within the lowest concentration of thioperamide but the yielded pK_b value of 6.82 ± 0.56 was in good agreement with literature data (pK_b = 6.88 ± 0.03) from the $miniG_{si}$ protein recruitment assay for the H_3R monomer (Figure 4.14, B and Table 4.16).[46] The calculated pK_b value of JNJ in the antagonist mode (pK_b = 9.33 ± 0.15) was comparable with the literature data[44] and the bivalent ligand MN240 achieved a pK_b value in nanomolar range (pK_b = 7.98 ± 0.20). Additionally, in both cases the pEC_{80} efficacy of 1 µM histamine was not reached within the lower concentrations of all three used H_3R antagonist as expected (Figure 4.14, B and Table 4.16).

From previous studies of Ferrada et al. 2008 at the $D_{2l}R$-H_3R heteromer a negative cooperativity was predicted[33]. Therefore, we tested the endogenous ligand histamine in the presence of one concentration of two D_2R standard ligands: the endogenous agonist dopamine (dopa) and the antagonist haloperidol (halo) (Figure 4.14, C). In the presence of 100 µM dopamine (dopa) as well as with 1 µM haloperidol (halo) the pEC_{50} value was right shifted to a higher nanomolar range ($pEC_{50,\ his\ +\ 100\ \mu M\ dopa}$ = 6.23 ± 0.18, $pEC_{50,\ his\ +\ 1\ \mu M\ halo}$ = 6.59 ± 0.06) compared to histamine alone at the $D_{2l}R$-H_3R heteromer ($pEC_{50,his}$ = 7.17 ± 0.23) (Table 4.16). Remarkably, histamine was not considered as a full agonist anymore in the presence of 100 µM dopamine (E_{max} = 47.0 ± 1.5) and 1 µM haloperidol (E_{max} = 84.4 ± 2.1) (Figure 4.14, C). These results led to the hypothesis that D_2R standard ligands might influence the potency of histamine ligands at the $D_{2l}R$-H_3R heteromer with a possible negative cooperativity between the two receptor protomers. However, further investigations are necessary.

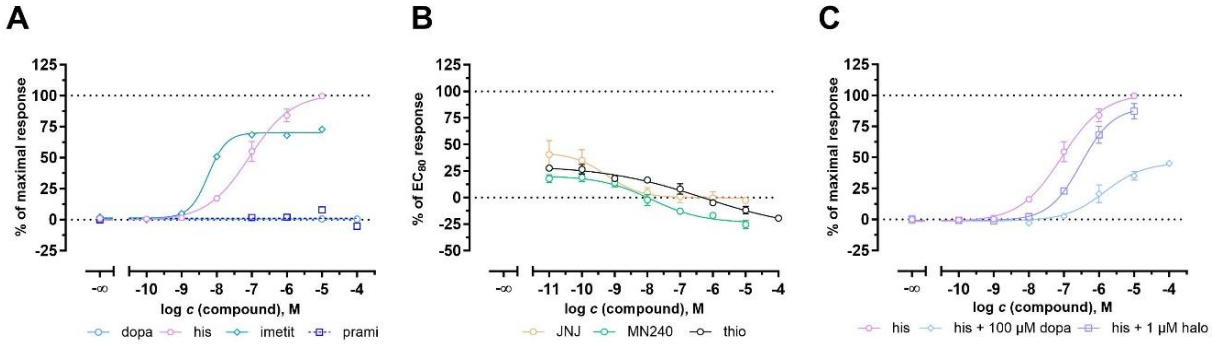

Figure 4.14: Characterization of agonists and antagonists at the $D_{2l}R$-H_3R heterodimer transiently expressed in HEK293T cells using the developed miniG protein-based assay. **A:** The concentration-dependent increase in luminescence of standard agonists in a time-resolved manner was determined for different agonists. Data were normalized according to the maximum level of 10 µM histamine. **B:** The concentration-dependent increase of luminescence in a time-resolved manner of the H_3R antagonist JNJ-5207852 (JNJ), the bivalent ligand MN240 in the presence of 1 µM histamine (antagonist mode). **C:** The concentration-dependent increase in luminescence of standard agonists in a time-resolved manner was determined for histamine alone and in the presence of dopamine (100 µM, dopamine receptor agonist) or haloperidol (1 µM, D_2R antagonist). Data were normalized according to the maximum level of the full agonist histamine for agonists (10 µM) and antagonists (1 µM). Ligand potencies (pEC_{50}) and efficacies (E_{max}) at the $D_{2l}R$-H_3R heteromer in the miniG Protein Recruitment Assay compared to literature data of pK_i values in HEK293T cells. Data are shown as mean ± SEM from two to four independent experiments, all performed in triplicate. Abbreviations used: dopa – dopamine, halo – haloperidol, his – histamine, prami – pramipexole, JNJ – JNJ-5207852, thio – thioperamide.

Table 4.16: Ligand potencies (pEC_{50}) and efficacies (E_{max}) at the $D_{2l}R$-H_3R heteromer in the miniG Protein Recruitment Assay compared to literature data (pK_i values) in HEK293T cells. Data are shown as mean ± SEM from two to four independent experiments, all performed in triplicate.

Cpd.	pEC_{50} ± SEM	E_{max} ± SEM / %	pK_b ± SEM	*N*	Ref.
dopa	< 4.0	n.a.	n.d.	2	7.69[93]
his	7.17 ± 0.23	100	n.d.	3	6.40[46]
imetit	7.85 ± 0.26	73.5 ± 0.5	n.d.	2	6.97[46]
prami	< 4.0	n.a.	n.d.	2	7.51[93]
MN240	n.d.	-	7.98 ± 0.20	4	-
thioperamide	n.d.	-	6.82 ± 0.56	2	6.43[46]
JNJ	n.d.	-	9.33 ± 0.15	2	9.20[44,a]
his + 100 µM dopa	6.23 ± 0.18	47.0 ± 1.5	n.d.	2	-
his + 100 µM halo	6.59 ± 0.06	84.4 ± 2.1	n.d.	2	-

n.d. not determined. n.a. not applicable. [a] pK_i value. Abbreviations used: dopa – dopamine, halo – haloperidol, his – histamine, prami – pramipexole, JNJ – JNJ-5207852, thio – thioperamide.

4.3.2.3. Limitations and Further Experiments

In this project, interesting pharmacological results of the $D_{2l}R$-H_3R were observed. However, more controls and changes in set-up are required in order to complete the understanding of this heteromer's signaling behavior. One limitation is, that the recruitment of the miniG_{si} protein is not traceable and no verification whether there is an asymmetric or symmetric miniG_{si} recruitment.[91,92] A possible control experiment could be, fusing the small bit of the split nano luciferase C-terminally to the $D_{2l}R$ and the large bit between the H_3R and the miniG_{si}. Additionally, a point-mutation could be introduced in the G protein binding domain of the respective receptor to reduce the ability for this receptor protomer to recruit the miniG_{si} protomer.[94] Furthermore, the linker length between the large bit and the miniG_{si} protein should be changed. The current linker length is about 56 base pairs, which should be increased and decreased to investigate a possible impact on the miniG_{si} recruitment. The transfection ratio remains to be examined, by transfecting different amounts of one plasmid DNA of one protomer, while leaving the other at a constant amount followed by the determination of the receptor ratio with radioligand experiments or a NanoBRET-based assay. Moreover, the miniG protein can be changed to other currently available miniG proteins like miniG_s, miniG_{sq} or miniG_o to investigate the possible recruitment of the $D_{2l}R$-H_3R heteromer and possible bias signaling of several H_3R, D_2R or bivalent ligands.

4.4. References

(1) Hamm, H. E. How activated receptors couple to G proteins. *Proceedings of the National Academy of Sciences of the United States of America* **2001**, *98* (9), 4819–4821. DOI: 10.1073/pnas.011099798.

(2) Fredriksson, R.; Lagerström, M. C.; Lundin, L.-G.; Schiöth, H. B. The G-protein-coupled receptors in the human genome form five main families. Phylogenetic analysis, paralogon groups, and fingerprints. *Molecular pharmacology* **2003**, *63* (6), 1256–1272. DOI: 10.1124/mol.63.6.1256.

(3) Milligan, G.; Kostenis, E. Heterotrimeric G-proteins: a short history. *British journal of pharmacology* **2006**, *147 Suppl 1* (Suppl 1), S46-55. DOI: 10.1038/sj.bjp.0706405.

(4) Sriram, K.; Insel, P. A. G Protein-Coupled Receptors as Targets for Approved Drugs: How Many Targets and How Many Drugs? *Molecular pharmacology* **2018**, *93* (4), 251–258. DOI: 10.1124/mol.117.111062.

(5) Alexander, S. P.; Kelly, E.; Marrion, N. V.; Peters, J. A.; Faccenda, E.; Harding, S. D.; Pawson, A. J.; Sharman, J. L.; Southan, C.; Buneman, O. P.; Cidlowski, J. A.; Christopoulos, A.; Davenport, A. P.; Fabbro, D.; Spedding, M.; Striessnig, J.; Davies, J. A. THE CONCISE GUIDE TO PHARMACOLOGY 2017/18: Overview. *British journal of pharmacology* **2017**, *174 Suppl 1* (Suppl Suppl 1), S1-S16. DOI: 10.1111/bph.13882.

(6) Moreno, E.; Casajuana-Martin, N.; Coyle, M.; Campos, B. C.; Galaj, E.; Del Torrent, C. L.; Seyedian, A.; Rea, W.; Cai, N.-S.; Bonifazi, A.; Florán, B.; Xi, Z.-X.; Guitart, X.; Casadó, V.; Newman, A. H.; Bishop, C.; Pardo, L.; Ferré, S. Pharmacological targeting of G protein-coupled receptor heteromers. *Pharmacological research* **2022**, *185*, 106476. DOI: 10.1016/j.phrs.2022.106476.

(7) Gomes, I.; Ayoub, M. A.; Fujita, W.; Jaeger, W. C.; Pfleger, K. D. G.; Devi, L. A. G Protein-Coupled Receptor Heteromers. *Annual review of pharmacology and toxicology* **2016**, *56*, 403–425. DOI: 10.1146/annurev-pharmtox-011613-135952.

(8) Angers, S.; Salahpour, A.; Bouvier, M. Dimerization: an emerging concept for G protein-coupled receptor ontogeny and function. *Annual review of pharmacology and toxicology* **2002**, *42*, 409–435. DOI: 10.1146/annurev.pharmtox.42.091701.082314.

(9) Jones, K. A.; Borowsky, B.; Tamm, J. A.; Craig, D. A.; Durkin, M. M.; Dai, M.; Yao, W. J.; Johnson, M.; Gunwaldsen, C.; Huang, L. Y.; Tang, C.; Shen, Q.; Salon, J. A.; Morse, K.; Laz, T.; Smith, K. E.; Nagarathnam, D.; Noble, S. A.; Branchek, T. A.; Gerald, C. GABA(B) receptors function as a heteromeric assembly of the subunits GABA(B)R1 and GABA(B)R2. *Nature* **1998**, *396* (6712), 674–679. DOI: 10.1038/25348.

(10) Kaupmann, K.; Malitschek, B.; Schuler, V.; Heid, J.; Froestl, W.; Beck, P.; Mosbacher, J.; Bischoff, S.; Kulik, A.; Shigemoto, R.; Karschin, A.; Bettler, B. GABA(B)-receptor subtypes assemble into functional heteromeric complexes. *Nature* **1998**, *396* (6712), 683–687. DOI: 10.1038/25360.

(11) Nelson, G.; Chandrashekar, J.; Hoon, M. A.; Feng, L.; Zhao, G.; Ryba, N. J. P.; Zuker, C. S. An amino-acid taste receptor. *Nature* **2002**, *416* (6877), 199–202. DOI: 10.1038/nature726.

(12) Rocheville, M.; Lange, D. C.; Kumar, U.; Patel, S. C.; Patel, R. C.; Patel, Y. C. Receptors for dopamine and somatostatin: formation of hetero-oligomers with enhanced functional activity. *Science (New York, N.Y.)* **2000**, *288* (5463), 154–157. DOI: 10.1126/science.288.5463.154.

(13) Angers, S.; Salahpour, A.; Joly, E.; Hilairet, S.; Chelsky, D.; Dennis, M.; Bouvier, M. Detection of beta 2-adrenergic receptor dimerization in living cells using bioluminescence resonance energy transfer (BRET). *Proceedings of the National Academy of Sciences of the United States of America* **2000**, *97* (7), 3684–3689. DOI: 10.1073/pnas.97.7.3684.

(14) Taura, J.; Fernández-Dueñas, V.; Ciruela, F. Visualizing G Protein-Coupled Receptor-Receptor Interactions in Brain Using Proximity Ligation In Situ Assay. *Current protocols in cell biology* **2015**, *67*, 17.17.1-17.17.16. DOI: 10.1002/0471143030.cb1717s67.

(15) Terrillon, S.; Bouvier, M. Roles of G-protein-coupled receptor dimerization. *EMBO reports* **2004**, *5* (1), 30–34. DOI: 10.1038/sj.embor.7400052.

(16) Nelson, G.; Hoon, M. A.; Chandrashekar, J.; Zhang, Y.; Ryba, N. J.; Zuker, C. S. Mammalian sweet taste receptors. *Cell* **2001**, *106* (3), 381–390. DOI: 10.1016/s0092-8674(01)00451-2.

(17) White, J. H.; Wise, A.; Main, M. J.; Green, A.; Fraser, N. J.; Disney, G. H.; Barnes, A. A.; Emson, P.; Foord, S. M.; Marshall, F. H. Heterodimerization is required for the formation of a functional GABA(B) receptor. *Nature* **1998**, *396* (6712), 679–682. DOI: 10.1038/25354.

(18) Lambert, N. A. GPCR dimers fall apart. *Science signaling* **2010**, *3* (115), pe12. DOI: 10.1126/scisignal.3115pe12.

(19) Hern, J. A.; Baig, A. H.; Mashanov, G. I.; Birdsall, B.; Corrie, J. E. T.; Lazareno, S.; Molloy, J. E.; Birdsall, N. J. M. Formation and dissociation of M1 muscarinic receptor dimers seen by total internal reflection fluorescence imaging of single molecules. *Proceedings of the National Academy of Sciences of the United States of America* **2010**, *107* (6), 2693–2698. DOI: 10.1073/pnas.0907915107.

(20) Moreno-Delgado, D.; Puigdellívol, M.; Moreno, E.; Rodríguez-Ruiz, M.; Botta, J.; Gasperini, P.; Chiarlone, A.; Howell, L. A.; Scarselli, M.; Casadó, V.; Cortés, A.; Ferré, S.; Guzmán, M.; Lluís, C.; Alberch, J.; Canela, E. I.; Ginés, S.; McCormick, P. J. Modulation of dopamine D1 receptors via histamine H3 receptors is a novel therapeutic target for Huntington's disease. *eLife* **2020**, *9.* DOI: 10.7554/eLife.51093.

(21) Maggio, R.; Innamorati, G.; Parenti, M. G protein-coupled receptor oligomerization provides the framework for signal discrimination. *Journal of neurochemistry* **2007**, *103* (5), 1741–1752. DOI: 10.1111/j.1471-4159.2007.04896.x.

(22) Ferrada, C.; Moreno, E.; Casadó, V.; Bongers, G.; Cortés, A.; Mallol, J.; Canela, E. I.; Leurs, R.; Ferré, S.; Lluís, C.; Franco, R. Marked changes in signal transduction upon heteromerization of dopamine D1 and histamine H3 receptors. *British journal of pharmacology* **2009**, *157* (1), 64–75. DOI: 10.1111/j.1476-5381.2009.00152.x.

(23) Rodríguez-Ruiz, M.; Moreno, E.; Moreno-Delgado, D.; Navarro, G.; Mallol, J.; Cortés, A.; Lluís, C.; Canela, E. I.; Casadó, V.; McCormick, P. J.; Franco, R. Heteroreceptor Complexes Formed by Dopamine D1, Histamine H3, and N-Methyl-D-Aspartate Glutamate Receptors as Targets to Prevent Neuronal Death in Alzheimer's Disease. *Molecular neurobiology* **2017**, *54* (6), 4537–4550. DOI: 10.1007/s12035-016-9995-y.

(24) Moreno, E.; Hoffmann, H.; Gonzalez-Sepúlveda, M.; Navarro, G.; Casadó, V.; Cortés, A.; Mallol, J.; Vignes, M.; McCormick, P. J.; Canela, E. I.; Lluís, C.; Moratalla, R.; Ferré, S.; Ortiz, J.; Franco, R. Dopamine D1-histamine H3 receptor heteromers provide a selective link to MAPK signaling in GABAergic neurons of the direct striatal pathway. *The Journal of biological chemistry* **2011**, *286* (7), 5846–5854. DOI: 10.1074/jbc.M110.161489.

(25) Olajide, O. J.; Chapman, C. A. Amyloid-β (1-42) peptide induces rapid NMDA receptor-dependent alterations at glutamatergic synapses in the entorhinal cortex. *Neurobiology of aging* **2021**, *105*, 296–309. DOI: 10.1016/j.neurobiolaging.2021.05.006.

(26) Liu, J.; Chang, L.; Song, Y.; Li, H.; Wu, Y. The Role of NMDA Receptors in Alzheimer's Disease. *Frontiers in neuroscience* **2019**, *13*, 43. DOI: 10.3389/fnins.2019.00043.

(27) Hübner, H.; Schellhorn, T.; Gienger, M.; Schaab, C.; Kaindl, J.; Leeb, L.; Clark, T.; Möller, D.; Gmeiner, P. Structure-guided development of heterodimer-selective GPCR ligands. *Nature communications* **2016**, *7*, 12298. DOI: 10.1038/ncomms12298.

(28) Kühhorn, J.; Hübner, H.; Gmeiner, P. Bivalent dopamine D2 receptor ligands: synthesis and binding properties. *Journal of medicinal chemistry* **2011**, *54* (13), 4896–4903. DOI: 10.1021/jm2004859.

(29) Salama, I.; Löber, S.; Hübner, H.; Gmeiner, P. Synthesis and binding profile of haloperidol-based bivalent ligands targeting dopamine D(2)-like receptors. *Bioorganic & medicinal chemistry letters* **2014**, *24* (16), 3753–3756. DOI: 10.1016/j.bmcl.2014.06.079.

(30) Shonberg, J.; Scammells, P. J.; Capuano, B. Design Strategies for Bivalent Ligands Targeting GPCRs. *ChemMedChem* **2011**, *6* (6), 963–974. DOI: 10.1002/cmdc.201100101.

(31) Valant, C.; Sexton, P. M.; Christopoulos, A. Orthosteric/allosteric bitopic ligands: going hybrid at GPCRs. *Molecular interventions* **2009**, *9* (3), 125–135. DOI: 10.1124/mi.9.3.6.

(32) Newman, A. H.; Battiti, F. O.; Bonifazi, A. 2016 Philip S. Portoghese Medicinal Chemistry Lectureship: Designing Bivalent or Bitopic Molecules for G-Protein Coupled Receptors. The Whole Is Greater Than the Sum of Its Parts. *Journal of medicinal chemistry* **2020**, *63* (5), 1779–1797. DOI: 10.1021/acs.jmedchem.9b01105.

(33) Ferrada, C.; Ferré, S.; Casadó, V.; Cortés, A.; Justinova, Z.; Barnes, C.; Canela, E. I.; Goldberg, S. R.; Leurs, R.; Lluis, C.; Franco, R. Interactions between histamine H3 and dopamine D2 receptors and the implications for striatal function. *Neuropharmacology* **2008**, *55* (2), 190–197. DOI: 10.1016/j.neuropharm.2008.05.008.

(34) Feng, Y.; Lu, Y. Immunomodulatory Effects of Dopamine in Inflammatory Diseases. *Frontiers in immunology* **2021**, *12*, 663102. DOI: 10.3389/fimmu.2021.663102.

(35) Ginés, S.; Hillion, J.; Torvinen, M.; Le Crom, S.; Casadó, V.; Canela, E. I.; Rondin, S.; Lew, J. Y.; Watson, S.; Zoli, M.; Agnati, L. F.; Verniera, P.; Lluis, C.; Ferré, S.; Fuxe, K.; Franco, R. Dopamine D1 and adenosine A1 receptors form functionally interacting heteromeric complexes. *Proceedings of the National Academy of Sciences of the United States of America* **2000**, *97* (15), 8606–8611. DOI: 10.1073/pnas.150241097.

(36) Soriano, A.; Ventura, R.; Molero, A.; Hoen, R.; Casadó, V.; Cortés, A.; Fanelli, F.; Albericio, F.; Lluís, C.; Franco, R.; Royo, M. Adenosine A2A receptor-antagonist/dopamine D2 receptor-agonist bivalent ligands as pharmacological tools to detect A2A-D2 receptor heteromers. *Journal of medicinal chemistry* **2009**, *52* (18), 5590–5602. DOI: 10.1021/jm900298c.

(37) Borroto-Escuela, D. O.; La Pérez de Mora, M.; Zoli, M.; Benfenati, F.; Narvaez, M.; Rivera, A.; Díaz-Cabiale, Z.; Beggiato, S.; Ferraro, L.; Tanganelli, S.; Ambrogini, P.; Filip, M.; Liu, F.; Franco, R.; Agnati, L. F.; Fuxe, K. Analysis and Quantification of GPCR Allosteric Receptor–Receptor Interactions Using Radioligand Binding Assays: The A2AR-D2R Heteroreceptor Complex Example. In *Receptor-Receptor Interactions in the Central Nervous System*; Fuxe, K., Borroto-Escuela, D. O., Eds.; Neuromethods; Springer New York, 2018; pp 1–14. DOI: 10.1007/978-1-4939-8576-0_1.

(38) Gehlert, D. R.; Schober, D. A.; Morin, M.; Berglund, M. M. Co-expression of neuropeptide Y Y1 and Y5 receptors results in heterodimerization and altered functional properties. *Biochemical pharmacology* **2007**, *74* (11), 1652–1664. DOI: 10.1016/j.bcp.2007.08.017.

(39) Fernández-Dueñas, V.; Gómez-Soler, M.; Jacobson, K. A.; Kumar, S. T.; Fuxe, K.; Borroto-Escuela, D. O.; Ciruela, F. Molecular determinants of A2AR-D2R allosterism: role of the intracellular loop 3 of the D2R. *Journal of neurochemistry* **2012**, *123* (3), 373–384. DOI: 10.1111/j.1471-4159.2012.07956.x.

(40) Wan, Q.; Okashah, N.; Inoue, A.; Nehmé, R.; Carpenter, B.; Tate, C. G.; Lambert, N. A. Mini G protein probes for active G protein-coupled receptors (GPCRs) in live cells. *The Journal of biological chemistry* **2018**, *293* (19), 7466–7473. DOI: 10.1074/jbc.RA118.001975.

(41) Forster, L.; Grätz, L.; Mönnich, D.; Bernhardt, G.; Pockes, S. A Split Luciferase Complementation Assay for the Quantification of β-Arrestin2 Recruitment to Dopamine D2-Like Receptors. *International journal of molecular sciences* **2020**, *21* (17). DOI: 10.3390/ijms21176103.

(42) Tropmann, K.; Bresinsky, M.; Forster, L.; Mönnich, D.; Buschauer, A.; Wittmann, H.-J.; Hübner, H.; Gmeiner, P.; Pockes, S.; Strasser, A. Abolishing Dopamine D2long/D3 Receptor Affinity of Subtype-Selective Carbamoylguanidine-Type Histamine H2 Receptor Agonists. *Journal of medicinal chemistry* **2021**, *64* (12), 8684–8709. DOI: 10.1021/acs.jmedchem.1c00692.

(43) Igel, P.; Schnell, D.; Bernhardt, G.; Seifert, R.; Buschauer, A. Tritium-labeled N(1)-3-(1H-imidazol-4-yl)propyl-N(2)-propionylguanidine ((3)HUR-PI294), a high-affinity histamine H(3) and H(4) receptor radioligand. *ChemMedChem* **2009**, *4* (2), 225–231. DOI: 10.1002/cmdc.200800349.

(44) Mönnich, D.; Nagl, M.; Forster, L.; Rosier, N.; Igel, P.; Pockes, S. Discovery of a Tritiated Radioligand with High Affinity and Selectivity for the Histamine H3 Receptor. *ACS medicinal chemistry letters* **2023**, *14* (11), 1589–1595. DOI: 10.1021/acsmedchemlett.3c00413.

(45) Cheng, Y.; Prusoff, W. H. Relationship between the inhibition constant (K1) and the concentration of inhibitor which causes 50 per cent inhibition (I50) of an enzymatic reaction. *Biochemical pharmacology* **1973**, *22* (23), 3099–3108. DOI: 10.1016/0006-2952(73)90196-2.

(46) Höring, C.; Seibel, U.; Tropmann, K.; Grätz, L.; Mönnich, D.; Pitzl, S.; Bernhardt, G.; Pockes, S.; Strasser, A. A Dynamic, Split-Luciferase-Based Mini-G Protein Sensor to Functionally Characterize Ligands at All Four Histamine Receptor Subtypes. *International journal of molecular sciences* **2020**, *21* (22). DOI: 10.3390/ijms21228440.

(47) Luke, G. A.; Felipe, P. de; Lukashev, A.; Kallioinen, S. E.; Bruno, E. A.; Ryan, M. D. Occurrence, function and evolutionary origins of '2A-like' sequences in virus genomes. *The Journal of general virology* **2008**, *89* (Pt 4), 1036–1042. DOI: 10.1099/vir.0.83428-0.

(48) Wang, Y.; Wang, F.; Wang, R.; Zhao, P.; Xia, Q. 2A self-cleaving peptide-based multi-gene expression system in the silkworm Bombyx mori. *Scientific reports* **2015**, *5*, 16273. DOI: 10.1038/srep16273.

(49) Zaman, G. J. R.; Roos, J. A. D. M. de; Blomenröhr, M.; van Koppen, C. J.; Oosterom, J. Cryopreserved cells facilitate cell-based drug discovery. *Drug discovery today* **2007**, *12* (13-14), 521–526. DOI: 10.1016/j.drudis.2007.05.008.

(50) Zhu, Z.; Puglisi, J.; Connors, D.; Stewart, J.; Herbst, J.; Marino, A.; Sinz, M.; O'Connell, J.; Banks, M.; Dickinson, K.; Cacace, A. Use of cryopreserved transiently transfected cells in high-throughput pregnane X receptor transactivation assay. *Journal of biomolecular screening* **2007**, *12* (2), 248–254. DOI: 10.1177/1087057106297828.

(51) Kunapuli, P.; Zheng, W.; Weber, M.; Solly, K.; Mull, R.; Platchek, M.; Cong, M.; Zhong, Z.; Strulovici, B. Application of division arrest technology to cell-based HTS: comparison with frozen and fresh cells. *Assay and drug development technologies* **2005**, *3* (1), 17–26. DOI: 10.1089/adt.2005.3.17.

(52) George, S. R.; Fan, T.; Xie, Z.; Tse, R.; Tam, V.; Varghese, G.; O'Dowd, B. F. Oligomerization of mu- and delta-opioid receptors. Generation of novel functional properties. *The Journal of biological chemistry* **2000**, *275* (34), 26128–26135. DOI: 10.1074/jbc.M000345200.

(53) Herrick-Davis, K.; Grinde, E.; Harrigan, T. J.; Mazurkiewicz, J. E. Inhibition of serotonin 5-hydroxytryptamine2c receptor function through heterodimerization: receptor dimers bind two molecules of ligand and one G-protein. *The Journal of biological chemistry* **2005**, *280* (48), 40144–40151. DOI: 10.1074/jbc.M507396200.

(54) Bourne, J. A. SCH 23390: the first selective dopamine D1-like receptor antagonist. *CNS drug reviews* **2001**, *7* (4), 399–414. DOI: 10.1111/j.1527-3458.2001.tb00207.x.

(55) Nagl, M.; Mönnich, D.; Rosier, N.; Schihada, H.; Sirbu, A.; Konar, N.; Reyes-Resina, I.; Navarro, G.; Franco, R.; Kolb, P.; Annibale, P.; Pockes, S. Fluorescent Tools for the Imaging of Dopamine D2 -Like Receptors. *Chembiochem: a European journal of chemical biology* **2023**, e202300659. DOI: 10.1002/cbic.202300659.

(56) Budzinski, J.; Maschauer, S.; Kobayashi, H.; Couvineau, P.; Vogt, H.; Gmeiner, P.; Roggenhofer, A.; Prante, O.; Bouvier, M.; Weikert, D. Bivalent ligands promote endosomal trafficking of the dopamine D3 receptor-neurotensin receptor 1 heterodimer. *Communications biology* **2021**, *4* (1), 1062. DOI: 10.1038/s42003-021-02574-4.

(57) Koschatzky, S.; Tschammer, N.; Gmeiner, P. Cross-receptor interactions between dopamine D2L and neurotensin NTS1 receptors modulate binding affinities of dopaminergics. *ACS chemical neuroscience* **2011**, *2* (6), 308–316. DOI: 10.1021/cn200020y.

(58) Vallone, D.; Picetti, R.; Borrelli, E. [Duplikat] Structure and function of dopamine receptors. *Neuroscience and biobehavioral reviews* **2000**, *24* (1), 125–132. DOI: 10.1016/s0149-7634(99)00063-9.

(59) Apodaca, R.; Dvorak, C. A.; Xiao, W.; Barbier, A. J.; Boggs, J. D.; Wilson, S. J.; Lovenberg, T. W.; Carruthers, N. I. A new class of diamine-based human histamine H3 receptor antagonists: 4-(aminoalkoxy)benzylamines. *Journal of medicinal chemistry* **2003**, *46* (18), 3938–3944. DOI: 10.1021/jm030185v.

(60) Diestler, D. J.; Knapp, E. W. Statistical thermodynamics of the stability of multivalent ligand-receptor complexes. *Physical review letters* **2008**, *100* (17), 178101. DOI: 10.1103/PhysRevLett.100.178101.

(61) Claveria-Gimeno, R.; Vega, S.; Abian, O.; Velazquez-Campoy, A. A look at ligand binding thermodynamics in drug discovery. *Expert opinion on drug discovery* **2017**, *12* (4), 363–377. DOI: 10.1080/17460441.2017.1297418.

(62) Pérez-Benito, L.; Henry, A.; Matsoukas, M.-T.; Lopez, L.; Pulido, D.; Royo, M.; Cordomí, A.; Tresadern, G.; Pardo, L. The size matters? A computational tool to design bivalent ligands. *Bioinformatics (Oxford, England)* **2018**, *34* (22), 3857–3863. DOI: 10.1093/bioinformatics/bty422.

(63) Sunahara, R. K.; Guan, H. C.; O'Dowd, B. F.; Seeman, P.; Laurier, L. G.; Ng, G.; George, S. R.; Torchia, J.; van Tol, H. H.; Niznik, H. B. Cloning of the gene for a human dopamine D5 receptor with higher affinity for dopamine than D1. *Nature* **1991**, *350* (6319), 614–619. DOI: 10.1038/350614a0.

(64) Rosier, N.; Grätz, L.; Schihada, H.; Möller, J.; Işbilir, A.; Humphrys, L. J.; Nagl, M.; Seibel, U.; Lohse, M. J.; Pockes, S. A Versatile Sub-Nanomolar Fluorescent Ligand Enables NanoBRET Binding Studies and Single-Molecule Microscopy at the Histamine H3 Receptor. *Journal of medicinal chemistry* **2021**, *64* (15), 11695–11708. DOI: 10.1021/acs.jmedchem.1c01089.

(65) Hao, J.; Beck, J. P.; Schaus, J. M.; Krushinski, J. H.; Chen, Q.; Beadle, C. D.; Vidal, P.; Reinhard, M. R.; Dressman, B. A.; Massey, S. M.; Boulet, S. L.; Cohen, M. P.; Watson, B. M.; Tupper, D.; Gardinier, K. M.; Myers, J.; Johansson, A. M.; Richardson, J.; Richards, D. S.; Hembre, E. J.; Remick, D. M.; Coates, D. A.; Bhardwaj, R. M.; Diseroad, B. A.; Bender, D.; Stephenson, G.; Wolfangel, C. D.; Diaz, N.; Getman, B. G.; Wang, X.-S.; Heinz, B. A.; Cramer, J. W.; Zhou, X.; Maren, D. L.; Falcone, J. F.; Wright, R. A.; Mitchell, S. N.; Carter, G.; Yang, C. R.; Bruns, R. F.; Svensson, K. A. Synthesis and Pharmacological Characterization of 2-(2,6-Dichlorophenyl)-1-((1S,3R)-5-(3-hydroxy-3-methylbutyl)-3-(hydroxymethyl)-1-methyl-3,4-dihydroisoquinolin-2(1H)-yl)ethan-1-one (LY3154207), a Potent, Subtype Selective, and Orally Available Positive Allosteric Modulator of the Human Dopamine D1 Receptor. *Journal of medicinal chemistry* **2019**, *62* (19), 8711–8732. DOI: 10.1021/acs.jmedchem.9b01234.

(66) Draper-Joyce, C. J.; Verma, R. K.; Michino, M.; Shonberg, J.; Kopinathan, A.; Klein Herenbrink, C.; Scammells, P. J.; Capuano, B.; Abramyan, A. M.; Thal, D. M.; Javitch, J. A.; Christopoulos, A.; Shi, L.; Lane, J. R. The action of a negative allosteric modulator at the dopamine D2 receptor is dependent upon sodium ions. *Scientific reports* **2018**, *8* (1), 1208. DOI: 10.1038/s41598-018-19642-1.

(67) Roberts, D. J.; Lin, H.; Strange, P. G. Investigation of the mechanism of agonist and inverse agonist action at D2 dopamine receptors. *Biochemical pharmacology* **2004**, *67* (9), 1657–1665. DOI: 10.1016/j.bcp.2003.12.030.

(68) Newton, C. L.; Wood, M. D.; Strange, P. G. Examining the Effects of Sodium Ions on the Binding of Antagonists to Dopamine D2 and D3 Receptors. *PloS one* **2016**, *11* (7), e0158808. DOI: 10.1371/journal.pone.0158808.

(69) Packeu, A.; Backer, J.-P. de; van Liefde, I.; Vanderheyden, P. M. L.; Vauquelin, G. Antagonist-radioligand binding to D2L-receptors in intact cells. *Biochemical pharmacology* **2008**, *75* (11), 2192–2203. DOI: 10.1016/j.bcp.2008.03.001.

(70) Verheijen, I.; Tourlousse, D.; Vanderheyden, P. M. L.; Backer, J.-P. de; Vauquelin, G. Effect of saponin and filipin on antagonist binding to AT 1 receptors in intact cells. *Biochemical pharmacology* **2004**, *67* (8), 1601–1606. DOI: 10.1016/j.bcp.2004.01.004.

(71) Dong, C.; Liu, Z.; Wang, F. Radioligand saturation binding for quantitative analysis of ligand-receptor interactions. *Biophysics reports* **2015**, *1* (3), 148–155. DOI: 10.1007/s41048-016-0016-5.

(72) Uhlén, S.; Schiöth, H. B.; Jahnsen, J. A. A new, simple and robust radioligand binding method used to determine kinetic off-rate constants for unlabeled ligands. Application at α2A- and α2C-adrenoceptors. *European journal of pharmacology* **2016**, *788*, 113–121. DOI: 10.1016/j.ejphar.2016.06.021.

(73) Bock, A.; Bermudez, M. Allosteric coupling and biased agonism in G protein-coupled receptors. *The FEBS journal* **2021**, *288* (8), 2513–2528. DOI: 10.1111/febs.15783.

(74) Nicholson, D. A.; Sengupta, A.; Sung, H.-L.; Nesbitt, D. J. Amino Acid Stabilization of Nucleic Acid Secondary Structure: Kinetic Insights from Single-Molecule Studies. *The journal of physical chemistry. B* **2018**, *122* (43), 9869–9876. DOI: 10.1021/acs.jpcb.8b06872.

(75) Salazar, A.; Keusgen, M.; Hagen, J. von. Amino acids in the cultivation of mammalian cells. *Amino acids* **2016**, *48* (5), 1161–1171. DOI: 10.1007/s00726-016-2181-8.

(76) Neve, K. A. Regulation of dopamine D2 receptors by sodium and pH. *Molecular pharmacology* **1991**, *39* (4), 570–578.

(77) Katritch, V.; Fenalti, G.; Abola, E. E.; Roth, B. L.; Cherezov, V.; Stevens, R. C. Allosteric sodium in class A GPCR signaling. *Trends in biochemical sciences* **2014**, *39* (5), 233–244. DOI: 10.1016/j.tibs.2014.03.002.

(78) Wittmann, H.-J.; Seifert, R.; Strasser, A. Mathematical analysis of the sodium sensitivity of the human histamine H3 receptor. *In silico pharmacology* **2014**, *2* (1), 1. DOI: 10.1186/s40203-014-0001-y.

(79) Wittmann, H.-J.; Seifert, R.; Strasser, A. Sodium binding to hH3R and hH 4R--a molecular modeling study. *Journal of molecular modeling* **2014**, *20* (8), 2394. DOI: 10.1007/s00894-014-2394-2.

(80) Christian, C. A.; Herbert, A. G.; Holt, R. L.; Peng, K.; Sherwood, K. D.; Pangratz-Fuehrer, S.; Rudolph, U.; Huguenard, J. R. Endogenous positive allosteric modulation of GABA(A) receptors by diazepam binding inhibitor. *Neuron* **2013**, *78* (6), 1063–1074. DOI: 10.1016/j.neuron.2013.04.026.

(81) Ehlert, F. J. The relationship between muscarinic receptor occupancy and adenylate cyclase inhibition in the rabbit myocardium. *Molecular pharmacology* **1985**, *28* (5), 410–421.

(82) Goupil, E.; Laporte, S. A.; Hébert, T. E. A simple method to detect allostery in GPCR dimers. *Methods in cell biology* **2013**, *117*, 165–179. DOI: 10.1016/B978-0-12-408143-7.00009-8.

(83) Shpakov, A. *Allosteric Regulation of G-Protein-Coupled Receptors: From Diversity of Molecular Mechanisms to Multiple Allosteric Sites and Their Ligands*, 2023. DOI: 10.20944/preprints202302.0009.v1.

(84) Herrera-Zúñiga, L. D.; Moreno-Vargas, L. M.; Ballaud, L.; Correa-Basurto, J.; Prada-Gracia, D.; Pastré, D.; Curmi, P. A.; Arrang, J. M.; Maroun, R. C. Molecular dynamics of the histamine H3 membrane receptor reveals different mechanisms of GPCR signal transduction. *Scientific reports* **2020**, *10* (1), 16889. DOI: 10.1038/s41598-020-73483-5.

(85) Keller, M.; Tränkle, C.; She, X.; Pegoli, A.; Bernhardt, G.; Buschauer, A.; Read, R. W. M2 Subtype preferring dibenzodiazepinone-type muscarinic receptor ligands: Effect of chemical homo-dimerization on orthosteric (and allosteric?) binding. *Bioorganic & medicinal chemistry* **2015**, *23* (14), 3970–3990. DOI: 10.1016/j.bmc.2015.01.015.

(86) Jastrzebska, B.; Maeda, T.; Zhu, L.; Fotiadis, D.; Filipek, S.; Engel, A.; Stenkamp, R. E.; Palczewski, K. Functional characterization of rhodopsin monomers and dimers in detergents. *The Journal of biological chemistry* **2004**, *279* (52), 54663–54675. DOI: 10.1074/jbc.M408691200.

(87) Navarro, G.; Cordomí, A.; Brugarolas, M.; Moreno, E.; Aguinaga, D.; Pérez-Benito, L.; Ferre, S.; Cortés, A.; Casadó, V.; Mallol, J.; Canela, E. I.; Lluís, C.; Pardo, L.; McCormick, P. J.; Franco, R. Cross-communication between Gi and Gs in a G-protein-coupled receptor heterotetramer guided by a receptor C-terminal domain. *BMC biology* **2018**, *16* (1), 24. DOI: 10.1186/s12915-018-0491-x.

(88) Wan, Q.; Okashah, N.; Inoue, A.; Nehmé, R.; Carpenter, B.; Tate, C. G.; Lambert, N. A. Mini G protein probes for active G protein-coupled receptors (GPCRs) in live cells. *The Journal of biological chemistry* **2018**, *293* (19), 7466–7473. DOI: 10.1074/jbc.RA118.001975.

(89) Frederick, A. L.; Yano, H.; Trifilieff, P.; Vishwasrao, H. D.; Biezonski, D.; Mészáros, J.; Urizar, E.; Sibley, D. R.; Kellendonk, C.; Sonntag, K. C.; Graham, D. L.; Colbran, R. J.; Stanwood, G. D.; Javitch, J. A. Evidence against dopamine D1/D2 receptor heteromers. *Molecular psychiatry* **2015**, *20* (11), 1373–1385. DOI: 10.1038/mp.2014.166.

(90) Leurs, R.; Bakker, R. A.; Timmerman, H.; Esch, I. J. P. de. The histamine H3 receptor: from gene cloning to H3 receptor drugs. *Nature reviews. Drug discovery* **2005**, *4* (2), 107–120. DOI: 10.1038/nrd1631.

(91) Kamal, M.; Maurice, P.; Jockers, R. Expanding the Concept of G Protein-Coupled Receptor (GPCR) Dimer Asymmetry towards GPCR-Interacting Proteins. *Pharmaceuticals* **2011**, *4* (2), 273–284. DOI: 10.3390/ph4020273.

(92) Vischer, H. F.; Watts, A. O.; Nijmeijer, S.; Leurs, R. G protein-coupled receptors: walking hand-in-hand, talking hand-in-hand? *British journal of pharmacology* **2011**, *163* (2), 246–260. DOI: 10.1111/j.1476-5381.2011.01229.x.

(93) Mönnich, D.; Humphrys, L. J.; Höring, C.; Hoare, B. L.; Forster, L.; Pockes, S. Activation of Multiple G Protein Pathways to Characterize the Five Dopamine Receptor Subtypes Using Bioluminescence Technology. *ACS Pharmacol. Transl. Sci.* **2024.** DOI: 10.1021/acsptsci.3c00339.

(94) Hiller, C.; Kühhorn, J.; Gmeiner, P. Class A G-protein-coupled receptor (GPCR) dimers and bivalent ligands. *Journal of medicinal chemistry* **2013**, *56* (17), 6542–6559. DOI: 10.1021/jm4004335.

5. Development of a NanoBRET Binding Assay for All Five Dopamine Receptors

Note: Prior to the submission of this thesis, parts of this chapter of, except for minor changes, was published in collaborations with partners:

Nagl, M.; Mönnich, D.; Rosier, N.; Schihada, H.; Sirbu, A.; Konar, N.; Reyes-Resina, I.; Navarro, G.; Franco, R.; Kolb, P.; Annibale, P.; Pockes, S. Fluorescent Tools for the Imaging of Dopamine D2 -Like Receptors. *Chembiochem: a European journal of chemical biology*, **2023**, e202300659. DOI: 10.1002/cbic.202300659.

Rosier, N.; Mönnich, D.; Nagl, M.; Schihada, H.; Sirbu, A.; Konar, N.; Reyes-Resina, I.; Navarro, G.; Franco, R.; Kolb, P.; Annibale, P.; Pockes, S. Shedding Light on the D1 -Like Receptors: A Fluorescence-Based Toolbox for Visualization of the D1 and D5 Receptors. *Chembiochem: a European journal of chemical biology*, **2023**, e202300658. DOI: 10.1002/cbic.202300658.

Co-workers performed the following experimental work:

Dr. Niklas Rosier: Synthesis and analytical characterization of the fluorescent ligands NR395, NR396, NR435, NR436, NR437, and NR438 (not shown).

Dr. Martin Nagl: Synthesis and analytical characterization of the fluorescent ligands MN193, MN206, and MN212 (not shown).

Dr. Lukas Grätz: Generation of plasmids pcDNA3.1. $5HT_{3A}$-Nluc-D_{2l}R-myc-his and pcDNA3.1. $5HT_{3A}$-Nluc-D_3R-myc-his.

5.1. Introduction

Dopamine is known as one of the most important neurotransmitters of the mammalian brain, where it is involved in several activities, e.g. in cognition,[1] emotion,[2] and endocrine regulation.[3] Otherwise, dysregulation of the catecholamine plays diverse roles in pathogenesis and therapy for different diseases such as schizophrenia, Parkinson's disease, drug addiction and bipolar disorders.[4,5] Dopamine receptors belong to the class A group of G protein-coupled receptors (GPCRs), one of the most common transmembrane proteins in the mammalian genome.[6–8] They consist of seven transmembranes with an extracellular N-terminus and intracellular C-terminus, connected through three extracellular (ECL) and three intracellular loops (ICL).[9,10] Due to the different pharmacological processes dopamine receptors are mediated by five subtypes.[11,12] The D_1-like family comprises the dopamine D_1 receptor (D_1R) and dopamine D_5 receptor (D_5R), which activate the second messenger pathway by stimulating adenylyl cyclase, leading to cyclic adenosin monophospahte (cAMP) production. The dopamine D_2 receptor (D_2R), dopamine D_3 receptor (D_3R), and dopamine D_4 receptor (D_4R) form the D_2-like family and, in contrast, block the cAMP-initiated second messenger cascade.[8,13,14]

The discovery of potential ligands for the human dopamine receptors is still affordable and indicates new assay systems, either for characterization of affinity or receptor subtype selectivity.[15,16] That should be achieved by simple, robust, and fast test systems. The classical technique to measure binding affinities are radioligand binding assays due to their robustness and high sensitivity.[17,18] Otherwise, the increasing costs and safety issues[19,20] are notable disadvantages for the need to develop other methods. A common technique to overcome these drawbacks is the NanoBRET binding assay established by Stoddart et al., that has been adapted to several GPCRs[21–24] so far, with comparable affinities as in radioligand binding studies.[25–27]

To perform the NanoBRET assay, a genetically engineered luciferase (NanoLuc), derived from a natural luciferase in the deep sea shrimp, is fused to the N-terminus of the respective receptor as a BRET donor.[28] In the presence of a substrate, oxidation is catalyzed by the luciferase and the resulting bioluminescent signal is measurable as the emission of blue light (λ = 460 nm).[28] The corresponding BRET acceptor is generally a fluorescence ligand with an excitation spectrum that overlaps with the emission spectrum of the NanoLuc and binds to the tagged GPCR of interest.[28] A bioluminescence energy transfer is accomplished by the close distance (approximately ≤ 10 nM) of the BRET donor to the acceptor and the favorable orientation of the luciferase to the respective fluorophore. This set-up enables to monitor the binding of a ligand in real-time, with low non-specific binding and high sensitivity and the possibility for high-throughput screening.[22,29]

To address this, a NanoBRET-based assay for all five (human) dopamine receptors was developed by fusing the NanoLuc to the N-terminus of these receptors and the generation of stable cell lines by transfecting HEK293T wild-type cells with the respective plasmid DNA. For the D_1-like receptors (D_1R, D_5R), six fluorescent ligands NR395, NR396, NR435, NR436, NR437, and NR438 were used to perform saturation binding and competition binding experiments. Likewise, for the D_2-like receptors ($D_{2l}R$, D_3R, D_4R), three fluorescent ligands MN193, MN206, and MN212 were applied for the characterization.

A

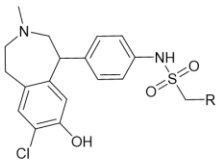

Compound	R
NR395 x TFA	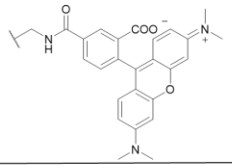
NR396 x 3 NH_3	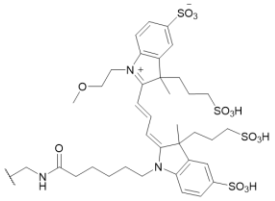
NR435 x 2 TFA	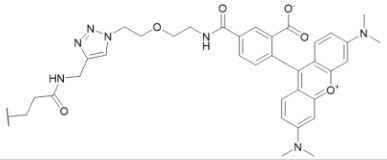
NR436 x 3 NH_3	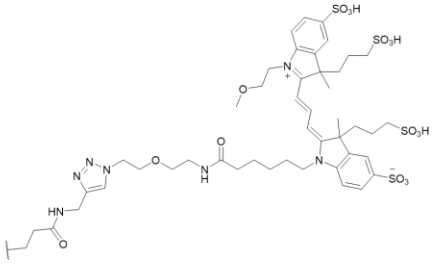
NR437 x 2 TFA	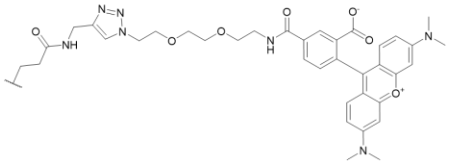
NR438 x 3 NH_3	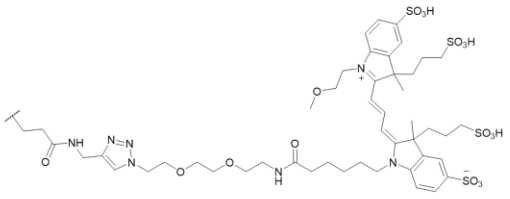

B

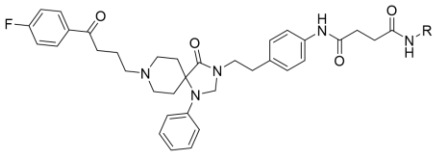

Compound	R
MN193 x 3 NH_3	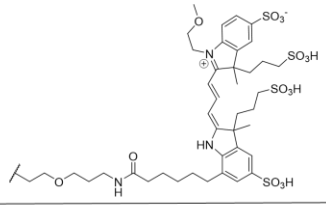
MN206 x TFA	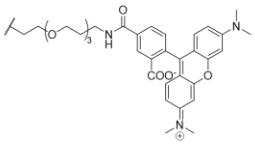
MN212 x TFA	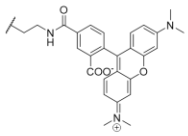

Figure 5.1: Structures of the investigated fluorescence ligands. **A:** Fluorescent ligands for the D_1-like receptors with a SCH-23390 analogue as pharmacophore linked with different alkyl or PEG linker to either a 5-Carboxytetramethylrhodamin (TAMRA) or DY-549P1 (Dyomics) fluorophore. **B:** Structures of fluorescent ligands for D_2-like receptors, consisting of a spiperone analogue as pharmacophore coupled through different PEG or alkyl linker to either a TAMRA or DY-549P1 (Dyomics) fluorescent dye.

5.2. Materials and Methods

5.2.1. Materials

Dulbecco's modified Eagle's medium high glucose (DMEM) and HEPES (1 M in distilled (d)H_2O, pH = 7.4, sterilised and stored at 4 °C) were from Sigma (Taufkirchen, Germany). Leibovitz's L-15 medium without phenol red (L-15) was from Gibco (Taufkirchen, Germany). Fetal calf serum (FCS), trypsin (0.05% trypsin, 0.02% EDTA in dH_2O) and geneticin (G418) were from Merck (Darmstadt, Germany). The NanoLuciferase substrate furimazine (Nano-Glo®) was from Promega (Walldorf, Germany). HEK293T cells (RRID:CVCL_0063) were a kind gift from Wulf Schneider (Institute for Medical Microbiology and Hygiene, Regensburg, Germany). The pcDNA3.1 vector was from Thermo Scientific (Nidderau, Germany). The cDNA of the dopamine receptors were purchased from the cDNA Resourse Center (Rolla, MO, USA). The restriction enzymes *Bam*HI and *Apa*I, were purchased from New England Biolabs (Frankfurt am Main, Germany).

Depending on their physicochemical properties, when possible, ligands were dissolved in dH_2O; otherwise DMSO (Merck) was used as a solvent. Dopamine dihydrochloride (dopa), (+)-butaclamol hydrochloride (buta), and pramipexole dihydrochloride (prami) were purchased from Sigma (Taufkirchen, Germany). Haloperidol (halo) was from TCI Deutschland GmbH (Eschborn, Germany). (-)-Quinpirole hydrochloride (quin), (*S*)-(-)-sulpiride (sulp), and spiperone hydrochloride (spip) were obtained from TOCRIS (Bristol, UK).

5.2.2. Molecular Cloning

The cDNA of the human dopamine receptors were purchased from the cDNA Resourse Center (Rolla, MO, USA). The plasmid encoding the NanoLuc (NLuc) was kindly provided by PROMEGA (Mannheim, Germany). The sequences of all five dopamine receptors and the luciferase sequence were amplified by standard PCR. Likewise the membrane signal peptide $5HT_{3A}$ was receptor upstream introduced by PCR. As described by Grätz et.al 2020[23] the respective dopamine receptor was cloned within a pcDNA3.1 vector backbone that encodes the NLuc N-terminally fused via a flexible glycine-serine-linker (-SGGGGS-) upstream of the inserted cDNA sequence with the restriction enzymes ApoI and BamHI. All plasmid DNA was quantified by UV-VIS absorbance using a NanoDrop spectrophotometer (ThermoFisher, Braunschweig, Germany) and sequences were verified by sequencing performed by Eurofins Genomics (Eurofins Genomics LLC, Ebersberg, Germany).

5.2.3. Cell Culture

HEK293T cells were cultured in DMEM supplemented with 10% FCS and 2 mM L-glutamine at 37 °C, 5% CO_2 in a H_2O saturated atmosphere. Cells were periodically inspected for mycoplasma contamination by Venor GeM Mycoplasma Detection Kit (Minerva Biolabs, Berlin, Germany).

5.2.4. Generation of Sable Cell Lines

HEK293T cells were seeded on a sterile 6 well dish at a cell density of 300,000 cells/ml in DMEM supplemented with 10% FCS and 2 mM L-glutamine. The next day, cells were transfected with 2 µg cDNA of pcDNA3.1.5HT_{3A}-NLuc-$D_{1,2l,3,5}$R-myc-his using the transfection reagent XtremeGene HP (Merk, Darmstadt, Germany) according to the supplier's protocol (1:3 cDNA (µg):XtremeGene (µl) ratio). After an incubation period of 48 h, cells were detached by using trypsin and seeded in a 175 cm^3 cell culture flask with 25 ml DMEM supplemented with 10% FCS, respectively. Cells were allowed to attach and thereafter treated with the antibiotic G418 (1,000 µg/ml) to achieve stable expression. The media was refreshed every three days, and G418 level was dropped to 600 µg/ml for continued selection pressure in later passages.

5.2.5. Radioligand Binding Experiment

To measure the receptor density for the stably expressed dopamine receptor cell lines and to ensure the NLuc tag has no impact on ligand binding, radioligand saturation binding assays were performed, as previously described, with minor changes.[30] The cell density was adjusted to 80,000 cells/well after counting in a "Neubauer" haemocytometer, followed by seeding 80 µl of the cell suspension in Leibovitz's L-15 media in each well of a 96-well plate (clear, u-bottom 96-well plate, Greiner Bio-One, Kremsmünster, Austria). The radioligand for D_1-like receptors was [^{3}H]SCH-23390 (81 Ci/mmol, Novandi Chemistry AB, Södertälje, Sweden; K_d = 0.2 nM D_1R/ 0.3 nM D_5R)[30,31] and [^{3}H]*N*-methyl-spiperone (77 Ci/mmol, Novandi Chemistry AB, Södertälje, Sweden; K_d = 0.014 nM D_2R/ 0.026 nM D_3R)[30] was used for D_2-like receptors, both with increasing concentrations in the range of approximately 1/10 K_d -10 K_d. Total binding was determined in the absence of any competitor and non-specific binding was measured by incubating the cell suspension in the presence of radioligand and (+)-butaclamol in a 2,000-fold excess with a total volume of 100 µl per well. Incubation periods of 1 h for D_2-like receptors or 1.5 h for D_1-like receptors were terminated by separating bound and free radioligand with an automated cell harvester (Brandel, Gaithersburg, USA) utilising rapid filtration through Whatman GF/C filters precoated with 0.3% polyethylenimine. Filters were transferred to flexible 96-well sample plates (Perkin Elmer, Rodgau, Germany) and incubated with scintillation cocktail for at least 5 h before

radioactivity was measured using a MicroBeta^2 1450 scintillation counter (Perkin Elmer, Rodgau, Germany). Data were analyzed using Prism 9 (GraphPad, La Jolla, CA, USA) and, after subtracting non-specific binding, K_i values were determined from IC_{50} values according to the Cheng-Prusoff-equation.[32]

5.2.6. NanoBRET Assay

NanoBRET saturation binding experiments were performed as described previously by Grätz et al. 2020 and Rosier et al. 2021[23,33] at 37° C using either a Tecan Infinite® Lumi plate reader (Tecan Trading AG, Switzerland,) or a CLARIOStar^{Plus} plate reader (BMG LABTECH, Ortenberg, Germany) and furimazine as a substrate (Promega, Mannheim, Germandy). HEK293T cells stably expressing Nluc-$D_{1,2l,3,5}R$ were seeded at a density of 1.25 x 10^6 cells/ml in Leibovitz's L-15 media supplemented with 10 mM HEPES and 5% FCS 16 h before the experiments in a white 96-well plate (BRANDplates® cellGrade 781965, VWR) and incubated at 37 °C overnight in a humidified atmosphere. The dilution of the substrate (furimazine, 1:5,000 final), the serial dilutions of the respective fluorescent ligands and competitors were prepared in Leibovitz's L-15 media supplemented with 10 mM HEPES and 1% bovines serum albumin (BSA) prior to the experiment and in 10-fold more concentrated than the final assay concentration. The concentration range in saturation binding experiment was chosen in the range of 0.1 K_d – 10 K_d of the respective fluorescent ligand. After the addition of 10 µl of the substrate and pre-diluted non-specific binding dilutions (in 1,000-fold excess to the respective fluorescent concentration: D_1-like: (+)-butaclamol; D_2-like: haloperidol) cells were incubated for 5 min, followed by the addition of 10 µl of the respective fluorescent ligand dilutions for saturation binding experiments. The luminescence was read for 20 cycles at 1 s integration time (CLARIOStar^{plus}: 2 s integration time) for both 'Blue' (< 470nm) and 'Red' (> 610nM) filter wavelengths. For competition binding experiments 10 µl of the respective competitor and 10 µl of the respective fluorescent ligand for the D_2-like receptors MN193 (c = 15 nM), MN206 (c = 15 nM) and MN212 (c = 3 nM) was added to the cells. A positive control (100% value) containing only the fluorescent ligand and a negative control with buffer (0% value) were always included in every experiment. The BRET ratio for each timepoint was calculated by dividing the 'Red' filtered light emission by the 'Blue' filtered light emission.

5.3. Results and Discussion

5.3.1. Investigation of Binding Affinities of D_1-like Fluorescent Ligands

To investigate the binding affinities of the six D_1-like fluorescent ligands NR395, NR396, NR435, NR436, NR437, and NR438 NanoBRET saturation binding experiments were performed at whole HEK293T cells stably expressing the D_1R, where the NanoLuc was fused N-terminally to the respective receptor. For all fluorescent ligand concentration dilutions, the Leibovitz's L-15 media was supplemented with 1% BSA to prevent non-specific binding at plate material or plastic vessels. For non-specific binding serial dilutions of (+)-butaclamol was used in 1,000-fold excess to the respective fluorescent ligand concentration.

The first set of fluorescent ligands consists of ligands containing a short alkyl linker with three C-atoms connecting the SCH-23390 analogue as pharmacophore with the fluorophore of either TAMRA (NR395) or DY-549P1 (NR396). In the case of NR435-438, the identical D_1R pharmacophore was coupled to the same two fluorescent dyes through a PEG-linker with different linker lengths (Figure 5.1, A). The TAMRA consisting fluorescent ligands were NR435 and 437, while NR436 and NR438 were coupled to the DY-549P1 dye.

The two fluorescent ligands NR395 and NR396 obtained no BRET signal, although the bioluminescence of the NanoLuc was measurable (λ = 480 nM) and the D_1R expression was verified by radioligand saturation binding experiments (Appendix, Figure 7.41 and 7.42). To investigate the binding characteristics of NR395 and NR396, further radioligand competition binding experiments on whole stable HEK293T-NLuc-D_1R cells were performed. Both fluorescence ligands showed bell-shaped curves in the presence of the specific D_1R radioligand [^{3}H]SCH-23390 (c = 0.5 nM) indicating a possible homodimerization of the D_1R, which was further investigated (Figure 5.2).[34]

A D_1R homodimerization was previously described in literature,[35,36] and was proved by Casado-Anguera et al. 2019 in competition binding experiments at sheep brain striatum membranes using two different concentration of the D_1R specific radioligand [^{3}H]SCH-23390.[34] The observed bell-shaped curves caused by homodimerization for the D_1R, were transformed to biphasic curves by the increase of the respective radioligand concentration.[34] For the data analysis in this study the one-site fit (monophasic curve) was compared with the two-site fit (biphasic curve) due a F-test and the calculated p-value was always indicated under the respective figure or table caption. A two-site fit was considered with a calculated p-value < 0.001 and rejection of the null-hypothesis.

Interestingly, the bell-shaped curves turned into monophasic curves by increasing the radioligand concentration and the calculated pK_i values differ between both experimental set-ups, except for

NR396 (Table 5.1). Therefore, the hypothesize of homodimerization of the D_1R was not confirmed. Additionally, radioligand competition binding experiments with the fluorescent ligands on HEK293T D_1R-CRELuc2P wildtype cells[37] were performed in the presence of both radioligand concentrations (c([^{3}H]SCH-23390)= 0.4 nM or 0.8 nM), to evaluate the impact of the NanoLuc-tag of the D_1R receptor to the binding affinity of NR395 and NR396. In both cases monophasic curves were observed, but with loss of affinity. This leads to the assumption, that the NanoLuc tag fused to the N-terminus revealed a negative impact on the binding properties of the florescent ligands and therefore, no BRET signal could be observed. The calculated pK_i values of both fluorescent ligands (NR395: 5.84 ± 0.31; NR396: 7.29 ± 0.41) were right-shifted after labelling with the fluorescent dyes TAMRA or DY-549P1 compared to the expected pK_i value for the used pharmacophore of SCH-23390 (with minor changes) and deviate by more than one order of magnitude (8.84 ± 0.07)[30]. In previously described studies, the introduction of labels can be associated with disadvantages for the binding affinities of the respective ligand.[38]

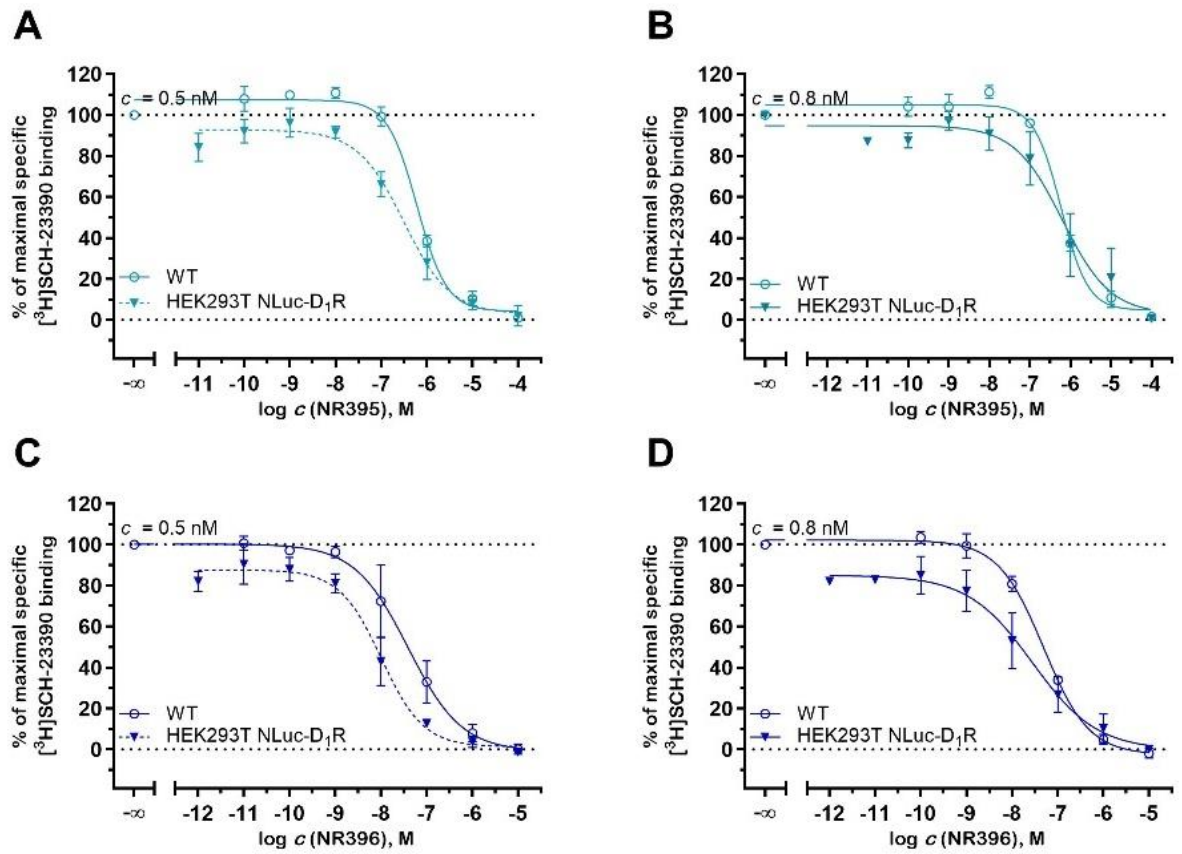

Figure 5.2: Radioligand competition binding experiment of **A:** NR395 in the presence 0.5 nM [^{3}H]SCH-23390 (turquoise)† or **B:** 0.8 nM [^{3}H]SCH-23390 (turquoise)† and **C:** NR396 in the presence 0.5 nM [^{3}H]SCH-23390 (dark blue)† or **D:** 0.8 nM [^{3}H]SCH-23390 (dark blue)† on whole HEK293T D_1R-CREluc2P cells and HEK293T NLuc-D_1R cells. To determine non-specific binding (+)-butaclamol was used in 1,000-fold excess. Data are shown as means ± SEM from two to four independent experiments, each performed in triplicate. †$p > 0.05$

Table 5.1: Calculated pK_i values of fluorescent ligands NR395 and NR396 in radioligand competition binding experiments in the presence of either 0.5 nM or 0.8 nM [^{3}H]SCH-23390 performed on HEK293T D_1R-CREluc2P cells and HEK293T Nluc-D_1R cells Data are shown as means ± SEM from two to four independent experiments, each performed in triplicate.

	HEK293T Nluc-D_1R		HEK393T D_1R-CREluc2P	
Cpd.	pK_i ± SEM	*N*	pK_i ± SEM	*N*
c ([^{3}H]SCH-23390) = 0.5 nM				
NR395	7.01 ± 0.31	4	5.84 ± 0.31	2
NR396	8.19 ± 0.35	4	7.93 ± 0.23	2
c ([^{3}H]SCH-23390) = 0.8 nM				
NR395	6.25 ± 0.34	4	6.70 ± 0.001	2
NR396	8.19 ± 0.31	3	7.29 ± 0.41	2

Furthermore, we suggest, the chosen linker length or linker polarity was insufficient either to bring the fluorophore of the fluorescent ligand in close proximity to the NanoLuc or in a favorable orientation to get a measurable BRET signal. To overcome this, four more fluorescent ligands were synthesized, with the same pharmacophore and fluorescent dyes, but different linker lengths and properties, to investigate the impact on pharmacological and physicochemical properties.[39]

By increasing the linker length and exchanging the alkyl linker trough a PEG linker in the second set of fluorescent ligands the BRET signal gained a saturation for NR435 (TAMRA dye) with low non-specific binding and an obtained pK_d value of 8.41 ± 0.11. Otherwise, for NR436 (DY-549P1 linked), no BRET signal revealed in a saturable manner (Figure 5.3, A and B). For both fluorescent ligands NR437 and NR348 a saturation binding curve was observed, but the affinities were up to 13-fold lower (NR437: pK_d = 7.73 and NR438: pK_d = 7.33) compared to NR436 (Figure 5.3, C and D).

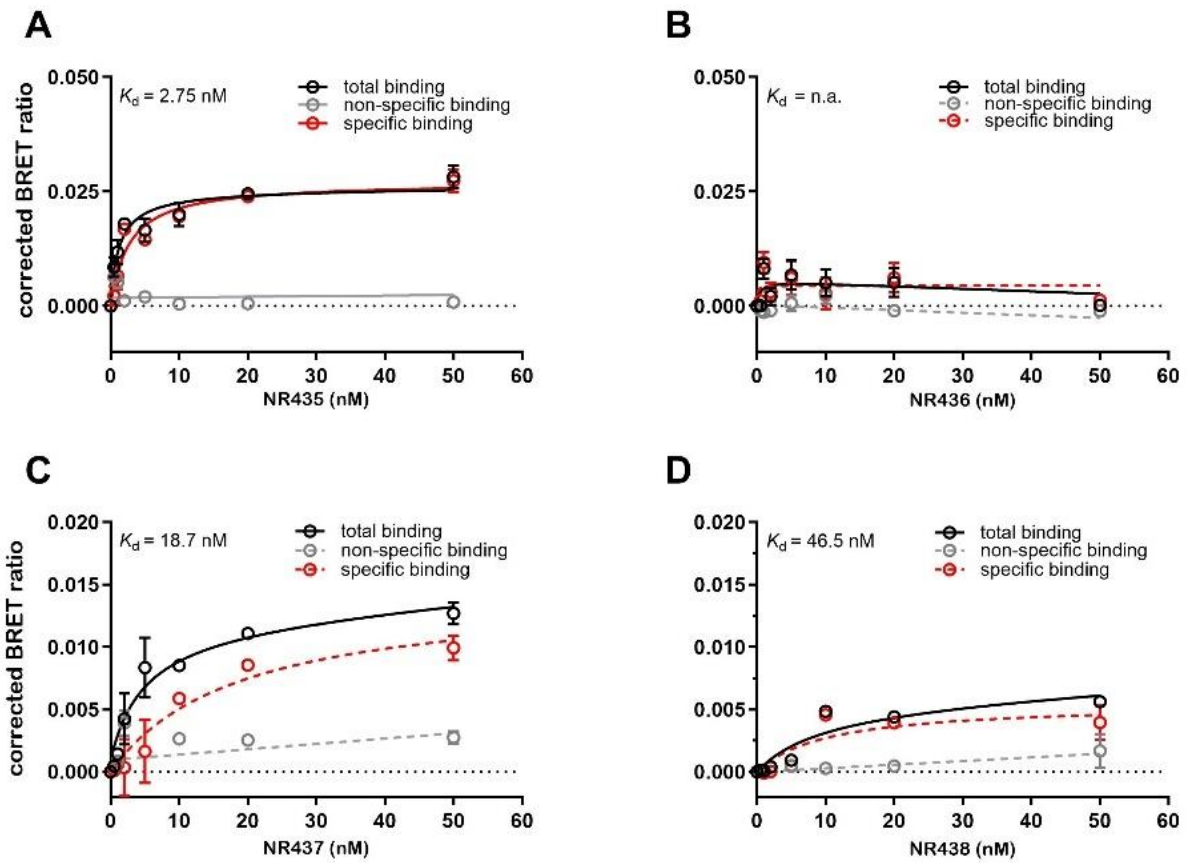

Figure 5.3: Representative NanoBRET saturation binding curves on HEK293T cells stably expressing Nluc-D_1R for NR435 (**A**), NR436 (**B**), NR437 (**C**), and NR438 (**D**). To determine non-specific binding (+)-butaclamol was used in 1,000-fold excess to the corresponding fluorescent concentration. Data represent means ± SEM from one to two independent experiments, each performed in triplicate.

Table 5.2: Binding affinities (pK_d values) of fluorescent ligands NR435, NR436, NR437 and NR438 on HEK293T Nluc-D_1R cells. Data represent means ± SEM from one to two independent experiments, each performed in triplicate.

Cpd.	pK_d	*N*
NR435	8.41 ± 0.11	2
NR436	n.a.	1
NR437	7.73	1
NR438	7.33	1

n.a. not applicable.

The impact of the linker length and change of the fluorophore to the binding affinity of a fluorescent ligand was previously described in literature[40,41], whereas in this project the shortest PEG linker coupled with the TAMRA dye achieved the highest affinity to the (human) D_1R. Besides, the fluorescent ligands with the DY-549P1 fluorophore showed less affinity and a worse signal-to-noise ratio than those consisting of the TAMRA dye. Please note, all latter experiments were

performed once and need to be verified and completed to *N* of 3 and the observed signal-to-noise ratio in all NanoBRET saturation binding experiments is improvable. This was due to a change in device (from Tecan Infinite® Lumi plate reader to CLARIOStar^{Plus} plate reader) and the limitation in time not achievable during this PhD project. We were not able to reproduce any result at the CLARIOStar^{Plus} under the same conditions. We suggest that due to a device specific signal-to-noise ratio the emission of the fluorescent ligand was not detectable anymore with the CLAIOStar^{Plus}, although we were able to detect the blue light emission of the NanoLuc (λ = 480 nM). It is known that, there is no direct correlation between the receptor expression and the observed BRET signal.[42] The optimal amount of NanoLuc-tagged receptor can be verified by transiently performed experiments.

5.3.2. Investigation of Binding Affinities of D_2-like Fluorescent Ligands

To investigate the $D_{2l}R$ and D_3R binding affinities of the three TAMRA-labeled D_2-like fluorescent ligands MN193, MN206, and MN212, NanoBRET saturation binding experiments were performed on whole HEK293T cells stably expressing the $D_{2l,3}R$, where the NanoLuc was N-terminally fused to the respective receptor. Please note, it was not possible to generate the plasmid for the NanoLuc-tagged D_4R and therefore, no results are shown for this D_2-like receptor. For all fluorescent ligand concentration dilutions, the Leibovitz's L-15 media was supplemented with 1% BSA to prevent non-specific binding at plate material or plastic vessels. For non-specific binding serial dilutions haloperidol was used in 1,000-fold excess to the respective fluorescent ligand concentration.

For both stable cell lines radioligand saturation binding experiments were performed, to verify that the NanoLuc-tag shows no impact of on the binding properties of the respective receptor (appendix, Figure 7.43 A and B). All obtained pK_d value a comparable with literature data[30] and confirmed that the N-terminally NanoLuc-tag had no influence either to the $D_{2l}R$ or D_3R characteristics (Appendix, Table 7.19).

All three fluorescent ligands consist of the same spiperone analogue as pharmacophore, coupled through different linker lengths to either a TAMRA- (MN206, MN212) or DY-549P1- dye (MN193) (Figure 5.1, B) and yielded in a saturation binding curve with pK_d values from nanomolar to sub-nanomolar range in the NanoBRET saturation binding assay (Figure 5.4, A - C). MN212 showed the highest affinity with a pK_d value of 9.32 ± 0.08, while the lowest was achieved by MN193 in the low nanomolar range (pK_d = 8.06 ± 0.03) (Table 5.3). The third fluorescent ligand MN206 obtained a pK_d value of 8.40 ± 0.08 (Table 5.3). The results were used to show the influence of the different linker lengths and properties or the different dyes, which have already been described in the literature.[40,41] In this project, the longest linker length in combination with the DY-549P1

dye achieved the lowest (MN193), while the shortest linker length in combination with the TAMRA dye led to the highest binding affinity in sub nanomolar range (MN212).

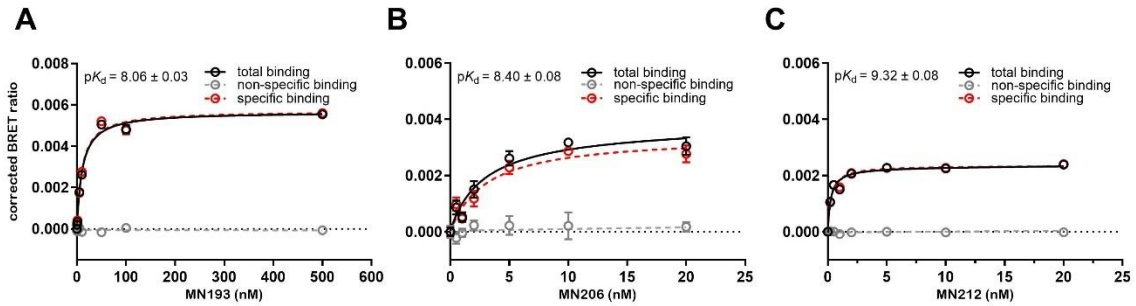

Figure 5.4: Representative NanoBRET saturation binding curves of the fluorescent ligands MN193 (**A**), MN206 (**B**), and MN212 (**C**) on whole HEK293T NLuc-D_{2l}R cells. Data of one representative experiment is shown from three to four independent experiments, each performed in triplicate.

Table 5.3: D_{2l}R binding affinities (pK_d values) of the fluorescent ligands MN193, MN206, and MN212 in NanoBRET saturation studies on HEK293T NLuc-D_{2l}R cells. Data are shown as means ± SEM from three to four independent experiments, each performed in triplicate.

Cpd.	pK_d± SEM	*N*
MN193	8.06 ± 0.03	3
MN206	8.40 ± 0.08	4
MN212	9.32 ± 0.08	4

With all three fluorescent ligands, competition binding experiments were performed in the presence of literature-described D_2-like standard ligands, whereas the concentrations of c = 15 nM (MN193), c = 15 nM (MN206), and c = 3 nM (MN212) were applied. As standard ligands (+)-butaclamol (buta), haloperidol (halo), pramipexole (prami), (+)-quinpirole (quin), spiperone (spip), and (*S*)-(-)-sulpiride (sulp) in six different concentrations diluted in Leibovitz's L-15 media supplemented with 1% BSA were used. Competition binding curves were normalized to the sample containing only fluorescent ligand (100% value) or buffer (0% value). All calculated pK_i values of the standard ligands were comparable, between all three used fluorescent ligands, except for the agonist quinpirole (quin). The pK_i values of this D_2-like standard ligand differ by more than one log unit between the fluorescent ligands MN193 (7.39 ± 0.29), MN206 (6.48 ± 0.34), and MN212 (6.07 ± 0.22) (Table 5.4). Besides, the pK_i values of several reference ligands were in good agreement with literature data.

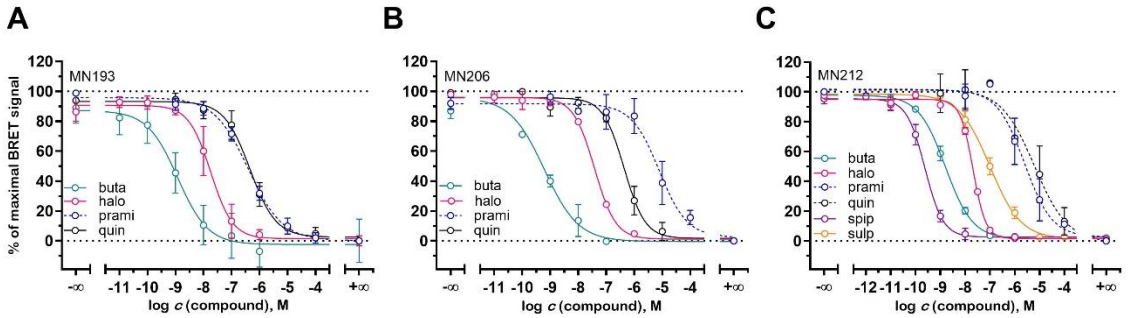

Figure 5.5: NanoBRET competition binding curves of various D_2-like standard ligands in the presence of the fluorescent ligands MN193 (**A**), MN206 (**B**), and MN212 (**C**) on whole HEK293T cells stably expressing NLuc-D_{2l}R. For both fluorescent ligands MN193 and MN206 a concentration of 15 nM was used and for MN212 a concentration of 3 nM. Dashed lines represent incomplete or flat curve fits. Data are shown as means ± SEM from two to five independent experiments, each performed in triplicate. Abbreviations used: buta = (+)-butaclamol, halo = haloperidol, prami = pramipexole, quin = (+)-quinpirole, spip = spiperone, and sulp = (*S*)-(-)-sulpiride.

Table 5.4: Calculated pK_i values of D_2-like standard ligands in the presence of either the fluorescent ligands MN193, MN206, or MN212 on stable HEK293T NLuc-D_{2l}R. Data are shown as means ± SEM from two to five independent experiments, each performed in triplicate.

	MN193		MN206		MN212		Ref.
Cpd.	pK_i ± SEM	*N*	pK_i ± SEM	*N*	pK_i ± SEM	*N*	
buta	9.33 ± 0.13	3	9.49 ± 0.23	3	9.72 ± 0.10	4	9.35[43,a]
halo	8.22 ± 0.26	4	8.15 ± 0.12	3	8.64 ± 0.08	4	8.54[44,b]
prami	6.89 ± 0.08	3	6.95 ± 0.48	2	6.52 ± 0.24	3	6.10[45,a]
quin	7.39 ± 0.29	3	6.48 ± 0.34	3	6.07 ± 0.22	2	6.04[46]
spip	n.d.	-	n.d.	-	10.6 ± 0.11	4	9.44[44,b]
sulp	n.d.	-	n.d.	-	7.87 ± 0.19	5	6.87[47,c]

n.d. = not determined.[a] CHO-D_2 cells. [b] CHO-D_{2S} cells. [c] [^{35}S]GTPγS binding to membranes of CHO-D_2 cells. Abbreviations used: buta = (+)-butaclamol, halo = haloperidol, prami = pramipexole hydrochloride, quin = (+)-quinpirole, spip = spiperone, and sulp = (*S*)-(-) sulpiride.

Due to the high homology of the D_{2L}R and D_3R, the fluorescent ligand MN212 with the highest affinity for the D_{2L}R was characterized on stable HEK293T NLuc-D_3R cells (Figure 5.6, A).[48] MN212 showed a three-fold lower affinity to the D_3R with a pK_d value of 8.54 ± 0.05 compared to the D_{2l}R (Table 5.5). The signal-to-noise ratio was comparable with the experiments performed on the stable HEK293T Nluc-D_{2l}R cells, although it was in both cases improvable.

Table 5.5: D_3 receptor binding affinity (pK_d-value) of fluorescent ligand MN212 on HEK293T NLuc-D_3R cells. Data are shown as means ± SEM from four independent experiments, each performed in triplicate.

Cpd.	pK_d± SEM	*N*
MN212	8.54 ± 0.05	4

Additionally, NanoBRET competition binding experiments were performed with literature described D_2-like standard ligands dopamine (dopa), pramipexole (prami), (+)-quinpirole (quin), and spiperone (spip) in the presence of 3 nM of the fluorescent ligand on stable HEK293T NLuc-D_3R cells (Figure 5.6, B). The yielded pK_i values of the three D_3R agonists pramipexole (6.39 ± 0.05) and quinpirole (6.42 ± 0.07) were more than one order of magnitude lower compared to literature data, while the pK_i value of the agonist dopamine (6.06 ± 0.16) and the antagonist spiperone (9.65 ± 0.03) were comparable with the references (Table 5.6).

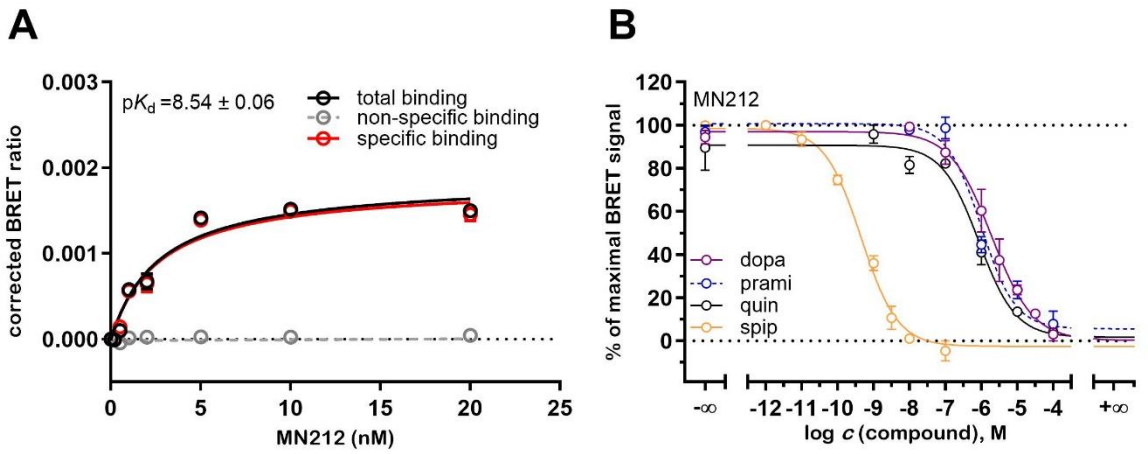

Figure 5.6: A: Representative NanoBRET saturation binding curve of MN212 and **B**: competition binding curves of four standard ligands in the presence of 3 nM of MN212 on stable HEK293T NLuc-D_3R cells. Data of one representative saturation binding experiment are shown from four independent experiments, each performed in triplicate. Data of competition binding experiments are shown as means ± SEM from two to four independent experiments, each performed in triplicate. Dashed lines represent incomplete or flat curve fits in competition binding experiments. Abbreviations used: Dopa = dopamine, prami = pramipexole, quin = (+)-quinpirole, and spip = spiperone.

Table 5.6: Binding affinity of D_2-like standard ligands in the presence of MN212 on stable HEK293T NLuc-D_3R. Data are shown as means ± SEM from two to four independent experiments, each performed in triplicate.

Cpd.	pK_i ± SEM	*N*	Reference
dopa	6.06 ± 0.16	4	6.27[43]
prami	6.39 ± 0.05	3	7.98[49]
quin	6.42 ± 0.07	2	7.39[49]
spip	9.65 ± 0.03	3	9.49[1]

Abbreviations used: Dopa = dopamine, prami = pramipexole, quin = (+)-quinpirole, and spip = spiperone.

Please note, due to the change of the device (from Tecan Infinite® Lumi plate reader to CLARIOStar^{Plus} plate reader) no kinetic studies, like association and dissociation experiments, were performed for the fluorescent ligands MN193, MN206, and MN212 on stable HEK293T Nluc-

$D_{2l,3}R$ cells. To find the optimal amount of the respective receptor to generate a high BRET signal transient experiments with different amounts of plasmid DNA of pcDNA3.1$_{neo}$ $5HT_{3A}$-Nluc-$D_{2l}R$-myc need to be performed.

5.4. Conclusion

In this study, the aim was to develop a NanoBRET-based binding assay for all five (human) dopamine receptors. Therefore, the NanoLuc was fused to the N-terminus of these receptors and generating stable cell lines by transfecting HEK293T wild-type cells with the respective plasmid DNA.[20] For the D_1-like receptors (D_1R, D_5R) two sets of fluorescent ligands NR395, NR396, and NR435–NR438 were characterized with saturation binding experiments. For the D_2-like receptors ($D_{2l}R$, D_3R, D_4R) three fluorescent ligands MN193, MN206, and MN212 were used for the characterization by saturation binding experiments and competition binding assays.

The first set of D_1-like fluorescent ligands NR395 and NR396 consist of an antagonistic SCH-23390 analogue as pharmacophore, which was coupled to either a TAMRA or DY-549P1 fluorescent dye, through an alkyl linker. Both saturation binding curves revealed in no saturable manner on stable HEK293T NLuc-D_1R cells, although the expression of the receptor was proven by radioligand binding experiments. Further comparison with radioligand competition binding studies on either wild-type HEK293T D_1R-CREluc2P or HEK293T NLuc-D_1R cells with two different radioligand concentrations (c = 0.4 nM and 0.8 nM) showed an increase in binding affinity on the tagged receptor of these two fluorescent ligands NR395 and NR396, compared to the wild-type receptor. Furthermore, a previously suggested homodimerization of the D_1R was not confirmed, but an impact of the NanoLuc-tag on the biding affinities of the fluorescent ligands.[38,40] Furthermore, we hypothesize, the chosen linker length or linker properties were insufficient, either to bring the fluorophore of the fluorescent ligand in close proximity to the NanoLuc or in a favorable orientation to get a measurable BRET-signal.

The second set of fluorescent ligands NR435, NR436, NR437, and NR438 consist of the identical D_1R pharmacophore tethered to either a TAMRA or a DY-549P1 fluorophore, but the nature of the linker was changed to more hydrophilic PEG linkers with different lengths. Thus, the NanoBRET saturation binding curve revealed in a saturable manner for NR435, leading to the highest affinity, where the D_1R pharmacophore was coupled to the TAMRA fluorophore. Besides, NR436 consisted of the same pharmacophore and linker length, but a different fluorescent dye (DY-549P1), resulting in no measurable BRET signal. Moreover, the same was observed for NR437 and NR438 with the identical composition (either SCH-23390 in combination with TAMRA or DY-549P1), but longer PEG linkers, compared to NR435 and NR436. Additionally, fluorescent ligand NR437 achieved a higher affinity (pK_d = 7.73) than the DY-549P1 linked NR438 (pK_d = 7.73). However, in this study the insertion of the DY-549P1 fluorophore led to a negative impact of the binding affinity to the respective receptor, as well as the increase of the linker length.

Due to a change of the device (from Tecan Infinite® Lumi plate reader to CLARIOStar^{Plus} plate reader), unfortunately, these results were not repeated and further investigated. Only the blue–light emission (λ = 480) was measurable, but not the red-light emission (λ = 610), perhaps due to the detection limit of the CLARIOStar^{Plus} compared to the Tecan Infinite® Lumi plate reader. For the same reason, no kinetic studies, like association and dissociation experiments, could be performed.

The three fluorescent ligands for the D_2-like receptors MN193, MN206, and MN212 were characterized on stable HEK293T NLuc-D_{2l}R cells and additionally, MN212 as well on HEK293T cells stably expressing the NanoLuc-tagged D_3R. All fluorescent ligands composed of the identical spiperone analogue as a pharmacophore coupled through different linker lengths of PEG- or alkyl linkers to either the TAMRA or DY-549P1 fluorescent dye. The fluorescent ligand MN212 consist of the shortest alkyl linker in combination with the TAMRA dye, while for MN193 the DY-549P1 fluorophore was used. The fluorescent ligand MN206 consists of the spiperone analogue coupled trough a PEG linker to a TAMRA dye.

At the D_{2l}R, MN212 achieved the highest binding affinity in sub nanomolar range, while MN193 and MN206 achieved values in the low nanomolar range. In this set of fluorescent ligands, the linker length, linker properties, and the chosen fluorophore implemented an impact to the binding affinity of the respective receptor. [40] As for the D_1R fluorescent ligands the shortest linker, without PEG units achieved the highest affinity (MN212), while the longest linker length in combination with the TAMRA dye achieved the lowest (MN193) binding affinity at the D_{2l}R. Due to the high homology of the D_{2l}R and D_3R,[48] NanoBRET saturation binding experiments were obtained at the NanoLuc-tagged D_3R. The fluorescent ligand MN212 showed a three-fold lower affinity to the D_3R compared to the D_{2l}R. Moreover, with all fluorescent ligands of the D_2-like family NanoBRET competition binding experiments at the D_2R and with MN212 at the D_3R were performed, with literature-described standard ligands like (+)-butaclamol, haloperidol, pramipexole, (+)-quinpirole, spiperone, and (*S*)-(-)-sulpiride. Several obtained pK_i values were comparable with literature data. It was not possible to generate the corresponding NanoLuc plasmid and thus the stable cell line for the D_4R within the scope of this work. Due to the change of the device (from Tecan Infinite® Lumi plate reader to CLARIOStar^{Plus} plate reader) no kinetic studies, like association and dissociation experiments, were performed.

5.5. References

(1) Vallone, D.; Picetti, R.; Borrelli, E. Structure and function of dopamine receptors. *Neuroscience and biobehavioral reviews* **2000**, *24* (1), 125–132. DOI: 10.1016/s0149-7634(99)00063-9.

(2) Missale, C.; Nash, S. R.; Robinson, S. W.; Jaber, M.; Caron, M. G. Dopamine receptors: from structure to function. *Physiological reviews* **1998**, *78* (1), 189–225. DOI: 10.1152/physrev.1998.78.1.189.

(3) Zhang, J.; Xiong, B.; Zhen, X.; Zhang, A. Dopamine D1 receptor ligands: where are we now and where are we going. *Medicinal research reviews* **2009**, *29* (2), 272–294. DOI: 10.1002/med.20130.

(4) Di Chiara, G. Drug addiction as dopamine-dependent associative learning disorder. *European journal of pharmacology* **1999**, *375* (1-3), 13–30. DOI: 10.1016/S0014-2999(99)00372-6.

(5) Di Chiara, G.; Bassareo, V.; Fenu, S.; Luca, M. A. de; Spina, L.; Cadoni, C.; Acquas, E.; Carboni, E.; Valentini, V.; Lecca, D. Dopamine and drug addiction: the nucleus accumbens shell connection. *Neuropharmacology* **2004**, *47 Suppl 1*, 227–241. DOI: 10.1016/j.neuropharm.2004.06.032.

(6) Dal Prà, I.; Armato, U.; Chiarini, A. Family C G-Protein-Coupled Receptors in Alzheimer's Disease and Therapeutic Implications. *Frontiers in pharmacology* **2019**, *10*, 1282. DOI: 10.3389/fphar.2019.01282.

(7) Wan, Q.; Okashah, N.; Inoue, A.; Nehmé, R.; Carpenter, B.; Tate, C. G.; Lambert, N. A. Mini G protein probes for active G protein-coupled receptors (GPCRs) in live cells. *The Journal of biological chemistry* **2018**, *293* (19), 7466–7473. DOI: 10.1074/jbc.RA118.001975.

(8) Fredriksson, R.; Lagerström, M. C.; Lundin, L.-G.; Schiöth, H. B. The G-protein-coupled receptors in the human genome form five main families. Phylogenetic analysis, paralogon groups, and fingerprints. *Molecular pharmacology* **2003**, *63* (6), 1256–1272. DOI: 10.1124/mol.63.6.1256.

(9) Rosenbaum, D. M.; Rasmussen, S. G. F.; Kobilka, B. K. The structure and function of G-protein-coupled receptors. *Nature* **2009**, *459* (7245), 356–363. DOI: 10.1038/nature08144.

(10) Hilger, D.; Kumar, K. K.; Hu, H.; Pedersen, M. F.; O'Brien, E. S.; Giehm, L.; Jennings, C.; Eskici, G.; Inoue, A.; Lerch, M.; Mathiesen, J. M.; Skiniotis, G.; Kobilka, B. K. Structural insights into differences in G protein activation by family A and family B GPCRs. *Science (New York, N.Y.)* **2020**, *369* (6503). DOI: 10.1126/science.aba3373.

(11) Fan, L.; Tan, L.; Chen, Z.; Qi, J.; Nie, F.; Luo, Z.; Cheng, J.; Wang, S. Haloperidol bound D2 dopamine receptor structure inspired the discovery of subtype selective ligands. *Nature communications* **2020**, *11* (1), 1074. DOI: 10.1038/s41467-020-14884-y.

(12) Jackson, D. M.; Westlind-Danielsson, A. Dopamine receptors: molecular biology, biochemistry and behavioural aspects. *Pharmacology & therapeutics* **1994**, *64* (2), 291–370. DOI: 10.1016/0163-7258(94)90041-8.

(13) Wang, Q.; Jolly, J. P.; Surmeier, J. D.; Mullah, B. M.; Lidow, M. S.; Bergson, C. M.; Robishaw, J. D. Differential dependence of the D1 and D5 dopamine receptors on the G protein gamma 7 subunit for activation of adenylylcyclase. *The Journal of biological chemistry* **2001**, *276* (42), 39386–39393. DOI: 10.1074/jbc.M104981200.

(14) Kebabian, J. W. Multiple classes of dopamine receptors in mammalian central nervous system: the involvement of dopamine-sensitive adenylyl cyclase. *Life sciences* **1978**, *23* (5), 479–483. DOI: 10.1016/0024-3205(78)90157-1.

(15) Zhuang, Y.; Xu, P.; Mao, C.; Wang, L.; Krumm, B.; Zhou, X. E.; Huang, S.; Liu, H.; Cheng, X.; Huang, X.-P.; Shen, D.-D.; Xu, T.; Liu, Y.-F.; Wang, Y.; Guo, J.; Jiang, Y.; Jiang, H.; Melcher, K.; Roth, B. L.; Zhang, Y.; Zhang, C.; Xu, H. E. Structural insights into the human D1 and D2 dopamine receptor signaling complexes. *Cell* **2021**, *184* (4), 931-942.e18. DOI: 10.1016/j.cell.2021.01.027.

(16) Di Martino, R. M. C.; Cavalli, A.; Bottegoni, G. Dopamine D3 receptor ligands: a patent review (2014-2020). *Expert opinion on therapeutic patents* **2022**, *32* (6), 605–627. DOI: 10.1080/13543776.2022.2049240.

(17) Finney, D. J. Radioligand Assay. *Biometrics* **1976**, *32* (4), 721. DOI: 10.2307/2529258.

(18) Maguire, J. J.; Kuc, R. E.; Davenport, A. P. Radioligand binding assays and their analysis. *Methods in molecular biology (Clifton, N.J.)* **2012**, *897*, 31–77. DOI: 10.1007/978-1-61779-909-9_3.

(19) Stoddart, L. A.; White, C. W.; Nguyen, K.; Hill, S. J.; Pfleger, K. D. G. Fluorescence- and bioluminescence-based approaches to study GPCR ligand binding. *British journal of pharmacology* **2016**, *173* (20), 3028–3037. DOI: 10.1111/bph.13316.

(20) Stoddart, L. A.; Kilpatrick, L. E.; Briddon, S. J.; Hill, S. J. Probing the pharmacology of G protein-coupled receptors with fluorescent ligands. *Neuropharmacology* **2015**, *98*, 48–57. DOI: 10.1016/j.neuropharm.2015.04.033.

(21) Stoddart, L. A.; Vernall, A. J.; Bouzo-Lorenzo, M.; Bosma, R.; Kooistra, A. J.; Graaf, C. de; Vischer, H. F.; Leurs, R.; Briddon, S. J.; Kellam, B.; Hill, S. J. Development of novel fluorescent histamine H1-receptor antagonists to study ligand-binding kinetics in living cells. *Scientific reports* **2018**, *8* (1), 1572. DOI: 10.1038/s41598-018-19714-2.

(22) Sakyiamah, M. M.; Nomura, W.; Kobayakawa, T.; Tamamura, H. Development of a NanoBRET-Based Sensitive Screening Method for CXCR4 Ligands. *Bioconjugate chemistry* **2019**, *30* (5), 1442–1450. DOI: 10.1021/acs.bioconjchem.9b00182.

(23) Grätz, L.; Tropmann, K.; Bresinsky, M.; Müller, C.; Bernhardt, G.; Pockes, S. NanoBRET binding assay for histamine H2 receptor ligands using live recombinant HEK293T cells. *Scientific reports* **2020**, *10* (1), 13288. DOI: 10.1038/s41598-020-70332-3.

(24) Christiansen, E.; Hudson, B. D.; Hansen, A. H.; Milligan, G.; Ulven, T. Development and Characterization of a Potent Free Fatty Acid Receptor 1 (FFA1) Fluorescent Tracer. *Journal of medicinal chemistry* **2016**, *59* (10), 4849–4858. DOI: 10.1021/acs.jmedchem.6b00202.

(25) Leyris, J.-P.; Roux, T.; Trinquet, E.; Verdié, P.; Fehrentz, J.-A.; Oueslati, N.; Douzon, S.; Bourrier, E.; Lamarque, L.; Gagne, D.; Galleyrand, J.-C.; M'kadmi, C.; Martinez, J.; Mary, S.; Banères, J.-L.; Marie, J. Homogeneous time-resolved fluorescence-based assay to screen for ligands targeting the growth hormone secretagogue receptor type 1a. *Analytical biochemistry* **2011**, *408* (2), 253–262. DOI: 10.1016/j.ab.2010.09.030.

(26) Nederpelt, I.; Georgi, V.; Schiele, F.; Nowak-Reppel, K.; Fernández-Montalván, A. E.; IJzerman, A. P.; Heitman, L. H. Characterization of 12 GnRH peptide agonists - a kinetic perspective. *British journal of pharmacology* **2016**, *173* (1), 128–141. DOI: 10.1111/bph.13342.

(27) Soave, M.; Stoddart, L. A.; Brown, A.; Woolard, J.; Hill, S. J. Use of a new proximity assay (NanoBRET) to investigate the ligand-binding characteristics of three fluorescent ligands to the human β1-adrenoceptor expressed in HEK-293 cells. *Pharmacology research & perspectives* **2016**, *4* (5), e00250. DOI: 10.1002/prp2.250.

(28) Hall, M. P.; Unch, J.; Binkowski, B. F.; Valley, M. P.; Butler, B. L.; Wood, M. G.; Otto, P.; Zimmerman, K.; Vidugiris, G.; Machleidt, T.; Robers, M. B.; Benink, H. A.; Eggers, C. T.; Slater, M. R.; Meisenheimer, P. L.; Klaubert, D. H.; Fan, F.; Encell, L. P.; Wood, K. V. Engineered luciferase reporter from a deep sea shrimp utilizing a novel imidazopyrazinone substrate. *ACS chemical biology* **2012**, *7* (11), 1848–1857. DOI: 10.1021/cb3002478.

(29) Cottet-Rousselle, C.; Ronot, X.; Leverve, X.; Mayol, J.-F. Cytometric assessment of mitochondria using fluorescent probes. *Cytometry. Part A : the journal of the International Society for Analytical Cytology* **2011**, *79* (6), 405–425. DOI: 10.1002/cyto.a.21061.

(30) Forster, L.; Grätz, L.; Mönnich, D.; Bernhardt, G.; Pockes, S. A Split Luciferase Complementation Assay for the Quantification of β-Arrestin2 Recruitment to Dopamine D2-Like Receptors. *International journal of molecular sciences* **2020**, *21* (17). DOI: 10.3390/ijms21176103.

(31) Bourne, J. A. SCH 23390: the first selective dopamine D1-like receptor antagonist. *CNS drug reviews* **2001**, *7* (4), 399–414. DOI: 10.1111/j.1527-3458.2001.tb00207.x.

(32) Cheng, Y.; Prusoff, W. H. Relationship between the inhibition constant (K1) and the concentration of inhibitor which causes 50 per cent inhibition (I50) of an enzymatic reaction. *Biochemical pharmacology* **1973**, *22* (23), 3099–3108. DOI: 10.1016/0006-2952(73)90196-2.

(33) Rosier, N.; Grätz, L.; Schihada, H.; Möller, J.; Işbilir, A.; Humphrys, L. J.; Nagl, M.; Seibel, U.; Lohse, M. J.; Pockes, S. A Versatile Sub-Nanomolar Fluorescent Ligand Enables NanoBRET Binding Studies and Single-Molecule Microscopy at the Histamine H3 Receptor. *Journal of medicinal chemistry* **2021**, *64* (15), 11695–11708. DOI: 10.1021/acs.jmedchem.1c01089.

(34) Casadó-Anguera, V.; Moreno, E.; Mallol, J.; Ferré, S.; Canela, E. I.; Cortés, A.; Casadó, V. Reinterpreting anomalous competitive binding experiments within G protein-coupled receptor homodimers using a dimer receptor model. *Pharmacological research* **2019**, *139*, 337–347. DOI: 10.1016/j.phrs.2018.11.032.

(35) Kong, M. M. C.; Fan, T.; Varghese, G.; O'Dowd, B. F.; George, S. R. Agonist-induced cell surface trafficking of an intracellularly sequestered D1 dopamine receptor homo-oligomer. *Molecular pharmacology* **2006**, *70* (1), 78–89. DOI: 10.1124/mol.105.021246.

(36) O'Dowd, B. F.; Ji, X.; Alijaniaram, M.; Rajaram, R. D.; Kong, M. M. C.; Rashid, A.; Nguyen, T.; George, S. R. Dopamine receptor oligomerization visualized in living cells. *The Journal of biological chemistry* **2005**, *280* (44), 37225–37235. DOI: 10.1074/jbc.M504562200.

(37) Tropmann, K.; Bresinsky, M.; Forster, L.; Mönnich, D.; Buschauer, A.; Wittmann, H.-J.; Hübner, H.; Gmeiner, P.; Pockes, S.; Strasser, A. Abolishing Dopamine D2long/D3 Receptor Affinity of Subtype-Selective Carbamoylguanidine-Type Histamine H2 Receptor Agonists. *Journal of medicinal chemistry* **2021**, *64* (12), 8684–8709. DOI: 10.1021/acs.jmedchem.1c00692.

(38) Yin, L.; Wang, W.; Wang, S.; Zhang, F.; Zhang, S.; Tao, N. How does fluorescent labeling affect the binding kinetics of proteins with intact cells? *Biosensors & bioelectronics* **2015**, *66*, 412–416. DOI: 10.1016/j.bios.2014.11.036.

(39) Vernall, A. J.; Stoddart, L. A.; Briddon, S. J.; Ng, H. W.; Laughton, C. A.; Doughty, S. W.; Hill, S. J.; Kellam, B. Conversion of a non-selective adenosine receptor antagonist into A3-selective high affinity fluorescent probes using peptide-based linkers. *Organic & biomolecular chemistry* **2013**, *11* (34), 5673–5682. DOI: 10.1039/C3OB41221K.

(40) Liu, T.; Nedrow-Byers, J. R.; Hopkins, M. R.; Berkman, C. E. Spacer length effects on in vitro imaging and surface accessibility of fluorescent inhibitors of prostate specific membrane antigen. *Bioorganic & medicinal chemistry letters* **2011**, *21* (23), 7013–7016. DOI: 10.1016/j.bmcl.2011.09.115.

(41) Middleton, R. J.; Kellam, B. Fluorophore-tagged GPCR ligands. *Current opinion in chemical biology* **2005**, *9* (5), 517–525. DOI: 10.1016/j.cbpa.2005.08.016.

(42) Grätz, L.; Müller, C.; Pegoli, A.; Schindler, L.; Bernhardt, G.; Littmann, T. Insertion of Nanoluc into the Extracellular Loops as a Complementary Method To Establish BRET-Based Binding Assays for GPCRs. *ACS pharmacology & translational science* **2022**, *5* (11), 1142–1155. DOI: 10.1021/acsptsci.2c00162.

(43) Freedman, S. B.; Patel, S.; Marwood, R.; Emms, F.; Seabrook, G. R.; Knowles, M. R.; McAllister, G. Expression and pharmacological characterization of the human D3 dopamine receptor. *The Journal of pharmacology and experimental therapeutics* **1994**, *268* (1), 417–426.

(44) Hall, D. A.; Strange, P. G. Evidence that antipsychotic drugs are inverse agonists at D2 dopamine receptors. *British journal of pharmacology* **1997**, *121* (4), 731–736. DOI: 10.1038/sj.bjp.0701196.

(45) Sautel, F.; Griffon, N.; Lévesque, D.; Pilon, C.; Schwartz, J. C.; Sokoloff, P. A functional test identifies dopamine agonists selective for D3 versus D2 receptors. *Neuroreport* **1995**, *6* (2), 329–332. DOI: 10.1097/00001756-199501000-00026.

(46) Millan, M. J.; Peglion, J. L.; Vian, J.; Rivet, J. M.; Brocco, M.; Gobert, A.; Newman-Tancredi, A.; Dacquet, C.; Bervoets, K.; Girardon, S. Functional correlates of dopamine D3 receptor activation in the rat in vivo and their modulation by the selective antagonist, (+)-S 14297: 1. Activation of postsynaptic D3 receptors mediates hypothermia, whereas blockade of D2 receptors elicits prolactin secretion and catalepsy. *The Journal of pharmacology and experimental therapeutics* **1995**, *275* (2), 885–898.

(47) Roberts, D. J.; Strange, P. G. Mechanisms of inverse agonist action at D2 dopamine receptors. *British journal of pharmacology* **2005**, *145* (1), 34–42. DOI: 10.1038/sj.bjp.0706073.

(48) Sokoloff, P.; Giros, B.; Martres, M. P.; Bouthenet, M. L.; Schwartz, J. C. Molecular cloning and characterization of a novel dopamine receptor (D3) as a target for neuroleptics. *Nature* **1990**, *347* (6289), 146–151. DOI: 10.1038/347146a0.

(49) Millan, M. J.; Maiofiss, L.; Cussac, D.; Audinot, V.; Boutin, J.-A.; Newman-Tancredi, A. Differential actions of antiparkinson agents at multiple classes of monoaminergic receptor. I. A multivariate analysis of the binding profiles of 14 drugs at 21 native and cloned human receptor subtypes. *The Journal of pharmacology and experimental therapeutics* **2002**, *303* (2), 791–804. DOI: 10.1124/jpet.102.039867.

6. Summary

6.1. Summary and Outlook

In the last decades various test systems were established to characterize pharmacological tools like radioligands and fluorescent ligands, as well as, evaluating binding affinities and selectivity of novel ligands. Furthermore, they are capable to investigate receptor monomers and heteromers and their functional properties.

In this thesis three different bioluminescent test systems comprising the spilt NanoLuc-based miniG recruitment method,[3] the further downstream CAMYEN BRET-based biosensor and a G-case sensor derived from the TRUPATH system[4] were applied to the five (human) dopamine receptors. Therefore, in case of the miniG recruitment assay the small bit of the split NanoLuc was fused to the C-terminus of the respective (human) dopamine receptor, while the large bit was introduced N-terminally to the canonical miniG protein. For the CAMYEN BRET assay the whole NanoLuc was cloned to the C-terminus of an Epac cAMP binding domain, and mCitrine to the N-terminus. In case of the G-case sensor the whole NanoLuc is cloned into the G_{α} subunit of a G protein trimer, and the cpVenus protein is fused to the N-terminus of the corresponding G_{γ} subunit. With the combination of these different techniques the five (human) dopamine receptors were characterized with respect to ligand induced efficacy, different G protein recruitment with involving bias signaling and comparison of close-receptor-signaling or further downstream signal trafficking. Those techniques enable to investigate a pharmacological profile of the dopamine receptor family and the characterization of G protein coupling, ligand efficacies and potencies, as well as the differentiation between agonist, antagonists and inverse agonists.

Moreover, a radioligand as a useful tool for radioligand binding experiments for the H_3R was characterized by overcoming drawbacks, of agonistic ligands such as receptor internalization in cell-based systems or selectivity issues within the histamine receptor family.[1,2] The chosen pharmacophore was a propionylated JNJ-5207852 scaffold, which was tritium labeled. In radioligand saturation binding experiments the radioligand revealed curves in a saturable manner with a binding affinity in the sub nanomolar range and obtained a high H_3R selectivity compared to the other members of the histamine receptor family. In kinetic studies the fast association and complete dissociation was verified. Furthermore, in competition binding experiments in the presence of the radioligand [^{3}H]UR-MN259 several H_3R standard agonists and antagonist were tested and the resulted pK_i values were comparable with literature data. Therefore, a selective and high affinity radioligand for the H_3R was developed and characterized as a novel tool for the investigation of new ligands in robust radioligand binding studies.

The investigation of the pharmacological properties of heterodimers of the class A family is necessary due to their involvement in e.g., neurodegenerative diseases like Parkinson's disease or

Alzheimer's disease. Furthermore, to address these drug targets novel bivalent ligands were synthesized in-house and needed to be evaluated in their binding affinities, efficacies and confirmed as true bivalent ligands. Therefore, a radioligand binding assay was developed for the reported D_1R-H_3R and $D_{2l}R$-H_3R heteromers. [5,6]

For the D_1R-H_3R the suggested stoichiometric receptor ratio *in vitro* of 1:2, leading to functional heterodimers,[5] was obtained and biphasic curves for the bivalent ligand NR330 were achieved. The resulting $pK_{i,high}$ value was not higher as at the monomer receptor. Further experiments with the bivalent ligand NR330 in the presence of an additional competitor were performed, in order to test whether the biphasic curve can be transformed to a monophasic curve by blocking one protomer of the D_1-H_3R heteromer. For the H_3R mode the D_1R antagonist SCH-23390 (c = 10 µM) and in the D_1R mode the antagonistic H_3R ligand JNJ-5207852 (c =10 µM) were used. The resulting monophasic curve of NR330 in the presence of either the D_1R or H_3R competitor was right shifted compared to the curve on the mono-expressed receptor and showed an additional decrease in the specific binding of both radioligands (D_1R protomer: [^{3}H]SCH-23390, H_3R protomer: [^{3}H]UR-MN259). We hypothesized a cross binding affinity of the D_1R competitor to the H_3R protomer and vice versa. Thus, the respective ligands were investigated on the respective D_1R and H_3R mono-expressing cell lines. The bivalent ligand NR330 resulted a monophasic curve in all three chosen buffers (sodium-free or sodium-containing) at the D_1R monomer, as expected, but different binding affinities which were negatively affected in the presence of sodium. At the H_3R monomer the expected monovalent curve was observed in sodium-free BB and BB supplemented with 100 mM NaCl. In contrast, in both buffers containing 140 mM NaCl (Leibovitz's L15 media and BB with 140 mM NaCl) no statistically correct binding mode was validated and both modes (monophasic and biphasic curves) were specified. With respect to the amount of the specific binding of the radioligand [^{3}H]SCH-23390 the observed plateau of NR330 at the H_3R was different compared to the resulted one of NR330 on D_1R-H_3R co-expressing HEK239T cells. Therefore, we assume a true bivalent binding mode of NR330 on D_1R-H_3R co-expressing HEK239T cells with a stoichiometric receptor ratio of 1:2.

The antagonistic H_3R ligands JNJ-5207852 and MN259 showed no binding affinity to the D_1R monomer, although a negative cooperativity was observed in combination with the D_1R standard antagonist SCH-23390. In case of the H_3R monomer the affinity of the D_1R antagonist SCH-23390 was dependent on the used buffers. In sodium containing buffer supplemented 140 mM NaCl, the binding affinity was in micromolar range, while in BB supplemented with 100 mM NaCl, the affinity was increased to the nanomolar range. In contrast, in BB without supplements a biphasic curve for SCH-23390 was observed. The observed two binding modes in sodium-free buffer were thus changed to a monovalent binding mode in sodium containing buffer, which implies a sodium-

dependent effect. Furthermore, the combination of the H_3R ligands JNJ-5207852 or MN259 with 10 µM SCH-23390 led to right-shifted curves and a drop in signal of the specific binding of the radioligand [^{3}H]UR-MN259 in all buffers. Therefore, we hypothesized a possible allosteric modulation of SCH-23390 to the H_3R ligands. Unfortunately, we could not confirm this hypothesis completely and further investigations are necessary.

For the $D_{2l}R$-H_3R heteromer a radioligand binding assay was likewise developed. The observed curves of the bivalent ligands MN079 and MN240 were primarily monophasic in different receptor ratios (1:1, 1:2.4 and 1:3.7), while MN240 achieved a biphasic curve only in the $D_{2l}R$-mode on co-expressing cells with a stoichiometric receptor ratio of 1:1.8. The assumed receptor ratio for the formation of functional heteromers of the class A GPCRs is 1:2 *in vitro*, which could not be achieved during this PhD.

However, to characterize the efficacies of bivalent ligands a functional miniG protein recruitment assay was applied to the $D_{2l}R$-H_3R heteromer. The small bit of the split Nano luciferase was fused to the C-terminus of the H_3R, whereas the large bit was cloned between the $D_{2l}R$ and the $miniG_{si}$ protein, tethered through flexible linkers. The recruitment of the $miniG_{si}$ could be observed in real-time after the activation by histamine and gave hints to the existence of the formation of the $D_{2l}R$-H_3R heteromer, compared to the observed traces on the H_3R monomer. All analyzed H_3R standard ligands gave robust concentration-response-curves, while in contrast no activation for the D_2-like agonist dopamine and pramipexole was achieved. Moreover, we were able to observe a possible cross-interaction between the $D_{2l}R$-H_3R heteromer. The affinity of histamine in the presence of 100 µM dopamine was right-shifted to nanomolar range and a drop in the signal was observed compared to histamine without additional competitor. A further possible explanation is the asymmetric recruitment of the $miniG_{si}$ protein by one protomer, due to an excess limitation. Thus, further experiments are necessary to confirm the negative cooperativity by introducing a point mutation in the G protein binding pocket of the $D_{2l}R^7$ and changing of the linker length to the miniG protein to evaluate a possible impact, as well as, the fusion of the small bit to the $D_{2l}R$ and the NLucN-$miniG_{si}$ construct to the H_3R.

In summary, it was not possible to develop a radioligand binding assay for both heteromers to characterize the respective novel bivalent ligands with sufficient replicates. However, the results are promising to confirm the ligands as true bivalent ligands, but further investigations are necessary. Thus, for competition binding experiments with an additional competitor the competitors should be changed to (+)-butaclamol in the H_3R mode and to GSK33449 in case of the D_1R mode to obtain monophasic curves of the bivalent ligand and to obtain monophasic curves without a decreased signal-to-noise ratio on co-expressing cells. Additionally, the end-capped ligands as further controls, should be included. For all following studies on the D_1R-H_3R

heteromer, the buffer needs to be changed to a sodium-containing buffer, like Leibovitz's L-15 media, to alleviate the sodium impact on the binding affinities and properties. Therefore, all previously obtained experiments with the bivalent ligand with or without an additional competitor need to be performed in this buffer. For the $D_{2l}R$-H_3R heteromer the correct stoichiometric receptor ratio i*n vitro* needs to be evaluated, followed by competition binding experiments in the presence of suitable competitors in both modes, for the complete characterization of the novel bivalent ligands.

The last project of this thesis was the development of a NanoBRET-based assay for the five (human) dopamine receptors to investigate the binding affinities of novel ligands with a reliable and robust test system like in radioligand binding experiments.[8] The NanoLuc as BRET donor was N-terminally fused to the respective (human) dopamine receptor where a fluorescent ligand can bind and the non-radioactive energy transfer takes place, referred as BRET. The investigated fluorescent ligands of either the D_1-like or D_2-like dopamine receptors consist of a selective pharmacophore (D_1-like: SCH-23390 analogue, D_2-like: spiperone analogue) connected through alkyl or PEG linker with the TAMRA or DY-549P1 dye.

For the D_1-like family the most promising fluorescent ligand NR435 consists of the SCH-23390 pharmacophore, a short linker and the TAMRA fluorophore and yielded an affinity in the nanomolar range. For the D_2-like family the fluorescent ligand MN212 with a spiperone analogue, the shortest linker and the TAMRA dye was characterized for the $D_{2l}R$ and obtained likewise the highest affinity. Due to the high homology between the D_2-like receptors MN212 was tested at the D_3R with an eight-fold lower affinity compared to the $D_{2l}R$. For both, competition binding experiments with different literature described D_2-like standard ligands were performed, with comparable pK_i values to published data. In this study, we could observe a negative modulation of the binding affinity by introducing the DY-549P1 dye to the fluorescent ligands. In previous work the respective linker length, properties like hydrophilic or lipophilic entities and the fluorophore are considered to affect the binding properties of the linker. [9,10]

Due to a change of the device (from Tecan Infinite® Lumi plate reader to CLARIOStar^{Plus} plate reader) all observed results were not reproducible at the CLARIOStar^{Plus} under the same conditions. We suggest, due to a device specific signal-to-noise ratio, that the emission of the fluorescent ligand was not detectable anymore with the CLAIOStar^{Plus}, although we were able to detect the blue light emission of the NanoLuc (λ = 480 nM). It is known that there is no direct correlation between the receptor expression and the observed BRET signal.[11] The optimal amount of NanoLuc-tagged receptor can be verified by transiently performed experiments. Due to the limitation in time kinetic studies, outstanding saturation or competition binding experiments for all dopamine receptor and the respective fluorescent ligands could not be performed.

6.2. References

(1) Esch, I. J. P. de; Thurmond, R. L.; Jongejan, A.; Leurs, R. The histamine H4 receptor as a new therapeutic target for inflammation. *Trends in pharmacological sciences* **2005**, *26* (9), 462–469. DOI: 10.1016/j.tips.2005.07.002.

(2) Osorio-Espinoza, A.; Escamilla-Sánchez, J.; Aquino-Jarquin, G.; Arias-Montaño, J.-A. Homologous desensitization of human histamine H_3 receptors expressed in CHO-K1 cells. *Neuropharmacology* **2014**, *77*, 387–397. DOI: 10.1016/j.neuropharm.2013.09.011.

(3) Wan, Q.; Okashah, N.; Inoue, A.; Nehmé, R.; Carpenter, B.; Tate, C. G.; Lambert, N. A. Mini G protein probes for active G protein-coupled receptors (GPCRs) in live cells. *The Journal of biological chemistry* **2018**, *293* (19), 7466–7473. DOI: 10.1074/jbc.RA118.001975.

(4) Olsen, R. H. J.; DiBerto, J. F.; English, J. G.; Glaudin, A. M.; Krumm, B. E.; Slocum, S. T.; Che, T.; Gavin, A. C.; McCorvy, J. D.; Roth, B. L.; Strachan, R. T. TRUPATH, an open-source biosensor platform for interrogating the GPCR transducerome. *Nature chemical biology* **2020**, *16* (8), 841–849. DOI: 10.1038/s41589-020-0535-8.

(5) Ferrada, C.; Moreno, E.; Casadó, V.; Bongers, G.; Cortés, A.; Mallol, J.; Canela, E. I.; Leurs, R.; Ferré, S.; Lluís, C.; Franco, R. Marked changes in signal transduction upon heteromerization of dopamine D1 and histamine H3 receptors. *British journal of pharmacology* **2009**, *157* (1), 64–75. DOI: 10.1111/j.1476-5381.2009.00152.x.

(6) Ferrada, C.; Ferré, S.; Casadó, V.; Cortés, A.; Justinova, Z.; Barnes, C.; Canela, E. I.; Goldberg, S. R.; Leurs, R.; Lluis, C.; Franco, R. Interactions between histamine H3 and dopamine D2 receptors and the implications for striatal function. *Neuropharmacology* **2008**, *55* (2), 190–197. DOI: 10.1016/j.neuropharm.2008.05.008.

(7) Hiller, C.; Kühhorn, J.; Gmeiner, P. Class A G-protein-coupled receptor (GPCR) dimers and bivalent ligands. *Journal of medicinal chemistry* **2013**, *56* (17), 6542–6559. DOI: 10.1021/jm4004335.

(8) Stoddart, L. A.; Kilpatrick, L. E.; Briddon, S. J.; Hill, S. J. Probing the pharmacology of G protein-coupled receptors with fluorescent ligands. *Neuropharmacology* **2015**, *98*, 48–57. DOI: 10.1016/j.neuropharm.2015.04.033.

(9) Liu, T.; Nedrow-Byers, J. R.; Hopkins, M. R.; Berkman, C. E. Spacer length effects on in vitro imaging and surface accessibility of fluorescent inhibitors of prostate specific membrane antigen. *Bioorganic & medicinal chemistry letters* **2011**, *21* (23), 7013–7016. DOI: 10.1016/j.bmcl.2011.09.115.

(10) Yin, L.; Wang, W.; Wang, S.; Zhang, F.; Zhang, S.; Tao, N. How does fluorescent labeling affect the binding kinetics of proteins with intact cells? *Biosensors & bioelectronics* **2015**, *66*, 412–416. DOI: 10.1016/j.bios.2014.11.036.

(11) Grätz, L.; Müller, C.; Pegoli, A.; Schindler, L.; Bernhardt, G.; Littmann, T. Insertion of Nanoluc into the Extracellular Loops as a Complementary Method To Establish BRET-Based Binding Assays for GPCRs. *ACS pharmacology & translational science* **2022**, *5* (11), 1142–1155. DOI: 10.1021/acsptsci.2c00162.

7. Appendix

7.1. Appendix Chapter 2

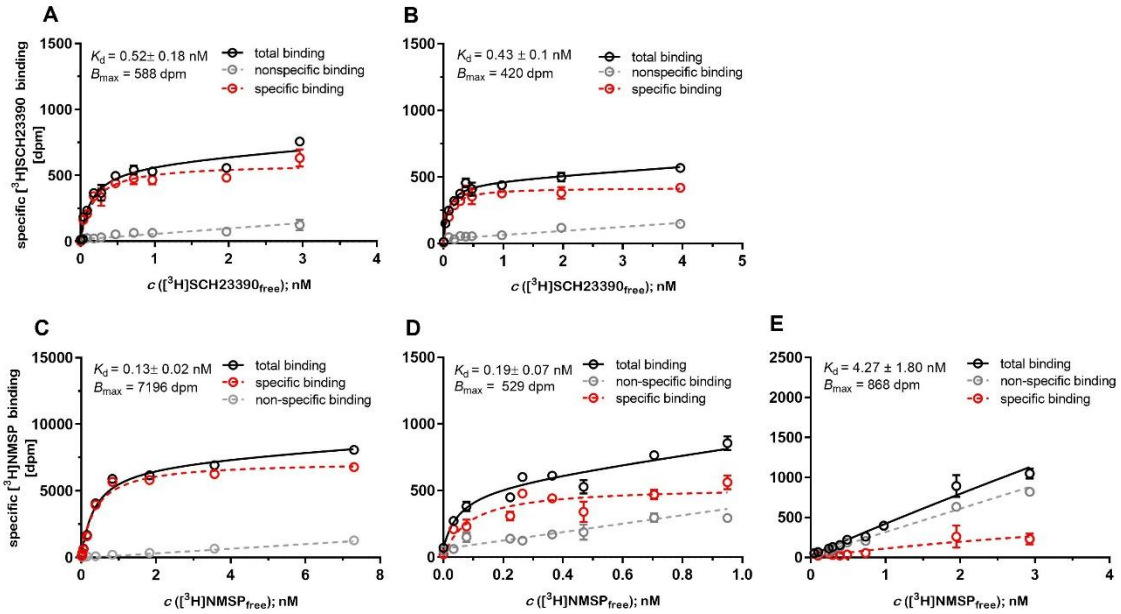

Figure 7.1: Radioligand saturation binding curves with whole HEK293T cells expressing NlucN-miniG$_x$_D$_y$R-NLucC. NLucN-miniG$_s$_D$_1$R-NlucC (**A**) or NLucN-miniG$_s$_D$_5$R-NlucC (**B**), NLucN-miniGs$_{i1}$_D$_{2l}$R-NlucC (**C**), NLucN-miniG$_o$_D$_3$R-NlucC (**D**) or NLucN-miniG$_o$_D$_4$R-NLucC (**E**) fusion proteins. Corresponding dissociation constants are provided in Table 7.1. [^{3}H]SCH-23390 (D$_1$-like receptors) and [^{3}H]NMSP (D$_2$-like receptors) were used as radioligands (concentrations of $1/K_d$ – 10 K_d). Non-specific binding was determined in the presence of (+)-butaclamol (D$_1$-like receptors), haloperidol (D$_{2l/3}$R) in 1,000-fold or, in the case of nemonapride (D$_4$R) 500-fold excess regarding the respective radioligand concentration. Saturation binding curves were fitted with a non-linear regression fit for one-site model. Graphs represent means ± SEM from one representative experiment performed in triplicate of five independent experiments (N = 3 for NLucN-miniG$_o$_D$_4$R-NLucC). K_d values are given as mean from five independent experiments (N = 3 for NLucN-miniG$_o$_D$_4$R-NLucC).

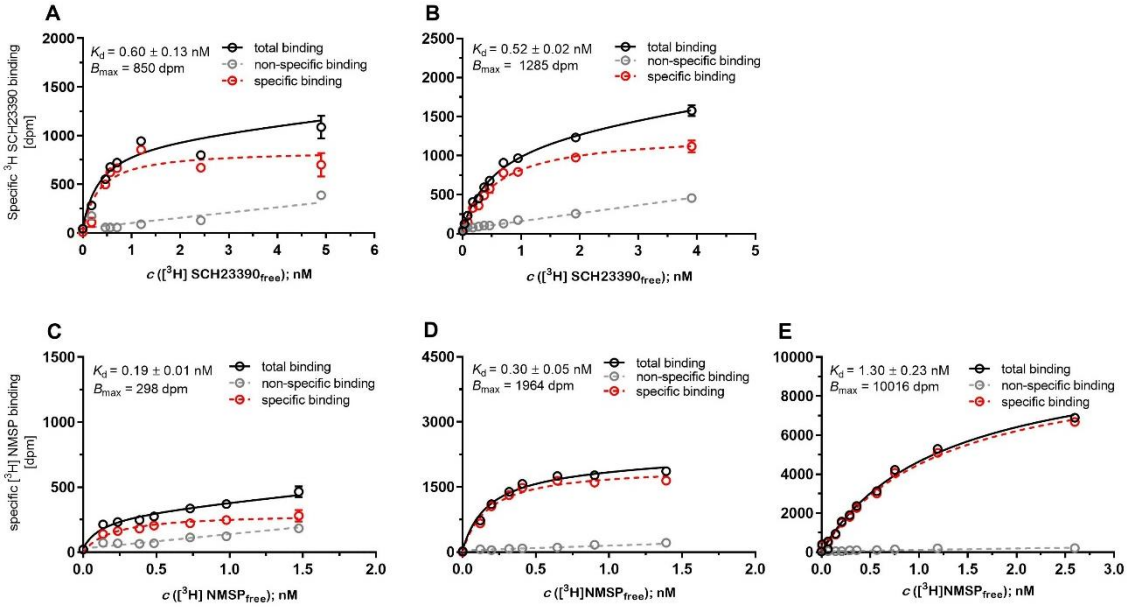

Figure 7.2: Radioligand saturation binding curves with whole HEK293T-CAMYEN_ D_xR cells. HEK-CAMYEN cells expressing D_1R (**A**), D_5R (**B**), $D_{2l}R$ (**C**), D_3R (**D**) or D_4R (**E**). Corresponding dissociation constants are provided in Table S1. [^{3}H]SCH23390 (D_1-like receptors) and [^{3}H]NMSP (D_2-like receptors) were used as radioligands (concentrations of $1/K_d$ – 10 K_d). Non-specific binding was determined in the presence of (+)-butaclamol (D_1-like receptors), haloperidol ($D_{2/3}R$) in 1000-fold or, in the case of nemonapride (D_4R), in 500-fold excess regarding the respective radioligand concentration. Saturation binding curves were fitted with a non-linear regression fit for one-site model. Graphs represent means ± SEM from one representative experiment performed in triplicate of five independent experiments. K_d values are given as mean from five independent experiments.

Table 7.1: Equilibrium dissociation constants (pK_d values) of radioligands [^{3}H]SCH-23390 (D_1-like) and [^{3}H]NMSP (D_2-like) and receptor densities (B_{max}) determined in radioligand saturation binding assays using HEK293T cells stably co-expressing NlucN-mini-G_x_D_yR-NlucC fusion proteins (except NlucN-mini-G_o_D_4R-NlucC, which was performed transiently) or the CAMYEN biosensor with the five dopamine receptors. Rec. = receptor number. Data are expressed as mean ± SEM of five independent experiments (N = 5) each performed in triplicate (N = 3 for NLucN-miniG$_o$_D_4R-NLucC).

D_xR	MiniG Protein Recruitment			CAMYEN cAMP			
	pK_d ± SEM	B_{max}	rec./cell	pK_d ± SEM	B_{max}	rec./cell	Ref. K_d / nM
D_1R	9.31 ± 0.13	2520	1.05 x 10^5	9.13 ± 0.16	3806	1.59 x 10^5	1.50[1]
$D_{2l}R$	9.85 ± 0.17	2808	1.24 x 10^5	9.64 ± 0.05	271	1.19 x 10^4	0.13[2]
D_3R	9.57 ± 0.21	3664	1.61 x 10^5	9.75 ± 0.06	2064	9.09 x 10^4	0.27[2]
D_4R	8.47 ± 0.21[a]	541	2.38 x 10^4	8.91 ± 0.31	12,007	5.29 x 10^5	0.29[3]
D_5R	9.54 ± 0.16	2042	8.54 x 10^4	9.24 ± 0.07	1699	7.10 x 10^4	0.58[4]

[a]performed under transient conditions.

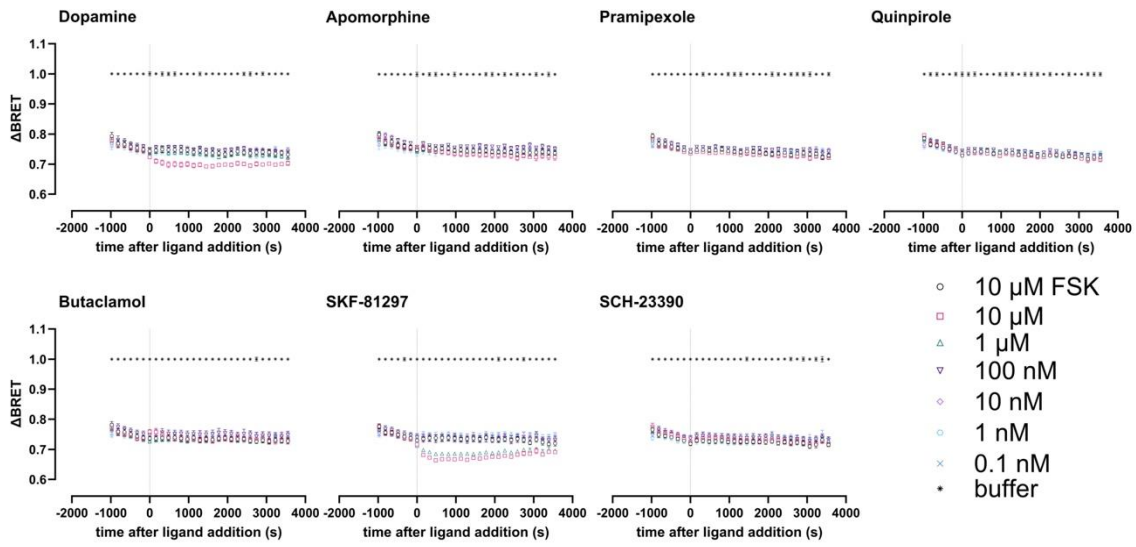

Figure 7.3 : Kinetic responses of HEK-CAMYEN cells in "cAMP inhibition mode". Stably transfected HEK293T-CAMYEN cells were treated with 2000x diluted furimazine and 10 μM forskolin for 30 min before ligand addition. FSK = forskolin. Each ligand concentration measured in triplicate, *N* = 5.

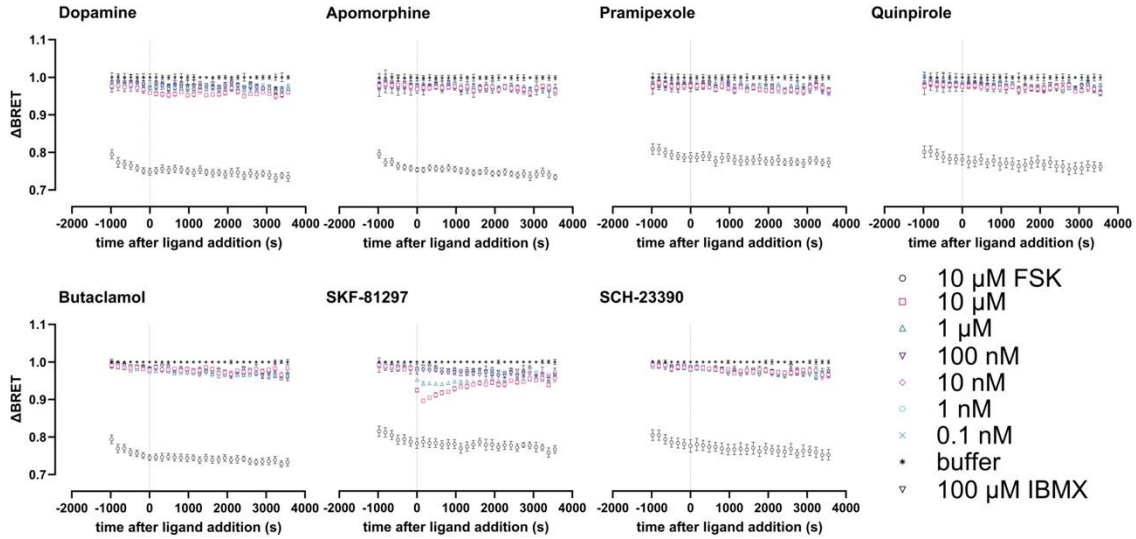

Figure 7.4: Kinetic responses of HEK-CAMYEN cells in "cAMP stimulation mode". Stably transfected HEK293T-CAMYEN cells were treated with 2000x diluted furimazine and 100 μM IBMX for 30 min before ligand addition. FSK = forskolin. Each ligand concentration measured in triplicate, *N* = 5.

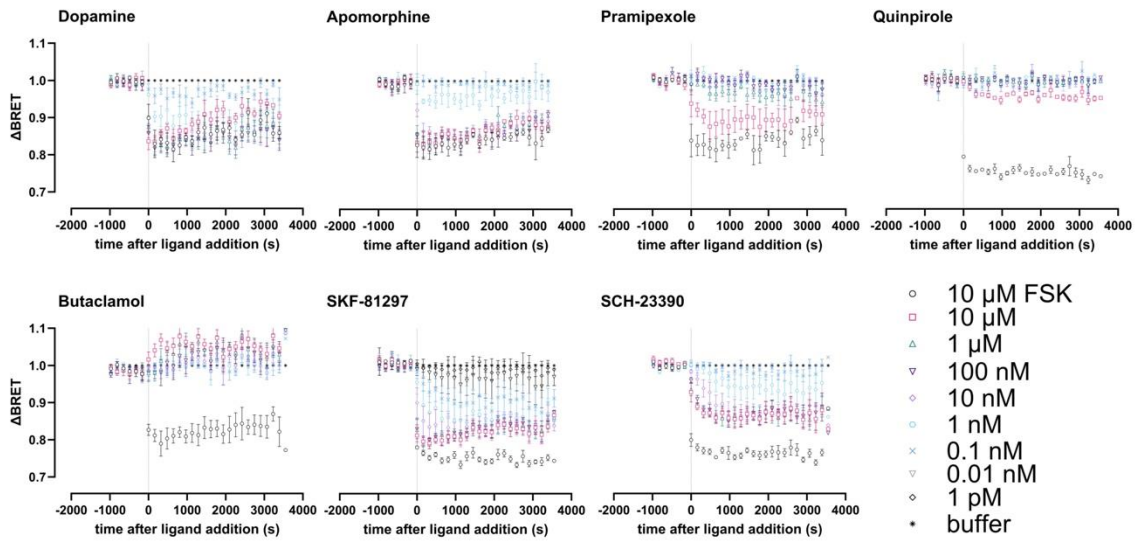

Figure 7.5: Kinetic responses of HEK-CAMYEN_D_1R cells. Stably transfected HEK293T-CAMYEN_D_1R cells were treated with 2000x diluted furimazine and 100 μM IBMX for 30 min before ligand addition. The AUC values from each experiment were used to generate the concentration response curves in Figure 4. FSK = forskolin. Each ligand concentration measured in triplicate, *N* = 5.

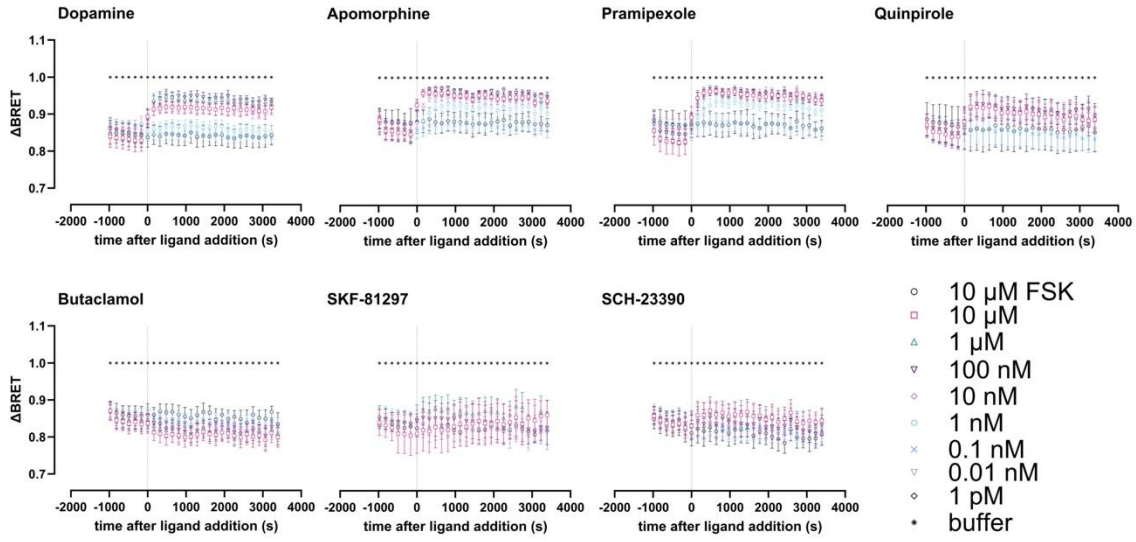

Figure 7.6: Kinetic responses of HEK-CAMYEN_D_{2l}R cells. Stably transfected HEK293T-CAMYEN_D_{2l}R cells were treated with 2000x diluted furimazine and 10 μM forskolin for 30 min before ligand addition. FSK = forskolin. Each ligand concentration measured in triplicate, *N* = 5.

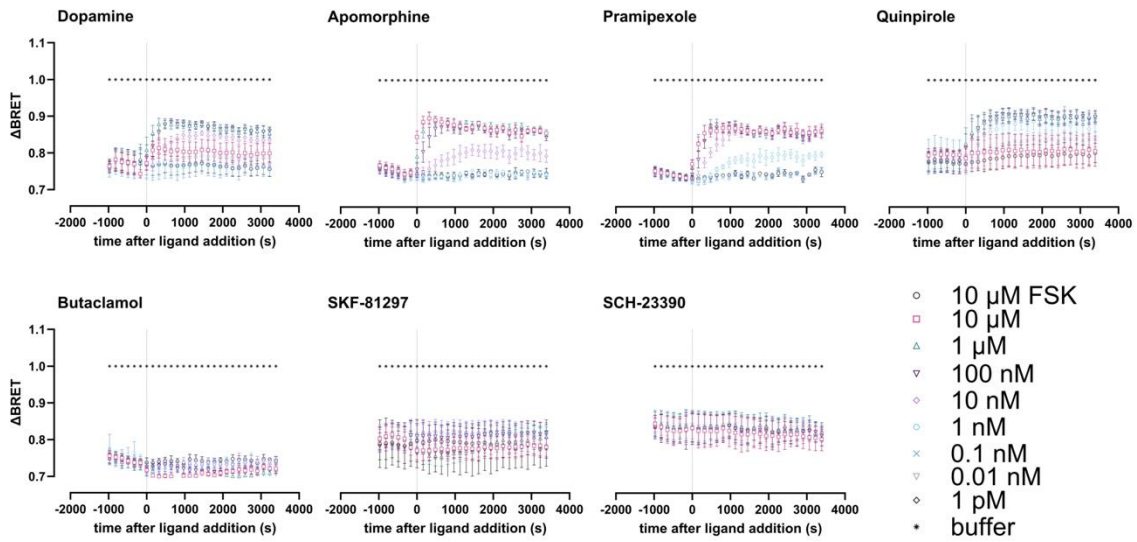

Figure 7.7: Kinetic responses of HEK-CAMYEN_D_3R cells. Stably transfected HEK293T-CAMYEN_D_3R cells were treated with 2000x diluted furimazine and 10 μM forskolin for 30 min before ligand addition. FSK = forskolin. Each ligand concentration measured in triplicate, *N* = 5.

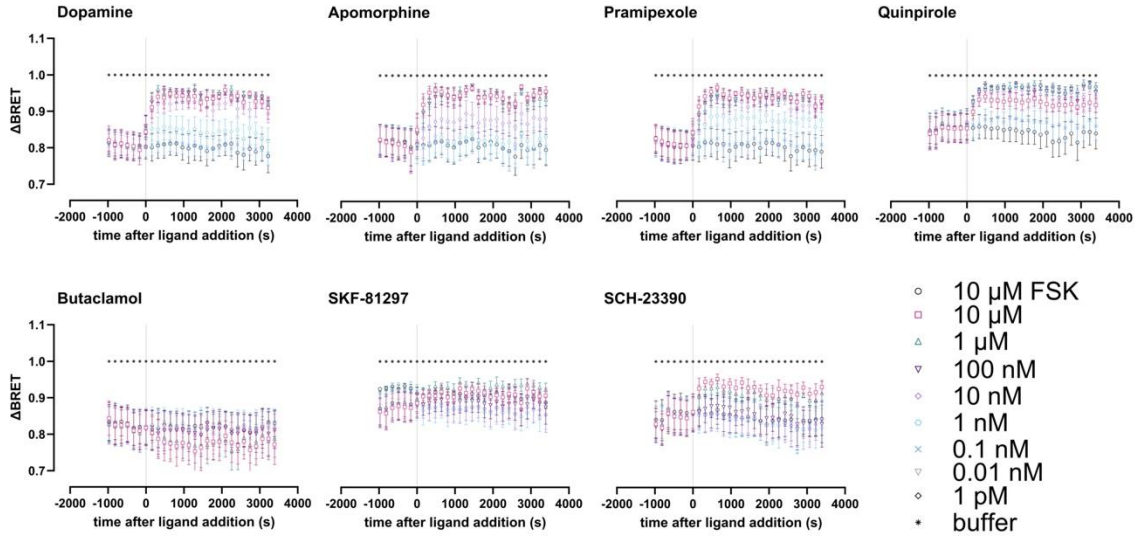

Figure 7.8: Kinetic responses of HEK-CAMYEN_D_4R cells. Stably transfected HEK293T-CAMYEN_D_4R cells were treated with 2000x diluted furimazine and 10 μM forskolin for 30 min before ligand addition. FSK = forskolin. Each ligand concentration measured in triplicate, *N* = 5.

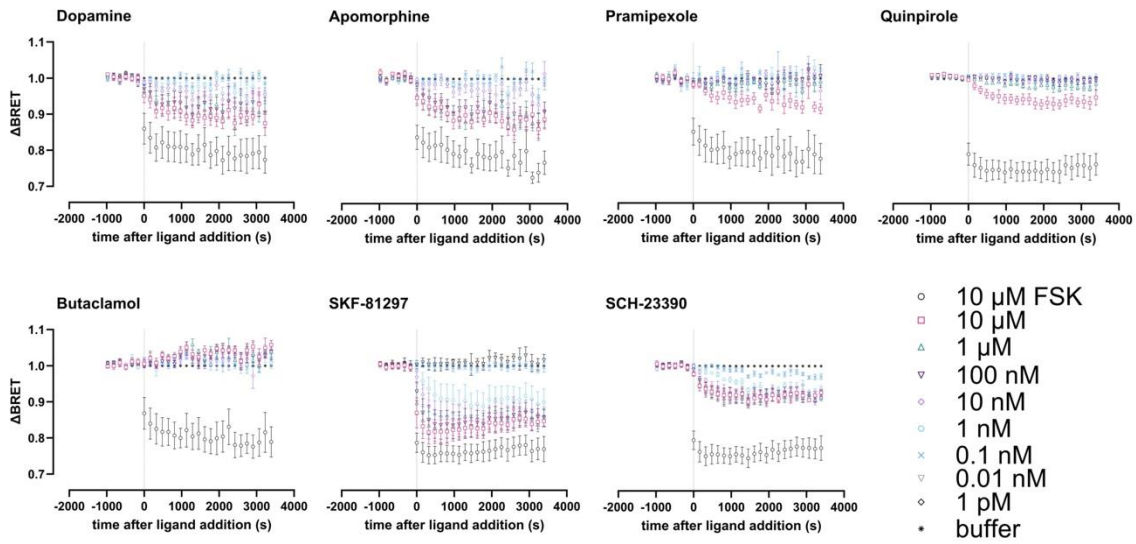

Figure 7.9: Kinetic responses of HEK-CAMYEN_D_5R cells. Stably transfected HEK293T-CAMYEN_D_5R cells were treated with 2000x diluted furimazine and 100 µM IBMX for 30 min before ligand addition. FSK = forskolin. Each ligand concentration measured in triplicate, *N* = 5.

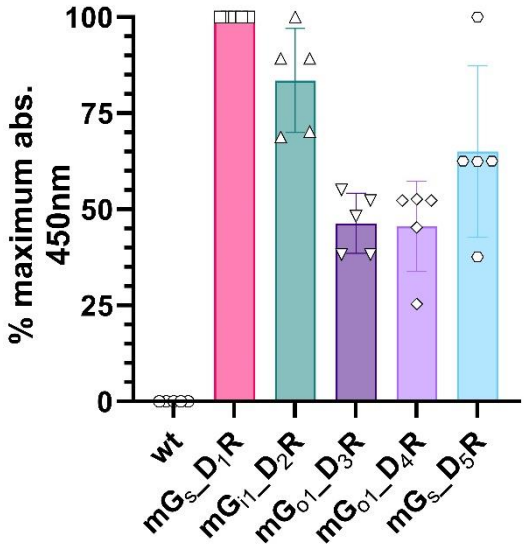

Figure 7.10: NLucN-miniG sensor expression when transfected with the respective dopamine receptor-NLucC constructs, measured using ELISA with an anti-NanoLuc antibody. The primary antibody was used against the NLucN tag expressed on the N-terminus of the respective miniG protein Receptors were transiently transfected into HEK293T cells alongside the relevant miniG protein (mG_s, mG_{i1}, and mG_{o1}). All variables were measured on the same day and plate. Data are normalized to HEK293T wild type cells (wt; 0%) and the maximum mean absorption at 450 nm on the day of the experiment (100%). *N* = 5 independent experiments.

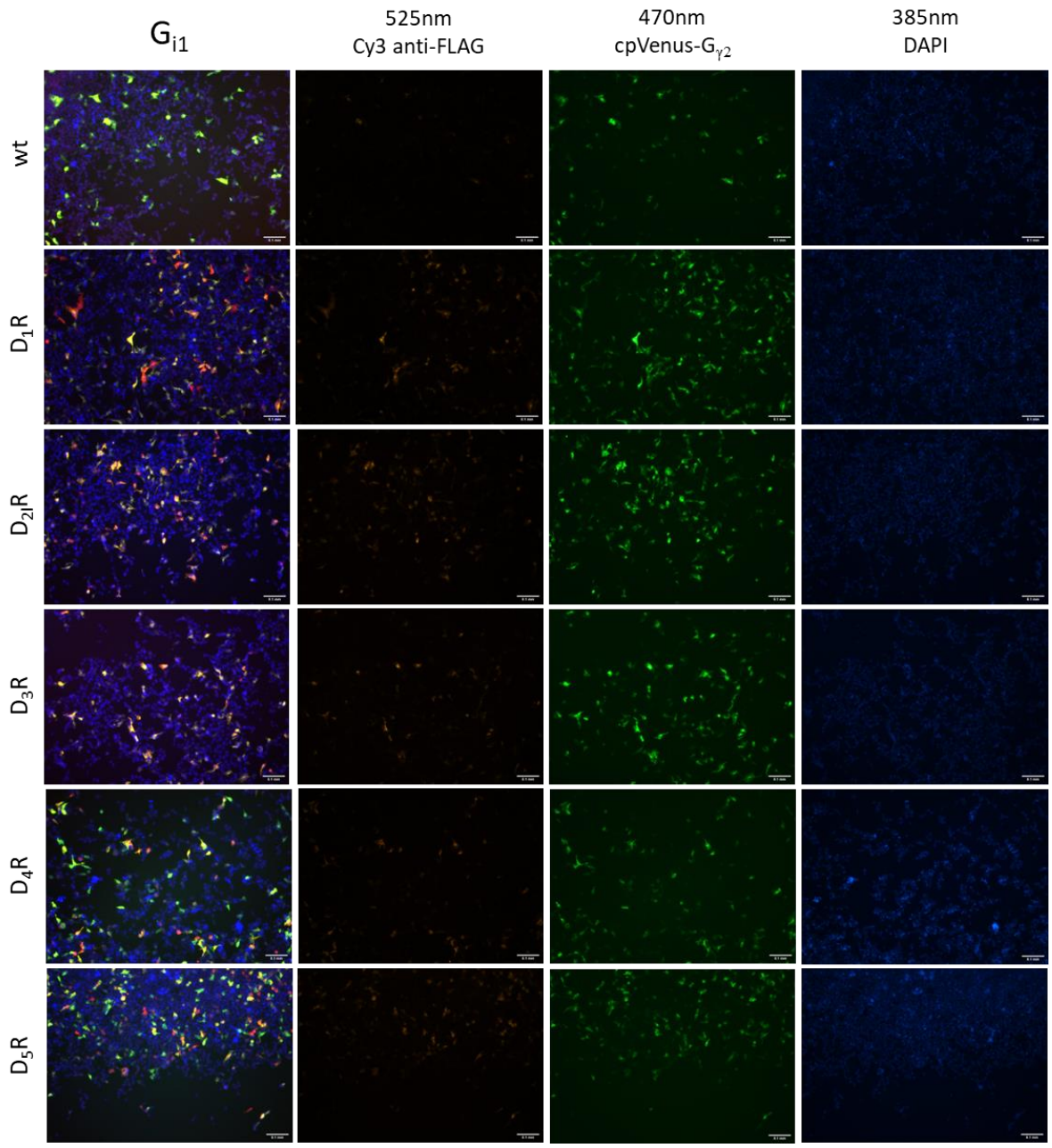

Figure 7.11: Immunofluorescence for expression and localization of the dopamine receptor subtypes in HEK293T cells transiently transfected along with G_{i1}-CASE. Cells were fixed with PFA and labelled with a mouse anti-FLAG monoclonal antibody (#MAB10026, 1:1000) and Cy3 conjugated goat anti-mouse secondary antibody, imaged at 525 nm. The cpVenus in the G-CASE sensor was imaged at 470 nM. Images were taken with a widefield inverted microscope with a 10x objective. The composite image on the left is automatically adjusted for brightness and contrast using ImageJ software, whereas the others remain unaltered. Scale bar shows 0.1 mm. Representative *N* = 1 of two wells on a 96-well plate.

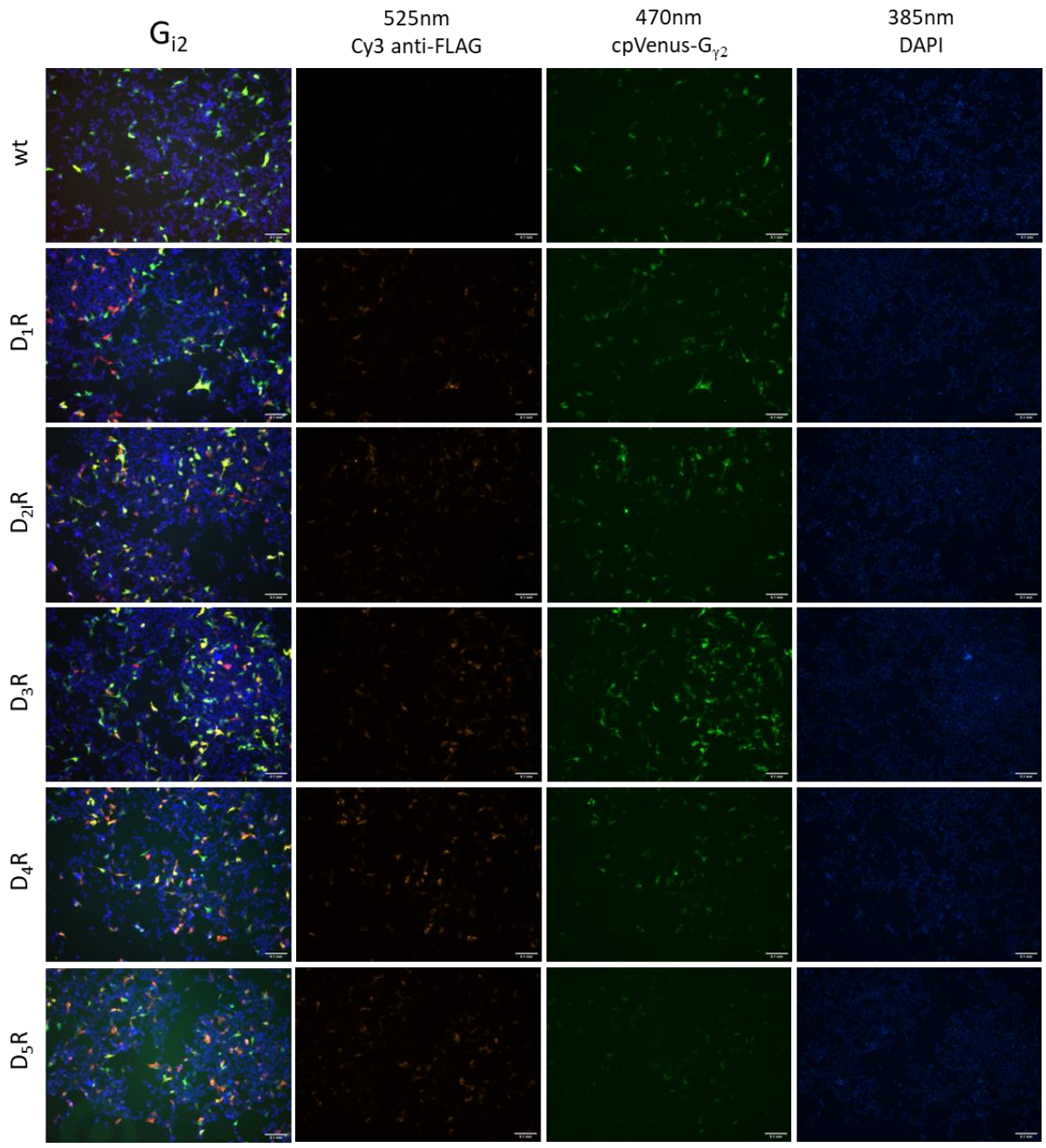

Figure 7.12: Immunofluorescence for expression and localization of the dopamine receptor subtypes, transiently transfected along with G_{i2}-CASE. Cells were fixed with PFA and labelled with a mouse anti-FLAG monoclonal antibody (#MAB10026, 1:1000) and Cy3 conjugated goat anti-mouse secondary antibody, imaged at 525 nm. The cpVenus in the G-CASE sensor was imaged at 470 nM. Images were taken with a widefield inverted microscope with a 10x objective. The composite image on the left is automatically adjusted for brightness and contrast using ImageJ software, whereas the others remain unaltered. Scale bar shows 0.1 mm. Representative $N = 1$ of two wells on a 96-well plate.

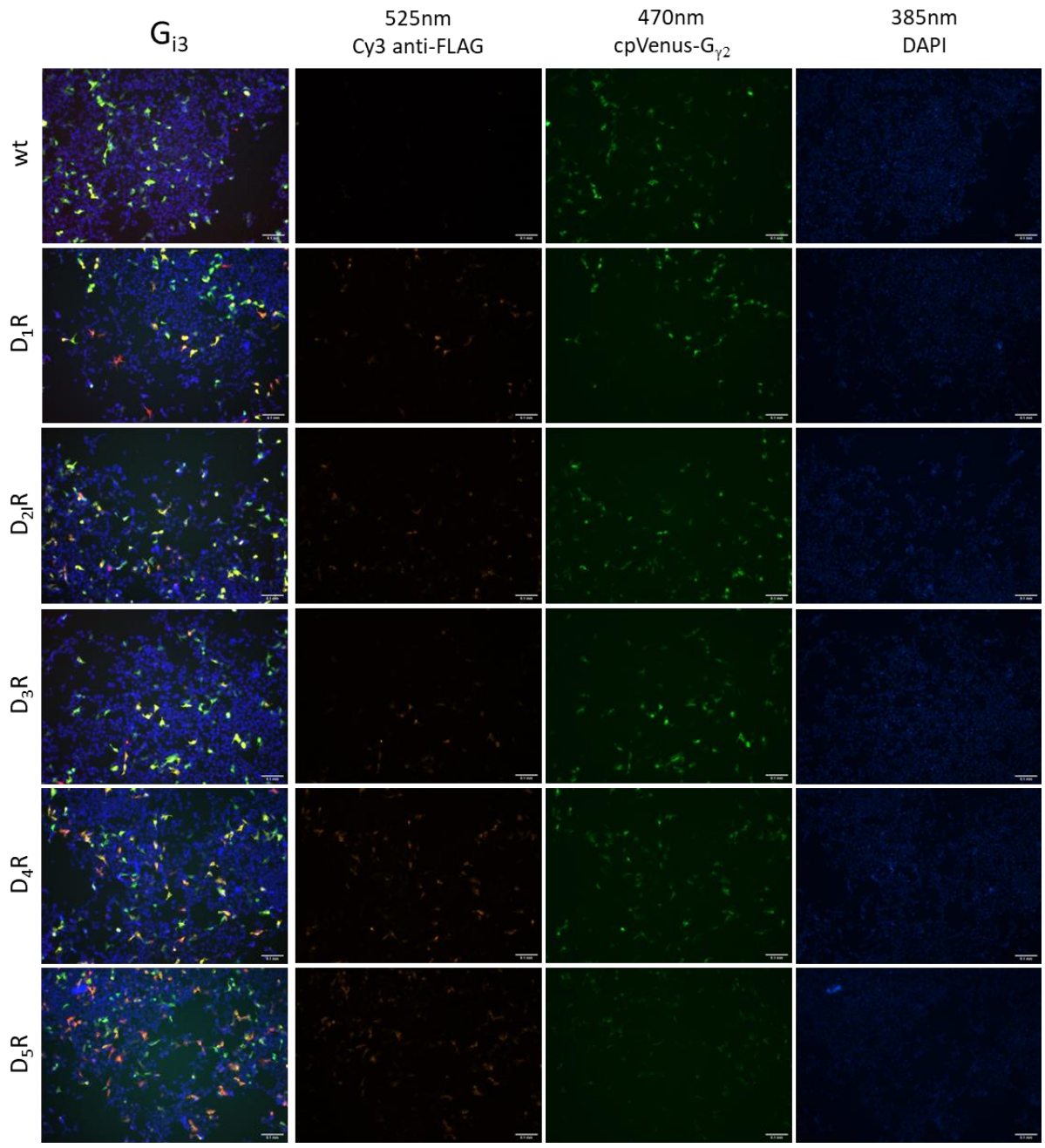

Figure 7.13: Immunofluorescence for expression and localization of the dopamine receptor subtypes, transiently transfected along with G_{i3}-CASE. Cells were fixed with PFA and labelled with a mouse anti-FLAG monoclonal antibody (#MAB10026, 1:1000) and Cy3 conjugated goat anti-mouse secondary antibody, imaged at 525 nm. The cpVenus in the G-CASE sensor was imaged at 470 nM. Images were taken with a widefield inverted microscope with a 10x objective. The composite image on the left is automatically adjusted for brightness and contrast using ImageJ software, whereas the others remain unaltered. Scale bar shows 0.1 mm. Representative $N = 1$ of two wells on a 96-well plate.

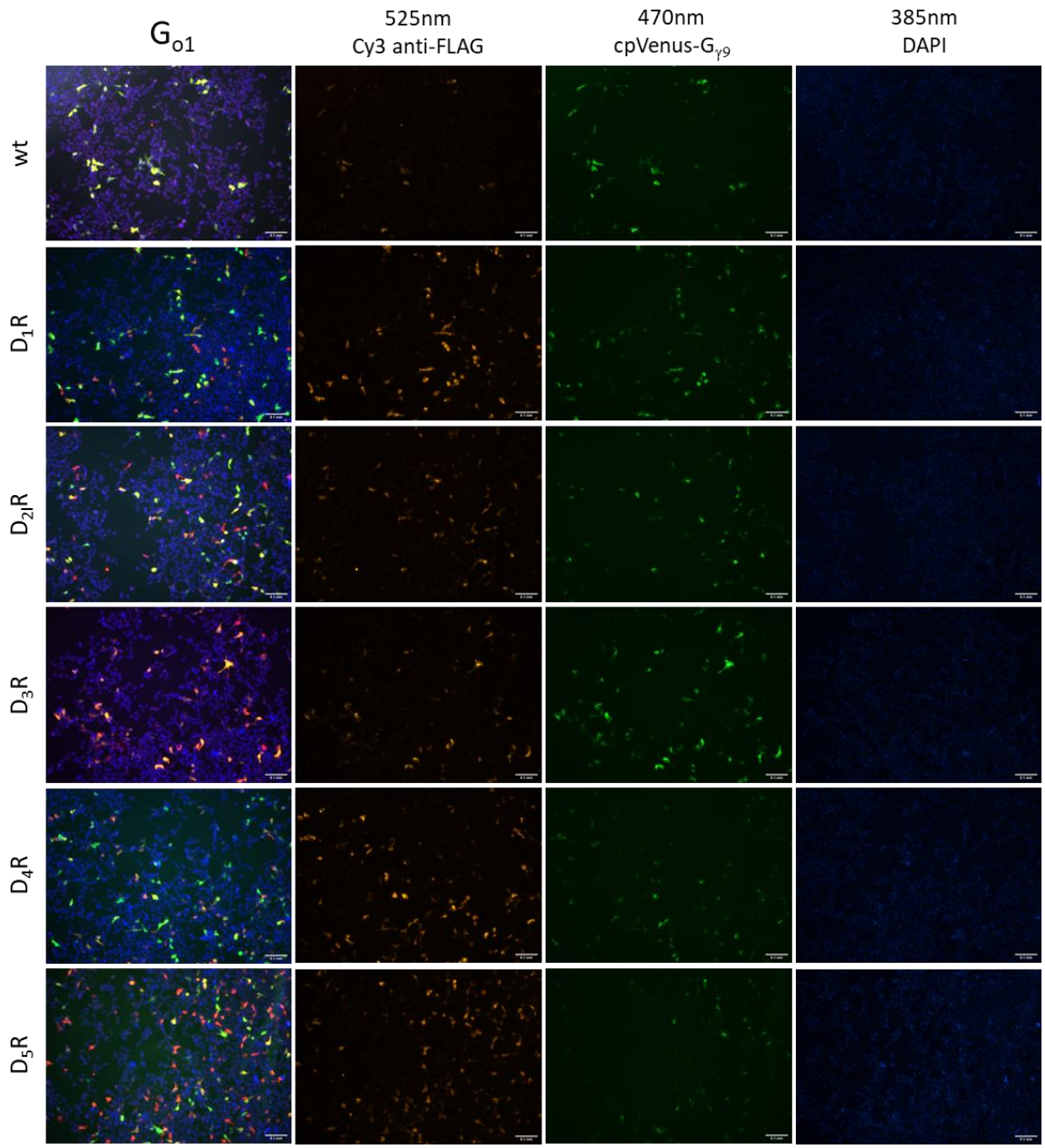

Figure 7.14: Immunofluorescence for expression and localization of the dopamine receptor subtypes, transiently transfected along with G_{o1}-CASE. Cells were fixed with PFA and labelled with a mouse anti-FLAG monoclonal antibody (#MAB10026, 1:1000) and Cy3 conjugated goat anti-mouse secondary antibody, imaged at 525 nm. The cpVenus in the G-CASE sensor was imaged at 470 nM. Images were taken with a widefield inverted microscope with a 10x objective. The composite image on the left is automatically adjusted for brightness and contrast using ImageJ software, whereas the others remain unaltered. Scale bar shows 0.1 mm. Representative $N = 1$ of two wells on a 96-well plate.

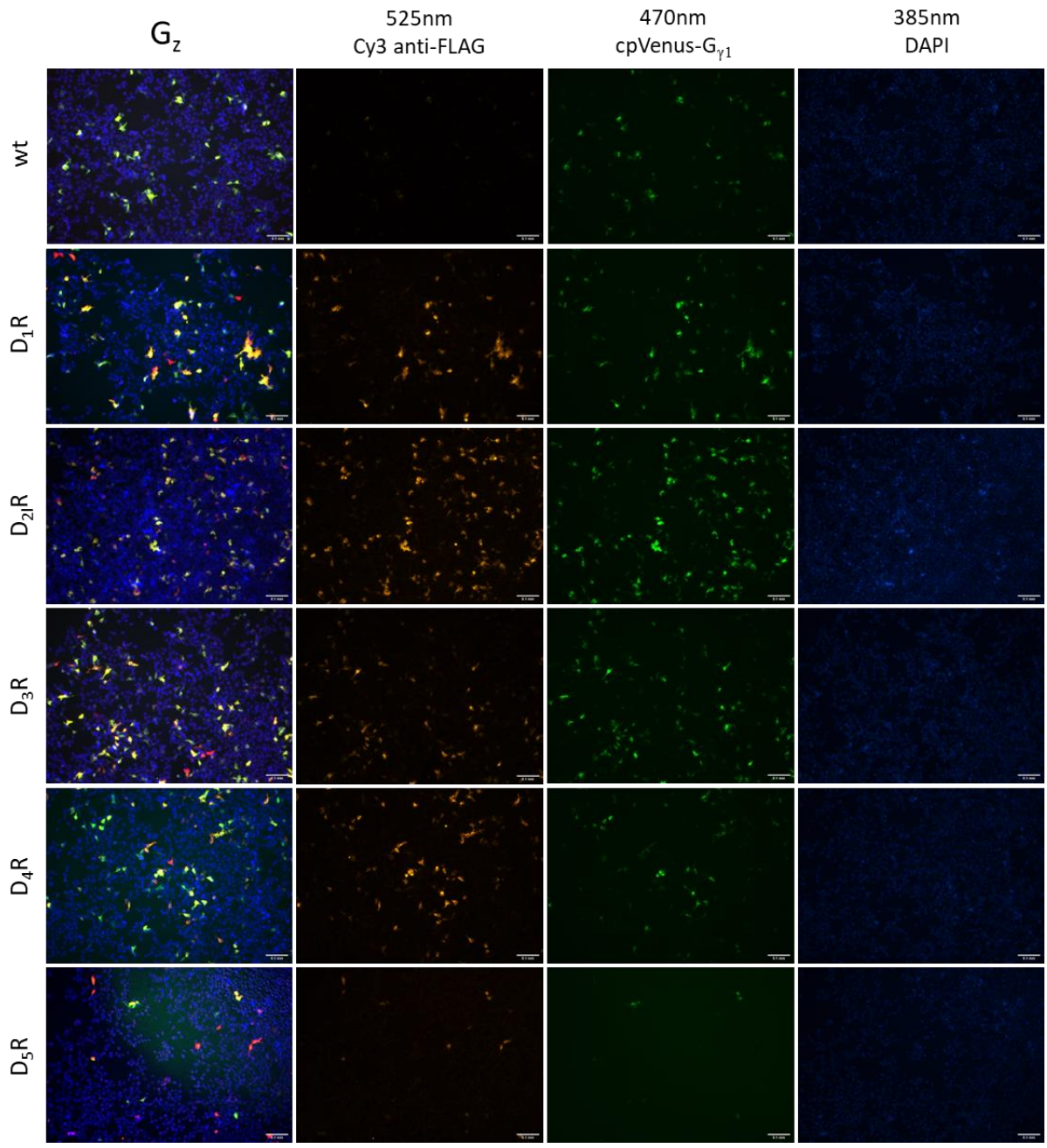

Figure 7.15: Immunofluorescence for expression and localization of the dopamine receptor subtypes, transiently transfected along with G_z-CASE. Cells were fixed with PFA and labelled with a mouse anti-FLAG monoclonal antibody (#MAB10026, 1:1000) and Cy3 conjugated goat anti-mouse secondary antibody, imaged at 525 nm. The cpVenus in the G-CASE sensor was imaged at 470 nM. Images were taken with a widefield inverted microscope with a 10x objective. The composite image on the left is automatically adjusted for brightness and contrast using ImageJ software, whereas the others remain unaltered. Scale bar shows 0.1 mm. Representative $N = 1$ of two wells on a 96-well plate.

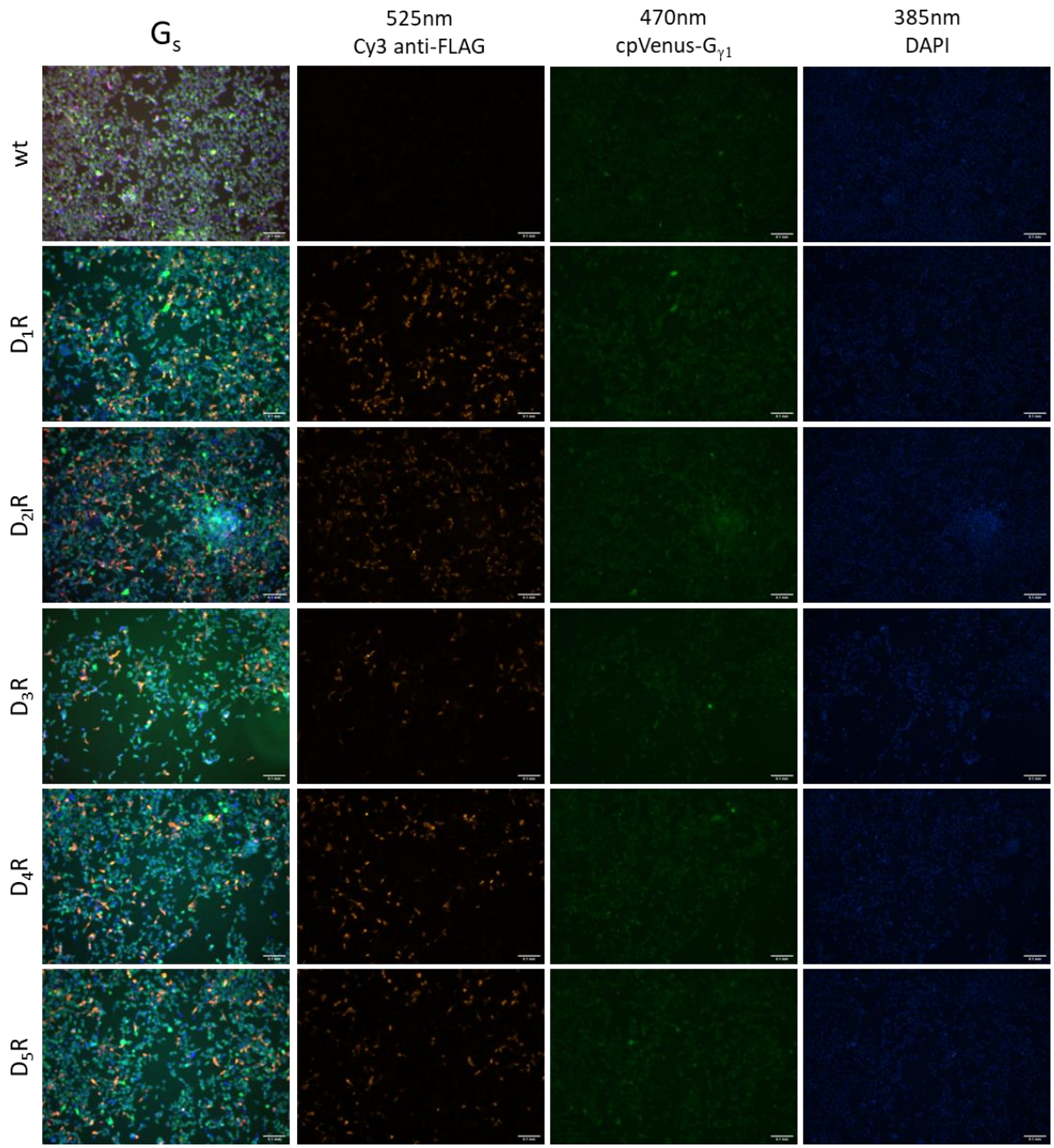

Figure 7.16: Immunofluorescence for expression and localization of the dopamine receptor subtypes, transiently transfected into the G_s-CASE stable cell line. Cells were fixed with PFA and labelled with a mouse anti-FLAG monoclonal antibody (#MAB10026, 1:1000) and Cy3 conjugated goat anti-mouse secondary antibody, imaged at 525 nm. The cpVenus in the G-CASE sensor was imaged at 470 nM. Images were taken with a widefield inverted microscope with a 10x objective. The composite image on the left is automatically adjusted for brightness and contrast using ImageJ software, whereas the others remain unaltered. Scale bar shows 0.1 mm. Representative $N = 1$ of two wells on a 96-well plate.

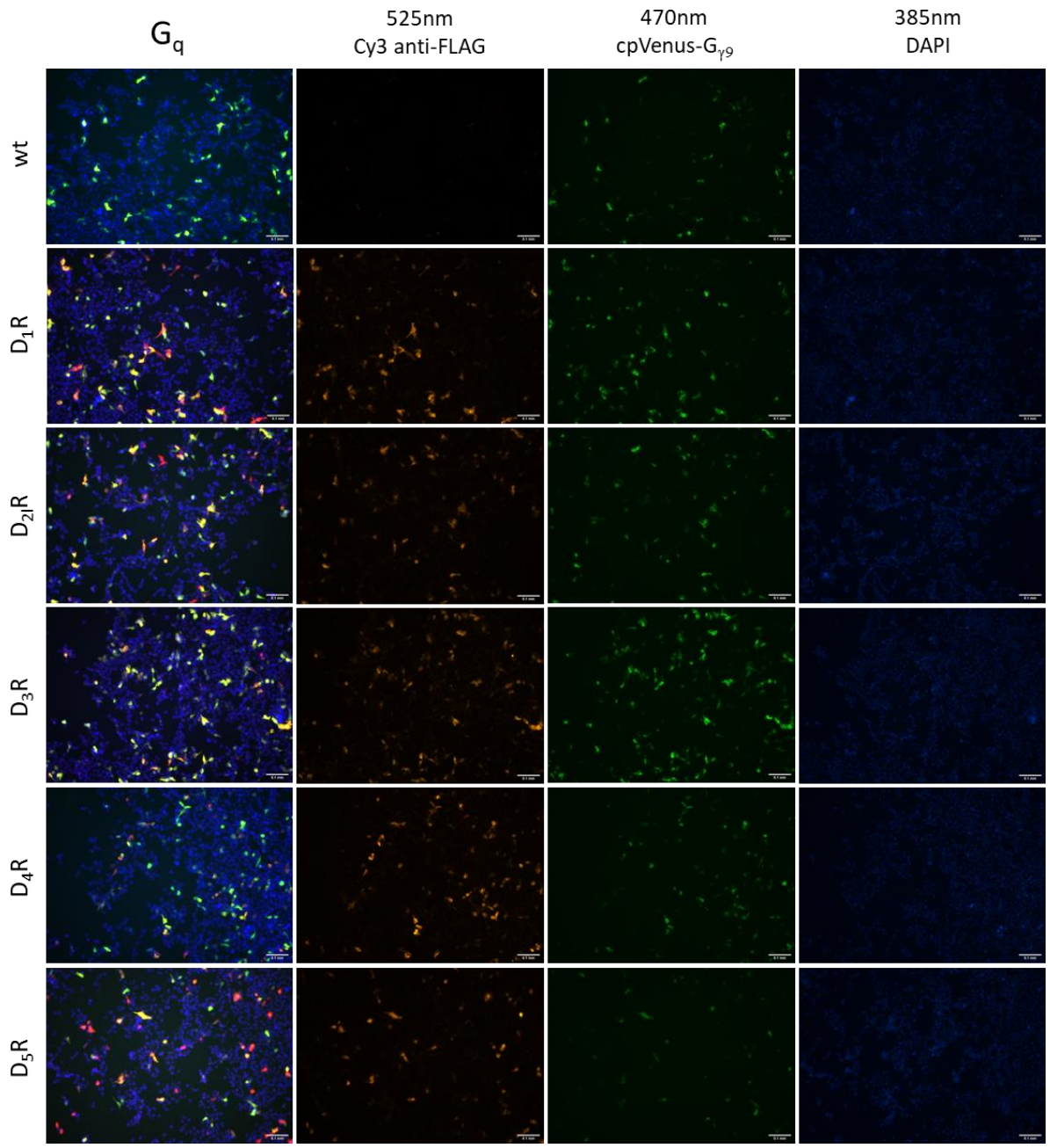

Figure 7.17: Immunofluorescence for expression and localization of the dopamine receptor subtypes, transiently transfected along with G_q-CASE. Cells were fixed with PFA and labelled with a mouse anti-FLAG monoclonal antibody (#MAB10026, 1:1000) and Cy3 conjugated goat anti-mouse secondary antibody, imaged at 525 nm. The cpVenus in the G-CASE sensor was imaged at 470 nM. Images were taken with a widefield inverted microscope with a 10x objective. The composite image on the left is automatically adjusted for brightness and contrast using ImageJ software, whereas the others remain unaltered. Scale bar shows 0.1 mm. Representative $N = 1$ of two wells on a 96-well plate.

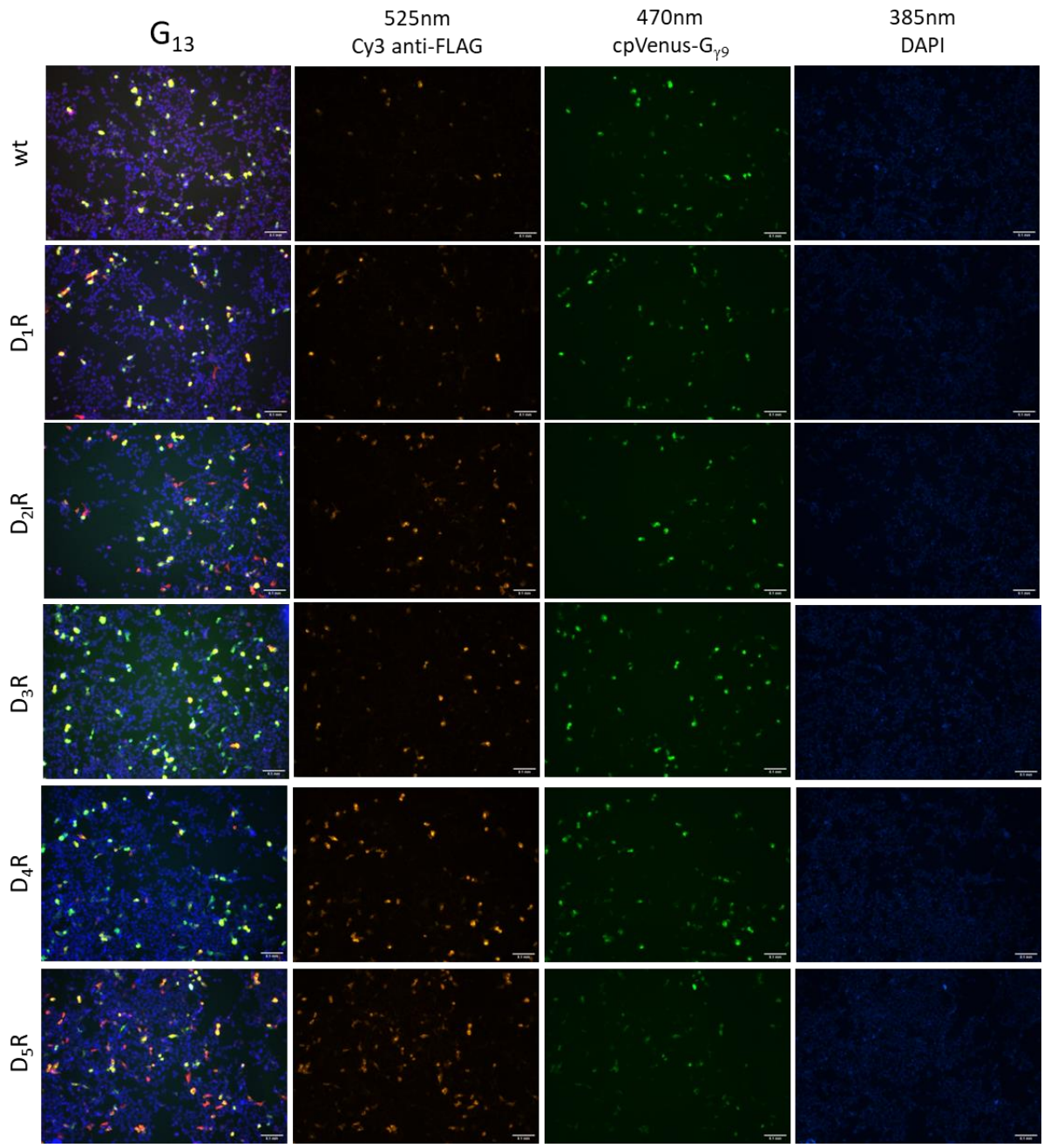

Figure 7.18: Immunofluorescence for expression and localization of the dopamine receptor subtypes, transiently transfected along with G_{13}-CASE. Cells were fixed with PFA and labelled with a mouse anti-FLAG monoclonal antibody (#MAB10026, 1:1000) and Cy3 conjugated goat anti-mouse secondary antibody, imaged at 525 nm. The cpVenus in the G-CASE sensor was imaged at 470 nM. Images were taken with a widefield inverted microscope with a 10x objective. The composite image on the left is automatically adjusted for brightness and contrast using ImageJ software, whereas the others remain unaltered. Scale bar shows 0.1 mm. Representative $N = 1$ of two wells on a 96-well plate.

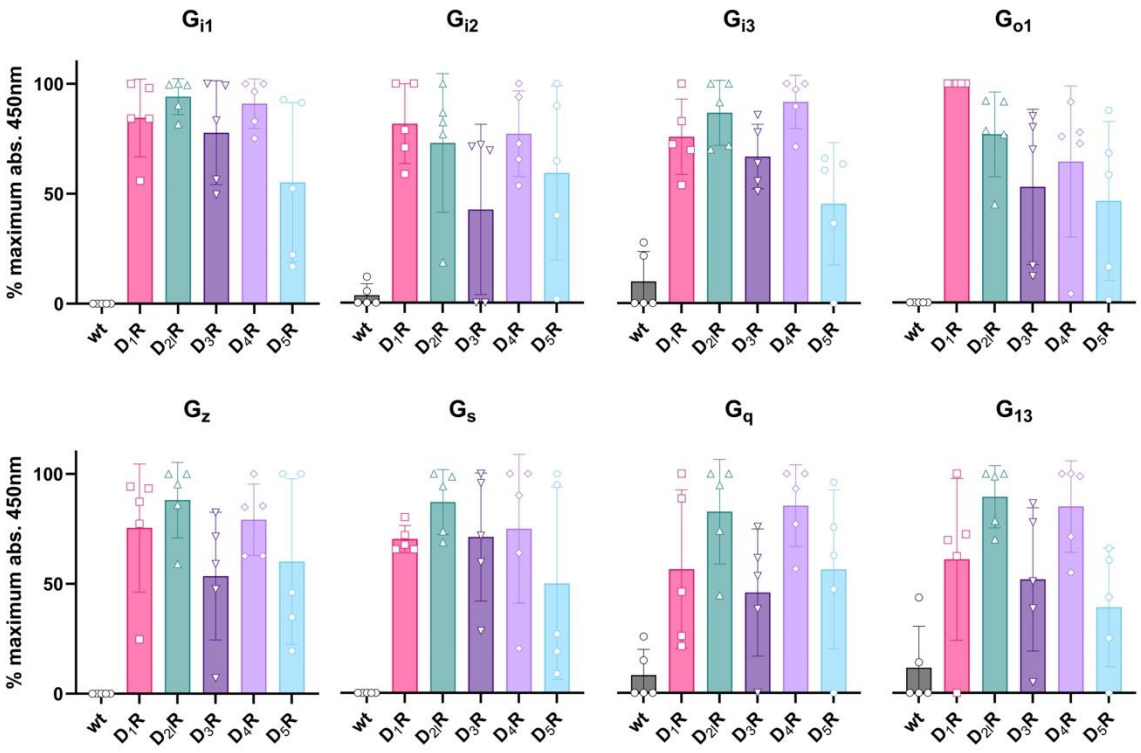

Figure 7.19: Dopamine receptor expression when transfected with G-CASE sensors, measured using ELISA with an anti-FLAG antibody. The primary antibody was used against the FLAG tag expressed on the receptor N-terminus. Receptors were transiently transfected into HEK293T cells alongside the relevant G-CASE sensor (G_{i1}, G_{i2}, G_{i3}, G_{o1}, G_z, G_q or G_{13}; G_s-CASE stable cell line). All variables were measured on the same day and plate. Data are normalized to the minimum (0%) and maximum (100%) mean absorption at 450 nm on the day of the experiment. *N* = 5 independent experiments in duplicate performed using different transient transfections on different days.

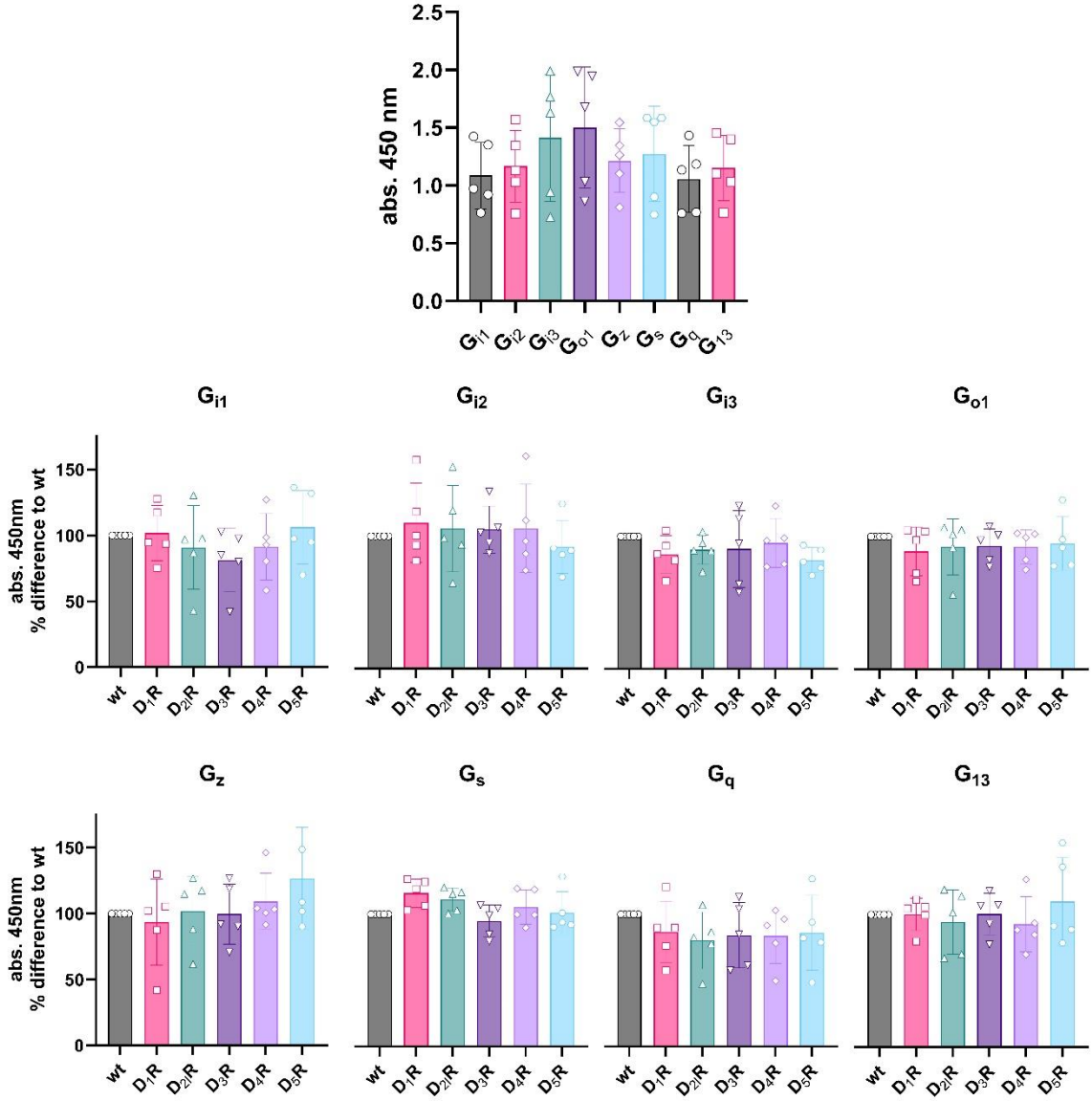

Figure 7.20: G-CASE Gα subunit expression when transfected with dopamine receptors, measured using ELISA with an anti-NLuc antibody. The primary antibody was used against the NLuc inserted into the Gα subunit. The top graph compares the expression of the different Gα subunits in wildtype HEK293T cells using the raw absorbance values. A Friedman non-parametric test with Dunn's multiple comparisons (data matched by transfection date) determined no significant difference in Gα subunit expression between the subtypes in wildtype cells ($\chi2(7) = 9.667$, $p = 0.2083$). Below, dopamine receptors were transiently transfected into HEK293T cells alongside the relevant G-CASE sensor (G_{i1}, G_{i2}, G_{i3}, G_{o1}, G_z, G_q or G_{13}; G_s-CASE stable cell line). All variables were measured on the same day and plate. Baseline correction was used to determine the % difference to G-CASE expressing cells without dopamine receptors (wt). For all variables, $N = 5$ independent experiments in duplicate performed using different transient transfections on different days.

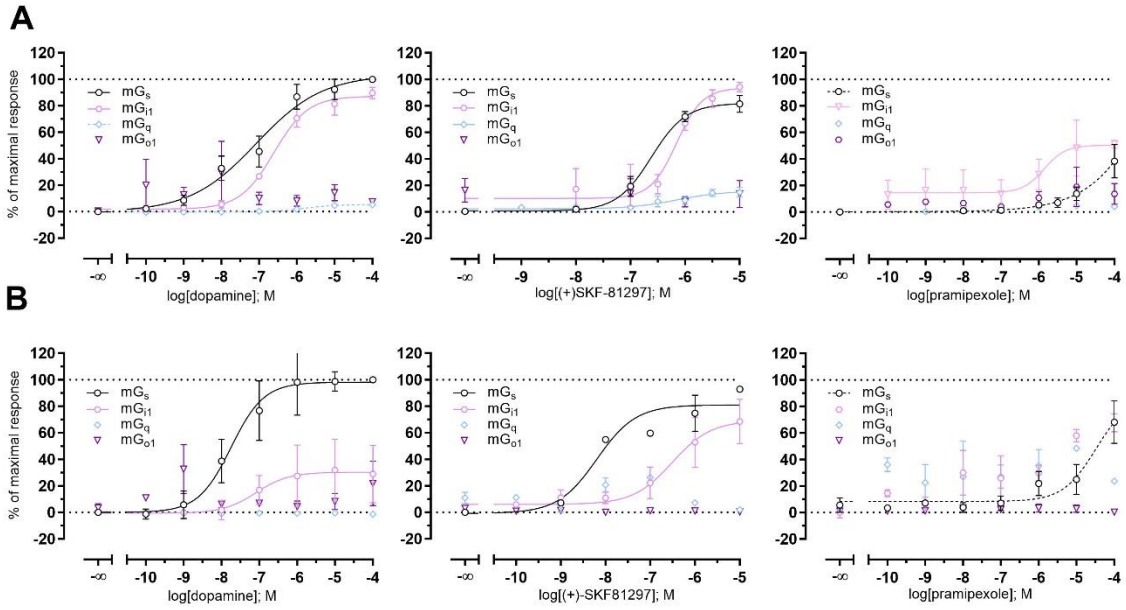

Figure 7.21: Functional coupling of miniG proteins with D_1-like dopamine receptors activated by dopamine, (+)SKF-81297, or pramipexole**.** Activation profile of D_1R (**A**) and D_5R (**B**) with $miniG_{s/si1/sq/o1}$, $N \geq 3$ independent experiments performed in triplicate.

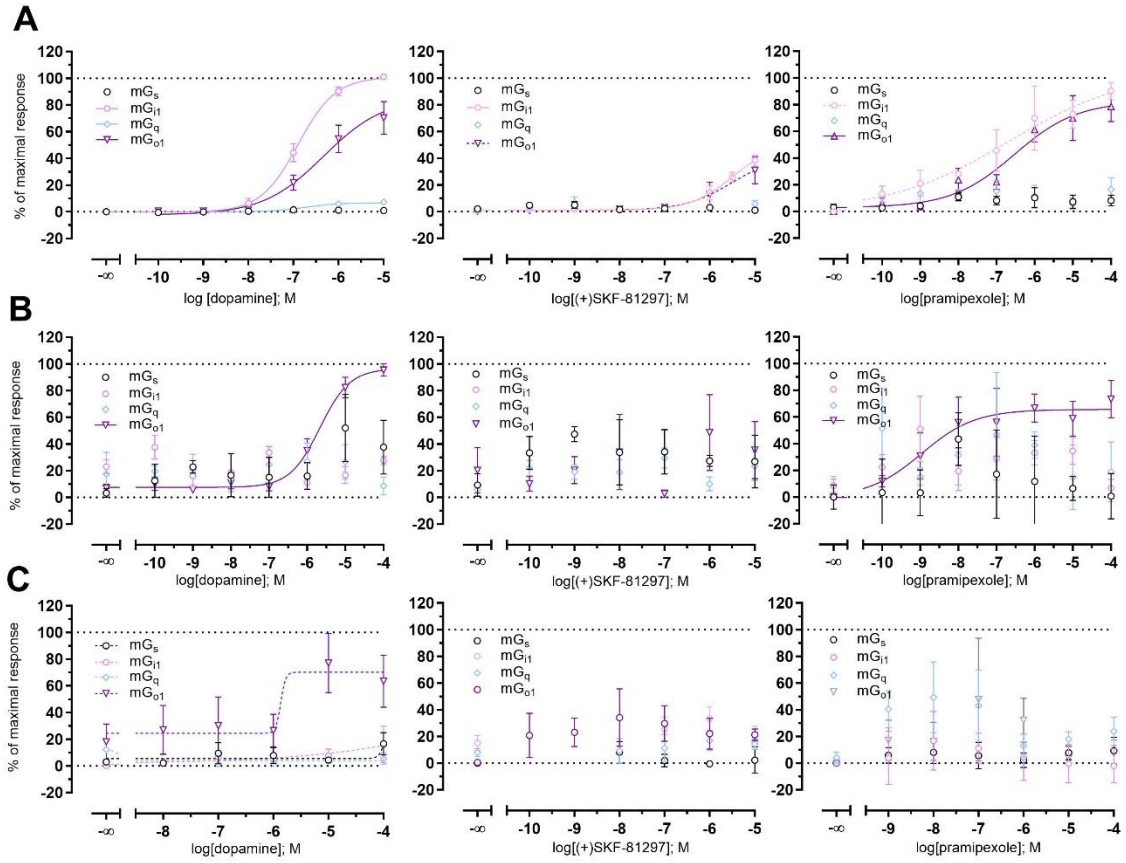

Figure 7.22: Functional coupling of miniG proteins with D_2-like dopamine receptors activated by dopamine, (+)SKF-81297, or pramipexole. Activation profile of the D_2R (**A**), D_3R (**B**), and D_4R (**C**) with $miniG_{s/si1/sq/o1}$, $N \geq 3$ independent experiments performed in triplicate.

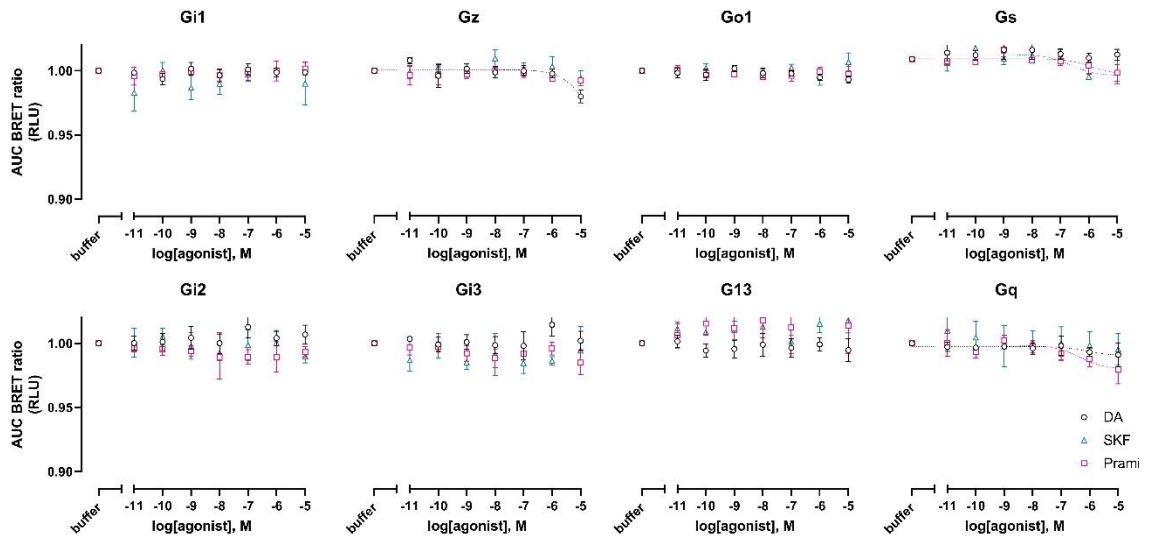

Figure 7.23: G-CASE activation in wild type HEK293T cells. HEK293T cells were transiently transfected with G-CASE sensor plasmids and control pcDNA. Experiments were performed using 5 µM coelenterazine H and concentration-response curves were generated using the AUC of 1 h BRET ratio/baseline traces. DA = dopamine, PR = pramipexole, SKF = (+)-SKF-81297; *N* = 5 independent experiments performed in duplicate.

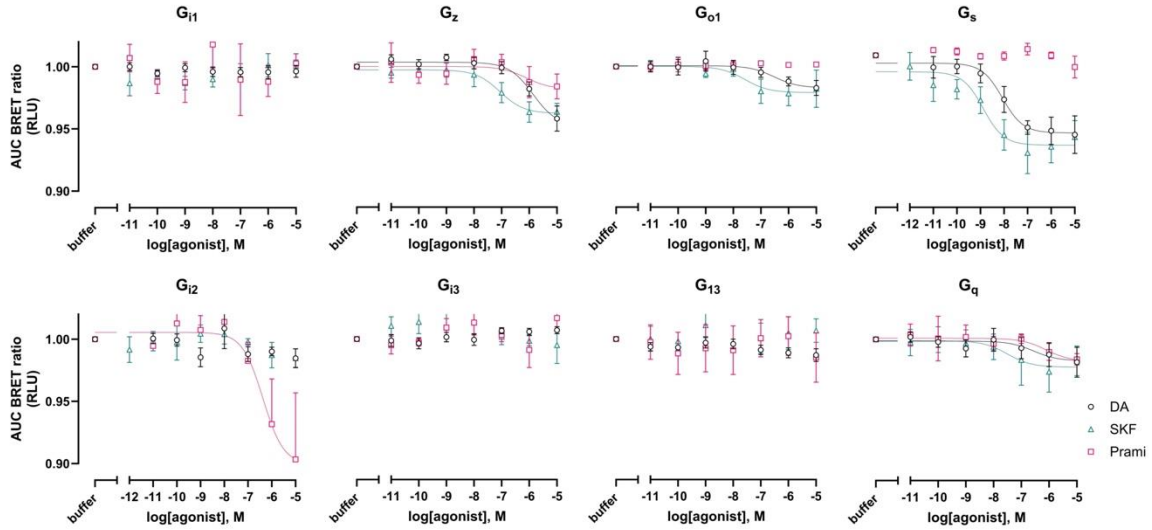

Figure 7.24: G-CASE activation in HEK293T cells expressing D_1R. HEK293T cells were transiently transfected with G-CASE sensor plasmids and D_1R. Experiments were performed using 5 µM coelenterazine H and concentration-response curves were generated using the AUC of 1 h BRET ratio/baseline traces. DA = dopamine, PR = pramipexole, SKF = (+)-SKF-81297; *N* = 5 independent experiments performed in duplicate.

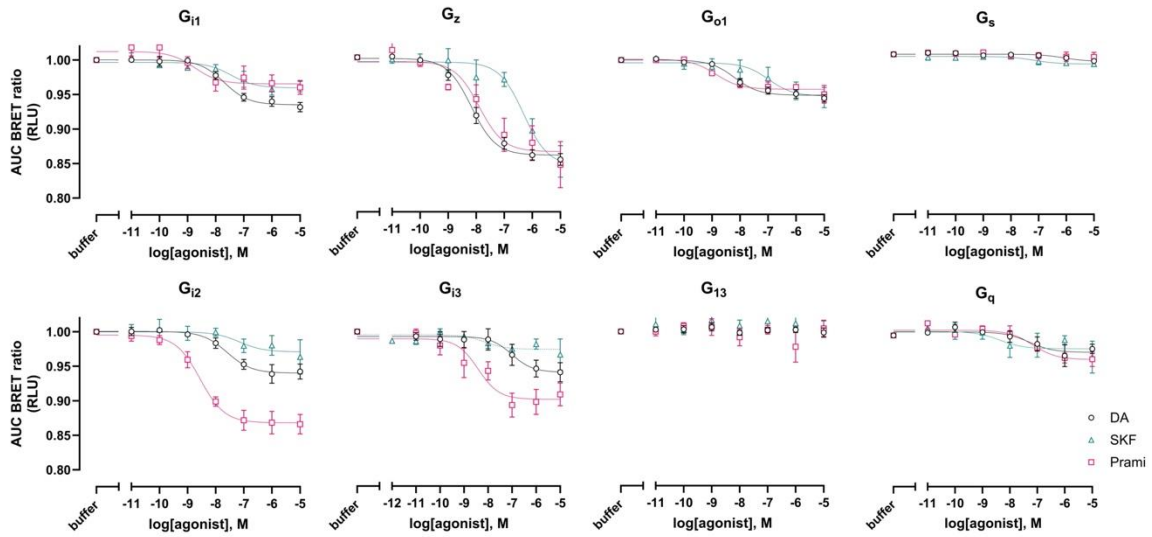

Figure 7.25: G-CASE activation in HEK293T cells expressing $D_{2l}R$. HEK293T cells were transiently transfected with G-CASE sensor plasmids and $D_{2l}R$. Experiments were performed using 5 µM coelenterazine H and concentration-response curves were generated using the AUC of 1 h BRET ratio/baseline traces. DA = dopamine, PR = pramipexole, SKF = (+)-SKF-81297; *N* = 5 independent experiments performed in duplicate.

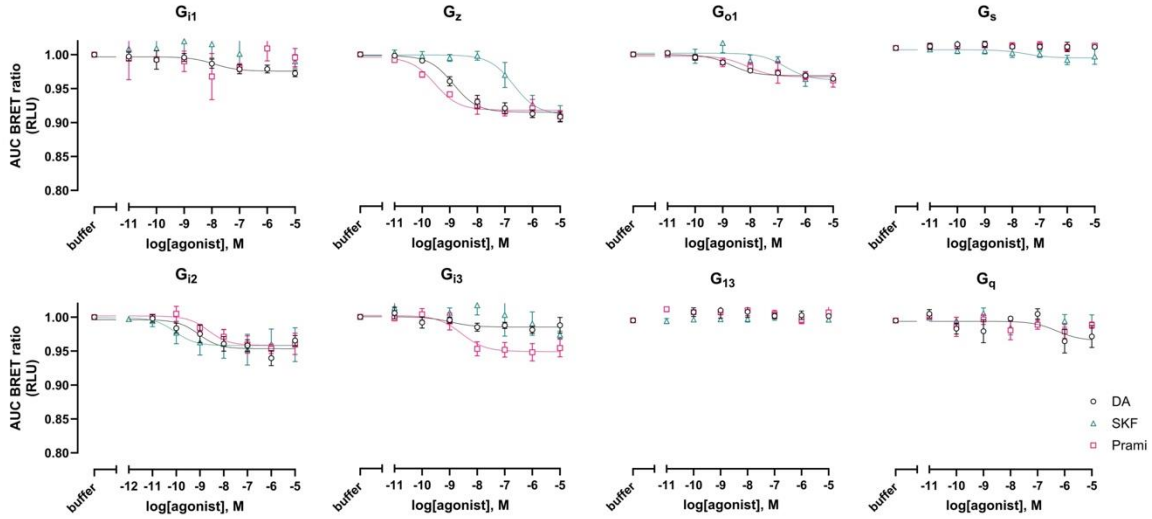

Figure 7.26: G-CASE activation in HEK293T cells expressing D_3R. HEK293T cells were transiently transfected with G-CASE sensor plasmids and D_3R. Experiments were performed using 5 µM coelenterazine H and concentration-response curves were generated using the AUC of 1 h BRET ratio/baseline traces. DA = dopamine, PR = pramipexole, SKF = (+)-SKF-81297; *N* = 5 independent experiments performed in duplicate.

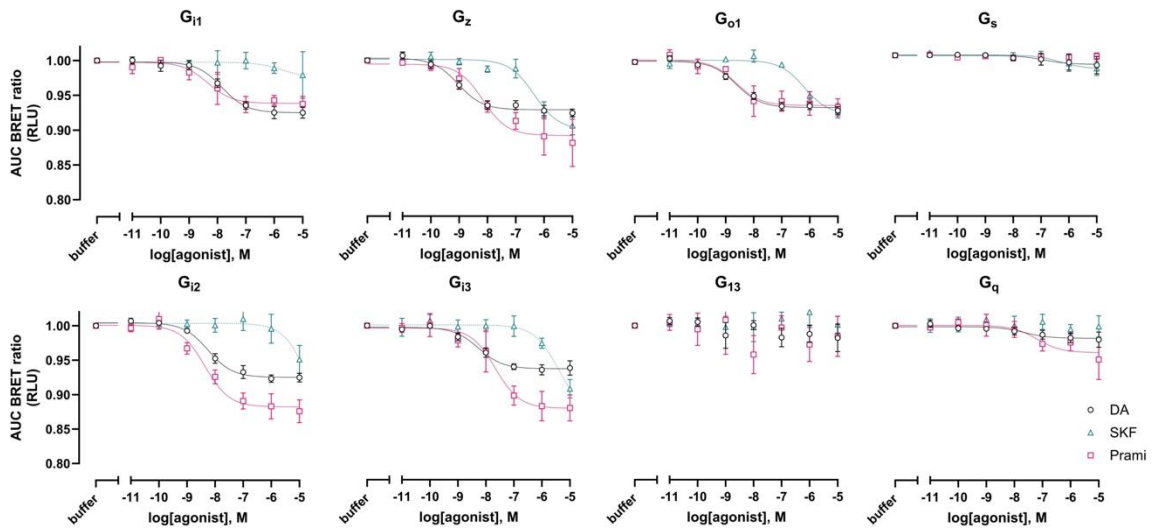

Figure 7.27: G-CASE activation in HEK293T cells expressing D_4R. HEK293T cells were transiently transfected with G-CASE sensor plasmids and D_5R. Experiments were performed using 5 µM coelenterazine H and concentration-response curves were generated using the AUC of 1 h BRET ratio/baseline traces. DA = dopamine, PR = pramipexole, SKF = (+)-SKF-81297; *N* = 5 independent experiments performed in duplicate.

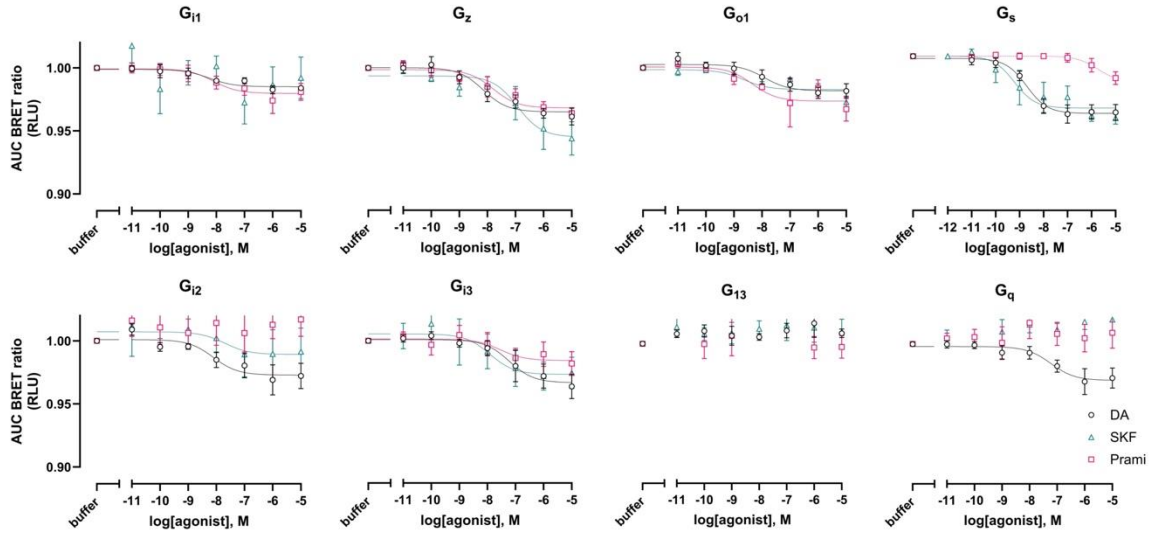

Figure 7.28: G-CASE activation in HEK293T cells expressing D_5R. HEK293T cells were transiently transfected with G-CASE sensor plasmids and D_5R. Experiments were performed using 5 µM coelenterazine H and concentration-response curves were generated using the AUC of 1 h BRET ratio/baseline traces. DA = dopamine, PR = pramipexole, SKF = (+)-SKF-81297; *N* = 5 independent experiments performed in duplicate.

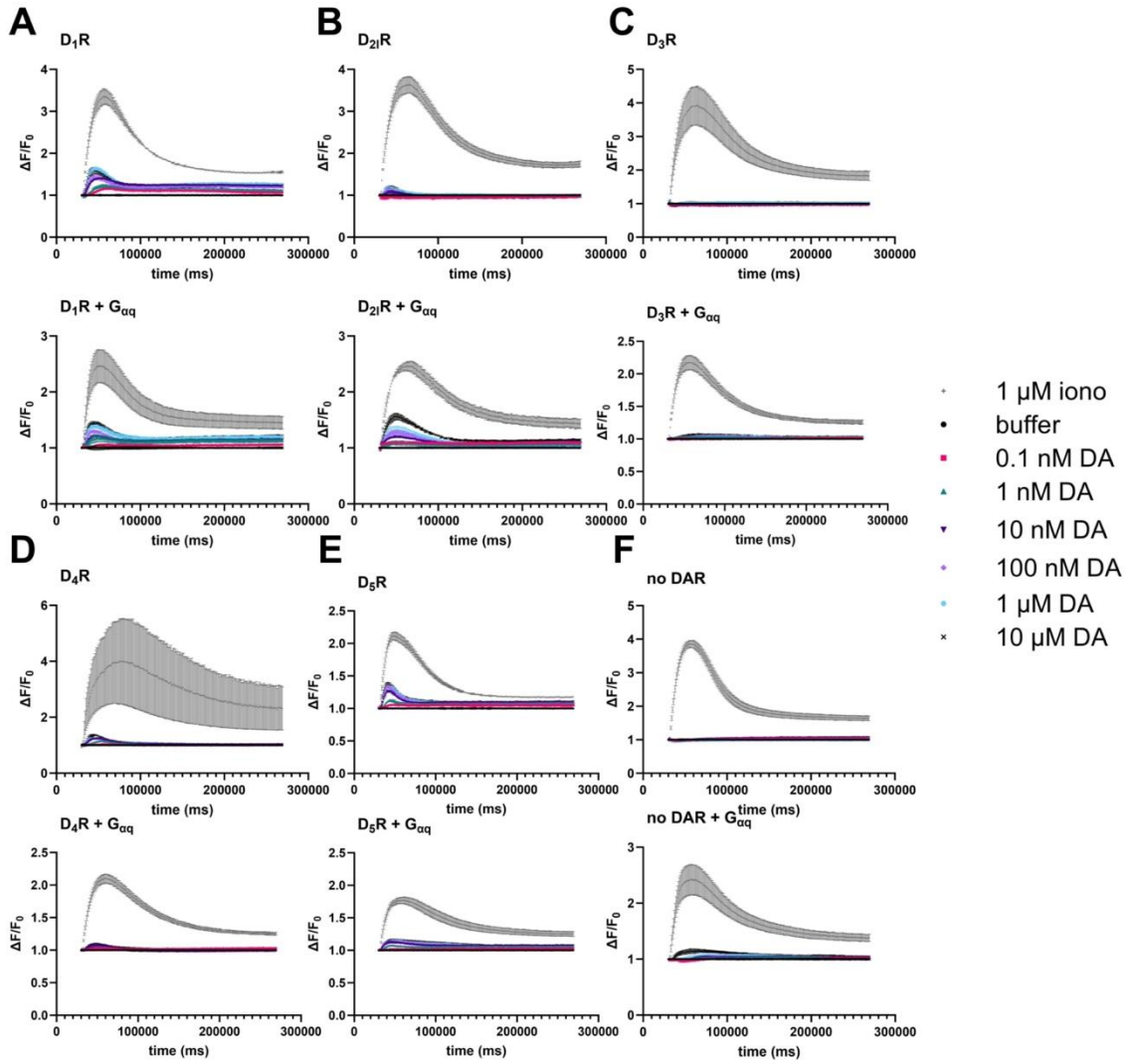

Figure 7.29: Calcium mobilization kinetics of HEK293A cells containing different dopamine receptors with or without overexpressing $G\alpha_q$. HEK293A cells were transiently transfected with 1 µg dopamine receptor cDNA with 1 µg $G\alpha_q$ or pcDNA3.1 empty vector. Data are corrected to the 30 sec baseline for each well divided by the buffer response. The top graph represents cells without added $G\alpha_q$, and below with overexpressed $G\alpha_q$ for (**A**) D_1R (**B**) $D_{2l}R$ (**C**) D_3R (**D**) D_4R (**E**) D_5R and (**F**) no dopamine receptor. DA = dopamine, iono = ionomycin, *N* = 1 representative of five independent experiments performed in triplicate.

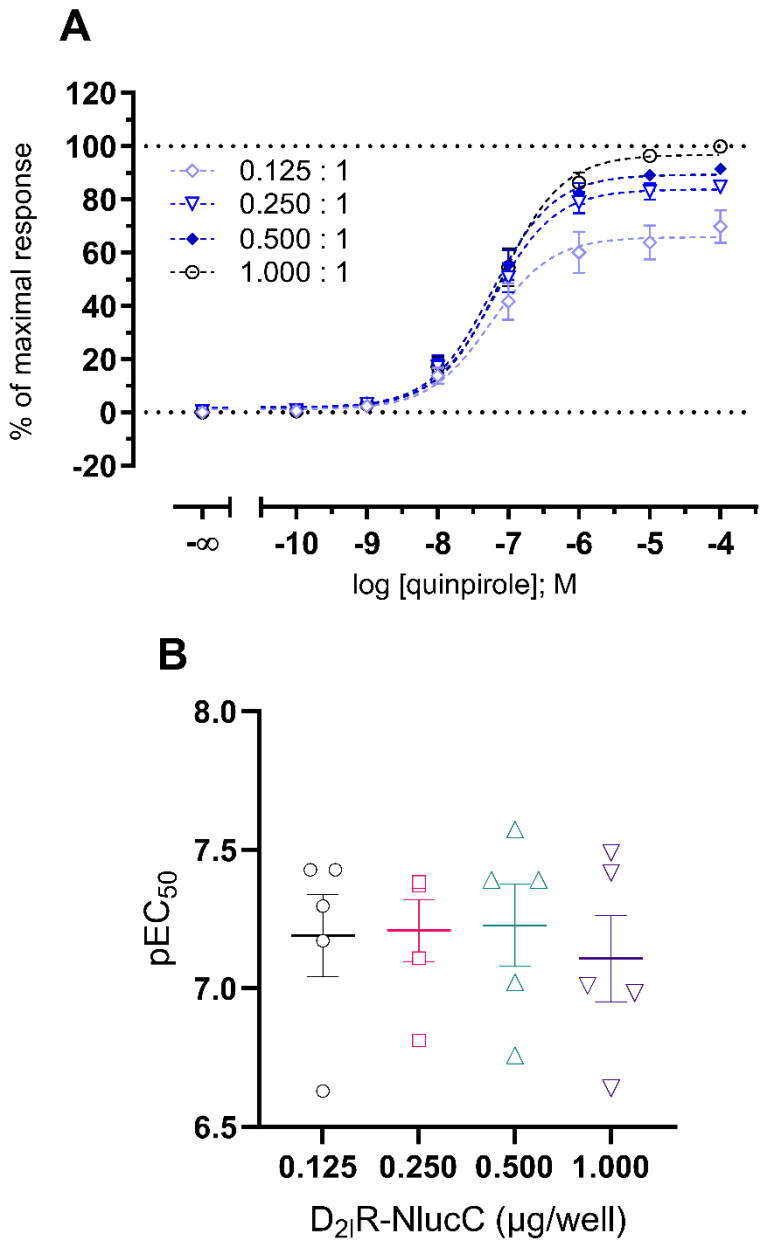

Figure 7.30: Recruitment of miniG$_i$ in split Nluc system with varied amounts of D$_{2l}$R-NlucC in HEK293T cells. Transient transfection with equivalent amounts of NlucN-miniGi (1 µg) and differing amounts of D$_{2l}$R-NlucC (1 – 0.125 µg). (**A**) Concentration response curves of miniG$_i$ recruitment to varied amounts of D$_{2l}$R-NlucC using quinpirole. Data are normalized to maximal response from each experiment (100 µM quinpirole with 1 µg receptor cDNA). (**B**) Comparison of pEC$_{50}$ values for each experiment in (A). A one-way ANOVA found no significant difference in pEC$_{50}$ ($F(3,12) = 1.025$, $p = 0.416$). Data are $N = 5$ with each experiment performed in triplicate.

Table 7.2: The transcripts per million (nTPM) of dopamine receptor and G protein genes in the basal ganglia, hypothalamus and stomach. Data taken from the Human Protein Atlas.[5]

Gene	nTPM		
	Basal ganglia	Hypothalamus	Stomach
GNAI1	23.8	34.1	17.1
GNAI2	108.1	108.2	71.3
GNAI3	1.9	1.8	8.8
GNAO1	130.9	84.9	10.6
GNAZ	26.7	29.6	11.2
GNAS	267.9	888.8	540.3
GNAQ	32.3	28.1	27.2
GNA13	14.5	12.3	17.5
DRD1	25.9	1.2	0.2
DRD2	65.2	11.1	0.1
DRD3	3.2	0.1	n.a.
DRD4	2.4	2.5	0.8
DRD5	1.5	1.3	4.3

7.2. Appendix Chapter 3

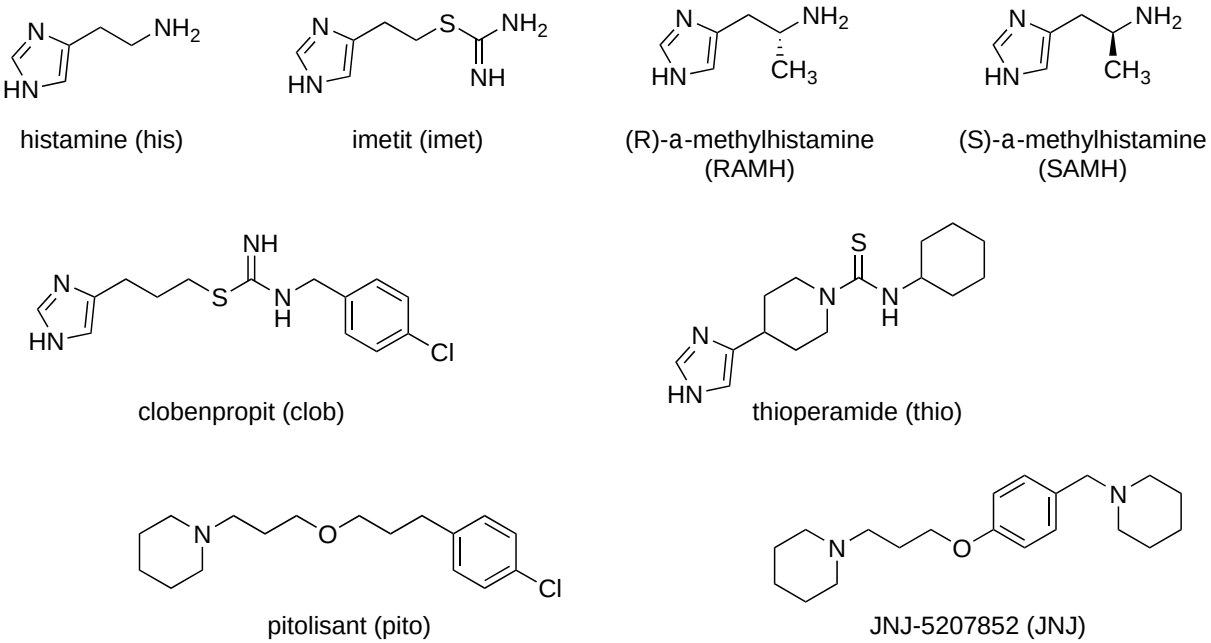

Figure 7.31: Structures of competitive ligands investigated in radioligand binding assays.

7.3. Appendix Chapter 4

D_1R-H_3R heteromer

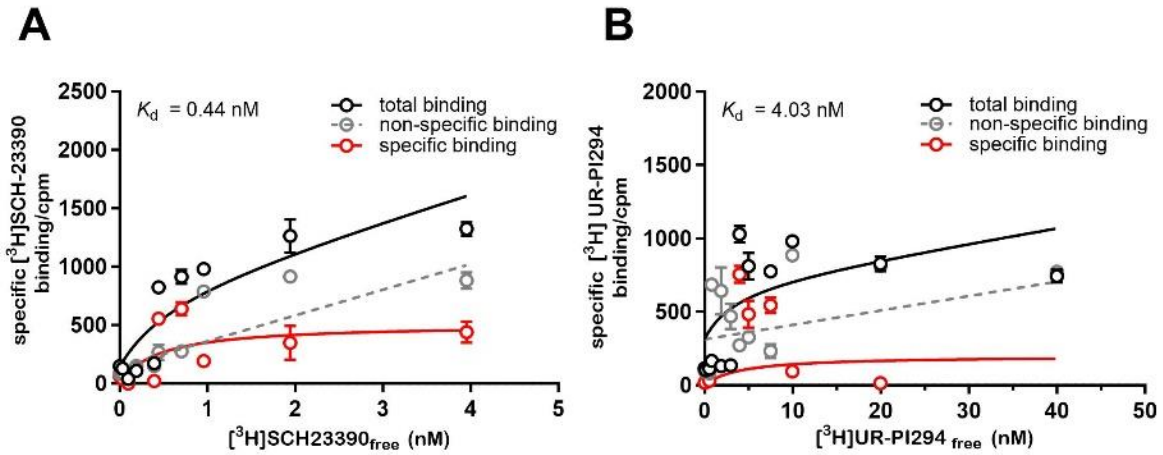

Figure 7.32: Radioligand saturation binding experiment for the D_1R-H_3R heteromer on stable HEK293T FlipIN D_1R-P2A-H_3R cells. **A**: Saturation binding experiment for the D_1R in the presence of different dilutions of the radioligand [^{3}H]SCH-23390 on D_1R-H_3R co-expressing cells . As non-specific binding (+)-butaclamol in 1,000-fold excess to the corresponding radioligand concentration was used. **B:** Saturation binding experiment for the H_3R in the presence of different dilutions of the radioligand [^{3}H]UR-PI294 on D_1R-H_3R co-expressing HEK293T cells. As non-specific binding thioperamide in 1,000-fold excess to the corresponding radioligand concentration was used. Data are shown as one representative from three independent experiments, each performed in duplicate.

Table 7.3: Dissociation constants (pK_d values) of specific radioligands [^{3}H]SCH-23390 for the D_1R protomer and [^{3}H]UR-PI294 for the H_3R protomer on co-expressing HEK293T cells stably expressing the D_1R-H_3R heteromer. Data are shown as means ± SEM from three independent experiments, each performed in duplicate.

cell line	D_1R protomer				H_3R protomer				ratio
	pK_d ± SEM	B_{max} ± SEM	*N*	Ref.	pK_d ± SEM	B_{max} ± SEM	*N*	Ref.	D_1R:H_3R
HEK293T D_1R-P2A-H_3R	n.a.	n.a.	3	8.33[6]	n.a.	n.a.	3	8.33[7]	n.a.

n.a. not applicable.

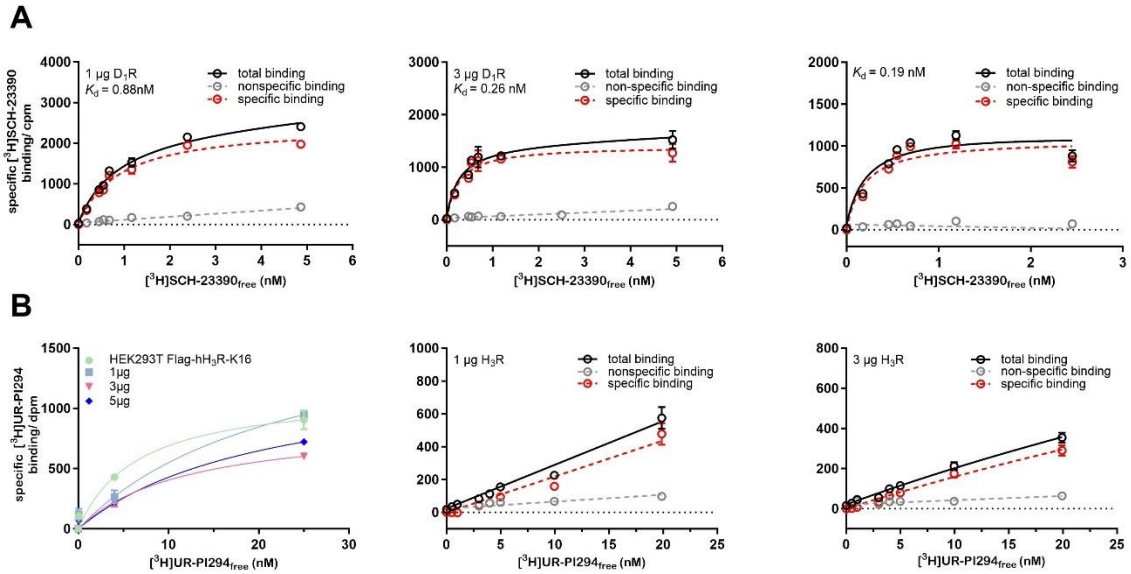

Figure 7.33: Radioligand dissociation experiments of [^{3}H]SCH-23390 on **A**: transient transfected HEK239T cells with 1 µg, 3 µg plasmid DNA of D_1R in comparison with stable HEK293T D_1R-CRELuc2P cells.as non-specific binding (+)-butaclamol in 1,000-fold excess to the corresponding radioligand concentration was used. **B:** Radioligand dissociation experiments of [^{3}H]UR-PI294 on transient transfected HEK239T cells with 1 µg, 3 µg or 5 µg plasmid DNA of H_3R in comparison with stable HEK293T Flag-hH_3R cells. As non-specific binding thioperamide in 1,000-fold excess to the corresponding radioligand concentration was used. Data are shown as one representative from one independent experiments, each performed in duplicate.

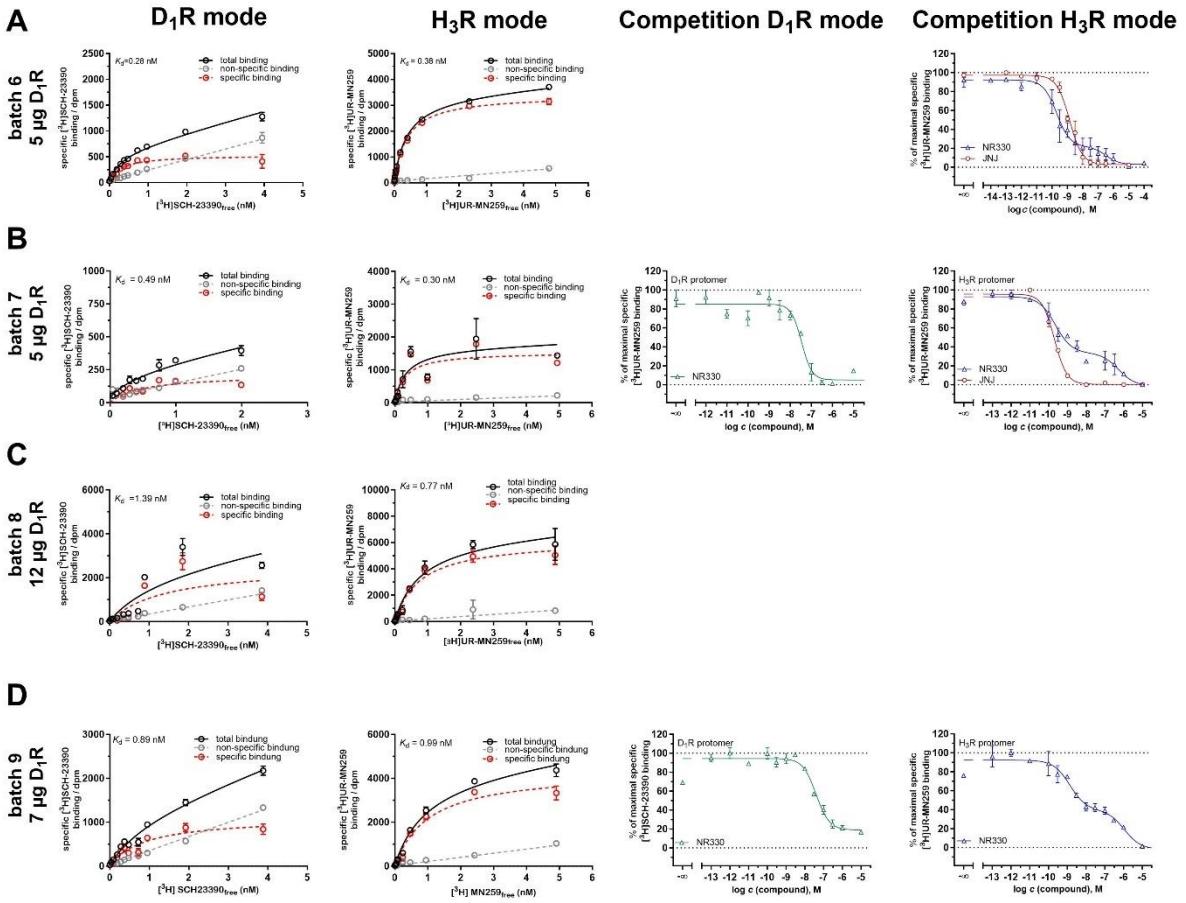

Figure 7.34: Radioligand saturation binding experiments and competition binding experiments in the D_1R-mode ([^{3}H]SCH-23390) or H_3R-mode ([^{3}H]UR_MN259) with four different batches of co-expressing D_1R-H_3R cells. **A:** Batch 6: with 5µg plasmid DNA. **B:** Batch 7: with 5 µg plasmid DNA of D_1R. **C:** Batch 8: 12 ug plasmid DNA of D_1R. **D:** Batch 9 where 7 µg plasmid DNA of D_1R were transfected. As non-specific binding (+)-butaclamol in case of D_1R-mode and clobenpropit in case of H_3R-mode in 1,000-fold excess to the corresponding radioligand concentration was used in saturation binding experiments. In radioligand competition binding experiments JNJ-5207852 (JNJ) and NR330 were used as competitors on the D_1R protomer and H_3R protomer in the presence of the respective radioligand (c ([^{3}H]SCH-23390) = 0.4 nM, c ([^{3}H]UR-MN259) = 0.5 nM) on co-expressing D_1R-H_3R HEK293T cells in each batch. As non-specific binding (+)-butaclamol in the D_1R-mode and clobenpropit in 1,000-fold for the H_3R-mode excess was used. Data of of saturation binding experiments are shown from one experiment (N = 1), performed in duplicate and competition binding experiments as means ± SEM from one or two independent experiments ($N \geq 1$), performed at least in duplicate. ***$p < 0.01$. †$p > 0.05$.

Table 7.4: Obtained pK_d vlues and maximal binding sites (B_{max}) of the D_1R radioligand [^{3}H]SCH-23390 on the D_1R protomer and the H_3R radioligand [^{3}H]UR-MN259 on the H_3R protomer on D_1R-H_3R co-expressing HEK293T cells (batch 6, transfected with 5 µg plasmid DNA of pcDNA3.1 $5HT_{2A}$-D_1R-myc). Data are shown from one experiment (N = 1), performed in duplicate.

receptor	pK_d	B_{max}/ dpm	receptors per cell	ratio D_1R:H_3R	Ref.
D_1R protomer	9.55	532	3.47E+04	1:5	9.70[6]
H_3R protomer	9.42	3398	1.83E+05		9.26[8]

Table 7.5: Obtained pK_d vlues and maximal binding sites (B_{max}) of the D_1R radioligand [^{3}H]SCH-23390 on the D_1R protomer and the H_3R radioligand [^{3}H]UR-MN259 on the H_3R protomer on D_1R-H_3R co-expressing HEK293T cells (batch 7, transfected with 5 µg plasmid DNA of pcDNA3.1$_{neo}$ D_1R-myc). Data are shown from one experiment (N = 1), performed in duplicate.

receptor	pK_d	B_{max}/ dpm	receptors per cell	ratio D_1R:H_3R	Ref.
D_1R protomer	9.31	211	8.82E+03	1:124	9.70[6]
H_3R protomer	9.52	3398	1.10E+05		9.26[9]

Table 7.6: Obtained pK_d vlues and maximal binding sites (B_{max}) of the D_1R radioligand [^{3}H]SCH-23390 on the D_1R protomer and the H_3R radioligand [^{3}H]UR-MN259 on the H_3R protomer on D_1R-H_3R co-expressing HEK293T cells (batch 8, transfected with 12 µg plasmid DNA of pcDNA3.1$_{neo}$ D_1R-myc). Data are shown from one experiment (N = 1), performed in duplicate.

receptor	pK_d	B_{max}/ dpm	receptors per cell	ratio D_1R:H_3R	Ref.
D_1R protomer	8.86	2549	1.07E+05	1:1.9	9.70[6]
H_3R protomer	9.11	6232	2.01E+05		9.26[9]

Table 7.7: Obtained pK_d vlues and maximal binding sites (B_{max}) of the D_1R radioligand [^{3}H]SCH-23390 on the D_1R protomer and the H_3R radioligand [^{3}H]UR-MN259 on the H_3R protomer on D_1R-H_3R co-expressing HEK293T cells (batch 9, transfected with 7 µg plasmid DNA of pcDNA3.1$_{neo}$ $5HT_{2A}$-D_1R-myc). Data are shown from one experiment (N = 1), performed in duplicate.

receptor	pK_d	B_{max}/ dpm	receptors per cell	ratio D_1R:H_3R	Ref.
D_1R protomer	9.05	1110	4.64E+04	1:3	9.70[6]
H_3R protomer	9.00	4349	1.40E+05		9.26[9]

Table 7.8: Binding affinities (pK_i values) of NR330 and JNJ-5207852 (JNJ) in the H_3R-mode with different batches of transient co-expressing HEK293T D_1R-H_3R cells. For batch 6: 5 µg, batch 7: 5 µg and batch 9: 7 µg of plasmid DNA of pcDNA3.1$_{neo}$ $5HT_{2A}$-D_1R-myc were used for transfection. Data are shown as means ± SEM from one or two independent experiments ($N \geq 1$), performed at least in duplicate.

	HEK293T D_1R-H_3R (H_3R protomer)				
Cpd.	pK_i ± SEM	p$K_{i,low}$ ± SEM	p$K_{i,high}$ ± SEM	curve-fit	N
Batch 6					
NR330		7.14 ± 0.36	10.08 ± 0.19	two-site***	2
JNJ	9.22± 0.15			one-site†	2
Batch 7					
NR330		6.54 ± 0.09	9.99 ± 0.36	two-site***	2
JNJ	10.12			one-site†	1
Batch 9					
NR330		6.13	9.04	two-site***	1

$^{***}p < 0.01$. $^{\dagger}p > 0.05$.

Table 7.9: Binding affinities (pK_i values) of NR330 and JNJ-5207852 (JNJ) in the H_3R-mode in different batches of transient co-expressing D_1R-H_3R. For batch 7: 5 µg and batch 9: 7 µg of plasmid DNA of pcDNA3.1$_{neo}$ $5HT_{2A}$-D_1R-myc were used for transfection. Data are shown as means ± SEM from one or two independent experiments ($N \geq 1$), performed at least in duplicate.

	HEK293T D_1R-H_3R (H_3R protomer)				
Cpd.	pK_i ± SEM	p$K_{i,low}$ ± SEM	p$K_{i,high}$ ± SEM	curve-fit	*N*
Batch 7					
NR330	7.98 ± 0.10			one-site†	2
JNJ	9.28			one-site†	1
Batch 9					
NR330	7.57			one-site†	1

†$p > 0.05$.

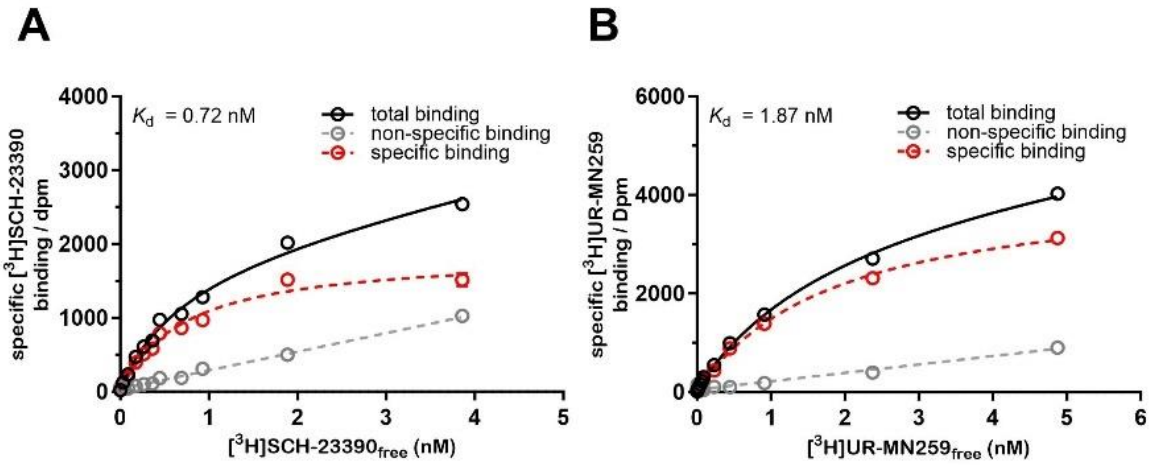

Figure 7.35: Performed radioligand saturation binding curves to determine the stoichiometric ratio of D_1R and H_3R on transient co-expressing HEK293T cells of batch 10 were 12 µg plasmid DNA of pcDNA3.1$_{neo}$ D_1R-myc was transfected, in two modes. **A:** Saturation curve of [^{3}H]SCH-23390 in different concentrations (D_1R-mode). As non-specific binding (+)-butaclamol in 1,000-fold excess was used. **B:** Saturation curve of [^{3}H]UR-MN259 in various concentrations (H_3R-mode). As non-specific binding clobenpropit in 1,000-fold excess was used. Data are shown from one experiment ($N = 1$), performed in duplicate.

Table 7.10: Obtained pK_d vlues and maximal binding sites (B_{max}) of the D_1R radioligand [^{3}H]SCH-23390 on the D_1R protomer and the H_3R radioligand [^{3}H]UR-MN259 on the H_3R protomer on transient D_1R-H_3R co-expressing HEK293T cells (batch 10, transfected with 12 µg plasmid DNA of pcDNA3.1$_{neo}$ $5HT_{2A}$-D_1R.myc). Data are shown from one experiment ($N = 1$), performed in duplicate.

receptor	pK_d	B_{max}/ dpm	receptors per cell	ratio D_1R:H_3R	Ref.
D_1R protomer	9.14	2549	1,07E+05	1:2	9.70[6]
H_3R protomer	8.73	6232	2,01E+05		9.26[9]

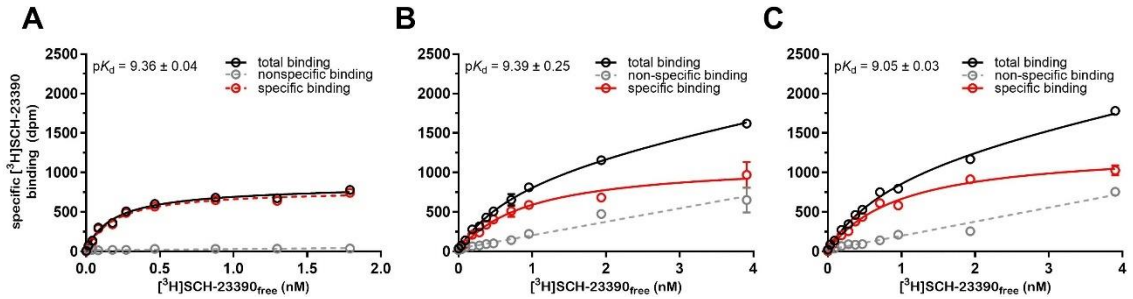

Figure 7.36: Representative radioligand saturation binding experiments of [^{3}H]SCH-23390 in sodium-free BB (**A**), Leibovitz's L15 media (**B**), and BB supplemented with 140 mM NaCl (**C**) on stable HEK293T D_1R-CRELuc2P cells. As non-specific binding (+)butaclamol in 1,000-fold excess was used. Calculated pK_d values are shown as means ± SEM from two to three independent experiments (N ≥ 2), each performed at least in duplicate.

Table 7.11: Determined dissociation constants (pK_d) of the specific D_1R radioligand [^{3}H]SCH-23390 in sodium-free BB, Leibovitz's L-15 media, and BB supplemented with 140 mM NaCl on stable HEK293T D_1R-CRELuc2P cells. Data are shown as means ± SEM from two to three independent experiments ($N \geq 2$), each performed at least in duplicate.

buffer	pK_d ± SEM	B_{max} ± SEM / dpm	N
BB	9.39 ± 0.25	738 ± 284	2
L15	9.64 ± 0.04	812 ± 13.7	3
BB + 140 mM NaCl	9.05 ± 0.03	2092 ± 557	2

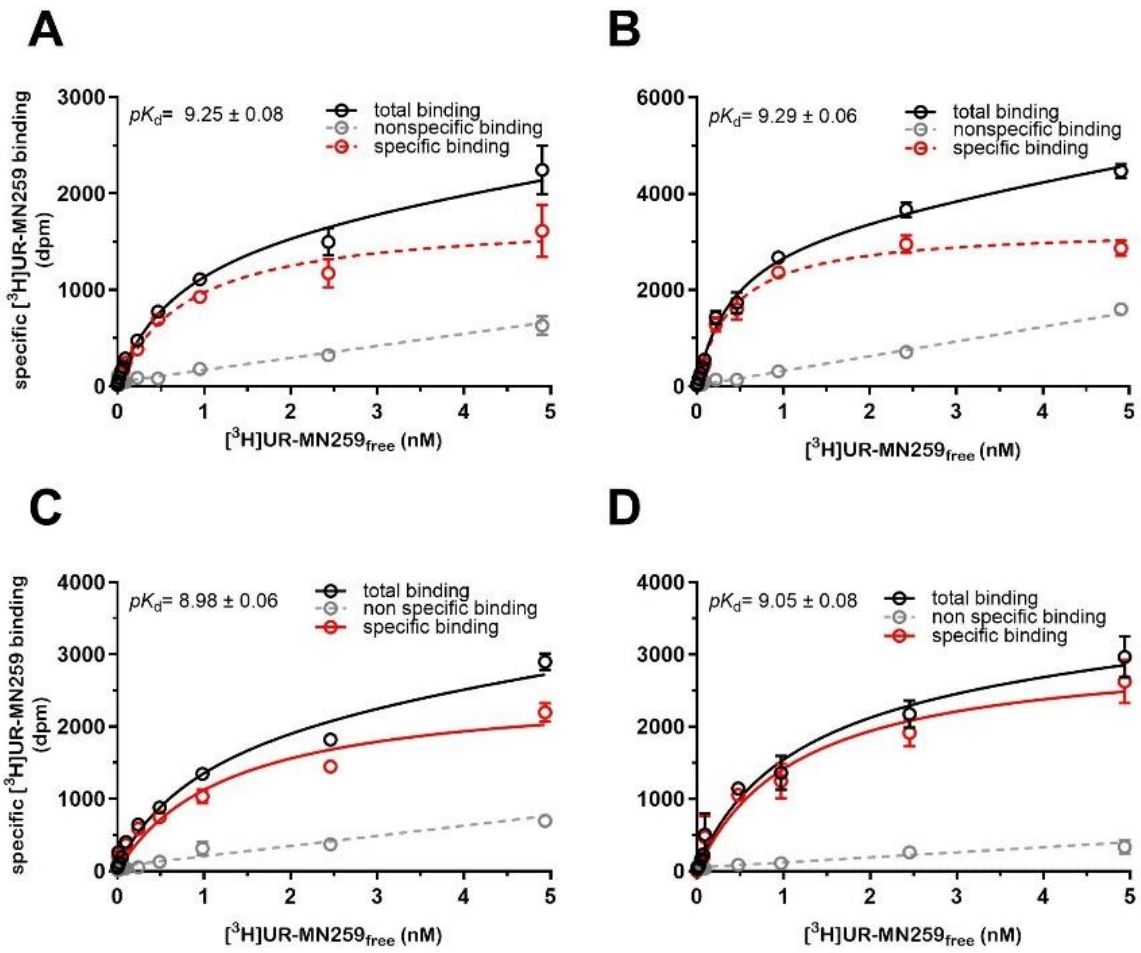

Figure 7.37: Representative radioligand saturation binding experiments of [^{3}H]UR-MN259 in sodium-free BB (**A**), Leibovitz's L15 media (**B**), BB supplemented with 100 mM NaCl (**C**), and BB supplemented with 140 mM NaCl (**D**) on stable HEK293T Flag-hH_3R cells. As non-specific binding clobenpropit in 1,000-fold excess was used. Calculated pK_d values are shown as means ± SEM from two to five independent experiments ($N \geq 2$), each performed at least in duplicate.

Table 7.12: Determined dissociation constants (pK_d) of the specific H_3R radioligand [^{3}H]UR-MN259 in sodium-free BB, Leibovitz's L-15 media, BB supplemented with 100 mM NaCl, and BB supplemented with 140 mM NaCl on stable HEK293T Flag-hH_3R cells. Data are shown as means ± SEM from two to five independent experiments ($N \geq 2$), each performed at least in duplicate.

buffer	pK_d ± SEM	B_{max} ± SEM / dpm	N
BB	9.25 ± 0.08	1668 ± 86	5
L15	9.29 ± 0.06	3596 ± 216	2
BB + 100 mM NaCl	8.98 ± 0.06	2199 ± 219	2
BB + 140 mM NaCl	9.05 ± 0.08	2468 ± 429	2

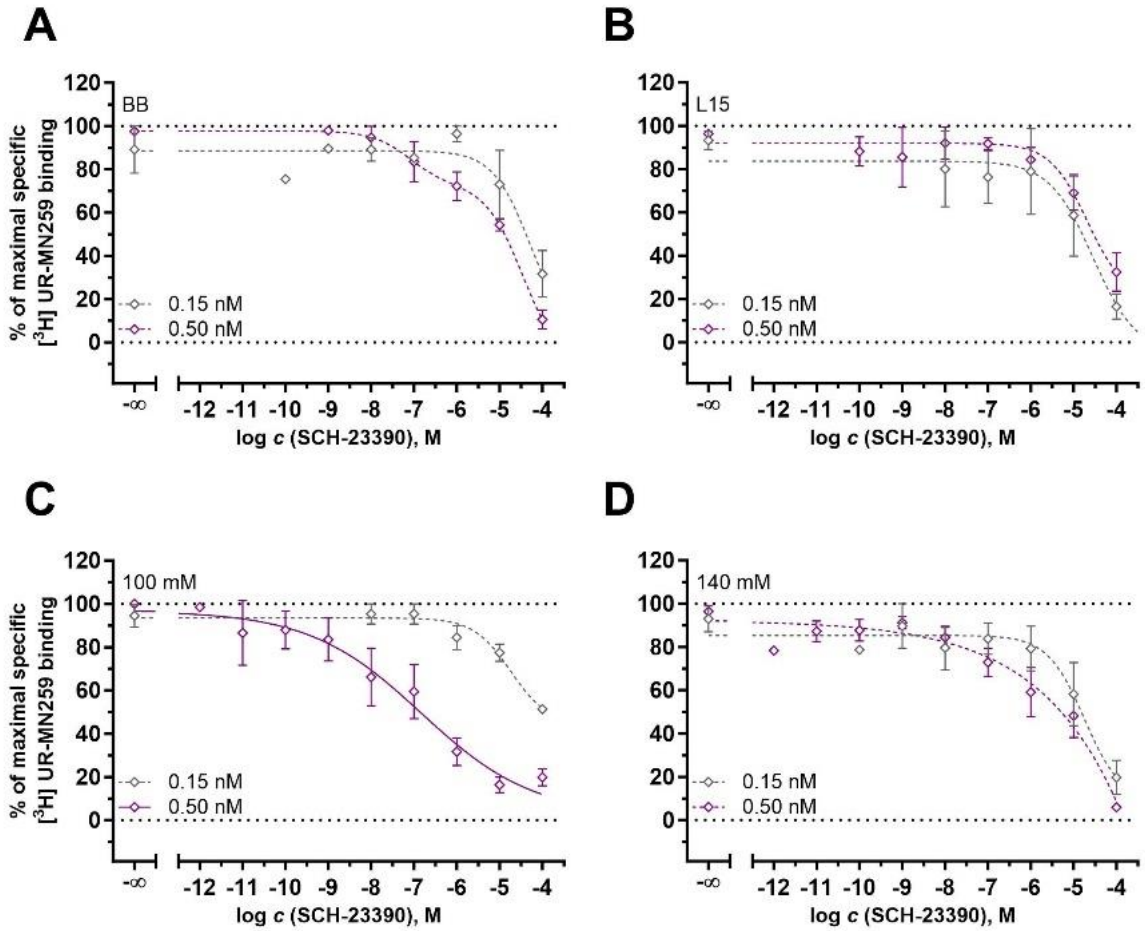

Figure 7.38: Displacement curves of a potential allosteric ligand SCH-23390 in the presence of different concentrations of [^{3}H]UR-MN259 (c= 0.15 nM or 0.50 nM) on stable HEK293T-Flag-hH_3R cells. Curves are shown for two values of radioligand ([A*]/K_d), where [A*] represents the respective radioligand concentration and K_d the dissociation constant of [^{3}H]UR-MN259 in sodium-freeBB (**A**), Leibovitz's L15 medium (**B**), BB supplemented with 100 mM NaCl (**C**) or 140 mM NaCl (**D**). Dashed lines mark incomplete curves where no curve-fit was possible. As non-specific binding clobenpropit in 1,000 -fold access for each buffer was used. Data are shown as means ± SEM of two to five independent experiments ($N \geq 2$), performed at least in duplicate.

Table 7.13: Calculated pK_i values of SCH-23390 for two different radioligand concentrations of [^{3}H]UR-MN259 (0.15 nM and 0.5 nM) in BB, Leibovitz's L15 medium (L15) and BB supplemented with 100 mM NaCl or 140 mM NaCl. Data are shown as means ± SEM of two to five independent experiments ($N \geq 2$), performed at least in duplicate.

	SCH-23390			
	c ([^{3}H]UR-MN259) = 0.50 nM		c ([^{3}H]UR-MN259) = 0.15 nM	
buffer	pK_i ± SEM	N	pK_i ± SEM	N
BB	5.57 ± 0.16	5	4.62 ± 0.20	2
L15	4.80 ± 0.12	5	4.83 ± 0.12	2
BB + 100 mM NaCl	7.79 ± 046	4	< 4.0	2
BB + 140 mM NaCl	5.58 ± 046	4	4.72 ± 0.26	3

$D_{2l}R$-H_3R heteromer

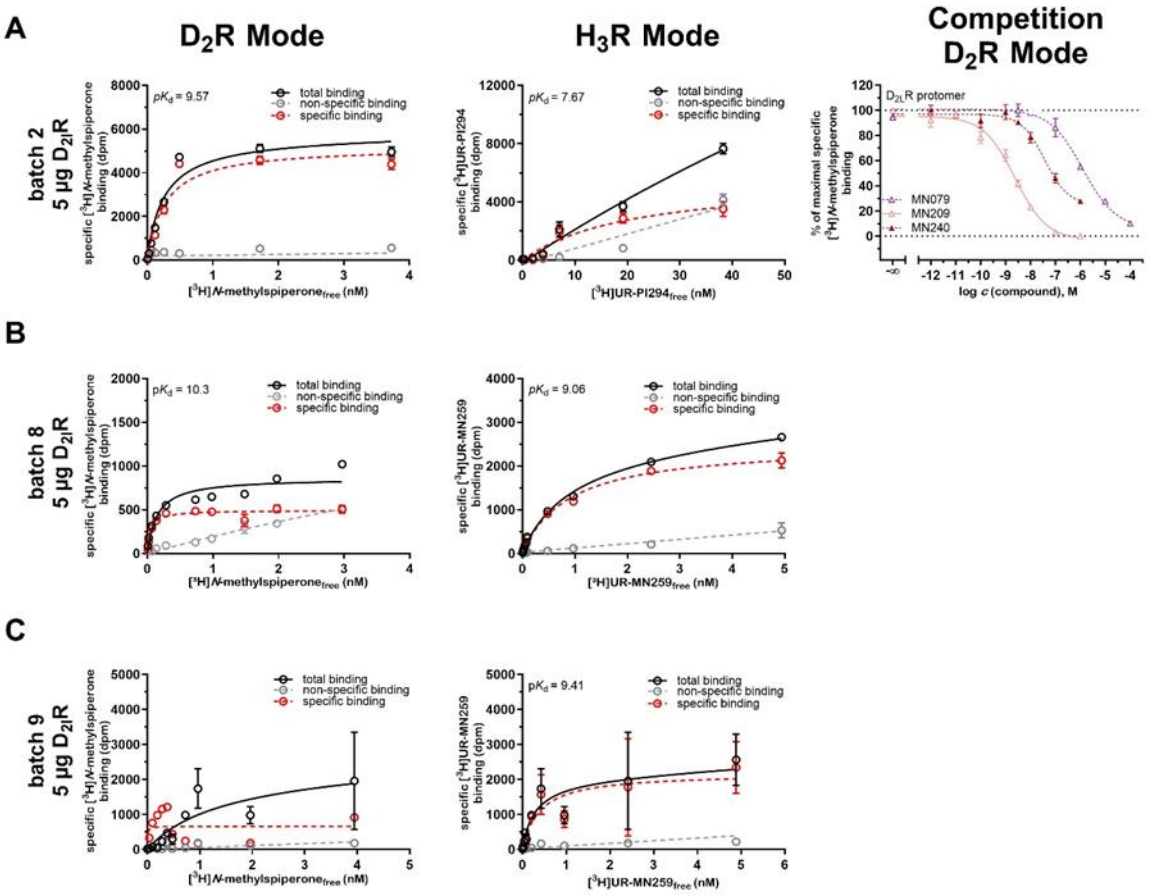

Figure 7.39: Radioligand displacement curves of either [^{3}H]*N*-methylspiperone ($D_{2l}R$ protomer), [^{3}H]UR-PI294 or [^{3}H]UR-MN259 (H_3R protomer) on transient $D_{2l}R$-H_3R co-expressing HEK293T cells in different batches. **A:** Batch 2: transient transfection of 5 µg plasmid DNA of pcDNA3.1$_{neo}$ $D_{2l}R$-myc. **B:** Batch 8: stable expressing H_3R cells line was transient transfected with 5 µg plasmid DNA of pcDNA3.1$_{neo}$ $D_{2l}R$-myc. **C:** Batch 9 stable expressing H_3R cell line was with 5 µg plasmid DNA of pcDNA3.1$_{neo}$ $D_{2l}R$-myc transient transfected. As non-specific binding haloperidol in case of D_2R-mode and thioperamide or clobenpropit in the H_3R-mode each in 1,000-fold excess were used. Data are shown from one experiment (*N* = 1), performed in duplicate.

Table 7.14: Equilibrium dissociation constants (pK_d vlues) and maximal binding sites (B_{max}) of the D_2R radioligand [^{3}H]*N*-methylspiperone on the $D_{2l}R$ protomer and the H_3R radioligand [^{3}H]UR-PI294 on the H_3R protomer on transient $D_{2l}R$-H_3R co-expressing HEK293T cells of batch 2 (transfected with 5 µg plasmid DNA of pcDNA3.1$_{neo}$ $D_{2l}R$-myc). Data are shown from one experiment (*N* = 1), performed in duplicate.

receptor	pK_d	B_{max}/ dpm	receptors per cell	ratio $D_{2l}R$:H_3R	Ref.
$D_{2l}R$ protomer	9.57	5204	3.82E+05	1: 1	10.8[10]
H_3R protomer	8.68	5678	3.44E+05		9.52[7]

Table 7.15: Equilibrium dissociation constants (pK_d vlues) and maximal binding sites (B_{max}) of the D_2R radioligand [^{3}H]*N*-methylspiperone on the $D_{2L}R$ protomer and the H_3R radioligand [^{3}H]UR-MN259 on the H_3R protomer on transient $D_{2l}R$-H_3R co-expressing HEK293T cells of batch 8 (transfected with 5 µg plasmid DNA of pcDNA3.1$_{neo}$ $D_{2l}R$-myc). Data are shown from one experiment (*N* = 1), performed in duplicate.

receptor	pK_d	B_{max}/ dpm	receptors per cell	ratio $D_{2l}R$:H_3R	Ref.
$D_{2l}R$ protomer	11.1	664.2	4.87E+04	1: 2.4	10.8[10]
H_3R protomer	9.41	2181	1.17E+05		9.26[8]

Table 7.16: Equilibrium dissociation constants (pK_d vlues) and maximal binding sites (B_{max}) of the D_2R radioligand [^{3}H]*N*-methylspiperone on the $D_{2l}R$ protomer and the H_3R radioligand [^{3}H]UR-MN259 on the H_3R protomer on transient $D_{2l}R$-H_3R co-expressing HEK293T cells of batch 9 (transfected with 5 µg plasmid DNA of pcDNA3.1$_{neo}$ $D_{2l}R$-myc). Data are shown from one experiment (*N* = 1), performed in duplicate.

receptor	pK_d	B_{max}/ dpm	receptors per cell	ratio $D_{2l}R$:H_3R	Ref.
$D_{2l}R$ protomer	10.3	495.3	3.63E+04	1: 3.7	10.8[10]
H_3R protomer	9.06	2504	1.35E+05		9.26[8]

Table 7.17: Binding affinities (pK_i values) of bivalent ligands in the D_2R-mode of transient co-expressing $D_{2l}R$-H_3R HEK293T cells in batch 2 (5 µg transfected plasmid DNA of pcDNA3.1$_{neo}$ $D_{2l}R$-myc). Data are shown from one experiment (*N* = 1), performed in duplicate.

Cpd.	pK_i ± SEM	curve-fit	*N*
MN079	6.22	one-site†	1
MN209	8.94	one-site†	1
MN240	7.76	one-site†	1

†$p > 0.05$.

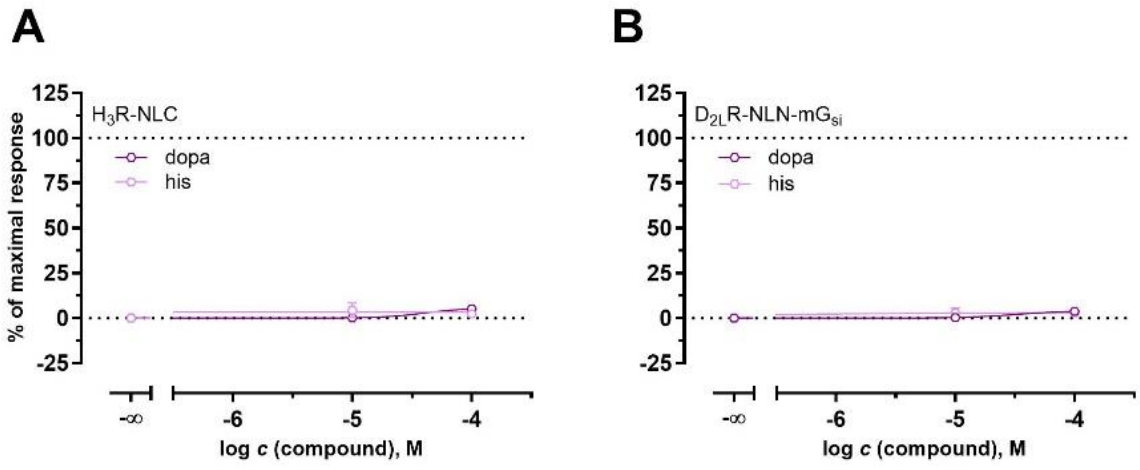

Figure 7.40: Verification of each construct of the split nano luciferase-based miniG protein recruitment assay alone in the presence of the substrate and the D_2R ligand dopamine (dopa) and the H_3R ligand histamine (his). **A:** Concentration-dependent curve of either dopamine or histamine on HEK293T cells transiently transfected with 2 µg of plasmid DNA of pcDNA3.1$_{neo}$ H_3R-NLC. **B:** Concentration-dependent curve of either dopamine or histamine on HEK293T cells transiently transfected with 2 µg of plasmid DNA of pIRES$_{puro}$ $D_{2l}R$-NLN-miniG_{si}.

7.4. Appendix Chapter 5

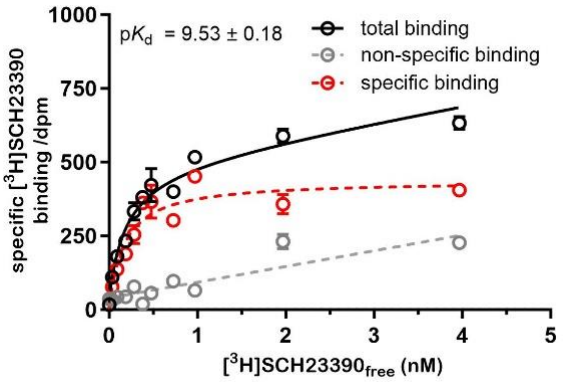

Figure 7.41: Representative radioligand displacement curve of [^{3}H]SCH-233390 on whole and stable HEK293T NLuc-D_1R cells. As non-specific binding (+) butaclamol in 1,000-fold excess to the corresponding radioligand [^{3}H]SCH233390 concentration was used. Representative experiment was performed in triplicate. Calculated pK_d value is shown as mean ± SEM from two independent experiments (N=2), all performed in triplicate.

Table 7.18: Dissociation constant (pK_d value) of the specific D_1R radioligand [3H]SCH-23390 on stable HEK293T Nluc-D_1R cells. Calculated pK_d value is shown as mean ± SEM from two independent experiments (N=2), all performed in triplicate.

	pK_d ± SEM	N	Ref.
Nluc-D_1R	9.53 ± 0.18	2	9.70[6]

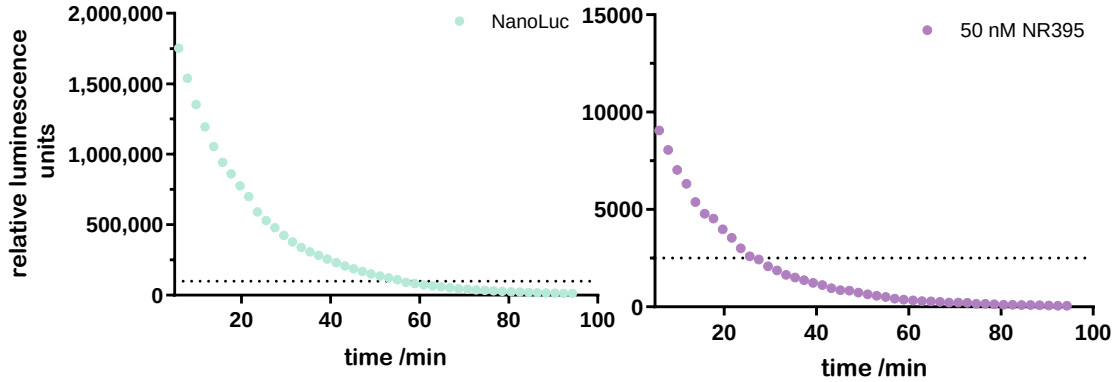

Figure 7.42: Representative relative luminescence unit tracers over a defined period of time for **A:** NanoLuc (λ = 480 nM) and **B:** fluorescens (λ = > 610 nM) observed in NanoBRET saturation binding experiments with NR395 for one representative concentration (c = 50 nM) on stable HEK293T NLuc-D_1R cells. Experiment was performed in triplicate.

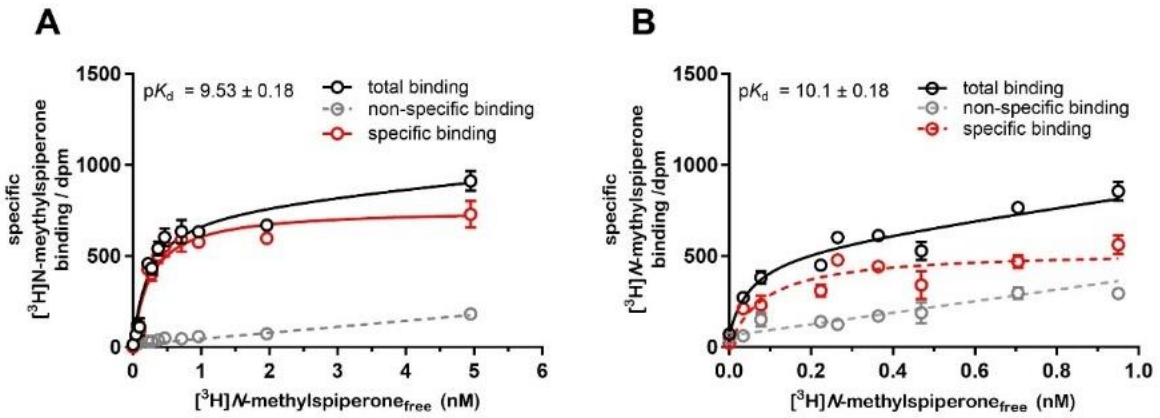

Figure 7.43: Representative radioligand displacement curve of [^{3}H]*N*-methylspiperone on **A:** whole HEK293T NLuc-D_{2l}R cells and **B:** whole HEK293T NLuc-D_3R cells. As non-specific binding haloperidol in 1,000-fold excess to the corresponding radioligand [^{3}H]*N*-methylspiperone concentration was used. Representative experiment was performed in triplicate. Calculated pK_d value is shown as mean ± SEM from two different experiments (*N*=2), all performed in triplicate.

Table 7.19: Dissociation constant (pK_d value) of the specific D_2R radioligand [^{3}H]*N*-methylspiperone on stable HEK293T Nluc-$D_{2l,3}$R cells. Calculated pK_d value is shown as mean ± SEM from two independent experiments (*N*=2), all performed in triplicate.

	pK_d ± SEM	*N*	Ref.
Nluc-D_{2l}R	9.53 ± 0.18	2	10.8[10]
NLuc-D_3R	10.1 ± 0.18	2	10.6[10]

7.5. Abbreviations

ADHD – attention hyperactivity deficit disorder;

Apo – *R*-(-)-apomorphine;

Aprox. – approximately;

ASD – autism spectrum disorder;

BRET – bioluminescence resonance technology;

BSA – bovine serum albumin;

Buta – (+)-butaclamol hydrochloride;

cAMP – cyclic adenosine monophosphate;

CAMYEN – cAMP sensor using YFP-Epac-Nluc;

cDNA – complementary DNA;

CNS – central nervous system;

Clo – clobenpropit;

Cpd – compound;

cpVenus – circular permutation Venus;

CZH – coelenterazine H;

DAG- diacylgycerol;

dH_2O – distilled water;

DMEM – Dulbecco's modified Eagle's medium high glucose;

Dopa – dopamine;

(h)DxR – (human) dopamine Dx receptor;

ECL extracellular loop;

ELISA – enzyme-linked immunosorbent assay;

ERK 1/ 2 - extracellular signal-regulated kinase 1/ 2;

Epac – exchange protein activated by cAMP;

FCS – fetal calf serum;

FMDV - foot-and-mouth disease virus;

Furi - Fuimazine

G-CASE – G protein-based, tricistronic activity sensor;

GPCR – G protein-coupled receptor;

Halo – haloperidol;

HEPES – 4-(2-hydroxyethyl)-1-piperazineethanesulfonic acid;

His – histamine;

ICL - intracellular loop;

IP_3 – inositol-1,4,5-trisphosphate;

JNJ - JNJ-5207852;

L-15 – Leibovitz's L-15 medium without phenol red;

MAPK or MEPK- mitogen-activated protein kinase;

miniG or mG – minimal G protein;

NAM - negative allosteric modulator;

NanoBiT – Nanoluciferase binary technology;

NanoLuc or Nluc – Nanoluciferase;

Nemo – nemonapride;

NlucC or smBiT – small C terminus part of the split Nanoluciferase;

NlucN or LgBiT – large N terminus part of the split Nanoluciferase;

NMSP – *N*-methylspiperone;

P2A - porcine teschovirus-1 2A protein;

PAM - positive allosteric modulators;

PBS – phosphate buffered saline;

PD -Parkinson's disease;

PEI – linear polyethylenamine;

PEG – polyethylene glycol;

PI3K – phosphoinositide-3-kinase;

PKA - protein kinase A;

PKB - protein kinase B;

PKC protein kinase C;

PLC-β - phospholipase C-β;

Prami – pramipexole dihydrochloride;

Quin – (-)-quinpirole hydrochloride;

RAS – rat sarcoma virus (protein);

RAF - rapidly accelerated fibrosarcoma (protein);

SCH – (+)-SCH-23390 hydrochloride;

SKF – (+)-SKF-81297 hydrobromide;

SLC - split luciferase complementation;

Spip – spiperone hydrochloride;

Sulp- (*S*)-(-)sulpirde;

TAMRA - Tetramethylrhodamin;

Thio - thioperamide

TM – transmembrane;

Wild-type – wt.

7.6. References

(1) Sun, W.; Jin, L.; Cao, Y.; Wang, L.; Meng, F.; Zhu, X. Cloning, expression, and functional analysis of human dopamine D1 receptors. *Acta pharmacologica Sinica* **2005**, *26* (1), 27–32. DOI: 10.1111/j.1745-7254.2005.00017.x.

(2) Zou, M.-F.; Keck, T. M.; Kumar, V.; Donthamsetti, P.; Michino, M.; Burzynski, C.; Schweppe, C.; Bonifazi, A.; Free, R. B.; Sibley, D. R.; Janowsky, A.; Shi, L.; Javitch, J. A.; Newman, A. H. Novel Analogues of (R)-5-(Methylamino)-5,6-dihydro-4H-imidazo4,5,1-ijquinolin-2(1H)-one (Sumanirole) Provide Clues to Dopamine D2/D3 Receptor Agonist Selectivity. *Journal of medicinal chemistry* **2016**, *59* (7), 2973–2988. DOI: 10.1021/acs.jmedchem.5b01612. P

(3) Schetz, J. A.; Benjamin, P. S.; Sibley, D. R. Nonconserved residues in the second transmembrane-spanning domain of the D(4) dopamine receptor are molecular determinants of D(4)-selective pharmacology. *Molecular pharmacology* **2000**, *57* (1), 144–152.

(4) Ricci, A.; Amenta, F. Dopamine D5 receptors in human peripheral blood lymphocytes: a radioligand binding study. *Journal of neuroimmunology* **1994**, *53* (1), 1–7. DOI: 10.1016/0165-5728(94)90057-4.

(5) Uhlén, M.; Fagerberg, L.; Hallström, B. M.; Lindskog, C.; Oksvold, P.; Mardinoglu, A.; Sivertsson, Å.; Kampf, C.; Sjöstedt, E.; Asplund, A.; Olsson, I.; Edlund, K.; Lundberg, E.; Navani, S.; Szigyarto, C. A.-K.; Odeberg, J.; Djureinovic, D.; Takanen, J. O.; Hober, S.; Alm, T.; Edqvist, P.-H.; Berling, H.; Tegel, H.; Mulder, J.; Rockberg, J.; Nilsson, P.; Schwenk, J. M.; Hamsten, M.; Feilitzen, K. von; Forsberg, M.; Persson, L.; Johansson, F.; Zwahlen, M.; Heijne, G. von; Nielsen, J.; Pontén, F. Proteomics. Tissue-based map of the human proteome. *Science (New York, N.Y.)* **2015**, *347* (6220), 1260419. DOI: 10.1126/science.1260419.

(6) Bourne, J. A. SCH 23390: the first selective dopamine D1-like receptor antagonist. *CNS drug reviews* **2001**, *7* (4), 399–414. DOI: 10.1111/j.1527-3458.2001.tb00207.x.

(7) Bartole, E.; Grätz, L.; Littmann, T.; Wifling, D.; Seibel, U.; Buschauer, A.; Bernhardt, G. UR-DEBa242: A Py-5-Labeled Fluorescent Multipurpose Probe for Investigations on the Histamine H3 and H4 Receptors. *Journal of medicinal chemistry* **2020**, *63* (10), 5297–5311. DOI: 10.1021/acs.jmedchem.0c00160.

(8) Mönnich, D.; Nagl, M.; Forster, L.; Rosier, N.; Igel, P.; Pockes, S. Discovery of a Tritiated Radioligand with High Affinity and Selectivity for the Histamine H3 Receptor. *ACS medicinal chemistry letters* **2023**, *14* (11), 1589–1595. DOI: 10.1021/acsmedchemlett.3c00413.

(9) Nagl, M.; Mönnich, D.; Rosier, N.; Schihada, H.; Sirbu, A.; Konar, N.; Reyes-Resina, I.; Navarro, G.; Franco, R.; Kolb, P.; Annibale, P.; Pockes, S. [Duplikat] Fluorescent Tools for the Imaging of Dopamine D2 -Like Receptors. *Chembiochem: a European journal of chemical biology* **2023**, e202300659. DOI: 10.1002/cbic.202300659.

(10) Forster, L.; Grätz, L.; Mönnich, D.; Bernhardt, G.; Pockes, S. A Split Luciferase Complementation Assay for the Quantification of β-Arrestin2 Recruitment to Dopamine D2-Like Receptors. *International journal of molecular sciences* **2020**, *21* (17). DOI: 10.3390/ijms21176103.

Eidesstattliche Erklärung

Ich erkläre hiermit an Eides statt, dass ich die vorliegende Arbeit ohne unzulässige Hilfe Dritter und ohne Benutzung anderer als der angegebenen Hilfsmittel angefertigt habe; die aus anderen Quellen direkt oder indirekt übernommenen Daten und Konzepte sind unter Angabe des Literaturzitats gekennzeichnet.

Teile der experimentellen Arbeiten wurden in Zusammenarbeit mit anderen Institutionen und Personen durchgeführt. Entsprechende Vermerke zu den Beiträgen der betreffenden Personen finden sich jeweils zu Beginn des entsprechenden Kapitels und unter „Acknowledgements".
Weitere Personen waren an der inhaltlich-materiellen Herstellung der vorliegenden Arbeit nicht beteiligt. Insbesondere habe ich hierfür nicht die entgeltliche Hilfe eines Promotionsberaters oder anderer Personen in Anspruch genommen. Niemand hat von mir weder unmittelbar noch mittelbar geldwerte Leistungen für Arbeiten erhalten, die im Zusammenhang mit dem Inhalt der vorgelegten Dissertation stehen.

Die vorliegende Arbeit wurde bisher weder im In- noch im Ausland in gleicher oder ähnlicher Form einer anderen Prüfungsbehörde vorgelegt.

Regensburg, den _____

Denise Mönnich